S
SEP 28 2000
STA# 4

4 ENGINEERING DATA TRANSMITTAL

Page 1 of 1

1. EDT 630480

2. To: (Receiving Organization)	3. From: (Originating Organization)	4. Related EDT No.:
Distribution	Inventory Control and Modeling	N/A
5. Proj./Prog./Dept./Div.:	**6. Design Authority/ Design Agent/Cog. Engr.:**	**7. Purchase Order No.:**
Data Observations on Double Shell Flamable Gas Watch List Tank Behavior/River Protection Project/IC&M/Nuclear Operations Project Services	D. C. Hedengren	N/A
8. Originator Remarks: This document is being released into the supporting document system for retrievability purposes.		**9. Equip./Component No.:** N/A **10. System/Bldg./Facility:** N/A
11. Receiver Remarks: For release. **11A. Design Baseline Document?** [ ] Yes [X] No		**12. Major Assm. Dwg. No.:** N/A **13. Permit/Permit Application No.:** N/A **14. Required Response Date:** 09/11/00

15. DATA TRANSMITTED

(A) Item No.	(B) Document/Drawing No.	(C) Sheet No.	(D) Rev. No.	(E) Title or Description of Data Transmitted	(F) Approval Designator	(G) Reason for Transmittal	(H) Originator Disposition	(I) Receiver Disposition
1	RPP-6655	N/A	0	Data Observations on Double-Shell Flammable Gas Watch List Tank Behavior	N/A	2	1	1

16. KEY

Approval Designator (F)	Reason for Transmittal (G)	Disposition (H) & (I)
E, S, Q, D or N/A (see WHC-CM-3-5, Sec.12.7)	1. Approval 4. Review 2. Release 5. Post-Review 3. Information 6. Dist. (Receipt Acknow. Required)	1. Approved 4. Reviewed no/comment 2. Approved w/comment 5. Reviewed w/comment 3. Disapproved w/comment 6. Receipt acknowledged

17. SIGNATURE/DISTRIBUTION
(See Approval Designator for required signatures)

(G) Reason	(H) Disp.	(J) Name	(K) Signature	(L) Date	(M) MSIN
		Design Authority			
		Design Agent			
2	1	Cog.Eng. D.C. Hedengren	D.C. Hedengren R2-11	9-18-00	
2	1	Cog. Mgr. B. G. Baide	B.G. Baide R3-12	9-18-00	
		QA			
		Safety			
		Env.			

(G) Reason	(H) Disp.	(J) Name	(K) Signature	(L) Date	(M) MSIN
1		R.J. Cash	R.J. Cash	9/21/00	R1-44
1	1	J.J. Zach	James Zach	9/19/00	R1-49

18.	19.	20.	21. DOE APPROVAL (if required)
A.E. Young Signature of EDT Originator — Date 9-18-00	N/A Authorized Representative for Receiving Organization — Date	D.G. Baide Design Authority/ Cognizant Manager — Date 9-18-00	Ctrl. No. [ ] Approved [ ] Approved w/comments [ ] Disapproved w/comments

BD-7400-172-2 (05/96) GEF097

DISTRIBUTION SHEET

To	From	Page 1 of 1
Distribution	Inventory Control and Modeling	Date 09/18/00
Project Title/Work Order		**EDT No.** EDT-630480
RPP-6655, Rev. 0, "Data Observations on Double-Shell Flammable Gas Watch List Tank Behavior"		**ECN No.** N/A

Name	MSIN	Text With All Attach.	Text Only	Attach./ Appendix Only	EDT/ECN Only
CH2M Hill Hanford Group, Inc.					
D. G. Baide	R3-72	X			
W. B. Barton	R2-11	X			
R. J. Cash	R1-44	X			
D. C. Hedengren	R2-11	3			
K. M. Hodgson	R2-11	X			
N. W. Kirch	R2-11	X			
C. E. Leach	R1-44	X			
T.C.S.R.C.	R1-10	X			
G & P Consulting, Inc.					
J. M. Grigsby	R1-44	X			
H & R Technical Associates					
L. J. Kripps	R1-44	X			
Lockheed Martin Services, Inc.					
Central Files	B1-07	X			
Longenecker and Associates					
J. J. Zach	R1-49	5			
Office of River Protection					
C. A. Groendyke	H6-60	6			
D. H. Irby	H6-60	X			
J. S. Shuen	H6-60	X			
DOE Reading Room	H2-53	X			
Pacific Northwest National Laboratory					
J. W. Brothers	K9-20	X			
J. M. Cuta	K7-15	X			
J. L. Huckaby	K7-15	X			
W. L. Kuhn	K7-15	X			
L. A. Mahoney	K7-15	X			
P. A. Meyer	K7-15	X			
C. W. Stewart	K7-15	X			
B. E. Wells	K7-15	X			

Data Observations on Double-Shell Flammable Gas Watch List Tank Behavior

D. C. Hedengren
CH2M HILL Hanford Group, Inc., Richland, WA 99352
Office of River Protection Contract DE-AC06-99RL14047

EDT/ECN: EDT-630480 UC: 2070
Org Code: 7M100 CACN/COA: 101898/BA10
B&R Code: EW 3120074 Total Pages: 254

Key Words: Data Observations, Data, Observations, Double-Shell, DSTs, Flammable Gas Watch List, Flammable Gas, Gas, Watch List, Tank Behavior, Hydrogen, Methane, Ammonia

Abstract: N/A

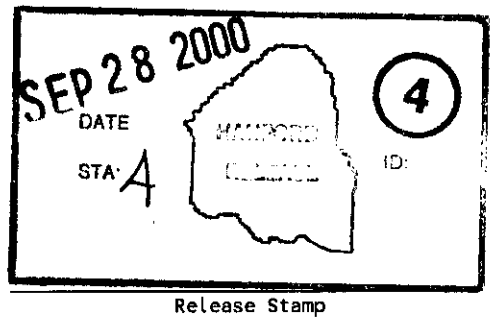

Release Approval 9/27/00 Date

Release Stamp

Approved for Public Release

RPP-6655
Revision 0

DATA OBSERVATIONS ON DOUBLE-SHELL FLAMMABLE GAS WATCH LIST TANK BEHAVIOR

D. C. Hedengren
K. M. Hodgson
W. B. Barton
CH2M HILL Hanford Group, Inc.

C. W. Stewart
J. M. Cuta
B. E. Wells
Pacific Northwest National Laboratory

Date Published
September 2000

CH2MHILL
Hanford Group, Inc.

Prepared for the U.S. Department of Energy
Office of River Protection

ABSTRACT

This report provides the data from the retained gas sampler, void fraction instrument, ball rheometer, standard hydrogen monitoring system, and other tank data pertinent to gas retention and release behavior in the waste stored in double-shelled Flammable Gas Watch List tanks at Hanford. These include tanks 241-AN-103, 241-AN-104, 241-AN-105, 241-AW-101, 241-SY-101, and 241-SY-103. The tanks and the waste they contain are described in terms of fill history and chemistry. The results of mixer pump operation and recent waste transfers and back-dilution in SY-101 are also described. In-situ measurement and monitoring systems are described and the data are summarized under the categories of thermal behavior, waste configuration and properties, gas generation and composition, gas retention and historical gas release behavior.

This page intentionally left blank.

SUMMARY

The main objective this report is to describe and document the waste configuration and the gas retention and release behavior in Hanford double-shell waste tanks (DSTs) in Facility Group 1. This group have significant spontaneous gas releases and the potential for significant induced releases. These include tanks 241-AN-103 (AN-103), 241-AN-104 (AN-104), 241-AN-105 (AN-105), 241-AW-101 (AW-101), and 241-SY-103 (SY-103). Tank 241-SY-101 (SY-101) is not in Facility Group 1, but is included in this report because it is on the Flammable Gas Watch List (FGWL) along with the other five tanks.

The five Facility Group 1 tanks exhibit buoyant displacement gas release, and it is important to record their behavior in terms of the gas release volume distribution, frequency, and duration. To help understand this behavior and develop models to predict it, the tank waste rheology and configuration, retained gas volume, and historic release behavior have been characterized using data from the retained gas sampler (RGS), void fraction instrument (VFI), ball rheometer, standard hydrogen monitoring system (SHMS), and other tank observations.

Prior to mixer pump installation in July 1993, SY-101 also exhibited buoyant displacement gas releases which were occasionally of sufficient volume not only to create a flammable headspace but to damage the tank dome if it had been burned. However, large gas releases were prevented by mixer pump operation, and the recent waste transfer and back dilutions have changed the waste such that gas retention and resumption of buoyant displacements is not expected and mixer pump operation is no longer necessary.

Observations from the last five years show that none of the gas releases from these tanks have challenged the lower flammability limit (LFL) and only rarely exceeded 25% of the LFL. While the tanks (except AW-101) contain just sufficient gas to damage the tank structure if all of it were hypothetically burned in the headspace, only a small fraction of the total is released in any one event. The largest gas release in SY-101 was only 63% of the tank inventory and the other tanks, on the average release only 10% or less of their inventory. Two tanks (AW-101 and SY-103) do not contain enough hydrogen to make their headspace flammable even if all the gas were suddenly released. The general trend over the past five years has been one of decreasing waste temperature, gas generation rate, retained gas volume and gas release volume. Only SY-103 has remained relatively constant in state and behavior.

Based on the available data and observations, it is concluded that the tanks do not present a serious flammable gas hazard, no new hazards have been identified, and the observed trends are of decreasing hazard.

This page intentionally left blank.

CONTENTS

APPENDICES

LIST OF FIGURES

This page cannot be converted.

Please view the native document

for the original page.

LIST OF TABLES

LIST OF TERMS

ATG	Advanced technology gauge
atm	atmosphere
BBI	Best-Basis Inventory
BD GRE	buoyant displacement gas release event
BPE	barometric pressure effect
cc	cubic centimeters
CCPLX	complex concentrate
cfm	cubic feet per minute
CHG	CH2M HILL Hanford Group, Inc.
cm	centimeter
cm/kPa	centimeter per kilo-Pascal
cm/s	centimeter per second
cm^3/in.	cubic centimeters per inch
cP	centiPoise
DACS	Data Acquisition and Control System
dL/dP	correlation of waste level with barometric pressure, cm/kPa or in./in.-Hg.
DOE	the U.S. Department of Energy
DOE-ORP	the U.S. Department of Energy, Office of River Protection
DOE-RL	the U.S. Department of Energy, Richland Operations Office
DST	double-shell tank
DSS	double-shell slurry
DSSF	double-shell slurry feed
EDS	energy dispersive spectroscopy
FGWL	Flammable Gas Watch List
FIC	Food Instrument Corporation
ft	feet
ft^3	cubic feet
FTIR	Fourier Transform Infra-Red Spectrometer
g/cc	grams per cubic centimeters
g/cm^3	grams per cubic centimeter
gal	gallon(s)
GC	Gas Chromatograph
GC-RGA	Gas Chromatograph Reduction Gas Analyzer

GC-TCD	Gas Chromatograph Thermal Conductivity Detector
GCS	Gas Characterization System
GMS-1	Gas Monitoring System-1
GMS-2	Gas Monitoring System-2
GRE	gas release event
HEPA	high-efficiency particulate air
HLAN	Hanford Local Area Network
hp	horsepower
Hz	Hertz
ILL	Interstitial Liquid Level
in.	inch(es)
in^2	square inches
in./d	inch per day
IR	infra-red/Infra-Red Photo Acoustic Multi-Gas Monitor
kg/m^3	kilograms per cubic meter
kgal	kilogallon
kJ/kg	kiloJoule per kilogram
kJ/mol	kiloJoule per mole
kJ/mol-K	kiloJoule per mole per degree Kelvin
kL	kiloliter
LANL	Los Alamos National Laboratory
lb	pound(s)
LFL	lower flammability limit
LOW	Liquid Observation Well
M	molar concentration
MT	manual tape
MT	metric ton
m	meter
m^3	cubic meters
mm	millimeter
mm/d	millimeter per day
MEV	million electron volts
mg/L	milligram per liter
MIT	multiple-function instrument tree
mol/kg-d	mole per kilogram per day
molecule/100 ev	molecules per 100 electron volts
MPa	MegaPascals
N	Newton
N/m	Newton per meter (unit of surface tension)
NMR	nuclear magnetic resonance
Pa	Pascal, N/m^2 (unit of pressure)
PMCS	Push Mode Core Sample
PNNL	Pacific Northwest National Laboratory
ppm	parts per million
ppmv	parts per million by volume
psi	pounds per square inch

PUREX	Plutonium-Uranium Extraction
RGS	Retained Gas Sampler
R/h	Rems per hour
RMCS	Rotary Mode Core Sample
rpm	revolutions per minute
RPP	River Protection Project
SACS	Surveillance Analysis Computer System
s^{-1}	per second
scf	standard cubic feet
scfd	standard cubic feet per day
scf/year	standard cubic feet per year
scfm	standard cubic feet per minute
scm	standard cubic meters
SHMS	standard hydrogen monitoring system
SST	single-shell tank
TC	thermocouple
TCD	Tank Characterization Database
TEM	transmission electron microscopy
TMACS	Tank Monitoring and Control System
TOC	total organic carbon
TWINS	Tank Waste Information Network System
USQ	unreviewed safety question
VFI	Void Fraction Instrument
WHC	Westinghouse Hanford Company
°C	degrees Celsius
°F	degrees Fahrenheit
K	Kelvin
%	percent
µg/g	microgram per gram

1.0 INTRODUCTION

The primary purpose of this report is to document the gas generation, retention and release behavior in DSTs on the FGWL at Hanford. This behavior is described in terms of tank history, waste chemistry and data from the RGS, VFI, ball rheometer, headspace gas monitoring systems, and other tank data. The goal of this presentation is to provide a better understanding and to aid in developing models that predict gas retention and release behavior in these tanks.

1.1 BACKGROUND

Radioactive waste is stored in 177 carbon steel tanks with capacities from 190 to 4,500 m^3 (50 to 1,200 kgal). Of these, 149 are single-shell tanks (SSTs) built in the 1940s, 1950s, and early 1960s, and 28 are newer DSTs constructed in the 1970s and 1980s. The SSTs were removed from active use in 1980. Since then, much of their pumpable liquid has been transferred to the DSTs. This has generally left the SSTs with less waste per tank, much of which is solid, while the DSTs are generally filled closer to their capacities and contain more liquid. However, the liquid transferred to the DSTs was typically concentrated by evaporation which, in some tanks, formed relatively deep layers of settled solids by precipitation as the waste cooled.

All Hanford wastes generate flammable gases by radiolysis of water, decomposition of organic compounds, and corrosion of the steel tank walls. The main fuel components of the waste gas mixture are hydrogen and ammonia. The gas also contains nitrous oxide (an oxidizer), nitrogen (inert component), and very small amounts of methane and other hydrocarbons.

Flammable gas generation by itself is not a hazard. When the gas is released continuously as fast as it is generated, the rate of release is very slow compared to the headspace ventilation rate and the mixing is rapid. The highest gas generation rates are less than 100 standard cubic feet per day while the nominal DST ventilation rate is at least 100 standard cubic feet per minute. Consequently, the background concentration of flammable gas in the headspace of each of the DSTs has remained well below the lower flammability limit (LFL).

Some DST wastes, however, can and do retain the gas mixture until a relatively large amount builds up and is released rapidly into the tank headspace (the portion of the tank that lies above the liquid or solid surface that defines the fill level). This type of release is termed a buoyant displacement. Such sudden releases potentially could result in the concentration of the flammable gas mixture in the headspace reaching the LFL and leading to deflagration if an ignition source is present at the time of the release. If the energy in the deflagration is sufficient, damage to the tank and release of radioactive waste could occur. Tanks AN-103, AN-104, AN-105, AW-101 and SY-103 currently exhibit buoyant displacement gas releases.

1.1.1 Flammable Gas Watch List

The flammable gas hazard in Hanford waste tanks was first recognized in the behavior of SY-101. The waste level in this tank began periodically rising and suddenly dropping, shortly after it was filled in 1980. The large, sawtooth level drops were taken as an indication of episodic gas releases that might pose a safety hazard. Some of them had sufficient volume to exceed the LFL in the entire headspace and probably would have damaged the tank had the gas been ignited.

In 1990, the gas release behavior of SY-101 was recognized as a situation requiring special attention and control. In April 1990, administrative controls were implemented to control various activities. In May 1990, the U.S. Department of Energy, Richland Operations Office, determined that hydrogen and nitrous oxide buildup in certain waste tanks and the possibility of their ignition constituted an Unreviewed Safety Question (USQ). The USQ was applied to SY-101 and 22 other tanks at that time. The USQ eventually led to the development of an effective set of administrative flammable gas controls and of the Facility Group concept as a method to apply the most stringent controls to the most hazardous tanks as discussed in the next section. After an intense period of study and negotiation, a mixer pump was selected to mitigate the large gas releases from SY-101 and was installed July 3, 1993. The mixer pump performed as expected, and no hazardous gas releases have occurred since.

The FGWL was a result of Public Law 101-510, which Congress passed in November 1990. Section 3137, also referred to as the Wyden Amendment, was part of this law. This section required the Secretary of Energy to identify within 90 days a "watch list" of the high-level nuclear waste tanks that may have a "serious potential for release of high-level waste due to uncontrolled increases in temperature or pressure." The same tanks defined by the USQ were also used for the initial FGWL.

The process by which the tanks were identified for the USQ and watch list was described in early 1991. An increase in the waste level, without waste additions, was called slurry growth. The original evaluation focused on the slurry growth phenomena; five DSTs and 15 SSTs were noted (by waste level data) as exhibiting slurry growth. Next, criteria were developed for both DSTs and SSTs regarding the slurry growth. The criteria for DSTs were: (1) level increase without liquid addition; (2) unexplained dome pressurization; and (3) unexplained temperature changes. For the SSTs, the criteria were: (1) level increase without liquid addition; (2) presence of a surface crust; (3) total organic carbon content above 3 grams/liter; and (4) B-Plant waste in the tank.

Use of these criteria resulted in the identification of two more tanks, bringing the total to 22. Tank SX-109 was added only because the ventilation system design for the 241-SX tank farm results in the headspace for 5 listed tanks being vented through the headspace of SX-109. Thus, the original number of tanks (with respect to flammable gases) identified in response to Public Law 101-510, Section 3137, was 23. Finally, two other tanks were added to the FGWL in 1993; one because of an observed level fluctuation and the other because of updated data that showed slurry growth. Thus, 25 tanks were put on the watch list due to the flammable gas safety issue.

In summary, tanks were put on the FGWL on the basis of process history and engineering judgment. By nature, it yielded a list that was "conservative." At the time the list was created there were no direct measurements of stored gas and there was very little information on the amounts of flammable gas in the dome spaces of the tanks. Based on today's knowledge, very few tanks would have been placed on the original list.

Formal criteria for selecting tanks for and removing tanks from the FGWL were approved by the U.S. Department of Energy (DOE) in 1997. The approved selection criterion is:

> "*Any tank that can have a flammable gas volume in the dome space that, when ignited, would result in pressure above a containment-related tank design limit will be categorized as a Flammable Gas Watch List tank.*"

The criterion for removal is:

> "*Any tank that no longer satisfies the selection criterion for the Flammable Gas Watch List will be removed from the Watch List.*"

The criterion for removing a tank from the FGWL has been interpreted (Johnson 1997) to mean that: (1) a tank has acceptable risk from the perspective of the FGWL if it cannot spontaneously release enough flammable gas to the dome space "which, if ignited would result in pressure above a containment-related tank design limit," and (2) this acceptable risk will be demonstrated by compliance with DOE orders in implementing an approved authorization basis.

1.1.2 The Flammable Gas Unreviewed Safety Question and Facility Group Concept

As introduced in the previous section, the flammable gas hazard in Hanford tanks were declared a Unreviewed Safety Question (USQ) in 1990 and the FGWL was established. The FGWL was populated with its current 25 tanks by 1993 and, by early 1995, all 177 tanks had been screened for retained gas using the Barometric Pressure Effect (BPE) method (Whitney 1995). The screening showed 58 tanks with detectable volumes of gas and flammable gas work controls were placed on the 37 tanks not already on the FGWL. In November 1995, flammability controls for ignition sources, ventilation and monitoring were placed on all 177 tanks.

The original USQ was updated and consolidated into one overall USQ in 1996. This expanded and replaced the original 1990 USQ and closed the USQ for SY-101 because of the proven effectiveness of the mixer pump. In 1998 the flammable gas USQ was closed for SSTs and the rest of the DSTs on the basis of improved understanding of the hazard and establishment of effective controls.

The flammable gas hazard control strategy is twofold. First, adequate passive or active ventilation is required to manage risk associated with steady background release of flammable gas. Second, controls are required to prevent ignition sources in the tanks to manage risk associated with flammable gas retention within waste and potential for sudden release.

The controls are graded based on perceived hazards and free less hazardous tanks from unnecessarily restrictive or burdensome controls. The grading of controls is based on whether a tank may be subject to large or small gas release events (GREs). Large GREs may cause the headspace concentration of flammable gas to exceed 25% of the LFL. Small releases may elevate the concentration of flammable gas beyond 25% of the LFL only in a localized area. GREs are further divided into spontaneous and induced releases where the latter are the result of some waste disturbing activity. The use of 25% of the LFL as the maximum allowed gas concentration is intended to provide a significant margin to the concentration where a deflagration is actually possible (100% of the LFL).

To assign graded control sets, each tank has been placed into one of three Facility Groups depending on which types of gas release events are associated with the tank. Tanks that have demonstrated a propensity for large spontaneous and induced GREs are in Facility Group 1. Tanks that may be susceptible to large induced GREs but only small spontaneous GREs are in Facility Group 2. All remaining large underground waste storage tanks are assigned to Facility Group 3, where it is judged that spontaneous releases do not occur, but small induced releases may be possible in some tanks. Facilities where a GRE is judged to not be a concern are included as non-GRE facilities.

The tank grouping is based, in part, on the methodology originally used for the hazard evaluation in 1996. Although this methodology cannot provide precise quantitative results, it does indicate which tanks have large volumes of retained gas. Despite the technical uncertainty, this methodology, coupled with physical observations and sample results, provides a workable basis for the tank grouping.

Facility Group 1 is made up of the facilities of greatest concern with respect to the flammable gas hazard. Specifically, the five tanks AN-103, AN-104, AN-105, AW-101, and SY-103 are assigned here. These tanks have exhibited significant GREs, and all are conservatively assumed to have the potential for large spontaneous and induced GREs. The level of rigor for these tanks is the maximum possible to manage the risk while continuing to perform essential waste storage functions.

It should be clear from the foregoing discussion that the Flammable Gas USQ and the Facility Group designation serve an entirely different function from the FGWL. The latter is a congressionally mandated list of potentially hazardous tanks whose temperature and pressure must be monitored and that are prevented from receiving waste. The USQ and Facility Groups determine how day-to-day tank farm operations are conducted and controlled. Removing a tank from the FGWL will not change its facility group or control set unless, as in the case of SY-101, the waste has also been treated to reduce its ability to retain and release gas.

1.2 DESCRIPTION OF THE FIVE FACILITY GROUP 1 TANKS

Tanks AN-103, AN-104, AN-105, AW-101, and SY-103 are cylindrical carbon steel tanks with a diameter of 75 ft (22.9 m) and a working depth of just over 35 ft (422 in. or 10.72 m) for a capacity of 1,160,000 gal (4.40 x 10^6 liters). A schematic of the tank is shown in Figure 1-1. An

outer concentric steel shell surrounds the inner one to a height of 450 in. (11.4 m) creating an annular space for leak detection and control. The dome begins at a height of 436 in. (11.1 m) and has a volume of 28,000 ft^3 (793 m^3). The maximum rated tank capacity, with waste to 436 in. (11.1 m) is 1,200,000 gal (4.54 x 10^6 liters). Both the tank headspace and the annulus are ventilated by separate systems. Typical ventilation rates are 100 scfm in the dome and 100 to 200 scfm in the annulus.

All of these tanks, except SY-103 and AN-103, are filled close to their capacity. The waste is a highly concentrated salt solution from which a relatively deep settled solids layer has precipitated to form the "typical" DST configuration of a relatively thin "crust" floating on a layer of supernatant liquid about as deep as the solids layer. The supernatant is called the "convective layer" because thermally driven convection keeps temperatures and concentrations uniform there. The settled solids is called the "nonconvective layer" because the strength of the material suppresses convection. The strength of the nonconvective layer allows it to retain gas. Large, rapid gas releases occur when the nonconvective layer accumulates enough gas to become buoyant with respect to the liquid above it.

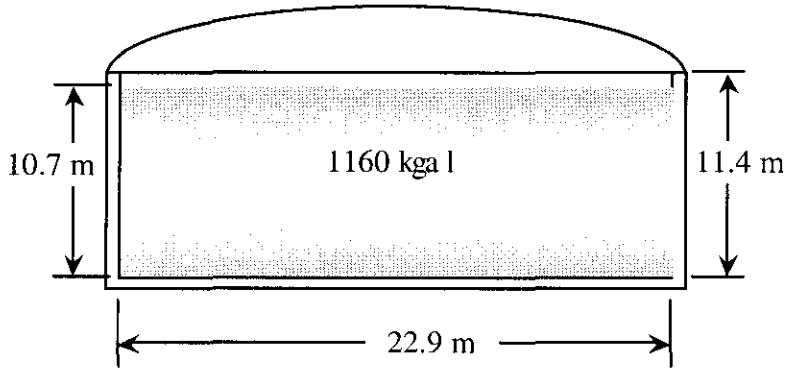

Figure 1-1. Double-Shell Tank Design

Only the tanks in Facility Group 1 now actually exhibit buoyant displacement GREs. Tank 241-SY-101, which is not designated as a Facility Group 1 tank, had by far the largest GREs prior to the mixer pump installation, with release volumes of 100 to 300 m^3 (3,500 to 10,000 ft^3) causing waste level drops of over 30 cm (12 in.). SY-101 is the only tank in which several of the largest gas releases may have made the tank headspace flammable. Next in line is AN-105, which has shown releases of up to 50 m^3 (1,800 ft^3) with level drops as high as 7 cm (3 in.). During these releases, the headspace has not been flammable but has exceeded 25% of the LFL. Typical releases in the other tanks are 10 to 25 m^3 (300 to 1,000 ft^3), which have not exceeded 25% of the LFL in the headspace. Release volumes have generally been decreasing since 1995 as discussed in Section 8.4.

1.2.1 Tank 241-AN-103

Tank 241-AN-103 initially received liquid removed from SSTs by saltwell pumping with regular transfers out to the 242-A Evaporator from 1982–1986. In February 1986, the tank was pumped out to a 224-cm (88-in.) heel before being filled to 835 cm (329 in.) with double-shell slurry feed (DSSF) from the 242-A Evaporator. By late 1989, the surface level had steadily risen to 43 cm (17 in.) because of gas accumulation. The level became steady at about 884 cm (348 in.) in 1997 with a small seasonal fluctuation. The tank headspace volume is currently 1,700 m^3 (60,400 ft^3).

Small sawtooth level fluctuations typical of this tank began in early 1990 with very small GREs about every 100 days. Since November 1993, the largest GRE period has been up to 270 days. The level fluctuations are so small that they do not serve to indicate gas releases. There have been only two small gas releases observed by headspace gas monitors since 1995. Tank 241-AN-103 has a crust nearly 1-m thick, second only to that in SY-101 prior to remediation, and a nonconvective layer 380 cm (150 in.) deep.

1.2.2 Tank 241-AN-104

Tank 241-AN-104 was initially used to receive slurry from the 242-A Evaporator and return the slurry to the evaporator feed tank for further concentration in converting dilute noncomplexed waste into DSSF. The tank was initially filled in several steps between late 1983 and mid-1984. It was pumped out to a 218-cm (86-in.) heel in October 1984 before receiving double-shell slurry (DSS) in 1985 to about 866 cm (341 in.). The surface level continued to rise until it reached a level of 870 cm (342.5 in.) in April 1985; additional slurry was then added, increasing the surface level to 978 cm (385 in.).

After its last fill, the waste level grew about 10 cm (4 in.) before incurring a large initial drop of almost 20 cm (8 in.) during January and February 1986. The level grew back by early 1988, when one more 20-cm (8-in.) drop occurred over about a month. It is not clear whether there were large gas releases associated with either of these drops. The current behavior, small 3 to 7-cm drops about every 100 days, began after the last large drop. However, level drop in this tank does not correlate well with gas release.

The waste level is currently about 979 cm (386 in.) and consists of a non-uniform layer of nonconvective material 380 to 415 cm (150 to 163 in.) in depth and 577 to 612 cm (227 to 241 in.) of supernatant liquid. There is also a thin crust layer about 40 cm (16 in.) thick. The headspace volume in tank AN-104 is about 1,300 m^3 (46,700 ft^3).

1.2.3 Tank 241-AN-105

Tank 241-AN-105 received slurry from the 242-A Evaporator and returned it to the evaporator feed tank for further concentration in converting dilute noncomplexed waste into DSSF. Tank AN-105 was pumped to an 81-cm (32-in.) heel in March 1985 and received DSSF to about the current level of 1,036 cm (408 in.).

After the last fill, the level grew about 15 cm (6 in.) before a 20-cm (8-in.) drop at the end of 1987. It is not known whether any large, rapid gas release was associated with this drop. Following the large initial drop, there were no significant level drops for about 3-1/2 years. The current cycle of 4 to 7-cm (1.6 to 2.8-in.) drops ensued in mid-1991. The GRE period in AN-105 has increased to about 270 days since January 1993.

The current waste level is about 1,041 cm (410 in.). The waste consists of a nonconvective layer 400 to 460 cm (160 to 180 in.) deep, convective liquid 580 to 640 cm (230 to 250 in.) deep, and a non-continuous floating crust layer that may be up to 30 cm (12 in.) thick. The headspace volume in tank AN-105 is about 1,050 m^3 (37,000 ft^3).

1.2.4 Tank 241-AW-101

Major additions to AW-101 began in late 1981 with transfers from the 242-A Evaporator. The tank was emptied and refilled several times during evaporator campaigns up to 1984. From mid-1984 to mid-1986, various process wastes from the Plutonium-Uranium Extraction (PUREX) Plant were collected in AW-101 and periodically transferred to the evaporator. In mid-1986, the tank was pumped out to about a 50-cm (20-in.) heel before being filled to about its current level with DSSF from the 242-A Evaporator.

Level fluctuations began immediately after the last fill and reached their current 2 to 5 cm (~2 in.) range by mid-1987. The GRE period in AW-101 until 1996 was almost random, ranging from 40 to 750 days. There were no significant gas releases from this tank from June 1996 to May 2000. Gas releases in this tank are quite slow, typically requiring several days. Level drop in AW-101 does not correlate with gas releases. The waste level is now about 1,040 cm (410 in.) and consists of a nonconvective layer 250 to 320 cm (100 to 125 in.) in depth, 660 to 730 cm (260 to 290 in.) of supernatant liquid, and a floating crust layer about 60 cm (24 in.) thick. The headspace volume in AW-101 is 1,070 m^3 (37,800 ft^3).

1.2.5 Tank 241-SY-103

From its initial fill in 1977 until 1980, SY-103 received concentrated complexant waste from B-Plant that was regularly pumped out to the 242-S Evaporator. In the third quarter of 1980, the tank was pumped down to a 120-cm (46-in.) heel before receiving DSS that filled it to a level of 500 cm (200 in.) on December 31, 1980. Uranium sludge from ion exchange processing was added in 1985 to 550 cm (216 in.). Interstitial liquid and water from SX-104 was added in 1988, bringing the level up to 660 cm (260 in.), and numerous other small additions brought the tank to its current level. Tank 241-SY-103 now contains about 691 cm (272 in.) of waste, of which

356 cm (140 in.) is supernatant liquid lying over a 335-cm (132-in.) nonconvective layer. The headspace is 2,500 m^3 (88,400 ft^3).

Between 1981 and mid-1985, when no large waste transfers occurred, waste surface level measurements showed a 1 to 2-in. level drop about once a year. Following the addition of uranium ion exchange wastes in 1985, the level drops began to occur about three times per year. These were of rather long duration, not the sudden drops typical of a buoyant displacement. However, after a liquid addition from SX-104 in 1988, sudden level drops of 2 to 3 cm (~1 in.), typical of buoyant displacement gas releases, began occurring. Level drops attained 3 to 5 cm (~2 in.) by 1992. The GRE period in SY-103 varies randomly from 20 to 200 days.

1.3 REMEDIATION OF TANK 241-SY-101

Tank 241-SY-101 was the most hazardous of all Hanford tanks and probably has been the most thoroughly studied. However, since 1993 its hazardous behavior has been mitigated such that it is no longer in the same class as the five DSTs in Facility Group 1. For this reason, discussion of SY-101 in this report will be limited mainly to comparison of the current tank to its pre-mitigation conditions and behavior. The remediation history of SY-101 is briefly reviewed in this section with references to recent documents that contain all the details.

Tank 241-SY-101 initially received about 260 cm (100 in.) of DSS, the most concentrated material produced by the evaporators, from the 242-S Evaporator between 1977 and 1980. Subsequent additions included complexed concentrate (similar to DSS but not as concentrated and containing a higher fraction of organics) and more DSS through 1980. These additions brought the level up to its nominal 1,042 cm (410 in.) (Sullivan 1995).

Level and temperature profile data (Antoniak 1993) show that the waste level began fluctuating in the typical "sawtooth" pattern indicative of buoyant displacement gas releases shortly after the final fill. Level drops were initially on the order of 8 cm (3 in.) but increased to 15 to 25 cm (6 to 10 in.) by 1986. The largest GREs, with level drops over 30 cm (12 in.), occurred in 1991-1992 over a period of ~140 days. Several of these releases were large enough to make the headspace flammable for a short period.

In response to this hazard, intense efforts began in 1991 to mitigate the large GREs. Concepts were developed by several working groups and from sources outside of Hanford. A total of 22 approaches were evaluated (Babad et al. 1992). Four concepts (heating, dilution, ultrasonic agitation, and mixing) were selected for further study (Lentsch 1992). The approach finally chosen for GRE mitigation was to mix the waste contents with a jet mixer pump (WHC 1992). A detailed safety assessment for mixer pump installation and operation was prepared by Los Alamos National Laboratory (LANL) (Sullivan 1995) and was approved by DOE. A modified 150-hp jet mixer pump originally designed for the Grout Program was installed on July 3, 1993, seven days after the last large GRE.

Significant GREs ceased after the waste was mixed from July to December 1993, and the waste level dropped to 1,019 cm (400 in.), indicating most of the stored gas had been released. Further testing in February to April 1994 established the capability of the mixer pump to mobilize waste

at least out to a 28-ft (8.5-m) radius. The waste on the bottom of the tank was "excavated" by repeated mixer pump runs in the same orientation through the spring and summer of 1994, and the normal mixer pump operation schedule of three runs per week at 1,000 rpm for 25 minutes was established in September 1994. Allemann et al. (1993, 1994), Stewart et al. (1994), and Brewster et al. (1995) contain the detailed history of the mitigation of SY-101.

The height of the waste surface in SY-101 and other tanks has been recognized and used as an indirect measure of retained gas inventory for many years. The surface level was discovered to be increasing at an accelerating rate in early 1996 in spite of, and almost certainly as a result of, regular mixer pump operations. Prior to this time regular water flushes necessitated by buildup of waste on the contact probe level instrument in Riser 1C had dissolved a cavity into the crust that obscured level growth. In December 1995 an ENRAF[1] level gauge was installed in a new Riser, 1A. Since this ENRAF™ did not required flushing, it allowed the level rise to be detected. An ENRAF™ was also installed in Riser 1C in December 1996, and a matching level increase was observed there also. The rate of level rise continued to increase during 1997 and 1998. In November 1998, the rate of surface-level rise was approximately 2 mm/d (0.08 in./d) which matched the high-level rise rate observed between large historic GREs.

On December 29, 1997, the Tank Waste Remediation System (TWRS) Plant Review Committee (PRC) declared that there was a "discovery" with respect to SY-101 because of potential inadequacy in the Authorization Basis (AB). The observed level rise that started in the latter part of 1996 was inconsistent with the model on which the mixer pump safety assessment was based (Sullivan 1995). The safety assessment controls were based on the assumption that the surface level was a measure of the retained gas volume in the tank and mixer pump operation was based on waste level criteria. However, even though the mixer pump was mixing the waste as effectively as ever, the continued level rise indicated that gas was accumulating within the waste. Increasing the frequency of mixer pump operation in the fall of 1997 was unable reduce the level rise and, in fact, appeared to accelerate it.

Because of this mismatch of expectation and observation, the contractor recommended that a USQ be declared for this condition in February 1998. The U.S. Department of Energy, Richland Operations Office (DOE-RL) concurred with the recommendation and declared the USQ on February 26, 1998. This USQ (TF-97-0975, Rev. 3) was called the surface level rise USQ because of the phenomenon from which it arose. As a result of the level rise USQ, the contractor established a project team that was responsible for developing and implementing options for remediating the unacceptable situation in SY-101 (Raymond 1999).

A series of workshops and analyses concluded that the source of the level rise was gas and solids accumulation in the crust layer. To confirm this, gas volume fractions in the lower half of the crust were measured in June and September 1998 using the VFI (Stewart et al. 1998). Gas volume fractions of 0.21 to 0.43 were measured in the lower half of the crust. The highest gas content appeared to be at the bottom of the crust, decreasing upward. An average crust gas fraction of 0.30 was estimated from the VFI results. Later in 1998 and early 1999 the RGS also

[1] ENRAF is a trademark of the ENRAF Corporation, Houston, Texas.

measured the void fraction in several crust samples. Void fractions exceeding 0.5 were measured in the lower part of the crust and 0.34 to 0.4 in mid-crust (Mahoney et al. 1999).

The VFI data also revealed that the crust thickness had increased from its historic value of about 40 in. to 54 in. (15.7 cm to 21.3 cm). In an attempt to gain more information about the crust a neutron/gamma probe, similar to that used in the liquid observation wells in SSTs, was deployed in the validation probe passage in the multi-function instrument trees (MIT). Neutron probe data throughout 1999 tracked the crust thickness increasing to 122 in. (3 m) after a redistribution event in April to May 1999. Based on comparison of neutron data and crust buoyancy calculations, the average void fraction in the submerged part of the crust was estimated to be 0.24, which resulted in a gas volume of about 10,000 scf (Rassat et al. 2000).

A number of options were evaluated for remediating the crust growth in SY-101 (Raymond 1998). The option selected was a series of waste transfers from SY-101 to SY-102 followed by back dilution of SY-101 with water. Dilution of the waste would dissolve the crust and the soluble solids elsewhere in the tank, which in turn would lead to a reduction in gas retention potential. The system consisted of a transfer pump, an over-ground, encased transfer line and drop leg connection at tank SY-102. A pressurized, heated water supply was also provided for in-line dilution of the waste being removed from SY-101. Dilution water could be placed on top of the waste or injected at the inlet to the transfer pump about 100 in. (254 cm) above the tank bottom.

Analyses and laboratory studies were conducted for dissolution of the crust and release of gas (Rassat et al. 1999 and 2000) and for postulated hazards during the transfer and back dilution operations (Stewart et al. 2000). A safety basis was prepared to support the operations (Ryan 2000), and a process control plan was used to cover the specific steps of all of the operations for transfer and back dilution (Estey 2000).

Three campaigns of transfers followed by back dilution were employed to mitigate the level rise issue. The first campaign from December 18 to December 19, 1999, dissolved a large fraction of the original, unsaturated crust above the liquid level and confirmed predictions and expectations of how the waste would react to dilution and transfer. The second transfer occurred over the period of January 25 to 27, 2000, and the subsequent back dilution was performed from February 21 to February 23, 2000. This dilution essentially destroyed the crust and released most of its stored gas. The third transfer started on February 27, 2000, and finished on March 2, 2000. The final back dilution was completed on March 15, 2000. This last dilution dissolved the balance of the readily soluble salts and brought the waste to its final state. Table 1-1 provides a summary of the transfer and back dilution volumes. Since the second and third transfers followed dilutions, they also removed some of the dilution water and less of the original, undiluted waste. The actual contents of the tank after each campaign are listed in the last two columns. The details of the remediation campaign are described by Mahoney et al. (2000).

The end result of the three campaigns was a dilution of 0.8:1 (water to waste). After an observation period of several months to confirm predictions of the end state and to detect any adverse trends, the plan is to formally remove SY-101 from the FGWL and return it to normal service.

Table 1-1. Tank 241-SY-101 Transfer and Dilution Volumes

(all volumes in gallons)	SY-101 Waste Transferred	Top Back Dilution	Low Back Dilution	Original Waste in Tank	Net Water in Tank
Campaign #1	89,500	26,000	36,000	974,500	62,000
Campaign #2	240,500	89,500	150,000	744,500	291,000
Campaign #3	286,000	36,500	187,000	539,000	434,000
Cumulative	616,000	152,000	373,000	539,000	434,000

1.4 OUTLINE OF THE REPORT

This report is organized into seven main sections consistent with the important aspects of the flammable gas safety issue in the six DSTs in focus: waste characterization and monitoring methods and equipment (Section 2); waste chemistry (Section 3); tank thermal behavior and temperature history (Section 4); waste configuration or layering and properties (Section 5); gas generation and composition (Section 6); gas retention and its distribution in the waste (Section 7); and spontaneous and induced gas release behavior (Section 8). The overall conclusions and summary are given in Section 9, and references are listed in Section 10.

This page intentionally left blank.

2.0 DESCRIPTION OF WASTE CHARACTERIZATION MEASUREMENTS

This section describes the kinds of measurements made, what information the data provide, and the location of the measurements taken in each tank. Waste level is discussed in Section 2.1, waste temperature in Section 2.2, and headspace gas monitoring in Section 2.3. The ball rheometer is described in Section 2.4, the VFI in Section 2.5, and core sampling in Section 2.6. Section 2.7 describes the RGS, and Section 2.8 discusses neutron and data logging. Section 2.9 summarizes the location of important instruments and measurements in each of the six DSTs on the FGWL.

2.1 WASTE LEVEL

The elevation of the waste surface above the tank bottom is a key indicator of tank status and waste behavior. Tanks with a high waste level are generally more hazardous because they store gas at a higher pressure, and less headspace is available to dilute episodic gas releases. A gradual increase in waste level may indicate accumulation of stored gas, while a quick drop is a sign of a sudden gas release. A gradual drop is usually associated with evaporation of liquid. The total stored gas volume in a tank can be computed from the correlation of waste level changes with barometric pressure fluctuations.

One of the primary objectives of VFI operation is to match an accurate estimate of retained gas volume with waste level at a fixed point in time, so that the past and future level measurements trace changes from the known gas volume. The level also serves as a reference for VFI sample elevation and as a consistency check with the measured height at which the ball rheometer passes through the liquid level.

Waste surface level is typically measured with three different devices: the Food Instrument Corporation (FIC) contact probe, a manual tape, and the ENRAF™ buoyancy gauge.[2] The FIC and manual tape level readings are available in each DST essentially from the time they started operation in the late 1970s. But only the period since the mid-1980s, since the last fill, is of interest as evidence of current and future gas release behavior. ENRAF™ level gauges have been installed only since about 1995, so their history is limited. Level measurements may be either manual or automatic. Early data are weekly; daily or once-per-shift readings have been available since the late 1980s.

The various instruments report different values and trends, mainly because of the irregularity of the crust surface but also because of the peculiarities of the measurement methods. The readings of each level gauge in SY-101 from January 1, 1994 to July 17, 1995 are shown in Figure 2-1 to illustrate the magnitude of the differences.

[2] SY-101 measured level by radar from 1993 to 1995, but the radar gauge was erratic at times, especially during gas releases, and it was unclear whether it indicated the actual waste surface or some related quantity sensitive to surface moisture. It eventually succumbed to radiation damage.

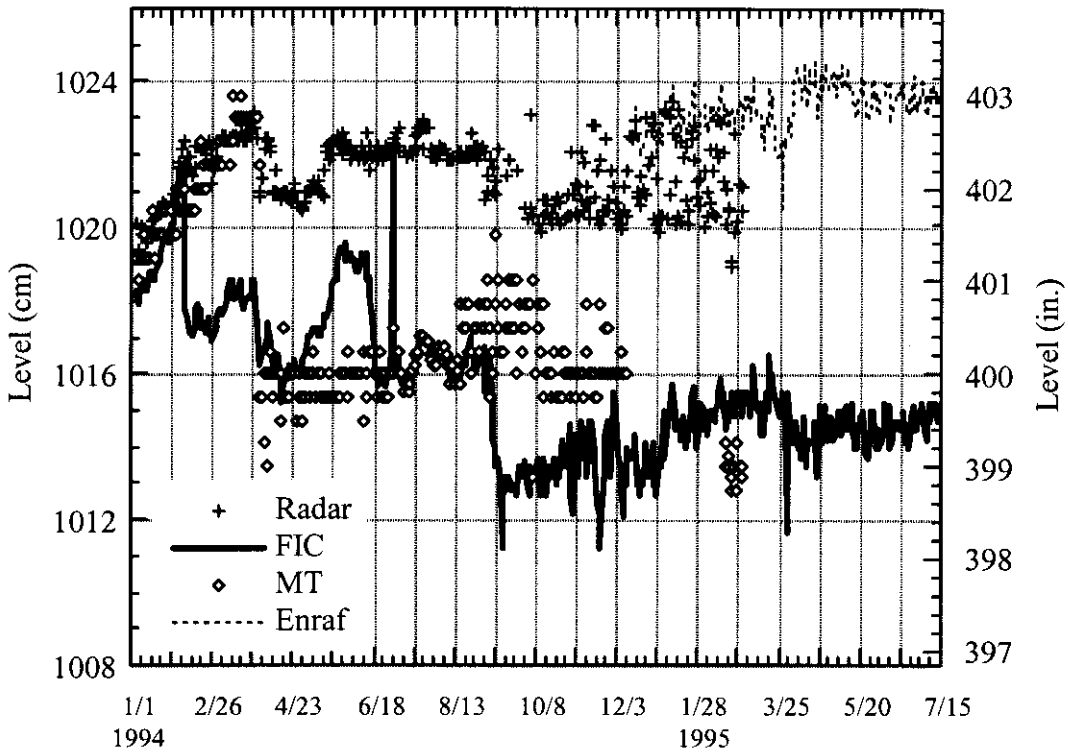

Figure 2-1. Tank 241-SY-101 Waste Level History - Example of Level Measurements

The FIC and manual tape must be flushed occasionally to remove accumulated deposits called "wastecicles." In-tank video in SY-101 showed that repeated flushing eroded the crust near the FIC, and repeated contact with the waste excavated a distinct cavity several centimeters deep. The short-term effect of flushing is not predictable. The flush water is much less dense than the waste liquid and tends to pool at a higher level until it mixes with the waste. This level rise may exceed the length of the wastecicle that was removed, therefore, the FIC actually reads higher for a week or so after the flush than before. The manual tape is also subject to wastecicle buildup but is seldom flushed and, thus, disturbs the crust less.

The ENRAF™ buoyancy gauge does not depend on electrical contact and merely sits stationary on the waste surface. Therefore, it is not subject to buildup of waste deposits, nor does it disturb the surface on which it rests. This makes the ENRAF™ potentially the most reliable level indicator.

The absolute accuracy of any of the waste level instruments depends on the degree of surface irregularity and the uncertainty in the reference position. Combined, these could produce a systematic error of 2 to 20 cm (1 in. to 8 in.) depending on the tank. Sensing level changes is far more important than absolute accuracy. A study of SY-101 data (Brewster et al. 1995) concluded that the ENRAF™ correlated most closely with gas releases and was the most precise level instrument. It records level in 0.025-cm (0.01-in.) increments and is easily able to resolve

level changes to within ± 0.25 cm (0.1 in). The FIC usually correlates closely with the ENRAF™ and reasonably well with gas release in SY-101. It records level in 0.25-cm (0.1-in.) increments, and its sensitivity is estimated at ± 0.6 cm (0.25 in.) for nearly consecutive readings, but wastecicle growth and periodic flushing adds an uncertainty of ± 5 cm (2 in.) in long-term values.

The manual tape is typically read in 0.64-cm (0.25-in.) increments; therefore, it senses changes only to within ± 2 cm (0.75 in.) at best. Because of this low sensitivity, the manual tape was not correlated with any of the other instruments or with gas release in the SY-101 study. In screening the tanks for trapped gas, Whitney (1995) found that the response of manual tape readings to barometric pressure changes was not as valid an indicator of gas retention as it was for the FIC and ENRAF™. The manual tape history is generally not used in this study.

2.2 WASTE TEMPERATURE

The shape of the temperature profile provides a valuable sounding of the nonconvective layer depth. Changes (or lack of changes) in the temperature profile sometimes indicate where GREs originate. Each of the tanks tested has temperature profiles in two locations by means of the recently installed MITs and the original thermocouple trees. Tank 241-SY-101 has two MITs.

Multi-function instrument trees (MITs) have 22 thermocouples spaced 30 to 60 cm (12 to 24 in.) apart, starting 10 cm (4 in.) from the tank bottom. These are usually read manually except in SY-101, where the readings are made automatically every 12 seconds. A validation probe that measures temperature every 10 cm (4 in.) with a high-precision resistance temperature detector (RTD) is operated occasionally to confirm thermocouple readings. The higher resolution of the validation probe profile allows a very accurate estimate of the nonconvective layer depth. Analysis of validation probe temperature profiles is essentially the only method that can determine the crust thickness.

Readings from the old thermocouple trees are made manually. The thermocouples are spaced approximately every 125 cm (50 in.) vertically with the first reading near the tank bottom. Because only one-half to one-third of the 20 thermocouples may be recorded, there is a large uncertainty in waste layer dimensions derived from these temperature profiles.

Temperatures of the tank bottom are also measured by 24 thermocouples welded to the outer surface of the tank bottom plate and embedded in the concrete pad that supports the inner shell. While these thermocouples are not exposed to the waste and have a very slow response time, they can provide some information about the thermal state of the tank. They reveal a "dished" radial temperature profile with the lowest temperature in the central part of the tank. This profile results from the annulus cooling flow entering at the bottom center of the tank. The bottom thermocouples are read manually on an approximately weekly schedule. Care must be taken in interpreting these data because several of the thermocouples in each tank are inoperative.

The uncertainty in the temperature read by a thermocouple, whether on an MIT or thermocouple tree, is estimated to be ±1.8 °C (3 °F) (Brewster et al. 1995). However, experience with SY-101

data (Stewart et al. 1994, 1995) has shown that MIT thermocouples are easily able to register temperature changes of 0.06 °C (0.1 °F). The uncertainty in the absolute temperature reading of the MIT validation probe is ±0.2 °C (0.3 °F).

2.3 HEADSPACE GAS MONITORING

The concentrations of hydrogen and other flammable gases in the tank headspace are monitored to ensure that the headspace is safe and to increase our understanding of the mechanisms for gas release and dilution. Several different systems are used. Depending upon the information desired from a tank, different monitoring instruments are combined into a tank-specific system. These instruments are listed in Table 2-1 with their measurement accuracies and ranges. The following sections describe how the instruments are applied in different monitoring systems.

Table 2-1. Gas Monitoring Instruments

Instrument	Gases Monitored	Range	Accuracy
Whittaker™ Electro-Chemical Cell and Transmitter	Hydrogen-Specific	0 to 1% and 0 to 10% H_2 by Volume	±0.2% by volume absolute (resolution of 50 ppm)
Gas Chromatograph Reduction Gas Analyzer (GC-RGA)	Hydrogen-Specific	Low Range 0 to 500 ppm H_2 High Range 500 to 30,000 ppm H_2	Low Range ±4 ppm <100 ppm and ±10% of reading >100 ppm High Range ±10% of reading
Gas Chromatograph Thermal Conductivity Detector (GC-TCD)	Hydrogen (H_2) Nitrous Oxide (N_2O) Methane (CH_4)	H_2 3 to 3,000 ppm N_2O 10 to 20,000 ppm CH_4 10 to 4,000 ppm	H_2, N_2O, CH_4 ±3 ppm <30 ppm and ±10% of reading >30 ppm
Fourier Transform Infra-Red Spectrometer (FTIR)	Ammonia (NH_3) Nitrous Oxide (N_2O) IR spectra for other species	NH_3 10 to 30,000 ppm N_2O 10 to 30,000 ppm Other species TBD	N_2O, NH_3 ±5 ppm <100 ppm ±10% of reading >100 ppm
Infra-Red Photo Acoustic Multi-Gas Monitor (IR)	Ammonia (NH_3) Selected filters for other species	NH_3 10 to 10,000 ppm Other species TBD	NH_3 ±10 ppm <100 ppm ±10% of reading >100 ppm
Grab Samples - Mass Spectrometer	Hydrogen (H_2) Nitrous Oxide (N_2O) Methane (CH_4) Argon (Ar) Nitrogen (N_2) Oxygen (O_2)	0 to 100% by volume	At least ± 10 ppm

2.3.1 Standard Hydrogen Monitoring Systems

The basic standard hydrogen monitoring system (SHMS) monitors hydrogen continuously. Gas is vacuum-pumped from the tank into a temperature-controlled cabinet that contains the monitoring instrument. For DSTs, the sample is obtained from the tank ventilation exhaust duct; for SSTs, the sample is obtained from a probe that is inserted well into the tank dome space.

The monitoring instrument is a Whittaker[3] electrochemical cell that is hydrogen-specific. The cell generates an electrical signal proportional to the volume percent hydrogen concentration. This signal is processed by a transmitter and sent to a digital data readout and data recorder. The recording channel of the data recorder is programmed to activate an alarm relay if a preset hydrogen concentration (currently 6,250 ppm) is reached. The alarm relay opens a normally closed contact that serves as the input to a programmable logic controller that controls the annunciation of a high hydrogen alarm and initiates an automatic vapor grab sample. Data are recorded by connection to the Tank Monitoring and Control System (TMACS) and by an on-board chart recorder. The SHMS also has a grab sample station that allows two 75 cc vapor samples to be taken simultaneously from the gas stream, isolated, and transported to a laboratory for analysis. Hydrogen and other gases can be measured from these samples.

These systems are calibrated quarterly. A mixture of 100 ppm hydrogen and air is used to adjust the low end of the hydrogen sensor, and a mixture of 5% hydrogen mixed with nitrogen is used to balance the high end of the sensor. A mid-range standard gas of 1,000 ppm hydrogen is used as an on-line calibration check during system operation (Schneider 1996).

The first SHMS was developed for continuous monitoring of hydrogen concentrations in SY-101. Three of the basic units are installed and operating on this tank; one monitors the vent header concentration, and the other two monitor locations within the headspace. Because of the success of these instruments, the system was upgraded by adding the capability to obtain a grab sample automatically on a high hydrogen reading. Also, the Whittaker™ cells were configured so that one covers a high range (0 to 10% by volume) and one a low range (0 to 1% by volume). This modified version is called the SHMS-B.

The SHMS-B is the most widely used of the SHMS instruments. It is installed on all FGWL tanks but SY-101 and AN-104. Data are recorded by connection to the TMACS and by the onboard chart recorder. As specific needs arose, the SHMS-B was modified to provide the needed capabilities. This resulted in several variations, including models C, D, E, and E+.

The SHMS-C is an SHMS-B modified to accommodate a dual-column gas chromatograph with thermal conductivity detectors (GC-TCD). Data for the Whittaker™ cells are recorded by connection to the TMACS and by the onboard chart recorder. The data for the gas chromatograph are recorded by a resident computer and retrieved via floppy disk for off-line analysis. The SHMS-C is designed to record accurately the baseline hydrogen concentrations that are well below the range of the Whittaker™ cells.

[3] Whittaker is a trademark of Whittaker Corporation, Garden Grove, California

The SHMS-D is an SHMS-B modified to accommodate an infrared (IR) photo-acoustic multi-gas monitor that measures ammonia. Data for the Whittaker™ cells are recorded by the on-board chart recorder and connection to TMACS. The data for the IR photo-acoustic multi-gas monitor are recorded by a resident computer and retrieved via floppy disk for off-line analysis. The SHMS-D was developed for monitoring ammonia concentrations in the ventilation exhaust of DSTs.

The SHMS-E is an updated version of the SHMS-B and accommodates (though they are not installed) a dual-column gas chromatograph with a thermal conductivity detector and an IR photo-acoustic multi-gas monitor. An onboard digital data logger records data with data retrieval via floppy disk. The upgrade in design from the SHMS-B is in the data recording (the strip-chart is eliminated) and the programmable logic controller. The SHMS-E is intended for use in the same applications as an SHMS-B but has the advantage of easily being upgraded to an E+.

The SHMS-E+ is an SHMS-E with the gas chromatograph and IR monitor installed. The Gas Chromatograph (GC) monitors hydrogen, nitrous oxide, and methane, and the IR monitor detects ammonia. An onboard digital data logger records data with data retrieval via floppy disk or by connection to a host computer via the Hanford Local Area Network (HLAN). The SHMS-E+ is intended for applications similar to those of the Gas Characterization System (GCS), which is described in Section 2.3.2. The SHMS-E+ provides nearly the same measurement capability as a GCS but at a significantly lower cost.

2.3.2 Other Monitoring Systems

Gas monitoring system-1 (GMS-1) monitors hydrogen and tank vapor space pressure for SY-101. The environmentally controlled enclosure contains one Whittaker™ electrochemical cell, a grab-sample station, and a pressure transmitter. It initially had a mass spectrometer for multi-gas analysis that has since been removed. Data from GMS-1 are recorded by the SY-101 mixer pump Data Acquisition and Control System (DACS).

Gas monitoring system-2 (GMS-2) is an environmentally controlled enclosure that contains a Fourier transform IR spectrometer (FTIR), two hydrogen-specific reduction gas analysis gas chromatographs, and one IR photo-acoustic monitor. GMS-2 monitors the vapor space of SY-101. The FTIR measures ammonia and nitrous oxide. One gas chromatograph (GC) has a single column and monitors low concentrations of hydrogen, and the other is dual-column and monitors both low and high concentrations of hydrogen. The IR monitor samples the ventilation exhaust stack of the SY farm (combined exhaust of SY-101, SY-102, and SY-103) for ammonia. The data are recorded by the SY-101 DACS. GMS-1 and GMS-2 provide the detailed concentration history necessary to support the mixer pump operation, and the data from these systems have significantly contributed to the understanding of this tank and the closure of the USQ for this tank.

The GCS is an environmentally controlled enclosure with an FTIR, two dual-column thermal-conductivity gas chromatographs, and a grab-sample station. The GCS is an upgraded version of the GMS-2. The FTIR monitors ammonia, one GC monitors hydrogen, and the other GC

measures nitrous oxide and methane. The data are recorded by the resident computer system and can be remotely accessed over the HLAN. The GCS is used to provide the detailed history of gas concentration over a wide range. These systems are currently installed on tanks AN-105 and AW-101.

The specific components of each of the monitoring systems described above are summarized in Table 2-2. A complete list of gas monitoring systems installed on the six FGWL DSTs is given in Table 2-3.

Table 2-2. Components of Gas Monitoring Systems

Systems	Components
SHMS	Whittaker™ cell for H_2, grab-sample station
SHMS-B	High- and low-range Whittaker™ cells for H_2, grab-sample station
SHMS-C	SHMS-B plus dual column GC-TCD for baseline H_2
SHMS-D	SHMS-B plus IR monitor for NH_3
SHMS-E	SHMS-B with improved data logging, space for two dual-column GC-TCDs (not installed) and an IR multi-gas monitor (not installed)
SHMS-E+	SHMS-E with GC-TCDs installed for H_2, N_2O, and CH_4, IR multi-gas monitor installed for NH_3
GMS-1	One Whittaker™ cell for H_2 and a grab-sample station (SY-101 only)
GMS-2	FTIR for NH_3 and N_2O, two GC-RGAs for H_2, and an IR monitor for SY farm stack NH_3 (SY-101 only)
GCS	FTIR for NH_3, two dual-column GC-TCD, one for H_2 and one for N_2O and CH_4

Table 2-3. Gas Monitoring Systems Installed on Double-Shell Tanks

Tank	Systems (date installed)
AN-103	SHMS-B (9/94)
AN-104	SHMS-C (9/94)
AN-105	SHMS-B (9/94), GCS (4/96)
AW-101	SHMS-B (9/94), GCS (4/96)
SY-101	SHMS (3/92) upgraded to SHMS-B, GMS-1 and GMS-2 (11/92)
SY-103	SHMS-B (5/92)
AN Farm exhaust	SHMS-D (6/96)
AW Farm Exhaust	SHMS-D (6/96) (removed 2/00)

2.4 BALL RHEOMETER

The ball rheometer concept originated from the need to measure in-situ rheological properties in Hanford DSTs. It is very difficult or impractical to measure rheological properties in the laboratory. Retrieving and handling the radioactive waste samples is very difficult. Preparing the sample for measurements can alter its rheological characteristics, as can the temperature changes that occur after the sample is removed from tank. In contrast, the rheology of the waste material can be estimated in-situ directly from the drag force on a ball as it moves through the waste at various speeds.

The ball rheometer system shown in Figure 2-2 consists of a 71-N (16-lb), 9.12-cm (3.6-inch) diameter tungsten alloy ball tethered to a steel cable that is wound onto a spool. The cable runs through a guide that distributes the line across the width of the spool, so only a single layer of cable is needed on the spool. Cable deployment and retrieval are performed with electric motors, clutches, reduction gears, and a driveline. The pulley rests on a load cell that measures the tension in the cable plus the pulley weight and any friction in the pulley when it is in motion. The motor automatically trips off when the cable tension falls below 7 N, to prevent unwinding slack cable into the tank.

Two motors are used to operate the spool, one for high speed (3 to 100 cm/s) and another for low speed (0.1 to 3.0 cm/s). A data acquisition system controls the ball and records the data. The ball position, velocity, and force as measured by the load cell are recorded as a function of time, typically at a rate of 15 Hz. The ball speed, direction, distance and the data collection rate are all adjustable. In addition to rising- and falling-ball tests, static measurements can also be made.

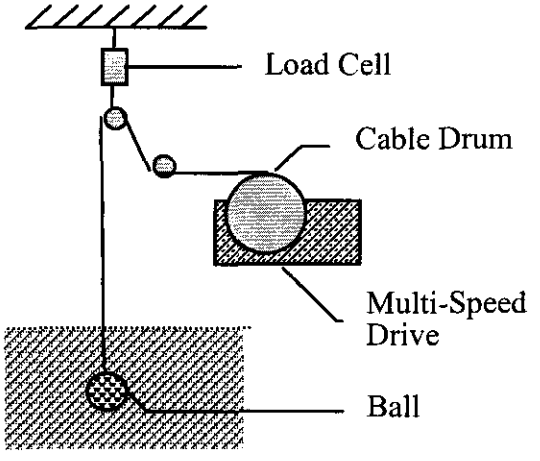

Figure 2-2. Ball Rheometer System

The first pass of the ball through the waste column was the only opportunity available to determine the rheology of the undisturbed waste. The ball was lowered into the nonconvective region at 0.1 cm/s for 20 cm. In SY-103 the ball was lowered all the way through the

nonconvective layer at this speed. In the later deployments in AN-103, AN-104, AN-105 and AW-101, the ball speed was increased after passing the nonconvective layer boundary to 1 cm/s for the next 20 cm and to 10 cm/s for the third 20-cm (8-in.) segment. The data rate at 10 cm/s velocity was increased to 100 samples/second. This sequence was repeated every 60 cm (24 in.) until the ball stopped, either reaching the tank bottom or waste with sufficient strength (about 900 Pa yield stress) to fully support the ball.

Four quantities are recorded during the tests: ball position with reference to "home," ball velocity, force at the load cell, and elapsed time since the start of a test. An encoder attached to the cable spool determines the ball position. A tachometer on each of the drive's electric motors measures ball velocity, but it can be derived more accurately from the ball position and elapsed time. The ball reference elevation, or home position, must be determined from tank drawings.

Cable tension data are measured with a nominal 445-N (100-lb) full-scale load cell. Because the cable runs over a pulley, the effective load limit is actually 222 N (50 lb), half the load cell value. The published error for this load cell is 0.1% of the full-scale reading, or 0.2 N, regardless of load. Indeed, the data show that the standard deviation of measurements made under static and dynamic conditions is, in almost all cases, 0.2 N.

The liquid density measurement depends on both ball volume and buoyancy force. The standard deviation in buoyancy force measured by the load cell is 0.2 N. To determine density, a reference measurement of the ball in air is required. This value is subtracted in all density determinations. The reference measurement is also uncertain by 0.2 N, but because it is used in all density determinations it represents a systematic error. The uncertainty in the ball volume is 1%, also a systematic error.

Ball position is determined with a multi-turn absolute rotary optical encoder that rotates with the cable spool. The encoder has 4,096 steps per revolution; thus, the positional accuracy is within 0.01 cm, a negligible error, if the cable spool diameter is known exactly. Uncertainty in the cable spool diameter is the largest source of error in position. The spool diameter, including the cable, was measured at 16.71 cm and is believed to be accurate to within 0.03 cm. With 1,000 cm of deployed cable, a positional error of about 2 cm is possible due to this uncertainty.

Velocity is determined by one of two methods. Tachometers are mounted to each drive motor for a direct velocity measurement. In addition, velocity can be determined from the change in ball position as a function of time. Because data are acquired at a known rate (usually 15 samples per second) and because positional accuracy is very good, ball velocity is most accurately determined by this second method. Errors in velocity are less than 1% and are negligible in their effect on the determination of rheological parameters, where force measurement errors and corrections to the load cell data dominate the uncertainties.

Home position is established when the ball approaches an inductive proximity sensor between the orifice plate and the isolation valve through which the riser is accessed. The volume between these two barriers is the designed resting position for the ball when in storage or transport. At the beginning of a test the sensor will indicate the presence of the ball, and the encoder is zeroed to establish home position. At the completion of a test, the ball is retrieved until the proximity

sensor is activated; at that time, software controls prevent further ball retrieval. Future tests then begin with the ball starting at this location. Home position is believed to be repeatable to well within 1 cm (0.4 in.).

Additional uncertainty exists in the elevation of home position above the tank bottom. The elevations of the top of the riser and tank bottom are taken from design drawings that represent conditions before the tanks were filled. Attempts have been made to reference the ball position to the indicated waste level, but, because the ball buoyancy transition indicates the free liquid level and the waste level device senses the top of the crust layer, a difference can be expected. For the six tanks tested, the liquid level indicated by the ball averages 2 cm (0.8 in.) higher than the surface level, which is opposite what would be expected for a floating crust. In SY-101, the ball indicated the liquid surface to be 2.4 cm (0.9 in.) below the level measured by the ENRAF™ gauge. Considering all sources, we ascribe an uncertainty of ± 4.5 cm (1.8 in.), or one ball radius, to all waste elevations indicated by the ball.

The location of the ball in the tank is measured from its center to the home position. To convert the indicated ball position to a height above the tank bottom, we subtract indicated position from the total distance from home to the tank bottom. The height of the ball center above the bottom, H_{BALL}, is then found by

$$H_{BALL} = (Z_{HOME} - Z_{BOTTOM}) - D_{BALL} \qquad (2\text{-}1)$$

where D_{BALL} is the indicated distance of the ball below home,
Z_{HOME} is the elevation of the home position, and
Z_{BOTTOM} is the elevation of the tank bottom.

Table 2-4 provides values for these elevations for each of the tanks tested.

Table 2-4. Ball Home Position Reference

Tank	Tank As-Built Elevations (ft) (home includes spool pieces)		Calculated Home Elevation (cm)
	Bottom	Home	(ref. tank bottom)
AN-103	613.07	670.38	1,746.8
AN-104	613.07	670.38	1,746.8
AN-105	613.07	670.38	1,746.8
AW-101	632.23	689.38	1,741.9
SY-103	617.24	674.16	1,734.9
SY-101	617.24	674.16	1,734.9

2.5 VOID FRACTION INSTRUMENT

The VFI is designed to measure the volume fraction of free (undissolved) gas (void) at specific locations in a tank. The VFI does not determine gas composition, and its response is very nearly independent of gas composition. The measurement is made by compressing the waste captured in a sample chamber of known size with nitrogen gas. The sample chamber is mounted on a rotating arm that is deployed vertically through a riser by means of a crane. Figure 2-3 is a sketch of the VFI deployed in a tank. Figure 2-4 shows the VFI sample chamber with the arm rotated to vertical while being flushed in the process of removing it from the AN-105 dome.

Once below the waste surface and any crust layer, the arm is rotated 90 degrees to become horizontal and lowered to the desired depth in the tank with the cover of the sample chamber open. At the measurement location, the cover is closed to capture a sample, and the waste is compressed with nitrogen gas by opening a valve between the connecting line and the source volume. Lowering the chamber with the cover open replaces the previous sample with fresh waste. The void fraction is calculated from the initial and final pressures and temperatures and known system volumes. The VFI can make measurements at a radius of 76 cm (30 in.) about the riser center about every 30 to 60 cm (12 to 24 in.) of elevation.

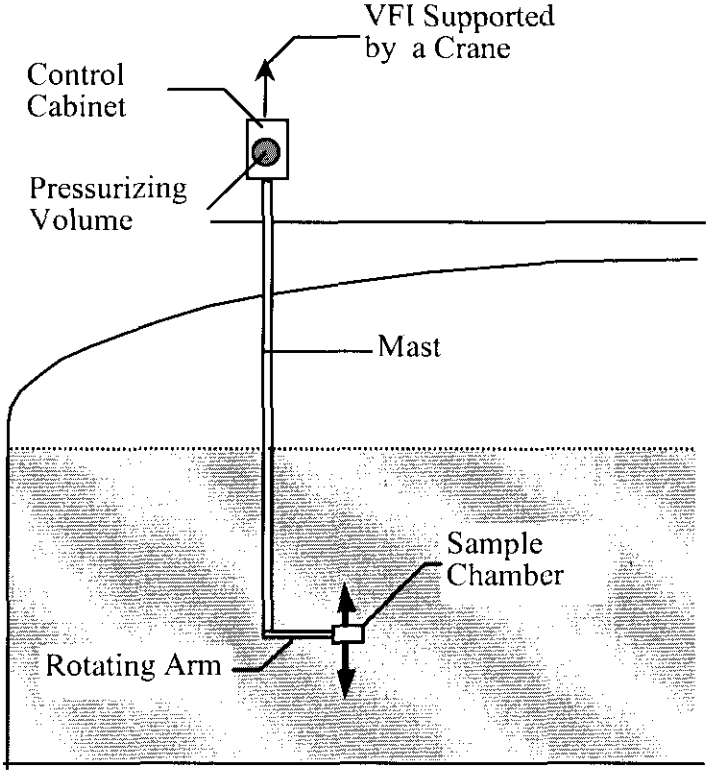

Figure 2-3. Void Fraction Instrument Deployed in a Tank

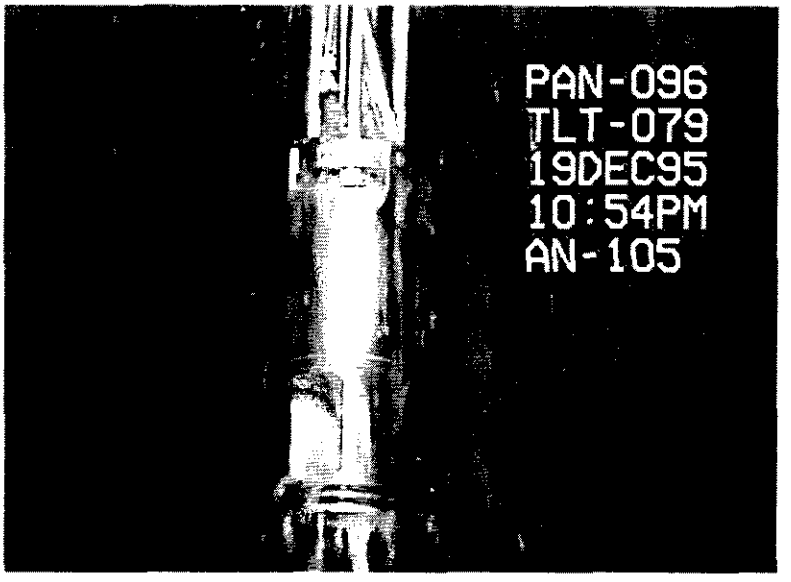

Figure 2-4. Void Fraction Instrument Sample Chamber in Tank 241-AN-105 Dome

The reference for the elevation of the sample chamber is the waste surface. The reference zero position is located by observing the elbow pivot for the lower arm passing into the waste on the in-tank video camera. The uncertainty in this observation is estimated as the radius of the pivot, which is about 4 cm. The uncertainty in relating the measured waste level elevation and the height of the liquid level penetrated by the VFI is taken to be the same as for the ball rheometer, ± 2 cm. The total uncertainty in the level, then, is ± 5 cm.

Sample locations are selected to provide the best possible understanding of the void fraction distribution for the available time in the tank. Three parameters describe the sample location in the tank: the selected riser, the angular orientation of the lower arm, and its elevation. The risers are selected based on availability and spatial distribution.

Up to four vertical traverses are planned for each riser. In the first traverse, the lower arm is normally pointed toward the center of the tank. For the second traverse, the lower arm is rotated 180 degrees to point away from the center. On the third traverse, the arm is rotated 90 degrees clockwise from the second, and the fourth is 180 degrees from the third. Because of limits on time and/or nitrogen gas supply, the fourth and sometimes even the third traverse is dropped. The measurement elevations on later traverses are usually varied based on what is found during the first.

The linear combination of uncertainties in the individual parameters yields an overall measurement uncertainty of ± 0.5% void fraction. The parameters with the largest contributions to the overall error are the connecting line volume, the parameter that models the real gas behavior of the trapped gases in the waste, and the compliance of the sample chamber. Other uncertainties and effects have also been considered, as described below.

If the increase in bubble pressure due to surface tension were significant, the VFI would underpredict the void fraction; however, calculations show that the pressure added by surface tension is significant only for bubbles less than one micron in diameter. Studies of gas release signatures and photomicrographs of core samples from SY-101 (Brewster et al. 1995) indicate that the volume-average bubble size is on the order of a few hundred microns. Tanks that are not forcibly mixed (all except SY-101) would be expected to have larger bubbles. In any event, if the over-pressure due to surface tension were large enough to cause an error in VFI measurements, it would also be enough to drive the gas in the bubble back into solution (Peurrung et al. 1998).

In a similar way, the strength of the waste could cause the void fraction to be over-predicted. As the sample is compressed, the pressure inside the bubbles may be slightly less than the pressure measured by the pressure transducer because the surrounding material supports some of the load. However, the ball rheometer indicates waste yield stresses less than 500 Pa, which is insignificant compared with the 3.5 MPa sample chamber pressure.

The temperatures inside the gas bubbles are not necessarily the same as those measured by the transducers. The bubble temperature tends to increase temporarily upon compression until heat transfer to the waste reestablishes equilibrium, but bubbles have negligible thermal mass compared with the waste and system hardware, therefore, the transient time is short and the initial and final temperatures are essentially equal. Thermal equilibrium of the sample due to gas compression is not an issue, even for the largest bubbles.

However, thermal equilibrium between the waste and the VFI structure must be considered, particularly for the first void fraction measurement after the VFI enters the waste. Transient heat transfer calculations indicate that a 10-minute wait is sufficient to reduce the maximum temperature difference to below 0.6 °C (1 °F). A 20-minute wait is used in actual testing to ensure thermal equilibrium.

There is also a sample capture error that was first quantified approximately in experiments conducted at LANL with both gassed SY-101 chemical simulant and neutrally buoyant spheres to investigate capture of bubbles in non-Newtonian fluids. Although the resemblance of those tests and analyses to actual VFI measurements in general tank waste is questionable, the results showed the void of the sample to be less than that of the undisturbed waste by a factor of about 0.1 with an uncertainty of ± 0.04.[4] Analysis of the RGS also raised the possibility of incomplete capture due to shear stress of the sludge on the container walls.[5] However, a zero error is predicted for shear strength below 1,500 Pa (0.2 psi), which is the case in all the tanks tested. Where both measurements were made in the same tanks, VFI and RGS void fractions match closely without detectable bias. Therefore, we assume that VFI capture error is negligible.

[4] Abbott, J. R., and C. Unal. November 16, 1994. *Sampling Ability of the In Situ Voidmeter Instrument.* LANL letter report TSA-6-94-316 (M110), Los Alamos National Laboratory, Los Alamos, New Mexico.

[5] Shekarriz, A., and J. D. Norton. September 15, 1995. *Retained Gas Sampler System Analysis.* Letter report PNL-FG-091595, Pacific Northwest Laboratory, Richland, Washington.

Overall, the uncertainties in the system are small compared with the typical scatter in the measurements of one-fifth to one-third of the void fraction; these small errors are neglected in computing the average void fraction and gas volume.

2.6 WASTE CORE SAMPLING

Core sampling is the task of remotely obtaining samples of materials store in River Protection Project (RPP) Tank Farm waste storage tanks. Push mode and rotary mode are two core sampling methods used to obtain solid and/or supernatant liquid samples of this waste. Sludge, saltcake, and liquid are the three general waste phases in the various tanks. The samples are obtained from the tanks using specially designed core-sampling trucks and sampling devices. A major part of tank waste characterization is core sampling. Prior to core sampling the headspace of the tank is monitored for flammability and organic vapors. A cylindrical cross-section of the tank contents is obtained by pushing or rotating a 2.5 cm x 48 cm (1 in. x 19 in.) stainless steel sampler and bit (Figures 2-5 and 2-6) into the waste through one of the tank risers.

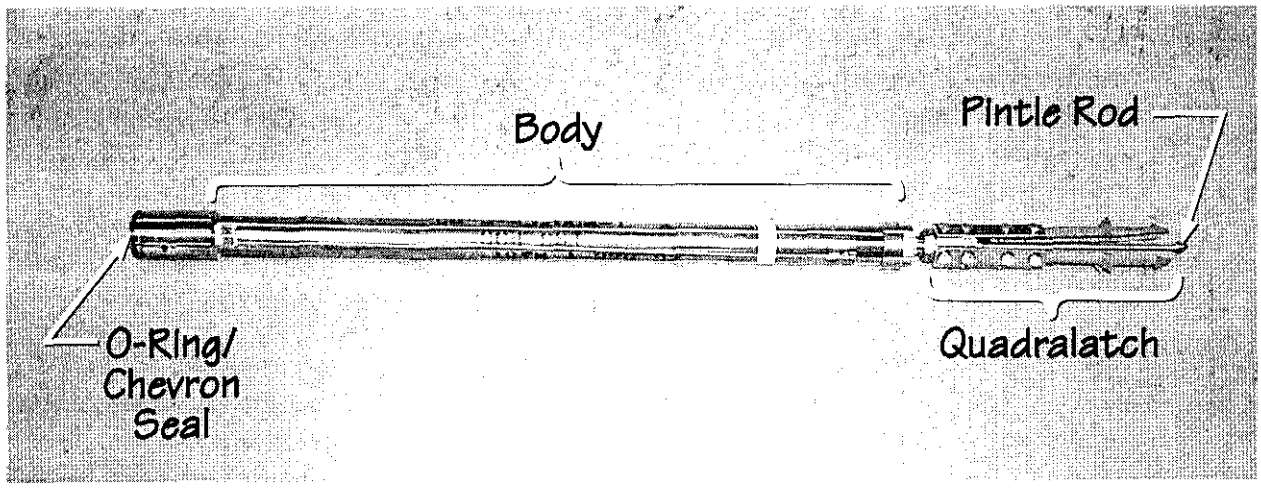

Figure 2-5. Sampler

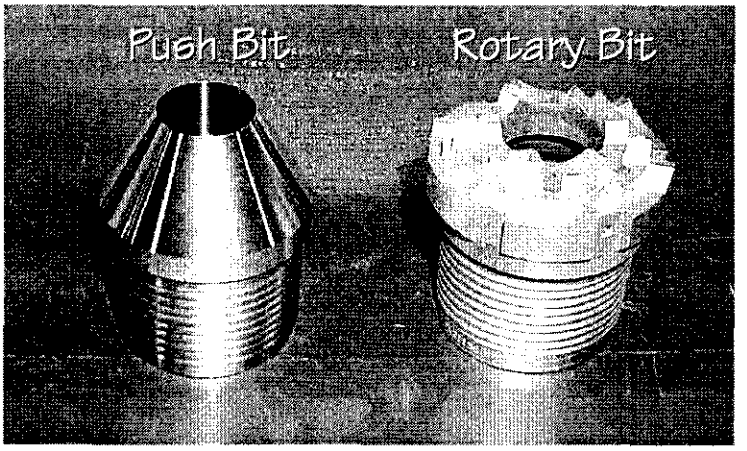

Figure 2-6. Push and Rotary Mode Bit

Push-mode sampling is performed on tanks containing liquids or soft sludge, by the first generation core sampling truck referred to as the Push Mode Core Sample (PMCS) truck. Rotary-mode sampling is primarily used to sample sludge or hard saltcake, although it may be used to sample the other waste types. Because of safety concerns, a second-generation truck, known as the Rotary Mode Core Sample (RMCS) truck was designed. The RMCS truck supplies nitrogen gas to limit drill bit temperature during drilling operations. The RMCS truck can also perform push mode sampling when sample material is soft.

During a sampling event, the stainless steel sampler is lowered down through the drill string, it locks into the core barrel, the drill string is then advanced (typically 19 in. [48 cm]) the sample then is raised and placed in a cask. A spring-loaded piston is used to create negative pressure, which helps draw the sample into the waste column. There is a ball valve at the bottom of the sampler, which is used to contain the collected sample in the tube once the sample has been taken. There are three types of samplers: the O-ring, Chevron, and Retained Gas Samplers.

Drill ram hydrostatic pressure is continuously monitored during the sampling operation to measure waste resistance. Core samples are repeatedly taken until the bottom of the tank is reached. The waste approximately 7.6 cm (3 in.) from the tank bottom of SSTs cannot be sampled because of the design and safety constraints of the sampling method (DeLorenzo 1994). An example of the cross-section or core profile is included as Figure 2.7.

The sampler has a 1.124 to 1.128 in. (2.85 to 2.87 cm) inside diameter which gives a nominal 1.00 in^2 cross section and makes the nominal capacity of the sampler for fluid samples 16.4 cm^3/in. Before the sample can enter the sampler it first must pass through a hole in the sampler bit. The diameter of this hole is 1.0 in (2.54 cm). Therefore, when taking a sample of rigid material, the diameter of the sample taken will be the same as the bit diameter, not the sampler diameter. This corresponds to a nominal 12.9 cm^3/in. For a full sampler, the volume of material which could theoretically be present in the current universal sampler is:

- 237 cm^3 for a rigid core sample (228 cm^3 for the top segment)
- 237 to 309 cm^3 for nonconvective layers depending on the viscosity of the material (228 to 298 cm^3 for the top segment)
- 309 cm^3 for liquids (298 cm^3 for the top segment) (Schofield 1996).

The most effective method available at this time for determining percent recovery with the universal sampler is with the x-ray imaging system, which permits a direct readout of how full a sampler is shortly after it has been removed from the tank, and before it is has been disturbed in the laboratory (Schofield 1996).

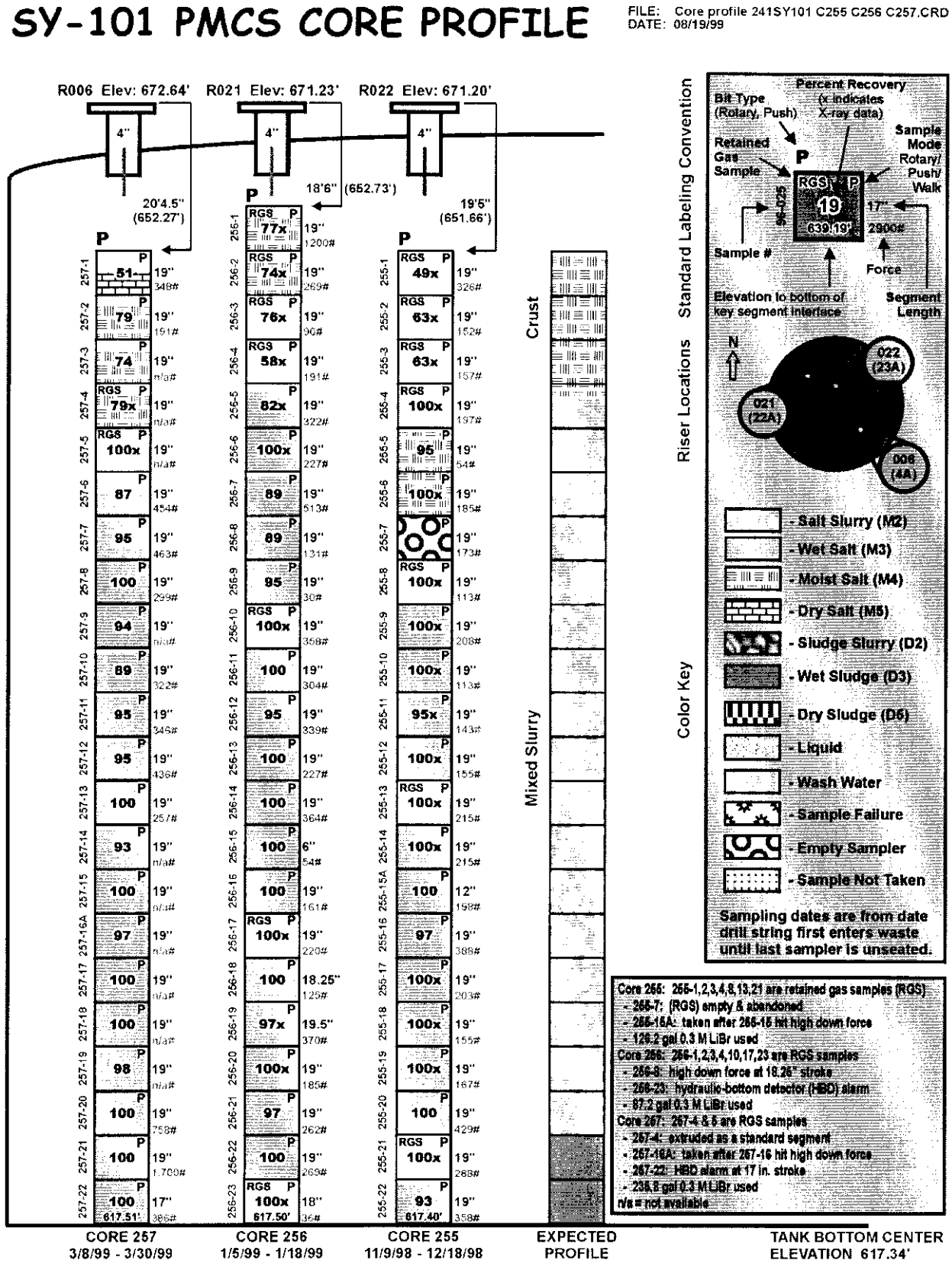

Figure 2-7. Example Core Profile

2.7 RETAINED GAS SAMPLER

The RGS system, which measures the in-situ composition of gases retained in the waste, is a version of the universal core sampler (see Figures 2-5 and 2-6) that was designed specifically for sampling waste that contains gas. Besides the modified sampler and sample extraction, the RGS sample is obtained in the same operation as a normal push-mode core sample. Details of the core sampler, modifications made, and operational constraints of the RGS are given in Webb (1994). The complete details of the sample extraction process and results for the four DSTs sampled with the RGS (AN-103, AN-104, AN-105, and AW-101) are described in Shekarriz et al. (1997). Mahoney et al. (1997) describe several improvements made in the sampler preparation and data reduction process as well as results for three SSTs. This section gives a brief description of the RGS system and operation.

To obtain a sample, an RGS is installed in the push-mode core drill string, lowered into the correct vertical position in the tank, and the sample taken by pushing the sampler down into the waste while the sampler piston is held in position. When the piston contacts the top end of the sampler, a spring is triggered that closes the sampler ball valve, hermetically sealing the waste sample solids, liquids, and gases in a chamber approximately 2.8 cm (1.125 in.) in diameter and 48 cm (19 in.) long.

After the valve is closed and the waste sealed in the sampler, the sampler is removed from the tank and transferred to the x-ray cart for imaging. The x-ray images confirm whether a full sample has been recovered and provides information about the gas structure (bubble shape, etc.) and density of the waste. It also allows a semi-quantitative estimate of the amount of gas present. After the x-ray, the sample is placed in a transport cask and delivered to the 222-S hot cell laboratory for extrusion and gas extraction.

To extract the waste, the sampler is connected to a previously evacuated extraction chamber in the hot cell. The sampler ball valve is opened, and a hydraulic ram pushes the sampler piston all the way forward to drive the sampler contents into the extractor. The waste is then stirred at ambient hot cell temperature to free most of the retained gas bubbles, after which the gas that has been released into the extractor is transferred to collector canisters using a mercury displacement pump. During this process, the sampler and canister pressures and temperatures are monitored and recorded for data reduction and analysis. The gases collected in the canisters are analyzed with a mass spectrometer.

The data analysis procedure uses the temperature, pressure, and volumes measured during extraction as well as the mass spectrometry results to compute the mole fraction and total volume of each gas constituent, the fraction of each component that exists in the gas and is dissolved in the liquid, and the total gas volume fraction at the local hydrostatic pressure from which the sample was taken. The x-ray images are analyzed to provide, in addition to qualitative observations of the phase distribution in the sample, an estimate of the density and gas volume.

Shekarriz (1994) performed a series of flow visualization tests to examine the effectiveness of the RGS drill bit in capturing bubbles in the nonconvective waste during sampling. A

transparent simulant with rheological properties similar to DST waste was used. These tests showed that bubble capture error was minimal and that a 60-degree bit was optimal in minimizing the waste disturbance during sampling.

Comprehensive studies were also performed to quantify the uncertainty in measuring retained gases using the RGS (Cannon and Knight 1995; Cannon 1996). It was found that, while the insoluble gas components could be measured with high accuracy, ammonia measurement was very difficult because it was absorbed within the system. The gas fraction in each sampler can also be determined quite accurately, but the limited number of samples per tank (usually no more than six) create a very high uncertainty in estimates of total gas inventory in the tank.

2.8 NEUTRON AND GAMMA LOGGING

Whenever a tank has had most of the drainable liquids removed, typically by saltwell pumping an SST, the liquid interface is left below a solid surface. This surface may consist either of drained saltcake or drained sludge, depending on the tank chemistry. This liquid level cannot be monitored by any of the conventional surface level devices previously discussed. The Interstitial Liquid Level (ILL) is monitored by installing a liquid observation well (LOW). An LOW consists of a hollow tube inserted into a riser from the surface to the bottom of the tank. It is typically jetted into place with high pressure water, and is capped on the bottom. This leaves the interior of the LOW isolated from the tank contents, but open to the surface, creating an uncontaminated environment from which to monitor the tank contents using neutron and gamma probes.

The LOW Surveillance Van can then drive up to the riser and lower a probe into the LOW opening. A computer program in the Surveillance Van lowers the probe to a pre-determined depth, typically about an inch above bottom, and retrieves the probe at variable speeds. The retrieval and data collection is controlled by a custom software script which is created specifically for the tank being evaluated. The probe can be slowed down to minimum speed across the zone of interest, (typically the ILL), and the frequency of data collection increased. In lesser zones of interest, (i.e., the vapor space above the waste), the speed can be increased and the data collection frequency decreased to reduce scanning time and file size.

A very basic but inaccurate system for obtaining this form of data has existed since 1980. The original system had many drawbacks, the most serious being a very inaccurate depth control system. The depth of major waste features, including the ILL, could only be determined within about 3 in. (7.6 cm) on a consistent basis. The primary reasons for this depth discrepancy were a lack of stabilization on the deployment boom, poor resolution of the depth encoder (20 pulses per inch, or about 0.60 in. (1.5 cm) between pulses), and a wide source-detector spacing on the neutron probe, leading to poor vertical resolution. The survey speed was also constant, and could not be optimized for various zones of interest. The Surveillance Analysis Computer System (SACS) database contains all scans obtained since 1980, and the data is available through either the PC-SACS or Tank Waste Information Network System (TWINS, CHG 2000) computer interface.

In 1997 a new LOW Surveillance System was designed and implemented, which allowed much more accurate measurements. The deployment boom was stabilized with a support leg, eliminating vertical movement. The depth encoder generated 140 pulses per inch, (about 0.007 in. [0.018 cm] per pulse). The source-detector spacing was minimized to help clearly define liquid interfaces. Finally, the scan speed and data collection intervals were programmable on a tank-by-tank basis. The liquid interface data available from the new system is advertised as being accurate within 0.25 in. in 100 ft (0.635 cm in 30.5 m), but in most cases it exceeds 0.10-in. (0.25-cm) resolution. The absolute accuracy and repeatability is variable on a tank-by-tank basis due to data analysis algorithms and the shape of the probe response profile.

The new neutron probe consists of a chemical source, (1.5 Curies of Americium-Beryllium, AmBe), threaded into the bottom of the probe which is immediately adjacent to the thermal neutron detector. The detector consists of a BF_3 gas tube, which only responds to neutrons which are moving slow enough to be captured. The AmBe source emits fast, high-energy neutrons at about 4.5 MEV, which are invisible to the BF_3. The fast neutrons are then moderated by the surrounding moisture, (primarily hydrogen), until they lose energy and become "thermal" neutrons. At that point they can be captured and detected by the BF_3. The detector response is a good indicator of the moisture content surrounding the LOW. In general, the higher the count rate, the higher the moisture content, although the response is not linear.

Areas of apparent low moisture content can be due to drained waste, reduced waste porosity, increased gas concentration, void space around the LOW above the ILL, and the presence of saltcake/sludge layers. The neutron profile can be very useful in identifying the tank waste layering characteristics, in addition to tracking the movement of the ILL.

The gamma probe is simply a low efficiency Geiger-Mueller tube with no artificial gamma source. It simply detects naturally occurring gamma radiation penetrating the LOW from the waste. Because the survey environment can exhibit very high gamma fields, the tube sensitivity is very low to avoid saturating the detector. The primary waste emitters are cesium and cobalt, although secondary gamma from strontium is also picked up. The gamma probe detects "total" gamma, and makes no attempt to identify the source isotope. Spectral gamma tools are available which can identify the parent isotope from their energy spectra, but they are not in common use. The basic rule in analyzing a gamma profile from a LOW is that cesium is usually the primary emitter, and that it is fairly soluble in water. This means that there should be a sudden change in total gamma concentration at the ILL interface, when the waste goes from liquid saturated to drained. As with the neutron probe, waste layers can often be delineated with the gamma probe. In general the gamma probe is not run nearly as often as the neutron, primarily because the liquid interface is not as definitive as the neutron for most tanks.

In 1998 it was realized that the existing neutron and gamma surveillance system could be modified to work in many DSTs. Many DSTs are equipped with MITs, which have temperature thermocouples installed at regular intervals inside a 4-in. (10-cm) tube. The bottom of the MIT is sealed from the waste, similar to the LOW. The interior of the MIT is a 2-in. (5-cm) tube, which is used to install a "validation probe" to check the accuracy of the thermocouples. The MIT is essentially a "tube within a tube," with the thermocouples being installed in the annulus space. Whenever the validation probe is removed the interior 2-in. (5-cm) tube is empty, and can

be used as a LOW for surveillance purposes. The normal neutron and gamma probes are 2-5/8 in. (6.67 cm) in diameter, and will not fit in the MIT. Special "slim hole" versions of the neutron and gamma probes were built to be run inside the MITs on selected DSTs, which are 100% compatible with the new LOW Surveillance Van data collection system. The data collected from the DSTs can now be evaluated in the same manner as the SSTs, identifying liquid interfaces and waste layer profiles. They are particularly useful for identifying the thickness of dense sludge layers on the bottom of the tanks. The neutron and gamma profiles are available from the SACS database.

2.9 SUMMARY OF MEASUREMENT HISTORY IN EACH TANK

This section summarizes thermocouple tree placement, level measurement locations, and risers through which in-situ measurement devices such as the ball rheometer, VFI, and RGS were deployed. Dates of deployment are also given. Gas monitoring systems are not included because they are discussed in detail in Section 2.3.

2.9.1 Tank 241-AN-103 Monitoring and Sampling

The placement of major in-tank instrumentation is shown in Figure 2-8. A color video camera was installed in Riser 5B in October 1995 to aid instrument installations and monitor any changes in the waste's crust. Waste surface level is currently measured by a manual tape in Riser 1A and an ENRAF™ buoyancy gauge in Riser 2A on the opposite side of the tank. The ENRAF™ gauge replaced an FIC contact probe in the same riser in August 1995. Tank dome pressure is monitored in Riser 10A.

Vertical temperature profiles are measured in two locations. An MIT was installed in Riser 15A in November 1995 and is currently being read manually. Validation probe runs in Riser 15A were made in August 1996, March 1999 and May 2000. An older thermocouple tree is mounted in Riser 4A; readings from this tree are monitored and recorded with the TMACS.

The sampling history of AN-103 is given in Table 2-5. The ball rheometer was deployed in Risers 16B and 1B on May 7 and 9, 1996, respectively. In Riser 16B, the ball went to within about 2 m (79 in.) of the tank bottom; in Riser 1B, it went to within about 1.5 m (59 in.) of the bottom. The VFI was operated in Riser 16B on May 14, 1996 and in Riser 1B on May 16, 1996. Three traverses were accomplished in Riser 1B and two in Riser 16B. Void measurements were obtained to within about 43 cm (17 in.) of the tank bottom in Riser 16B and within 63 cm (25 in.) in Riser 1B. No gas releases were evident on the surface or via the SHMS in any of the tests. Core samples and RGS measurements were obtained in AN-103 in two additional risers in September 1996, four months after VFI and ball rheometer testing.

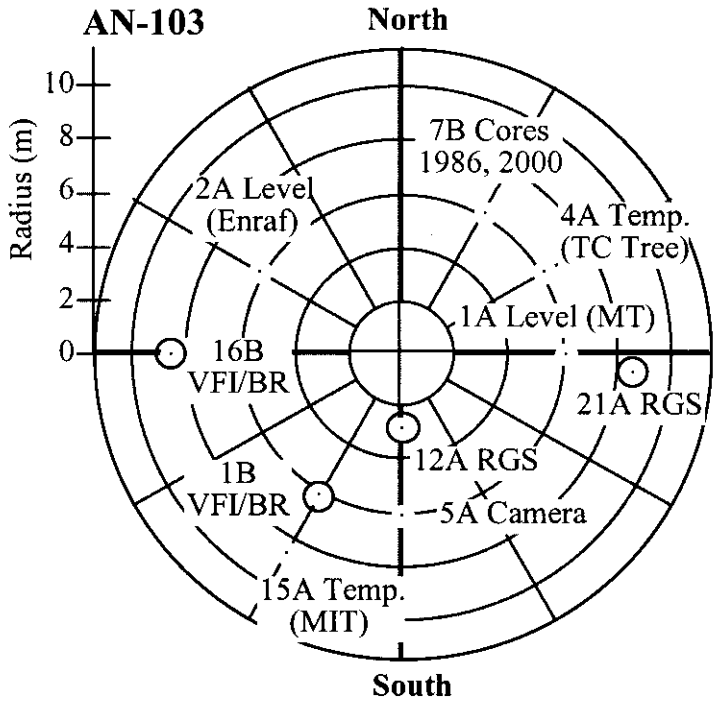

Figure 2-8. Tank 241-AN-103 Sample and Monitoring Risers

Table 2-5. Sampling and Measurement History for Tank 241-AN-103

Date	Type	Riser	Radius		Angle (deg. CW from North)
			(m)	(ft)	
2/86	Core samples	7B	6.1	20	30
5/6/96	Ball rheometer	16B	8.5	28	270
5/10/96	Ball rheometer	1B	6.1	20	210
5/14/96	VFI	16B	8.5	28	270
5/16/96	VFI	1B	6.1	20	210
8/28/96	Validation Probe (Temperature)	15A	8.5	28	210
9/20/96	Core samples and RGS	21A	8.5	28	95
9/96	Core samples and RGS	12A	2.75	9	180
3/18/99	Validation Probe (Temperature)	15A	8.5	28	210
1/14/00	Neutron and gamma scan	15A	8.5	28	210
2/24/00	Neutron and gamma scan	15A	8.5	28	210
3/10/00	Neutron and gamma scan	15A	8.5	28	210
4/21/00	Neutron and gamma scan	15A	8.5	28	210
5/31/00	Validation Probe (Temperature)	15A	8.5	28	210
2/00	Core samples	7B	6.1	20	30

2.9.2 Tank 241-AN-104 Monitoring and Sampling

The placement of important in-tank instrumentation is shown in Figure 2-9. Waste surface level is currently measured by a manual tape in Riser 1A and an ENRAF™ buoyancy gauge in Riser 2A on the opposite side of the tank. The ENRAF™ gauge replaced FIC contact probe in the same riser in August 1995. Temperature profiles are measured with an MIT, which was installed in Riser 15A in November 1995, and a thermocouple tree in Riser 4A. The MIT is currently being read manually. Validation probe runs were performed in the MIT in August 1996, April 1999 and June 2000.

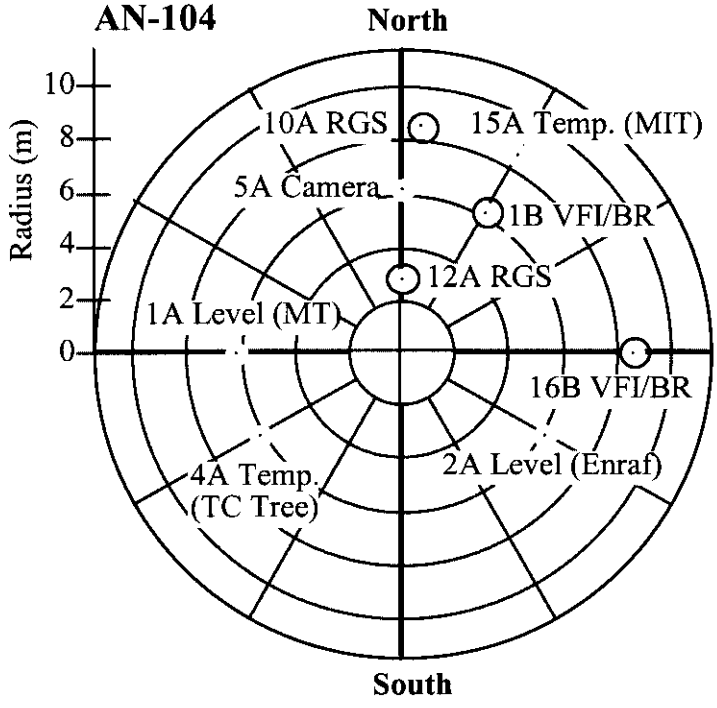

Figure 2-9. Tank 241-AN-104 Sample and Monitoring Risers

The sampling history of AN-104 is shown in Table 2-6. The VFI was operated in Riser 16B on April 2, 1996, and in Riser 1B on April 4, 1996. Two traverses were accomplished in Riser 1B and three in Riser 16B. Interference with the scaffolding around the riser prevented VFI measurements below about 100 cm (39 in.) in Riser 16B and below about 80 cm (31 in.) in Riser 1B. Since this test, scaffold height checks were made part of the pre-test review. The ball rheometer was deployed in Riser 16B on March 27, 1996, and in Riser 1B on April 1, 1996. In August and September 1996, four and five months after VFI and ball rheometer testing, core samples and RGS void measurements were obtained in two additional risers.

Table 2-6. Sampling and Monitoring History for Tank 241-AN-104

Date	Type	Riser	Radius		Angle (deg. CW from North)
			(m)	(ft)	
4/2/96	VFI	16B	8.5	28	90
3/27/96	Ball rheometer	16B	8.5	28	90
4/1/96	Ball rheometer	1B	6.1	20	30
4/4/96	VFI	1B	6.1	20	30
8/27/96	Validation Probe (Temperature)	15A	8.5	28	30
9/96	Core samples and RGS	10A	8.5	28	5
8/96	Core samples and RGS	12A	2.75	9	0
4/5/99	Validation Probe (Temperature)	15A	8.5	28	30
1/14/00	Neutron and gamma scan	15A	8.5	28	30
2/24/00	Neutron and gamma scan	15A	8.5	28	30
4/21/00	Neutron and gamma scan	15A	8.5	28	30
6/6/00	Validation Probe (Temperature)	15A	8.5	28	30
7/00	Core samples				

2.9.3 Tank 241-AN-105 Monitoring and Sampling

The placement of important in-tank instrumentation in tank AN-105 is shown in Figure 2-10. Waste surface level is currently measured by a manual tape in Riser 1A and an ENRAF™ buoyancy gauge in Riser 2A on the opposite side of the tank. The ENRAF™ gauge replaced an FIC contact probe in the same riser in August 1995. Vertical temperature profiles are measured with an MIT that was installed in Riser 15A in October 1995 and an older thermocouple tree in Riser 4A. The MIT is currently being read manually. Validation probe runs were performed in August 1996, April 1999 and June 2000.

The sampling history of AN-105 is given in Table 2-7. The ball rheometer and VFI were run in AN-105 in Riser 1B on December 15 and 18, 1995, and in Riser 16B on December 20 and 22, 1995, respectively. Two traverses were accomplished with the VFI in Riser 1B and three in Riser 16B. No significant gas releases were observed on the waste surface or on the gas monitoring equipment during VFI operation. No VFI measurements could be taken below about 150 cm (59 in.) because of interference by a plastic sleeve required for contamination control. The sleeve used in AN-105 was made of thicker material than those encountered in previous tests. Core samples and RGS void measurements were obtained in two additional risers in AN-105 in June 1996, six months after VFI and ball rheometer testing.

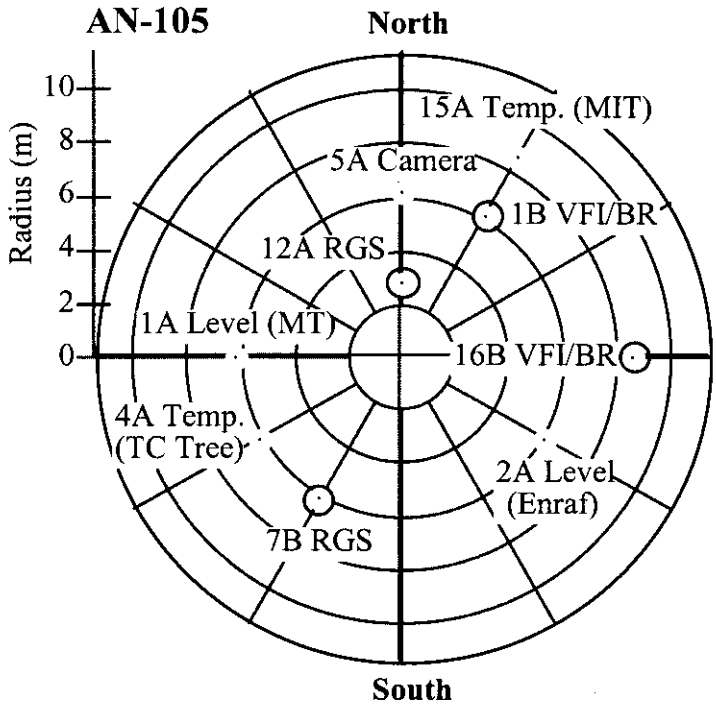

Figure 2-10. Tank 241-AN-105 Sample and Monitoring Risers

Table 2-7. Waste Configuration Measurement History for Tank 241-AN-105

Date	Type	Riser	Radius		Angle (deg. CW from North)
			(m)	(ft)	
12/15/95	Ball rheometer	1B	6.1	20	30
12/18/95	Ball rheometer	16B	8.5	28	90
12/20/95	VFI	1B	6.1	20	30
12/22/95	VFI	16B	8.5	28	90
6/96	Core samples and RGS	7B	6.1	20	210
6/96	Core samples and RGS	12A	2.75	9	0
8/20/96	Validation Probe (Temperature)	15A	8.5	28	30
4/8/99	Validation Probe (Temperature)	15A	8.5	28	30
1/14/00	Neutron and gamma scan	15A	8.5	28	30
2/24/00	Neutron and gamma scan	15A	8.5	28	30
6/1/00	Validation Probe (Temperature)	15A	8.5	28	30

2.9.4 Tank 241-AW-101 Monitoring and Sampling

The placement of important in-tank instrumentation is shown in Figure 2-11. Waste surface level is currently measured by both a manual tape (MT) in Riser 1A and an ENRAF™ buoyancy gauge in Riser 2A, on the opposite side of the tank. The ENRAF™ gauge replaced an FIC

contact probe in the same riser on August 18, 1995. Vertical temperature profiles are measured in two locations: (1) an MIT installed in Riser 15A in 1995 that is currently being read manually and, (2) an older thermocouple tree mounted in Riser 4A with six of its thermocouples recorded manually; readings spaced approximately every 125 cm (50 in.), the first near tank bottom. Validation probe runs were made in the MIT in June 1997, January 1999, and May 2000.

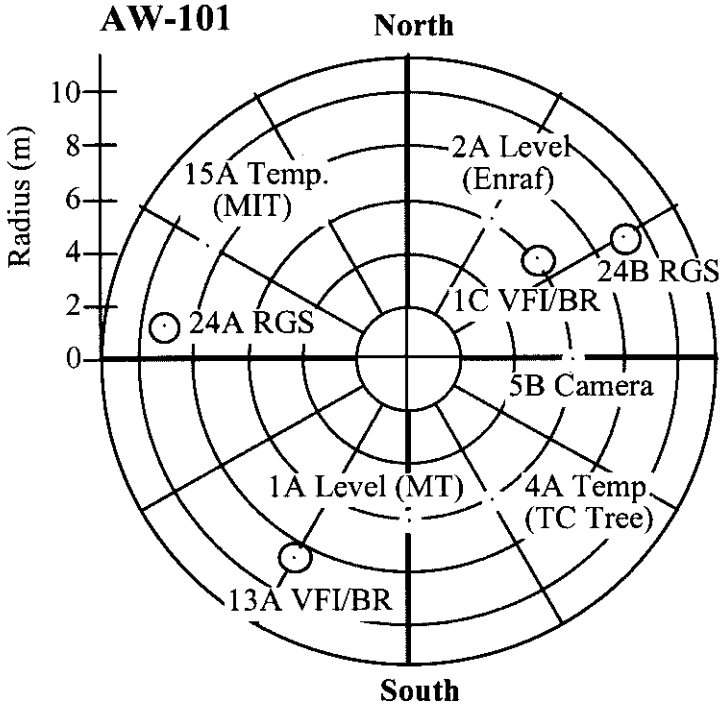

Figure 2-11. Tank 241-AW-101 Sample and Monitoring Risers

The sampling history of AW-101 is listed in Table 2-8. The ball rheometer and VFI were both run in Risers 13A and 1C; the ball rheometer was run in Riser 13A on September 18, 1995, and in Riser 1C on September 20, 1995. The VFI was deployed in Riser 13A on September 22, 1995, and in Riser 1C September 24, 1995. Water lancing was performed to penetrate the crust layer for the ball in Riser 13A on September 15 and in Riser 1C on September 18, 1995. Core samples and RGS void measurements were obtained from two additional risers in AW-101 in March and May 1996, six and seven months after VFI and ball rheometer testing.

Tank 241-AW-101 was the first tank sampled with the RGS; segments 8, 17, 19, and 21 were taken from Riser 24A and segments 18 and 22 from Riser 24B. Segment 8 is from the convective layer, and the rest are from the nonconvective layer. Laboratory analysis showed that the insoluble fraction of the stored gas contained about 25% hydrogen and 60% nitrogen, with the remaining 15% composed of oxygen, nitrous oxide, methane, argon, and small amounts of other hydrocarbons (Shekarriz et al. 1997).

Table 2-8. Sampling and Measurement History for Tank 241-AW-101

Date	Type	Riser	Radius		Angle (deg. CW from North)
			(m)	(ft)	
9/18/95	Ball rheometer	13A	8.5	28	210
9/20/95	Ball rheometer	1C	6.1	20	52
9/24/95	VFI	1C	6.1	20	52
9/22/95	VFI	13A	8.5	28	278
5/96	Core samples and RGS	24A	9.1	30	278
5/96	Core samples and RGS	24B	9.1	30	60
6/27/97	Validation Probe (Temperature)	15A	8.5	28	300
1/20/99	Validation Probe (Temperature)	15A	8.5	28	300
1/19/00	Neutron and gamma scan	15A	8.5	28	300
2/11/00	Neutron and gamma scan	15A	8.5	28	300
3/3/00	Neutron and gamma scan	15A	8.5	28	300
4/20/00	Neutron and gamma scan	15A	8.5	28	300
6/20/99	Validation Probe (Temperature)	15A	8.5	28	300
5/30/00	Validation Probe (Temperature)	15A	8.5	28	300

2.9.5 Tank 241-SY-101 Monitoring and Sampling

Tank 241-SY-101 is the most heavily monitored tank at Hanford. Brewster et al. (1995) contains a complete description of all the instrumentation and readings. The locations of the MITs and other important instruments in the tank are shown in Figure 2-12 along with the location of the mixing pump. Tank conditions can be inferred from temperature profiles and transient thermocouple response to pump operation indicated by the two MITs in Risers 17B and 17C.

Table 2-9 summarizes the waste sampling history of SY-101. Quarterly validation probe runs and weekly neutron/gamma logs are not shown in table because of their high frequency. The VFI was first operated in Riser 11B on December 21, 1994, and in Riser 4A on January 17, 1995. Two traverses were accomplished in Riser 11B and three in Riser 4A. A fourth traverse in Riser 4A was canceled because of a low battery in the crane dynamometer. The VFI could not penetrate below about 60 cm (24 in.) in Riser 11B because of crane unloading. The ball rheometer was deployed three months after the VFI tests because of difficulty in penetrating the crust. The ball was lowered through Riser 4A on March 27, 1995, and through Riser 11B on April 5, 1995. It found the bottom in Riser 4A but became supported by the waste at about 80 cm in Riser 11B.

In 1998 and 1999 the VFI and RGS were deployed through several risers to help confirm that gas accumulation in the crust was causing the accelerated level rise observed since 1997. The VFI obtained several measurements in the crust on June 29, 1998, and September 11, 1998, that show void fractions exceeding 40% near the base. Several RGS segments were obtained from the crust layer in November and December 1998 that confirmed these values (Stewart et al. 1998; Mahoney et al. 1999).

Table 2-9. Waste Sampling History of Tank 241-SY-101

Date	Type	Riser	Radius		Angle (deg. CW from North)
			(m)	(ft)	
5/91	Core sample (Window C)	22A	6.1	20	330
12/91	Core sample (Window E)	11B	8.5	28	150
12/21/94	VFI	11B	8.5	28	150
1/17/95	VFI	4A	6.1	20	150
3/28/95	Ball rheometer	4A	6.1	20	150
4/5/95	Ball rheometer	11B	8.5	28	150
6/29/98	VFI	11B	8.5	28	150
7/22/98	VFI	11B	8.5	28	150
9/11/98	VFI	1C	6.1	20	60
11-12/98	Core sample and RGS	23A	2.75	9	0
1/99	Core sample and RGS	22A	6.1	20	330
3/99	Core sample	4A	6.1	20	150

2.9.6 Tank 241-SY-103 Monitoring and Sampling

Locations of tank instruments are shown in Figure 2-13. The waste surface level is measured using an ENRAF buoyancy gauge located in Riser 2A. This gauge replaced the FIC contact probe in 1994. A manual tape is located in Riser 17A. Waste temperatures are monitored with a thermocouple tree in Riser 4A and an MIT in Riser 17B. Validation probe runs have been made in the MIT about every six months since April 1996.

The sampling history of SY-103 is summarized in Table 2-10. The ball rheometer was operated in Riser 17C on July 14, 1995 and in Riser 22A on August 8, 1995. The ball became supported by the waste about 120 cm (47 in.) and 135 cm (53 in.) above the bottom in Risers 17C and 22A, respectively. The VFI was first deployed on July 19, 1995 in Riser 17C, and on August 18, 1995 in Riser 22A. Three traverses were conducted in each riser.

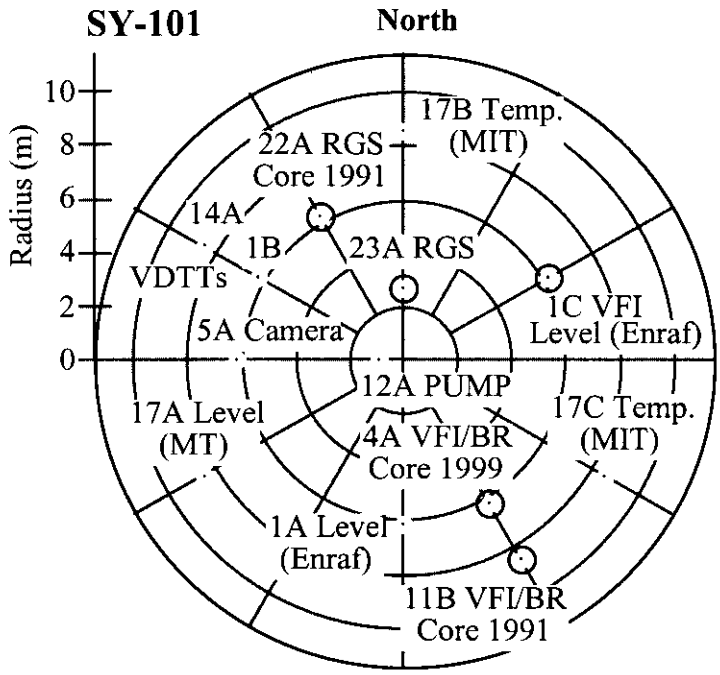

Figure 2-12. Tank 241-SY-101 Sample and Monitoring Risers

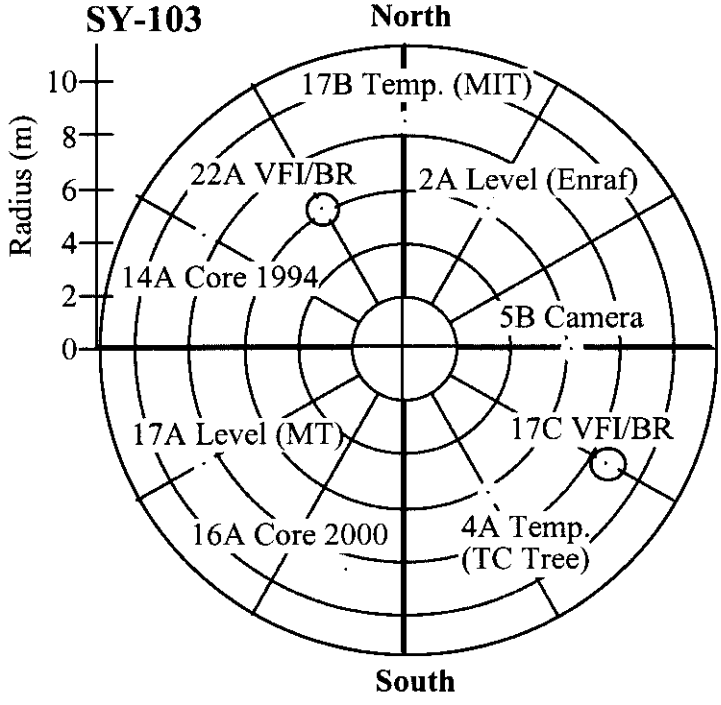

Figure 2-13. Tank 241-SY-103 Sample and Monitoring Risers

Table 2-10. Sampling & Measurement History for Tank 241-SY-103

Date	Type	Riser	Radius		Angle (deg. CW from North)
			(m)	(ft)	
8/94	Core sample	14A	8.5	28	300
7/14/95	Ball rheometer	17C	8.5	28	120
7/19/95	VFI	17C	8.5	28	120
8/8/95	Ball rheometer	22A	6.1	20	330
8/18/95	VFI	22A	6.1	20	330
4/25/96	Validation Probe (Temperature)	17B	8.5	28	0
4/24/97	Validation Probe (Temperature)	17B	8.5	28	0
10/31/98	Validation Probe (Temperature)	17B	8.5	28	0
4/29/98	Validation Probe (Temperature)	17B	8.5	28	0
10/13/98	Validation Probe (Temperature)	17B	8.5	28	0
4/13/99	Validation Probe (Temperature)	17B	8.5	28	0
10/5/99	Validation Probe (Temperature)	17B	8.5	28	0
1/29/00	Neutron scan only (no gamma)	17B	8.5	28	0
2/10/00	Neutron and gamma scan	17B	8.5	28	0
3/00	Core sample	16A	8.5	28	195
3/00	Core sample	22A	6.1	20	330
3/9/00	Neutron and gamma scan	17B	8.5	28	0
3/30/00	Validation Probe (Temperature)	17B	8.5	28	0
4/13/00	Neutron and gamma scan	17B	8.5	28	0

3.0 WASTE CHEMISTRY

3.1 BEST-BASIS INVENTORY FOR EACH TANK

Double-shell tanks 241-AN-103, 241-AN-104, 241-AN-105, 241-AW-101, 241-SY-101, and 241-SY-103 contain saltcake wastes and associated supernatant. The waste reported for SY-101 is for the pre-pump out and pre-dilution condition existing prior to the recent remediation of the waste in SY-101. Total quantities in kilograms of the major constituents in each of these tanks are presented in Figure 3-1 and Table 3-1 for the various tanks. The predominant constituents represented are sodium, nitrate, nitrite, hydroxide, and aluminum. Other noticeable constituents, which are of lesser significance, are chloride, potassium, phosphate, carbonate, and total organic carbon (TOC). Concentrations of various analytes in the total waste of each tank are given in Table 3-2. Waste-layer concentrations of the analytes used to predict hydrogen generation rates are given by Kufahl and Hedengren (2000). Total quantities by waste layer of the major constituents in each of these tanks are presented in Table 3-3 for the various tanks. The total water in the waste is not reported.

Tables 3-1 through 3-3, which list inorganic species, contain data obtained from the Best-Basis Inventory (BBI) subject area in TWINS (CHG 2000) on June 7, 2000. The BBI effort involves developing and maintaining waste tank inventories comprising 25 chemical and 46 radionuclide components in the 177 Hanford Site underground storage tanks. These BBIs provide waste composition data necessary as part of the RPP process flowsheet modeling work, safety analyses, risk assessments, and system design for waste retrieval, treatment, and disposal operations. It must be noted that the SY-101 tank data comes from pre-transfer pump conditions, i.e., before December 1999, and this data was provided by Conner (2000a).

Information presented is from tank characterization data, tank interpretative reports, and tank characterization reports.

3.1.1 Tank 241-AN-103 Chemistry

Water was initially added to AN-103 in the second quarter of 1982 in order to test the tank's integrity. The first waste transfers occurred in the fourth quarter of 1982, with the receipt of dilute non-complexed waste from SY-102. By the end of January 1983, the tank was nearly empty, having transferred most of its waste to AW-102. Beginning in the third quarter of 1983 and continuing through the third quarter of 1984, AN-103 received saltwell liquor from saltwell pumping of a variety of SSTs. Also, during this time the tank received dilute, non-complexed waste from the 300 and 400 Areas and from B-Plant cesium processing, and waste from AN-104. A transfer of waste from AN-103 to AN-101 is recorded in the fourth quarter of 1984. Between the first quarter of 1984 and the first quarter of 1986, AN-103 participated in several evaporator campaigns, exchanging waste with AW-102. With the conclusion of the evaporator campaign in the first quarter of 1986, transfers of waste to AN-103 ceased. Small amounts of water have been added to the tank over the years. Minor fluctuations in the surface level have been

observed as a result of slurry growth caused by the gas generation in the waste. Occasional lancing of the crust has been performed attempting to release the retained gas.

Table 3-1. Best-Basis Inventory for Selected Double-Shell Tanks

Analyte Name	Analyte	AN-103	AN-104	AN-105	AW-101	SY-101	SY-103
Aluminum	Al	224,000	141,000	164,000	119,000	213,000	145,000
Calcium	Ca	480	692	1,480	881	1,040	945
Chloride	Cl^-	28,800	29,700	38,500	28,400	55,600	31,400
Chromium	Cr	2,760	4,870	6,950	1,380	23,500	22,000
Fluoride	F^-	3,550	2,220	5,220	11,000	2,280	3,360
Iron	Fe	190	360	319	1060	1,650	5,840
Mercury	Hg	4.7	0	0	0	0	0
Potassium	K	48,600	24,300	25,400	157,000	20,900	12,900
Manganese	Mn	26.7	57	46.5	850	369	1,150
Sodium	Na	1,100,000	1,070,000	1,100,000	1,060,000	1,250,000	719,000
Nickel	Ni	53.6	180	132	130	897	290
Nitrite	NO_2^-	497,000	445,000	473,000	482,000	684,000	377,000
Nitrate	NO_3^-	727,000	688,000	705,000	743,000	778,000	504,000
Total Hydroxide	OH^-	796,000	567,000	600,000	719,000	185,000	447,000
Lead	Pb	400	242	251	331	520	630
Phosphate	PO_4^{3-}	9,030	16,800	18,200	12,600	45,800	40,600
Silicon	Si	2,170	2,180	987	1,450	1,910	107
Sulfate	SO_4^{2-}	11,400	38,800	27,500	14,700	28,400	17,000
Carbonate	TIC as CO_3^{2-}	92,400	184,000	198,000	113,000	182,000	94,600
Total organic carbon	TOC	10,500	19,300	37,300	19,700	73,800	37,900
Total Uranium	U	141	461	259	3,550	373	1,670
Zirconium	Zr	27.1	60.7	40.5	261	50.9	123

Notes:

Results are in kilograms.

Table 3-2. Concentrations of Various Constituents Based on Best-Basis Inventory and Waste Volume for Selected Double-Shell Tanks

Analyte Name	Analyte	AN-103	AN-104	AN-105	AW-101	SY-101	SY-103
Aluminum	Al	2.29	1.30	1.42	1.12	2.02	1.91
Calcium	Ca	3.31E-03	4.31E-03	8.63E-03	4.31E-03	6.63E-03	8.39E-03
Chloride	Cl-	0.224	0.209	0.254	0.150	0.401	0.315
Chromium	Cr	0.015	0.023	0.031	0.004	0.116	0.151
Fluoride	F-	0.052	0.029	0.064	0.089	0.031	0.063
Iron	Fe	9.40E-04	1.61E-03	1.33E-03	3.28E-03	7.57E-03	0.037
Mercury	Hg	0	0	0	0	0	0
Potassium	K	0.343	0.155	0.152	0.902	0.137	0.117
Manganese	Mn	1.34E-04	2.59E-04	1.98E-04	1.97E-03	1.72E-03	7.45E-03
Sodium	Na	13.2	11.6	11.2	10.8	13.9	11.1
Nickel	Ni	2.52E-04	7.65E-04	5.25E-04	4.82E-04	3.91E-03	1.76E-03
Nitrite	NO2-	2.98	2.41	2.40	2.18	3.80	2.92
Nitrate	NO3-	3.24	2.77	2.66	2.79	3.21	2.89
Hydroxide	OH- TOTAL	12.9	8.31	8.24	8.98	2.78	9.35
Lead	Pb	5.33E-04	2.91E-04	2.83E-04	4.33E-04	6.42E-04	1.08E-03
Phosphate	PO43-	0.026	0.044	0.045	0.020	0.123	0.152
Silicon	Si	0.021	0.019	8.21E-03	0.012	0.017	1.36E-03
Sulfate	SO42-	0.033	0.101	0.067	0.025	0.076	0.063
Carbonate	TIC as CO32-	0.425	0.765	0.771	0.331	0.774	0.561
Total organic carbon	TOC	0.242	0.401	0.726	0.346	1.571	1.123
Uranium	U TOTAL	1.64E-04	4.83E-04	2.54E-04	2.48E-03	4.01E-04	2.50E-03
Zirconium	Zr	8.21E-05	1.66E-04	1.04E-04	4.87E-04	1.43E-04	4.80E-04

Notes:

Results are in Molarity (moles per liter of total waste)

Table 3-3. Compositions of the Solid and Liquid Layers of Selected Double-Shell Tanks Based Upon Best-Basis Calculations

Results are in kg

Crust

Constituent	AN-103	AW-101	SY-101
Al	21500	5890	36200
Ca	N/A	114	242
Cl	870	1310	8980
Cr	224	132	5490
F	192	838	673
Fe	N/A	106	485
Hg	0	0	0
K	1550	8810	3260
Mn	N/A	74.9	88.5
Na	67600	57800	268000
Ni	N/A	13.1	222
NO_2	17500	24200	124000
NO_3	36400	50900	217000
Pb	N/A	16.4	99.1
PO_4	489	1590	14700
Si	299	154	828
SO_4	742	1370	7400
TIC as CO_3	N/A	12400	57100
TOC	N/A	1770	16000
U	N/A	298	81.1
Zr	N/A	21.3	10.9

Slurry

Constituent	AN-103	AN-104	AN-105	AN-105	SY-101	SY-103
Al	145000	53000	3120	61900	148218.2	3990
Ca	N/A	555	70.7	1290	678.8	28.1
Cl	9590	11300	875	13800	39224.1	655
Cr	1470	4100	589	5830	14864.8	4.49
F	2120	2030	1080	3400	1336.1	N/A
Fe	N/A	291	31.6	229	962.3	6.96
Hg	0	0	0	0	0.0	0
K	15400	9070	462	9310	14821.8	394
Mn	N/A	43.3	10.6	24.1	230.7	N/A
Na	501000	489000	38500	469000	820570.4	30700
Ni	N/A	153	7.22	101	558.5	4.93
NO_2	168000	160000	10300	173000	468283.6	8060
NO_3	374000	302000	34600	281000	463987.4	51600
Pb	N/A	105	10.7	111	354.9	N/A
PO_4	5440	10600	9820	5400	25949.0	2800
Si	1300	1620	102	364	910.8	N/A
SO_4	7910	30700	935	19700	17399.5	197
TIC as CO_3	N/A	160000	8870	161000	106330.5	N/A
TOC	N/A	12300	963	21700	49406.1	N/A
U	N/A	453	17.7	233	242.3	0.0031
Zr	N/A	42.8	12	16.4	34.2	N/A
Note:			Slurry/ Lower	Slurry/ Upper		Salt Slurry

Liquid

Constituent	AN-103	AN-104	AN-105	AW-101	SY-103
Al	56900	87800	98600	85200	55900
Ca	96.5	137	119	18.8	159
Cl	18400	18400	23800	20700	15700
Cr	1070	764	533	309	44.6
F	1240	186	734	2720	N/A
Fe	48.3	68.5	59.3	30.6	28.4
Hg	0	0	0	0	0
K	31700	15200	15600	108000	5280
Mn	9.65	13.7	11.9	11.3	N/A
Na	535000	582000	590000	694000	286000
Ni	19.3	27.3	23.9	17.3	66.2
NO_2	311000	284000	290000	340000	193000
NO_3	317000	387000	389000	481000	242000
Pb	230	137	130	208	N/A
PO_4	3100	6160	2930	2500	4210
Si	569	555	521	691	107
SO_4	2730	8050	6840	3490	3.81
TIC as CO_3	9310	24300	28400	26000	N/A
TOC	4900	7080	14600	9000	N/A
U	2.95	8.37	8.54	9.99	N/A
Zr	10.1	17.8	12.2	40.5	N/A
Note:	Supernatant	Supernatant	Supernatant	Drain/Liq	Drain/Liq

Solids

Constituent	AN-103	AW-101	SY-101	SY-103
Al	N/A	27800	28582.6	85200
Ca	383	748	118.3	757
Cl	N/A	6450	7441.3	15100
Cr	N/A	939	3178.6	21900
F	N/A	7440	274.3	3360
Fe	141	920	204.5	5810
Hg	4.7	0	0.0	0
K	N/A	40500	2817.2	7180
Mn	17.1	764	49.5	N/A
Na	N/A	311000	159340.0	402000
Ni	34.3	99.3	117.5	219
NO_2	N/A	118000	91990.1	176000
NO_3	N/A	211000	96918.1	211000
Pb	171	107	66.0	N/A
PO_4	N/A	8510	5162.4	33600
Si	N/A	602	173.3	N/A
SO_4	N/A	9790	3572.8	16800
TIC as CO_3	83000	74400	18110.5	94600
TOC	5640	8940	8377.7	N/A
U	138	3250	49.7	1670
Zr	17.1	200	5.8	123
Note:		Saltcake		Sludge

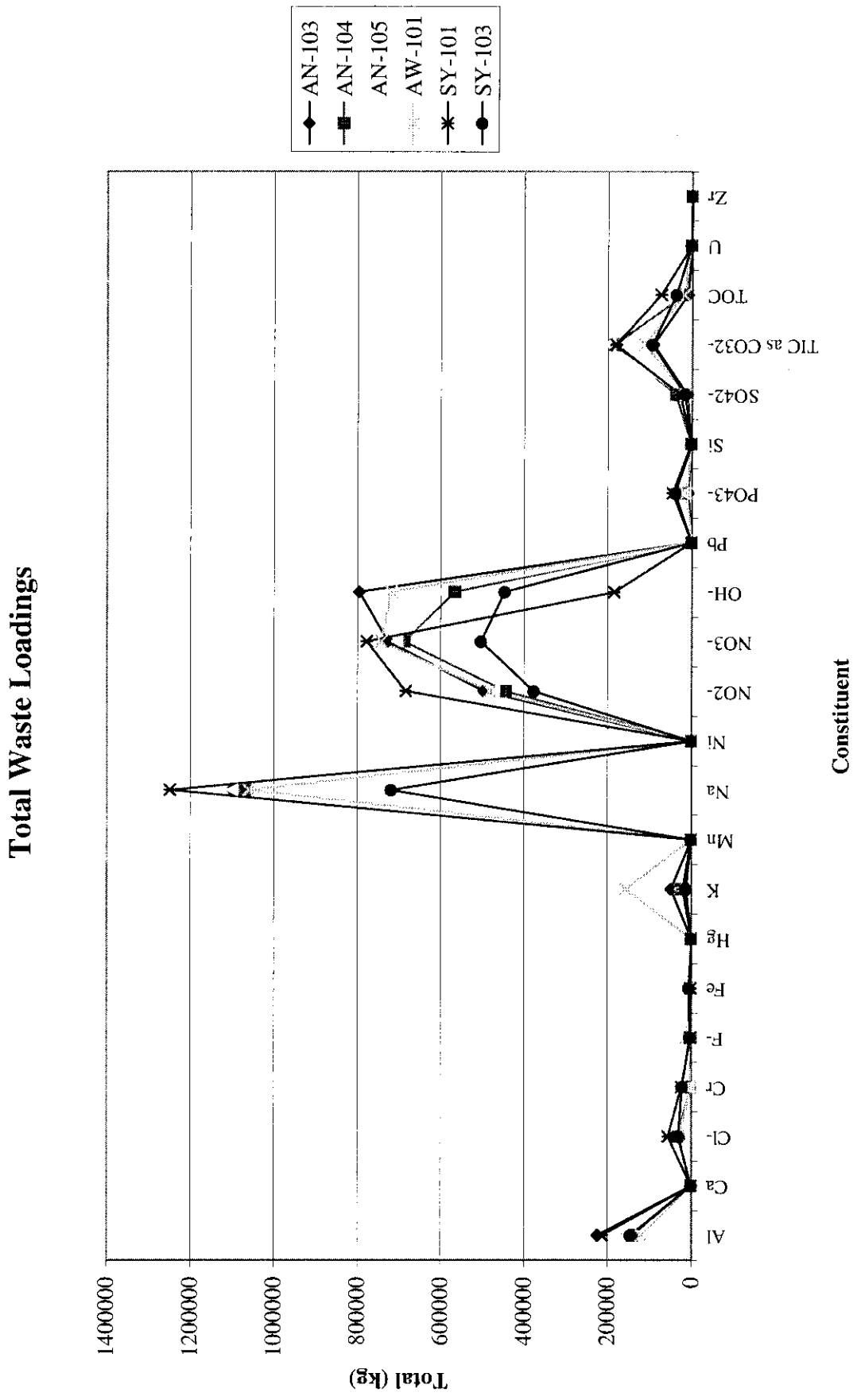

Figure 3-1. Total Waste in Kilograms of Major Constituents for Selected Double-Shell Tank

Tank 241-AN-103 presently contains an estimated 3,618 m^3 (128,000 ft^3) of DSS waste made up of three layers: a floating crust, a convective (supernatant) layer, and a non-convective (salt slurry) layer. The estimated volumes for these layers are 150 m^3 (5,300 ft^3) for the crust, 1,881 m^3 (66,400 ft^3) for the supernatant, and 1,386 m^3 (48,900 ft^3) for the salt slurry. A total of 201 m^3 (7,100 ft^3) of retained gas is estimated in the tank waste.

3.1.2 Tank 241-AN-104 Chemistry

Tank 241-AN-104 went into service in 1982 and received water during the second quarter of 1982. The tank received DSSF from AW-102 in the fourth quarter of 1982 and the first quarter of 1984. In the fourth quarter of 1983, the tank received PUREX waste. In the first quarter of 1984, waste was sent to tanks 241-AZ-102 and 241-AN-105. In the third quarter of 1984, 310 m^3 (10,900 ft^3) of flush water was added to the tank, and waste was sent to AN-103. During the fourth quarter of 1984 and the second quarter of 1985, the tank received DSSF from AW-102 via the evaporator. The last transfer for this tank was a small amount of flush water added in 1996.

This tank contains an estimated 3,982 m^3 (141,000 ft^3) of DSSF made up of two layers: a convective (supernatant) layer and a non-convective (salt slurry) layer. The total waste volume was derived from surface level measurements. The tank is estimated to contain 2,275 m^3 (80,300 ft^3) of supernatant and 1,593 m^3 (56,300 ft^3) of salt slurry some of which is a thin crust. A total of 114 m^3 (4,030 ft^3) of retained gas is estimated in the tank waste; 8 m^3 (283 ft^3) in the supernatant layer and 106 m^3 (3740 ft^3) in the salt slurry layer.

3.1.3 Tank 241-AN-105 Chemistry

Tank 241-AN-105 entered service in 1982. Water was initially added to AN-105 in the second quarter of 1982. During the fourth quarter of 1982 through the first quarter of 1983, the tank received DSSF from AW-102. A small amount of waste from an unknown source was added in the third quarter of 1984. The tank received non-complexed waste from AN-104 in the first quarter of 1984. Most of the waste was then removed to AW-102 during the first quarter of 1985 for an evaporator campaign, leaving approximately 583 m^3 (20,600 ft^3) waste in AN-105. During the first two quarters of 1985, the tank received DSSF waste from AW-102 via the evaporator, then waste reception ceased. The only transfer since that time has been an addition of flush water from miscellaneous sources from the fourth quarter of 1995 to the first quarter of 1996.

Tank 241-AN-105 has an operating capacity of 4,391 m^3 (155,000 ft^3), and presently contains an estimated 4,262 m^3 (151,000 ft^3) of DSSF. This total waste volume was derived from surface level measurements. The tank is estimated to contain 1,772 m^3 (62,600 ft^3) of salt slurry part of which is in a thin crust, 2,400 m^3 (84,800 ft^3) of supernatant, and 87 m^3 (3,070 ft^3) of retained gas.

3.1.4 Tank 241-AW-101 Chemistry

Tank 241-AW-101 went into service in 1980 and had an active transfer history until 1986. The major waste types received by the tank were dilute-noncomplexed waste, Plutonium-Uranium Extraction (PUREX) process miscellaneous low level-2 (PL2) waste, DSSF, saltwell liquor, as well as N Reactor sulfate and phosphate waste. The tank currently contains DSSF.

Tank 241-AW-101 presently contains 4,258 m^3 (150,000 ft^3) of DSSF waste. This waste volume was based on an ENRAF™ reading. This waste consists of 2839 m^3 (100,000 ft^3) of supernatant and 1419 m^3 (50,100 ft^3) of saltcake part of which is a thin crust.

3.1.5 Tank 241-SY-101 Chemistry

Tank 241-SY-101 was designed for use as a concentrated waste holding tank and went into service in 1977 with the receipt of DSS from the 242-S Evaporator/Crystallizer. In addition to periodic transfers of DSS, the tank has received concentrated complexant waste originally from B-Plant and a small amount of water. Although the tank remains in service, it no longer receives waste due to its inclusion on the FGWL.

The tank has an operational capacity of 4,320 m^3 (153,000 ft^3) and as of August 1995 contained 4,160 m^3 (147,000 ft^3) of waste. The major constituents of SY-101 waste included water, aluminum, chloride, chromium, hydroxide, nitrate, nitrite, phosphate, potassium, sodium, sulfate, total inorganic carbon, and total organic carbon. At the time, core sampling results and temperature profile measurements indicated the waste existed in three well-defined layers: the crust, convective, and non-convective layers.

3.1.6 Tank 241-SY-103 Chemistry

Tank 241-SY-103 began operating in 1977 and received concentrated wastes. Two years later the tank contained more than 3,600 m^3 (127,000 ft^3) of complex concentrate (CCPLX) waste. During 1980, the tank was pumped down to a non pumpable waste heel of about 466 m^3 (16,500 ft^3), then received DSS. During 1985, the tank received small transfers of uranium ion exchange sludge. The uranium sludge was generated from groundwater pumped from beneath a crib near U-Plant, then processed through ion-exchange resins. During 1988 and 1989, the tank received saltwell liquid and waster water from the 200 West Area. No waste has been added since 1990.

Waste, which was added to the tank at various times, has settled into layers that vary from sludge (lower depths) to liquid (toward the top). From the bottom up, the solids in the lowest region are expected to consist of the following: a heel of CCPLX from the early process history, DSS, and uranium ion-exchange sludge. A less dense layer of supernate is on top of the solids layer; it consists of waste water and other liquid waste transfers. Sampling confirms the existence of a crust layer at the waste surface. Similar to SY-101 waste, the solid layers of waste on the SY-103 bottom appear to be nonconvective, and the supernate region farther up appears to be convective so that the waste appears to circulate naturally.

SY-103 bottom appear to be nonconvective, and the supernate region farther up appears to be convective so that the waste appears to circulate naturally.

3.2 ORGANIC SPECIATION RESULTS

Tables 3-4 through 3-10 list the organic data obtained from the Tank Characterization Database (TCD). Specifically, the organic species tables were obtained from the Sample Analysis subject area in TCD on July 18, 2000. Only pre-mixer pump data samples were obtained for the SY-101 tank, i.e., before July 1993. Any replicate measurements were arithmetically averaged to produce a single data point. Tables 3-4, 3-7, and 3-9 list the major organic constituents present in solid samples obtained from tanks AN-103, AN-104, AW-101, SY-101, and SY-103. Tables 3-5, 3-6, and 3-8 show the major organic constituents present in the liquid samples. Additionally, Table 3-10 contains the major and minor organic constituents obtained from the tank and core composite samples for tanks AW-101 and SY-101.

Table 3-4. Organic Constituents Obtained from the Solid Core Composite Samples for Tanks 241-AN-103, 241-AN-104, 241-AN-105, 241-AW-101, 241-SY-101, and 241-SY-103

Analyte	AN-103	AN-104	AN-105	AW-101	SY-101	SY-103
Acetate	565	636	275	N/A	N/A	1,750
Aroclor 1016	0.61	0.33	0.54	N/A	N/A	N/A
Aroclor 1221	0.61	0.33	0.54	N/A	N/A	N/A
Aroclor 1232	0.61	0.33	0.54	N/A	N/A	N/A
Aroclor 1242	0.61	0.33	0.54	N/A	N/A	N/A
Aroclor 1248	0.61	0.33	0.54	N/A	N/A	N/A
Aroclor 1254	0.61	0.33	0.54	N/A	N/A	N/A
Aroclor 1260	0.61	0.33	0.54	N/A	N/A	N/A
Formate	1,290	732	1,170	N/A	N/A	3,515
Oxalate	10,400	9,670	5,630	8,050	N/A	11,000
Total organic carbon	1,710	4,710	5,610	3,950	18,200	6,890

Notes:

Units: (μg/g)
N/A = not available

Table 3-5. Organic Constituents Obtained from the Liquid Core Composite Samples for Tanks 241-AN-103, 241-AN-104, 241-AN-105, 241-SY-101, and 241-SY-103

Analyte	AN-103	AN-104	AN-105	SY-101	SY-103
Acetate	2,870	1,880	641	N/A	1,350
Formate	1,630	3,440	1,620	N/A	4,250
Oxalate	806	825	435	N/A	2,550
Total organic carbon	3,050	3,110	4,350	11	9,650

Notes:

Units: mg/L
N/A = not available

Table 3-6. Organic Constituents Obtained from the Drainable Liquid Samples for Tanks 241-AN-103, 241-AN-104, 241-AN-105, 241-AW-101, 241-SY-101, and 241-SY-103

Analyte	AN-103	AN-104	AN-105	AW-101	SY-101	SY-103
Acetate	3,880	612	622	N/A	N/A	1,330
Formate	3,180	961	1,560	N/A	N/A	4,290
Oxalate	554	707	766	N/A	N/A	2,550
Total organic carbon	N/A	N/A	N/A	3,320	11,800	10,040

Notes:

Units: mg/L
N/A = not available

Table 3-7. Organic Constituents Obtained from the Solid Subdivision Samples for Tanks 241-AN-103, 241-AN-104, 241-AN-105, 241-AW-101, 241-SY-101, and 241-SY-103

Analyte	AN-103	AN-104	AN-105	AW-101	SY-101	SY-103
Acetate	1,030	532	594	694	N/A	N/A
Citrate	N/A	N/A	N/A	506	N/A	N/A
Formate	748	759	1,080	634	N/A	N/A
Oxalate	4,070	8,470	6,880	16,000	N/A	N/A
Total organic carbon	N/A	N/A	N/A	4,080	16,400	8,100

Notes:

Units: (μg/g)
N/A = not available

Table 3-8. Organic Constituents Obtained from the Liquid Tank Composite Samples for Tanks 241-AN-105 and 241-AW-101 (mg/L)

Analyte	AN-105	AW-101
Aroclor 1016	0.012	0.004
Aroclor 1221	0.012	0.004
Aroclor 1232	0.012	0.004
Aroclor 1242	0.012	0.004
Aroclor 1248	0.012	0.004
Aroclor 1254	0.012	0.004
Aroclor 1260	0.012	0.004
Oxalate	683	646
Total organic carbon	2,680	3,020

Table 3-9. Organic Constituents Obtained from Solid Tank Composite Samples for Tanks 241-AW-101, 241-SY-101, and 241-SY-103 (μg/g)

Analyte	AW-101	SY-101	SY-103
Aroclor 1016	0.728	N/A	N/A
Aroclor 1221	0.728	N/A	N/A
Aroclor 1232	0.728	N/A	N/A
Aroclor 1242	0.728	N/A	N/A
Aroclor 1248	0.728	N/A	N/A
Aroclor 1254	0.728	N/A	N/A
Aroclor 1260	0.728	N/A	N/A
Total organic carbon	5,920	23,100	9,290

Notes:
N/A = not available

Table 3-10. Organic Constituents Obtained from the Tank and Core Composite Samples for Tanks 241-AW-101 and 241-SY-101 (4 Sheets)

Constituent Name	AW-101 TANK COMPOSITE LIQUID (mg/L)	SY-101 CORE COMPOSITE SOLID (μg/g)	SY-101 CORE COMPOSITE LIQUID (mg/L)
1,1,1-Trichloroethane	0.1	N/A	N/A
1,1,2,2-Tetrachloroethane	0.1	N/A	N/A
1,1,2-Trichloroethane	0.1	N/A	N/A
1,1-Dichloroethane	0.1	N/A	N/A

Table 3-10. Organic Constituents Obtained from the Tank and Core Composite Samples for Tanks 241-AW-101 and 241-SY-101 (4 Sheets)

Constituent Name	AW-101 TANK COMPOSITE LIQUID (mg/L)	SY-101 CORE COMPOSITE SOLID (µg/g)	SY-101 CORE COMPOSITE LIQUID (mg/L)
1,1-Dichloroethene	0.1	N/A	N/A
1,2,4-Trichlorobenzene	50	72	3.3
1,2-Dichlorobenzene	50	72	3.3
1,2-Dichloroethane	0.1	N/A	N/A
1,2-Dichloroethylene	0.1	N/A	N/A
1,2-Dichloropropane	0.1	N/A	N/A
1,3-Dichlorobenzene	50	72	3.3
1,4-Dichlorobenzene	50	72	3.3
2,4,5-Trichlorophenol	250	359	16.5
2,4,6-Trichlorophenol	50	72	3.3
2,4-Dichlorophenol	50	72	3.3
2,4-Dimethylphenol	50	72	3.3
2,4-Dinitrophenol	250	359	16.5
2,4-Dinitrotoluene	50	72	3.3
2,6-Dinitrotoluene	50	72	3.3
2-Butanone	0.2	N/A	N/A
2-Chloronaphthalene	50	72	3.3
2-Chlorophenol	50	72	3.3
2-Fluoro-4-nitrophenol	N/A	N/A	1.6
2-Hexanone	0.2	N/A	N/A
2-Methylnaphthalene	50	72	3.3
2-Methylphenol	50	72	3.3
2-Nitroaniline	250	354	16.5
2-Nitrophenol	50	72	3.3
3,3 -Dichlorobenzidine	100	144	6.5
3-Nitroaniline	250	359	16.5
4,6-Dinitro-o-cresol	250	359	16.5
4,4-Dichlorodiphenyl sulphone	N/A	42	N/A
4-Bromophenylphenyl ether	50	72	3.3
4-Chloro-3-methylphenol	50	72	3.3
4-Chloroaniline	50	72	3.3
4-Chlorophenylphenyl ether	50	72	3.3
4-Methyl-2-Pentanone	0.2	N/A	N/A
4-Methylphenol	50	72	3.3
4-Nitroaniline	250	359	16.5
4-Nitrophenol	250	359	16.5
Acenaphthene	50	72	3.3

Table 3-10. Organic Constituents Obtained from the Tank and Core Composite Samples for Tanks 241-AW-101 and 241-SY-101 (4 Sheets)

Constituent Name	AW-101 TANK COMPOSITE LIQUID (mg/L)	SY-101 CORE COMPOSITE SOLID (µg/g)	SY-101 CORE COMPOSITE LIQUID (mg/L)
Acenaphthylene	50	77	3.3
Acetone	0.2	N/A	N/A
Anthracene	50	72	3.3
Aroclor 1016	0.004	N/A	N/A
Aroclor 1221	0.004	N/A	N/A
Aroclor 1232	0.004	N/A	N/A
Aroclor 1242	0.004	N/A	N/A
Aroclor 1248	0.004	N/A	N/A
Aroclor 1254	0.004	N/A	N/A
Aroclor 1260	0.004	N/A	N/A
Benzene	0.1	N/A	N/A
Benzo(a)anthracene	50	72	3.3
Benzo(a)pyrene	50	71	3.3
Benzo(b)fluoranthene	50	72	3.3
Benzo(ghi)perylene	50	71	3.3
Benzo(k)fluoranthene	50	72	3.3
Benzoic acid	250	359	0.5275
Benzyl alcohol	50	72	3.3
Bis(2-Chloroethoxy)methane	50	72	3.3
Bis(2-chloroethyl) ether	50	72	3.3
Bis(2-Chloroisopropyl) ether	50	72	3.3
Bis(2-ethylhexyl)phthalate	6.2	72	3.3
Bromodichloromethane	0.1	N/A	N/A
Bromoform	0.1	N/A	N/A
Bromomethane	0.2	N/A	N/A
Butylbenzylphthalate	50	72	3.3
Carbon disulfide	0.1	N/A	N/A
Carbon tetrachloride	0.1	N/A	N/A
Chlorobenzene	0.1	N/A	N/A
Chloroethane	0.2	N/A	N/A
Chloroform	0.1	N/A	N/A
Chloromethane	0.2	N/A	N/A
Chrysene	50	72	3.3
Cis-1,3-Dichloropropene	0.1	N/A	N/A
Dibenz[a,h]anthracene	50	72	3.3
Dibenzofuran	50	72	3.3
Dichlorocyclohexane	N/A	N/A	1.0
Dibromochloromethane	0.1	N/A	N/A

Table 3-10. Organic Constituents Obtained from the Tank and Core Composite Samples for Tanks 241-AW-101 and 241-SY-101 (4 Sheets)

Constituent Name	AW-101 TANK COMPOSITE LIQUID (mg/L)	SY-101 CORE COMPOSITE SOLID (µg/g)	SY-101 CORE COMPOSITE LIQUID (mg/L)
Diethylphthalate	50	71	3.3
Dimethyl phthalate	50	72	3.3
Di-n-butylphthalate	50	71	0.3
Di-n-octylphthalate	50	72	3.3
Dodecane	N/A	125	N/A
Ethylbenzene	0.1	N/A	N/A
Fluoranthene	50	72	3.3
Fluorene	50	72	3.3
Hexachlorobenzene	50	72	3.3
Hexachlorobutadiene	50	72	3.3
Hexachlorocyclopentadiene	50	72	3.3
Hexachloroethane	50	72	3.3
Indeno(1,2,3-cd)pyrene	50	72	3.3
Isophorone	50	72	3.3
Methylenechloride	0.1	N/A	N/A
Naphthalene	50	72	3.3
Nitrobenzene	33	72	3.3
N-Nitroso-di-n-propylamine	50	72	3.3
N-Nitrosodiphenylamine	50	72	3.3
Oxalate	647	N/A	N/A
Pentachlorophenol	250	359	16.5
Pentadecane	N/A	19	N/A
Phenanthrene	50	72	3.3
Phenol	50	72	3.3
Pyrene	50	72	3.3
Styrene	0.1	N/A	N/A
Tetrachloroethene	0.1	N/A	N/A
Tetradecane	N/A	289	N/A
Toluene	0.1	N/A	N/A
Total organic carbon	3020	18200	10.7
Trans-1,3-Dichloropropene	0.1	N/A	N/A
Trichloroethene	0.1	N/A	N/A
Tridecane	N/A	389	N/A
Triphenylphosphine oxide	N/A	153	7.2
Vinyl acetate	0.114	N/A	N/A
Vinyl chloride	0.2	N/A	N/A
Xylenes (total)	0.1	N/A	N/A

Notes:

N/A = not available

3.3 DISSOLUTION STUDIES

3.3.1 Tank 241-AN-104 Dissolution Studies

Tank 241-AN-104 has been identified as a tank to be retrieved for low level waste pretreatment and immobilization. Retrieval of the tank waste will require dilution to dissolve solids. Laboratory tests have been performed to determine the amount and type of dilution with water required for safe retrieval of the tank waste. The behavior of the AN-104 waste was very similar to the AN-105 waste, which was tested earlier.

Although the settled solids layer in the tanks take up over 40% of the total waste volume in the tank, the actual solids account for just over 5% by weight of the total. The rest of the settled solids layer is interstitial liquid. Approximately 80% of the solids by weight can be dissolved at moderate dilution to 50% by volume of the whole-tank-composite, or 80% dilution of the settled solids. Most of the solids in the undiluted samples are sodium carbonate. Most of the solids that remain undissolved at moderate dilution are sodium oxalate. The laboratory work indicated that the waste exhibited Newtonian behavior, i.e., the viscosity did not change with shear rate except for minor deviations. Values of viscosity clearly increased with increasing fraction of solids and decreased with increasing temperature. The total inventory of sodium is approximately 1,190 metric tons (MT). Approximately 520 MT (44% by weight) of sodium is retrievable without dilution and 1015 MT (85%) is retrievable at moderate dilution of 80% by volume of the settled solids (Herting 1998).

3.3.2 Tank 241-AN-105 Dissolution Studies

Tank 241-AN-105 has been identified as a tank to be retrieved for low level waste pretreatment and immobilization. Retrieval of the tank waste will require dilution to re-dissolve major soluble sodium salts while not precipitating out other salts. Laboratory tests have been conducted to determine the amount and type of dilution required for safe retrieval. The dilution parameters evaluated were volume percent dilution, type of diluent (water or 2 M NaOH), and temperature. It was determined that, the volume of settled solids falls with increasing dilution. Additionally, the other parameters have little or no effect on the volume of settled solids. Dissolution kinetics were very fast; the solids generally dissolved faster than the laboratory was able to measure. The solid phase organic salt, most likely sodium oxalate, did not dissolve appreciable under any of the tested conditions. Other insoluble waste components included unspecified forms of chromium oxide and sodium silicate or aluminosilicate. The laboratory work indicated that the waste exhibited Newtonian behavior, i.e., the liquid viscosity did not change with shear rate. Values of viscosity clearly increased with increasing fraction of solids and decreased with increasing temperature. All the diluted samples settled into three layers after initial mixing, settled solids, supernatant liquid, and a floating layer of solids adhering to small gas bubbles. Gas is much less soluble in the waste solutions than in the diluent. Thus addition of 500,000 L of water to tank AN-105 could release 10,000 L of gas, which could be a significant factor in selection of mixing and transfer pump equipment. The total inventory of sodium is approximately 1,100 MT. Approximately 500 MT of sodium (46% by weight) is retrievable without dilution. With dilution, at least 900 MT (82%) is retrievable at 25% by volume and at least 1,000 MT (91%) at 75% dilution by volume (Herting 1997).

3.3.3 Tank 241-AW-101 Dissolution Studies

Tank 241-AW-101 has been identified as a tank to be retrieved for low activity waste pretreatment and immobilization. Retrieval of the tank waste will require dilution to dissolve solids. Laboratory tests have been performed to determine the amount and type of dilution by water required for safe retrieval of the tank waste.

Currently, AW-101 contains approximately 68% supernatant liquid by volume and 32% solids in the crust and settled at the bottom. As with most typical tank wastes, the actual solid phase is a relatively small fraction; the undiluted whole-tank-composite samples contained 3.4% true solids by weight at 45°C. These true solids are made up of 60% Na_2CO_3, 20% $Na_2C_2O_4$, 15% Na-F-PO_4-SO_4 (combination of various double salts) and 5% other (oxides or hydrous oxides of U, Si, Al, Ca, Fe, Cr, and Mn in order of abundance). At 50% dilution of the settled solids by volume nearly all the carbonate and phosphate salts dissolved. At 100% dilution, nearly all the sulfate and fluoride also dissolved, and the remaining solids are approximately 75% $Na_2C_2O_4$, and 25% Other. The fraction of total sodium inventory in the tank that is retrievable in the supernatant liquid is 60-65% at zero dilution. This increases to 95% with 124 volume percent dilution of the settled solids (Herting et al. 1999).

3.3.4 Tank 241-SY-101 Dissolution Studies

Laboratory results from 1999 indicate both the centrifuged solids and the true (dry) solids decrease with dilution and temperature in SY-101 waste. At tank temperature, only minor fractions of nitrite and nitrate seem to be in solids. The primary remaining ions in solid form at 30% dilution are sodium salts of oxalate and carbonate, followed by lesser amounts of $Al(OH)_3$ (or other Al solids) and $Cr(OH)_3$. The SY-101 waste exhibited Newtonian behavior of liquid viscosity remaining constant with shear rate. Values for viscosity clearly decreased with increasing temperature (Person 1999).

3.3.5 Tank 241-SY-103 Dissolution Studies

Laboratory work from November 1988 indicates that there is a large effect of temperature on solids dissolution in SY-103 waste. Higher temperature, greater dilution (2:1 water to waste) and agitation resulted in the greatest dissolution. Temperature and agitation had greater effects than dilution ratio. At high temperature (38°C) and 1:1 dilution of water to waste 77% of the solids by weight were dissolved and at 2:1 dilution of water to waste 88% were dissolved (Prignano 1988).

3.4 TRANSMISSION ELECTRON MICROSCOPY RESULTS

The crystallinity, morphology, chemical composition, and crystalline phase of several SY-101 and SY-103 solid samples were studied by transmission electron microscopy (TEM), electron energy dispersive spectroscopy (EDS), and electron diffraction. The main focus of the preliminary investigation in fiscal year (FY) 1995 was on the identification of aluminum hydroxide thought to be present in these tank samples. The results were compared with nuclear magnetic resonance (NMR). The results of these studies are summarized by Liu et al. (1995) and in the following bullets:

- Aluminum hydroxide is observed in SY-103. Other soluble nitrate and sulfate phases are also observed in SY-103.
- Both sodium and aluminum salts are observed in SY-101.
- The study of $Al(OH)_3$ is consistent with the tank chemistry. Tank 241-SY-101 composition falls under the solubility limits of sodium aluminate, and the SY-103 composition is near the solubility limit of $Al(OH)_3$. Therefore, it is expected that $Al(OH)_3$ can precipitate in SY-103.
- Nuclear magnetic resonance (NMR) experiments suggest that aluminum hydroxide will precipitate at low hydroxide concentration, and sodium aluminate will form for a higher OH/Al ratio.
- Within the experimental range, all soluble aluminum is tetrahedral (aluminate). All $Al(OH)_3$ is in the solid phase, and no $Al(OH)_3$ is observed in the liquid phase. This suggests that drying the sample is unlikely to cause precipitation of $Al(OH)_3$ and, therefore, the TEM study of $Al(OH)_3$ is reliable.
- All the soluble aluminate exists as sodium aluminate. The narrow peak at a lower hydroxide suggests that the aluminum is truly a soluble species, but the broader peak at high hydroxide concentrations suggests that the aluminum species begins to aggregate into clusters and ultrafine colloidal particles.
- The TEM study on tank samples and the NMR study on simulants is consistent with reported literature results.
- Insoluble solid phases containing Cr, Fe, and Mn are observed in SY-103; they are not affected by washing.

4.0 TANK THERMAL BEHAVIOR

The waste temperature has a strong influence on tank behavior. Over the past five years, from January 1, 1995, through January 1, 2000, the temperatures measured near the bottom of each tank have shown a net drop of about 5 °F. Temperatures measured in the middle of the nonconvective layer have also dropped, by a slightly lesser amount, as have the temperatures measured in the convective layer. (The exception is the waste in SY-101, which has shown a modest increase of 3 to 5 °F over this period due to the insulating effects of the thick crust, prior to its dissolution as a result of waste transfer and back-dilution operations from December 1999 through March 2000.) This has apparently resulted in a marked change in gas generation, retention and release behavior as will be discussed in Sections 5.0 through 8.0.

The waste temperature and temperature distribution in a DST depends on a complex balance of heat generation and dissipation. The heat generated in the waste stored in DSTs is dissipated primarily by means of ventilation of the tank headspace and of the annulus between the inner and outer shells. A smaller amount of heat is also radiated to the soil through the sidewalls and from the waste surface to the tank dome. The relative fraction of the total heat load removed through these various paths is influenced by many factors including the waste configuration (e.g., crust and nonconvective layer thickness, waste level, etc.), the ventilation flow rates, and the ambient air temperature.

This section presents a brief summary of heat transfer considerations and discusses the thermal behavior and history of each tank. Heat transfer paths available for heat removal are discussed in Section 4.1, and waste configuration effects are described in Section 4.2. The waste temperature histories over the last five-years for the six FGWL DSTs are presented in Section 4.3, and an overall summary of thermal behavior is provided in Section 4.4.

4.1 HEAT DISSIPATION PATHS

The primary means of heat removal from DSTs is ventilation of both the tank headspace and of the annular space between the inner and outer shells. The tanks in each farm are manifolded together. The headspace vent systems are each driven by single induced draft fan that serves the entire farm. The headspace ventilation fans in the AN and AW farms are nominally capable of about 600 scfm total flow that is distributed among the tanks in the farm by adjusting dampers in the tank inlet ducts. The SY farm fan is capable of 800 scfm.

The headspace ventilation system draws ambient air into the tank through inlet filters. The headspace exhaust is then drawn through high-efficiency particulate air (HEPA) filters into a manifold and discharged to the atmosphere through the tank farm stack. The induced draft creates a vacuum of 2 to 5 in. of water in the headspace. The nominal flow rate is maintained at about 100 scfm in AN-103, AN-104, AN-105, and AW-101 by inlet flow controllers. (Prior to their installation in mid-1996, the flow rates in many tanks were on the order of 20 to 30 scfm.) Tank 241-SY-101 headspace vent flow has been 500 to 550 scfm, and SY-103's has been 100 to 200 scfm.

The annulus ventilation systems in the AN and AW farms are each driven by two fans with a combined capacity of 800 scfm per tank (5,600 scfm total for the seven AN tanks and 4,800 for the six AW tanks). Approximately 80% (640 scfm/tank) of this flow is directed at the sides of the tanks and 20% (160 scfm/tank) flows through the slots in the tank bottom. The annulus ventilation system in the SY farm is driving by one fan rated at 750 scfm or 250 cfm for each of the three tanks. The side-to-bottom flow in the SY farm can be adjusted external to the tank. The flow through the bottom slots in SY-101 and SY-103 is estimated to be 200 cfm.

Though its original purpose was leak detection, annulus ventilation also provides considerable cooling of the non-convective layer at the bottom of the tank. Four main conduits beneath the tank bring inlet air into a plenum under the center of the tank. The air then flows out through an array of small radial channels from the central plenum to the main annulus at the tank periphery. Since the coolest ventilation air at the highest flow rate is exposed to the central portion of the tank bottom, the temperature distribution forms a "dished" pattern typical of DSTs, with the coolest bottom temperatures at the center. The importance of heat transfer to air through the bottom of the tank is illustrated by the dramatic seasonal oscillation in the lowest thermocouple in the waste (indicated by TC1 at 4 in. from the bottom in most tanks). Annulus vent flows in the Facility Group 1 DSTs are on the order of 200 scfm.

The temperature response of the tanks show that the thermal response of the tanks is dominated by the seasonal temperature cycle. During the summer months, the incoming air can be as hot or hotter than the surface of the waste in the tank most of the time. (The Hanford Weather Station has registered ambient air temperatures up to 120 °F in August, with highs typically 99 to 105 °F and minimum temperatures no lower than 85 °F for periods of two weeks or more at a time.) During the fall, winter, and early spring seasons, however, conditions are usually more moderate, and the ambient air temperature is typically 20 to 60 °F below the waste surface temperature. This is reflected in the seasonal oscillation in temperature seen on all thermocouples in the waste and also in those embedded in the concrete bottom, sides, and domed top of a tank.

In addition to forced convection heat transfer, headspace ventilation potentially allows evaporative cooling of the waste surface. The ambient air at Hanford is generally dry (exceedingly so in the winter) with relative humidity typically in the range 20 to 30% during the day. Evaporation removes heat at a rate of approximately 2,400 kJ/kg of water evaporated. However, the high dissolved salt concentration in the liquid waste along with the universal presence of a covering crust layer all but prevents evaporation in the FGWL DSTs. Even SY-101 prior to remediation, which had the highest ventilation flow and highest temperature actually showed a yearly net gain of water in some years due to its high salt concentration and thick crust layer.

Thermal conduction through the concrete structure of the tank to the earth surrounding the buried tank is the only other available path for heat transfer, besides annulus and headspace ventilation. Heat radiates from the waste surface to the interior surface of the tank dome and between the inner and outer sidewalls across the annulus. Heat is also conducted directly to the soil through the concrete in the tank bottom. The earth forms an essentially infinite heat sink at a temperature of about 40 °F, which initially constitutes a respectable temperature difference with the waste

(typically at 80 to 100 °F). However, the soil temperature increases over time and decreases the effective temperature gradient. Eventually the soil temperature near the tank becomes sufficiently high that more heat is transferred vertically to the surface and radiated to the atmosphere than is transported radially outward. Past analyses have shown that this mode of heat dissipation accounts for only 5 to 10% of the total tank heat load. As a result, tank thermal behavior is dominated by the headspace and annulus ventilation.

4.2 WASTE CONFIGURATION EFFECTS

The crust, convective layer and nonconvective layer each generate heat approximately uniformly. The thickness of these layers affects the balance of heat flow between the various dissipation paths available and has a strong influence on the temperature profile. The most important factors are crust thickness, nonconvective layer thickness, and waste level. Each of these effects is discussed below.

The crust layer mainly acts as an insulator for heat dissipation from the waste below it. The heat generated within the crust is a small fraction of the heat transfer through it. Heat transport through the crust is by conduction. The thicker the crust, the greater the top-to-bottom temperature difference required for a given heat transfer rate. Therefore, as the crust becomes thicker, the temperature of the convective layer below the crust increases. However, this also causes the temperature difference across the nonconvective layer on the bottom to increase, driving a larger fraction of the heat load into the annulus ventilation system and out the tank bottom. Tanks with a thick crust will, therefore, tend to have a high convective layer temperature that will be close to the peak nonconvective layer temperature.

Like the crust, heat transfer in the nonconvective layer is also by conduction, but it is much thicker than the crust and generates much more heat. In most tanks more heat is generated in the nonconvective layer than can be conducted to the annulus cooling system and as much as half is conducted upward into the convective layer. This produces the characteristic parabolic temperature profile with the peak temperature approximately midway through the layer. Above the peak temperature elevation, heat flows upward into the convective layer. Below the peak temperature elevation, heat flows down into the tank floor. The peak temperature is proportional to the square of the layer depth. Therefore, a deep nonconvective layer will tend to have a much higher peak temperature than a shallow one.

The overall effect of these heat transfer mechanisms is illustrated in the form of temperature profiles in Figure 4-1. Temperature profiles for a typical thin-crust and thick-crust tank are shown as the dashed line. The direction of primary heat flow paths is shown by the arrows.

The final consideration is the effect of changing the waste surface area-to-volume ratio. Ignoring heat transfer through the sidewalls, the area-to-volume ratio increases in inverse proportion to the waste level. Since heat generation is proportional to the volume and dissipation is proportional to the area, a high area-to-volume ratio indicates a cool tank. This means that removing the convective layer would reduce the peak waste temperature significantly, even though heat transfer in the remaining waste would be entirely by conduction. It also implies that tanks with a

low waste level such as SY-103 and AN-103 should tend to be cooler than full tanks such as AN-105 and AW-101, all other things being equal.

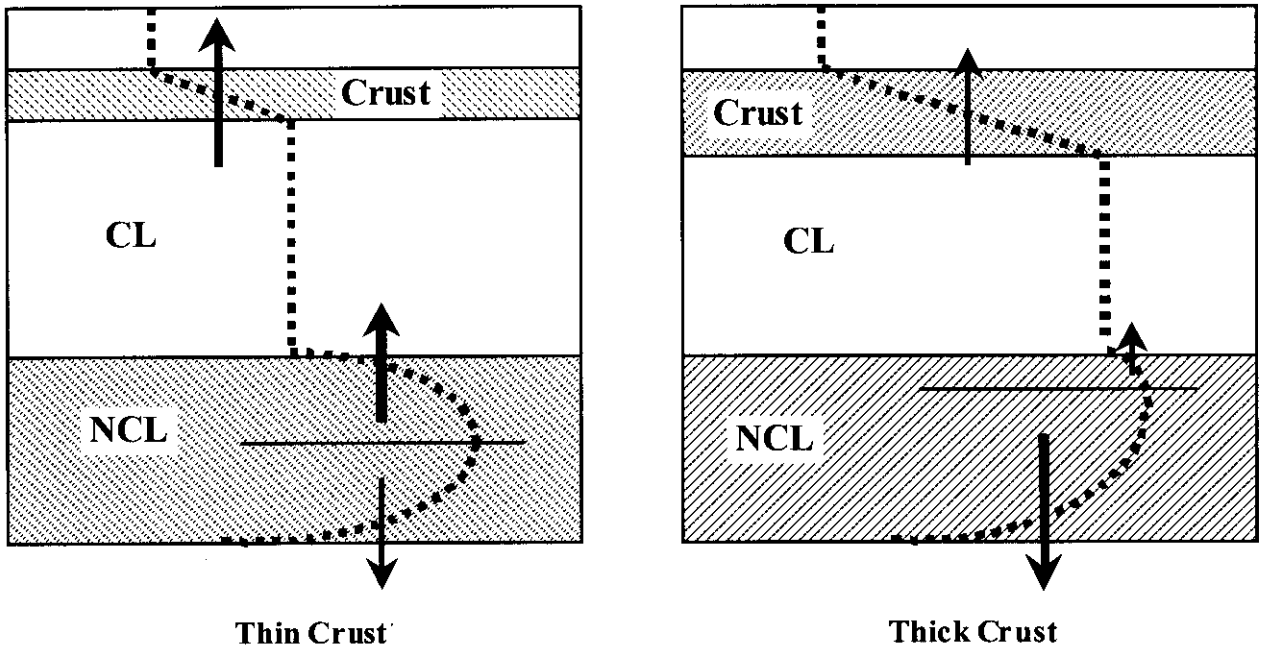

Figure 4-1. Influence of Crust Thickness on Heat Flow and Temperature Profiles

4.3 WASTE TEMPERATURE HISTORY

The temperature history of each of the six FGWL tanks over the period January 1, 1995, to January 1, 2000, is characterized using measurements at three different axial locations on a single thermocouple tree at one radial/azimuthal location in the tank. The original thermocouple trees are used rather than the newer MITs because MIT data do not cover the desired time period. Table 4-1 describes the locations of these instruments in detail. The three axial locations were selected to obtain representative temperature measurements in the waste near the bottom of the non-convective layer, near the middle of the non-convective layer, and in the convective layer, which consists of supernatant liquid overlying the waste.

Table 4-1. Selected Thermocouples for Waste Temperature History

Tank	thermocouple tree location			lowest TC		middle TC		highest TC	
	Riser	radius (ft)	azimuth angle (°F.) [a]	ID	elevation (in.)	ID	elevation (in.)	ID	elevation (in.)
AN-103	4A	20	60	TC1	4	TC5	100	TC11	244
AN-104	4A	20	210	TC1	4	TC5	100	TC11	244
AN-105	4A	20	210	TC1	4	TC5	100	TC11	244
AW-101	4A	20	150	TC1	4	TC5	100	TC11	244
SY-101	17B[b]	28	0	TC1	4	TC5	100	TC11	244
SY-103	4A	20	150	TC2	33	TC4	81	TC12	273

Notes:

(a) azimuth angle for thermocouple tree location is given in degrees clockwise from North.
(b) an MIT was installed in SY-101 in 1992 replacing the original thermocouple tree.
TC = thermocouple

The temperature behavior for three axial levels at the given riser location is assumed to be sufficient to characterize the thermal behavior of the whole tank. The temperature is not expected to be radially uniform at a given level in the waste, but the significant gradients are in all cases axial rather than radial. There is some heat transfer radially at the tank wall to the air in the annulus, but most of the heat transfer is in the axial direction, at the waste surface, and at the tank bottom. At the waste surface, evaporative cooling and forced convection heat transfer due to the ventilation air flow are the primary means of heat removal. Beneath the tank, forced convection in the ventilation channels within the concrete pad that the tank sits on provide an efficient path for heat removal through the bottom of the tank.

This pattern of top-and-bottom cooling results in the typical "camel hump" axial temperature profile observed in these tanks. Generally, the coldest temperature is indicated by the thermocouple near the tank bottom (TC1), the hottest temperature is found near the middle of the non-convective waste layer (TC5). The liquid supernatant layer (TC11) is generally cooler than the non-convective layer it overlays. Figure 4-2 shows a typical waste temperature axial profile for each tank. For all of the tanks, the thermocouple in the middle of the non-convective layer, TC5 (TC4 in SY-103), registers at or near the hottest temperature in the non-convective layer. Similarly, TC11 (TC12 in SY-103) registers temperatures representative of the supernatant liquid layer. The temperature at 4 in. from the bottom of the tank, as indicated by TC1, is also the lowest temperature measured in the non-convective layer in all tanks.

The profile for SY-103 shows that the selection of TC2, which is at 33 in., rather than TC1 (at 9 in.), results in a slightly higher estimate of the bottom waste temperature in this tank. For this tank, TC2 is used instead of TC1, for continuity of the temperature history data. Prior to November 1994, information was recorded only for the even-numbered thermocouples on the TC tree in Riser 4A. An MIT was installed in Riser 17B in October 1994, and from that point on, daily temperature readings were recorded for all thermocouples on both risers via TMACS.

While the temperatures in SY-101 increased in 1997-1999 due to crust growth and those in SY-103 remained relatively constant, the general trend in the three AN tanks and AW-101 is one

of decreasing temperature. This trend is due to increased ventilation flow rates. In mid-1995, the AN farm annulus ventilation rates were increased to approximately 200 cfm. The tank headspace ventilation flow rates were increased from about 20 to 30 cfm to around 100 cfm in AW-101 in mid-1996, and in AN-103, AN-104, and AN-105 in early 1997. As a result, these tanks show an acceleration in the rate of temperature decrease. The increased flow rate through the annulus also resulted in a more marked seasonal oscillation in the tank temperatures. This effect is particularly noticeable on the lowest thermocouple in the waste (TC1). The following subsections present the temperature history for each tank, with a brief discussion of the factors that affect the temperature trends and significant local changes.

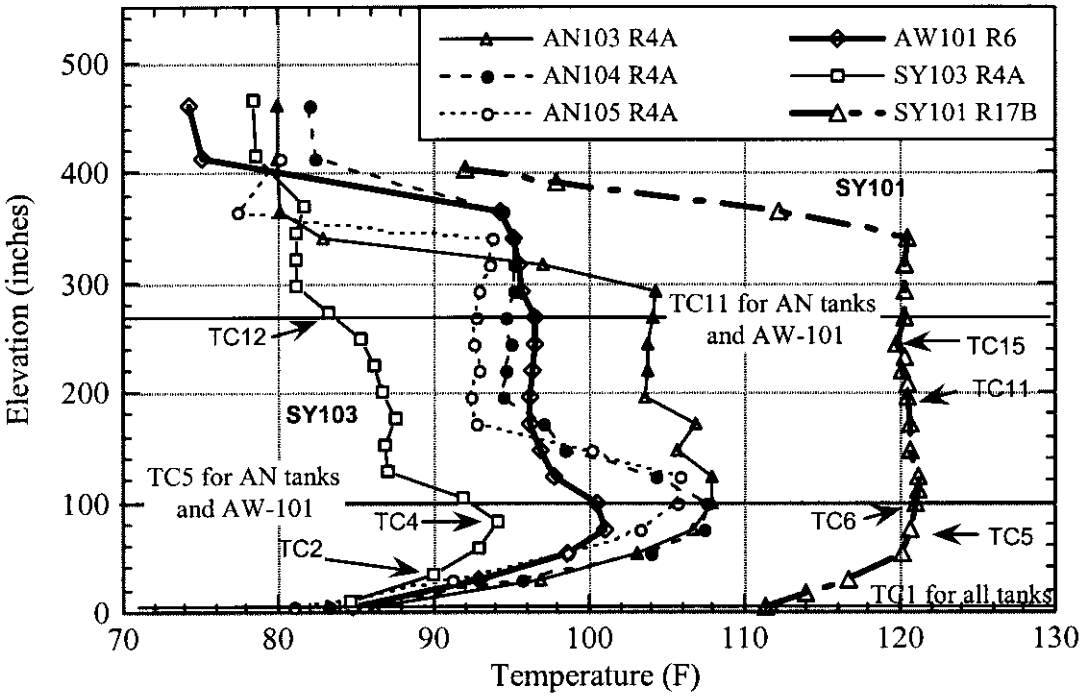

Figure 4-2. Typical Temperature Profiles in Flammable Gas Watch List Tanks

4.3.1 Tanks 241-AN-103, 241-AN-104, 241-AN-105, and 241-AW-101

The temperature histories from 1995 to 2000 for AN-103, AN-104, AN-105, and AW-101 are shown in Figures 4-3 through 4-6. For all four of these tanks, the thermocouples show virtually no response to GREs, except for a few cases in which the thermocouple in the middle of the non-convective layer (TC5) shows a sudden drop that coincides with a GRE. The only significant external factors affecting the temperatures at all levels in the waste appear to be the headspace and annulus ventilation rates and the temperature of the incoming ambient air. The temperature indicated by the thermocouple in the waste at the bottom of the tank (TC1) is particularly sensitive to the annulus ventilation rate. This is indicated by the sudden increase in seasonal temperature variation at all levels of the tank with the increase in headspace and

annulus ventilation rates in January 1997, and the somewhat erratic variations in TC1 prior to 1997, which are traceable to changes in annulus ventilation rate.

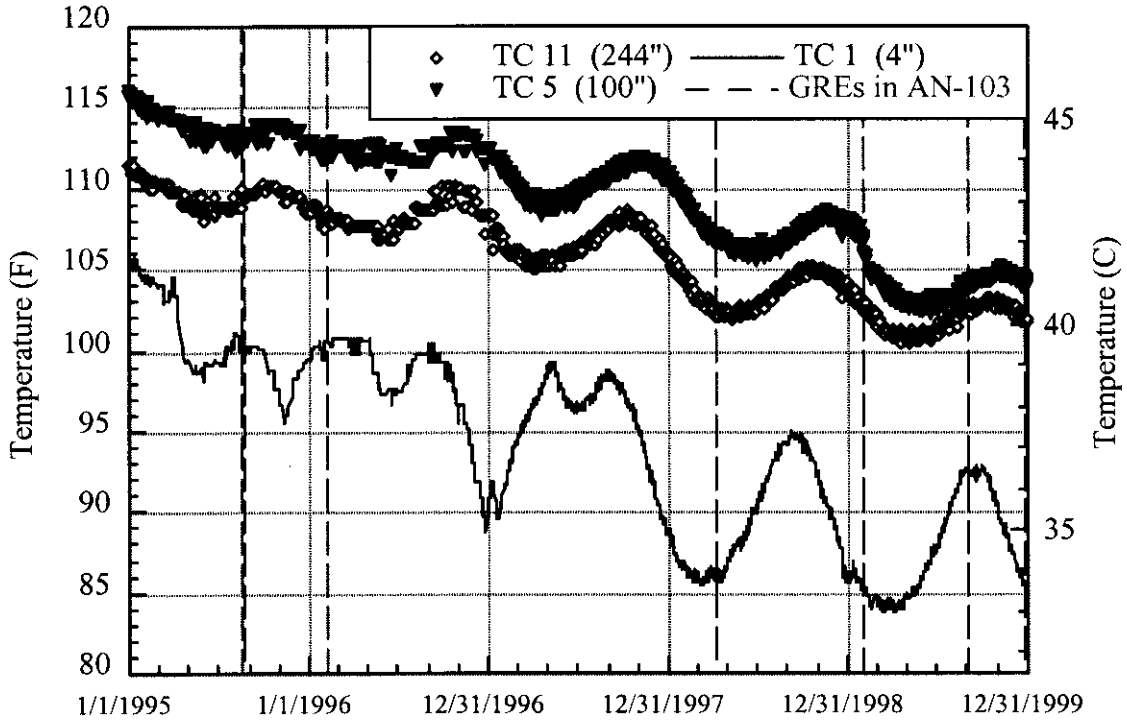

Figure 4-3. Tank 241-AN-103 Temperature History

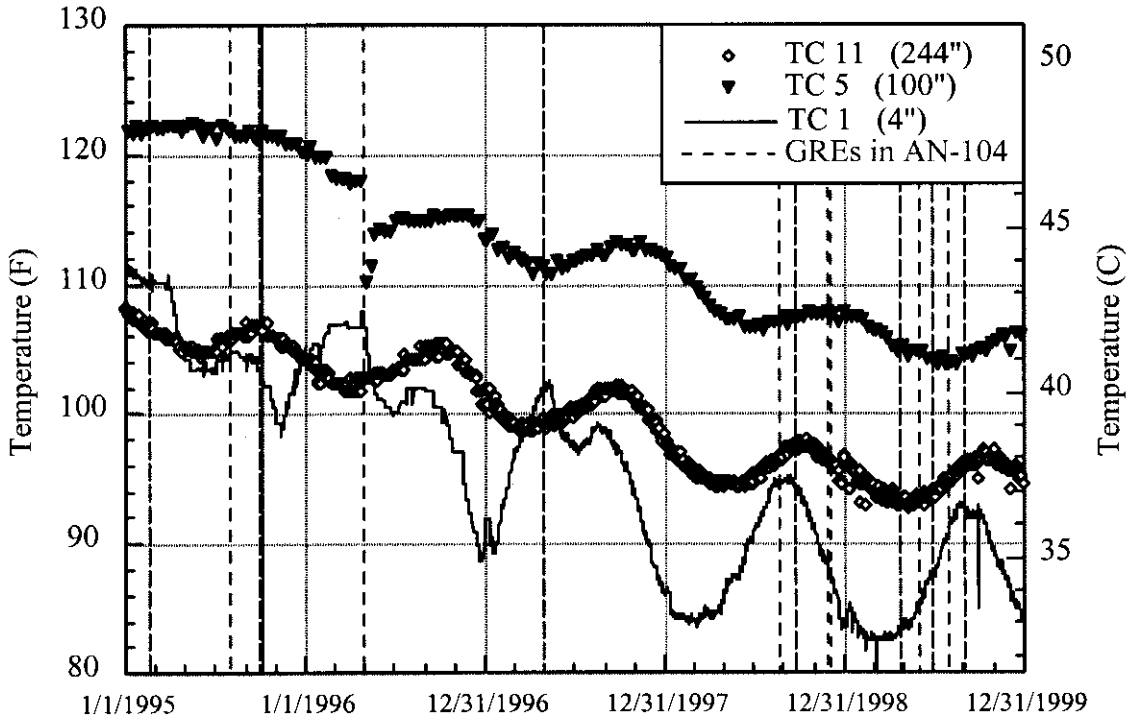

Figure 4-4. Tank 241-AN-104 Temperature History

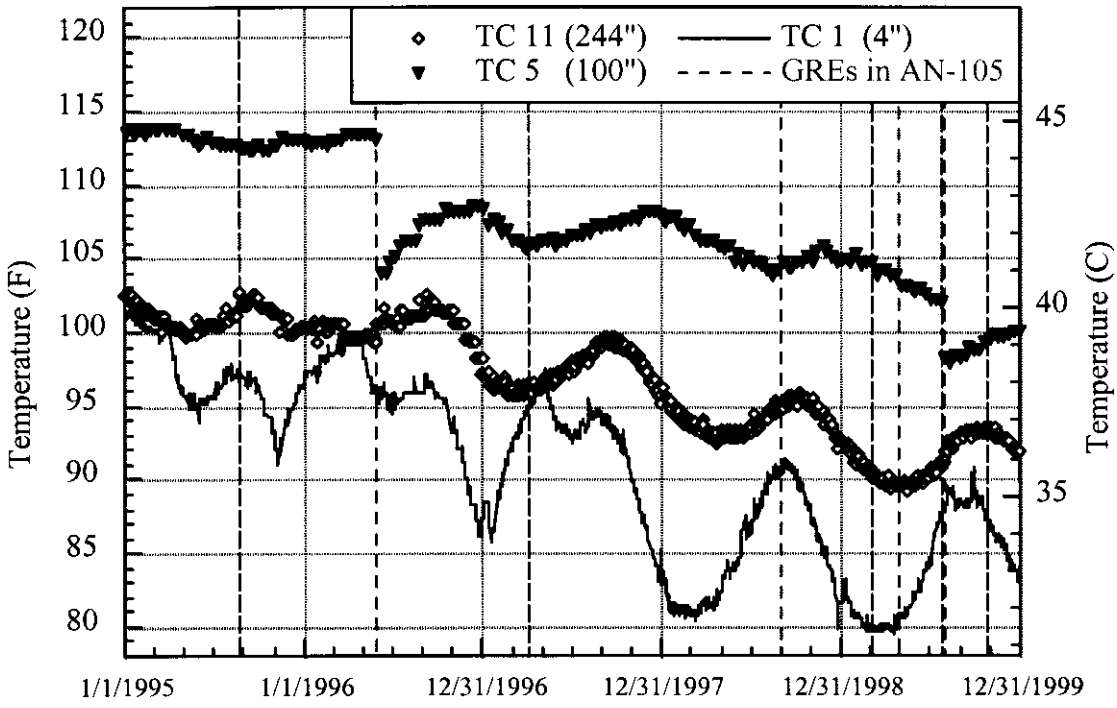

Figure 4-5. Tank 241-AN-105 Temperature History

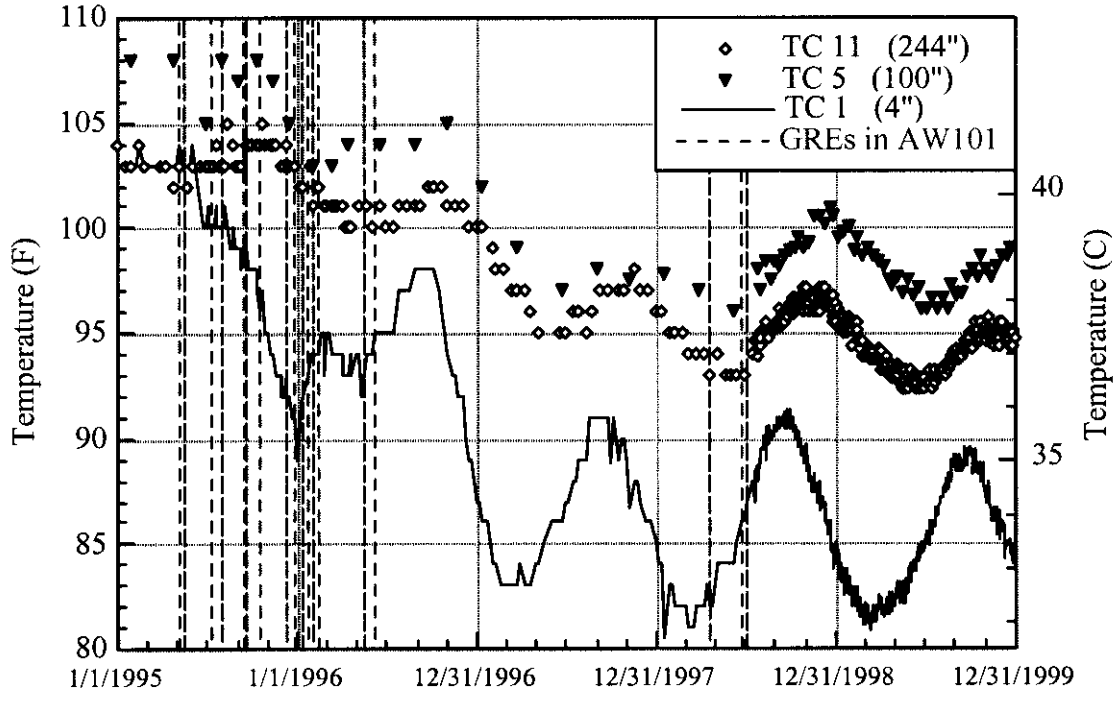

Figure 4-6. Tank 241-AW-101 Temperature History

The temperatures indicated by these three thermocouples in all three AN tanks and in AW-101 are for the most part insensitive to the occurrence of GREs. Two events in AN-105 (in June 1996 and in September 1998) and one event in AN-104 (in May 1996) resulted in noticeable temperature changes on TC5. The magnitude of the change in each of these cases and the subsequent rapid recovery suggest that a local disturbance of the waste brought cooler material, probably liquid from above, into contact with the thermocouples. For the most part, however, there was no change in the temperature indicated by the thermocouples in the waste during a GRE. This supports the conclusion that GREs in these tanks during this 5-year period were mainly local disturbances, and did not generally result in global movement of the waste.

Figure 4-7 shows the response of TC1, 4 in. from the bottom of the tank, over the 5-year period for the three AN tanks. The temperature traces have essentially identical patterns, and are quite obviously in response to changes in annulus ventilation flow rate and temperature variations (seasonal and unseasonal) in the incoming ambient air.

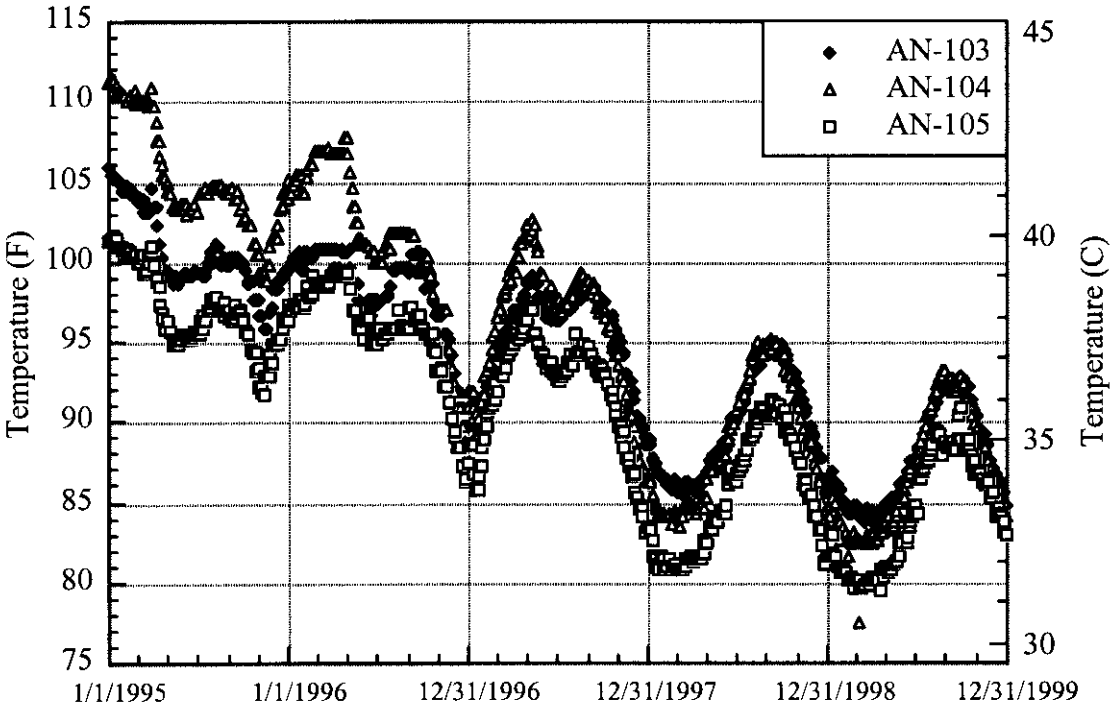

Figure 4-7. Comparison of TC1 Temperature History in Tanks 241-AN-103, 241-AN-104, and 241-AN-105

4.3.2 Tanks 241-SY-101 and 241-SY-103

The temperature histories from 1995 to 2000 for SY-101 and SY-103 are shown in Figures 4-8 and 4-9. Since the installation of the mixer pump in July 1993, there have been no GREs in SY-101. The temperature traces in Figure 4-8 show the effect of mixer pump operation. The small local increases in the temperature on the lowest thermocouple (TC1) result from excavation of the material around the thermocouple tree when the pump jet was aimed at it. Thermocouple TC5 and TC11 are both in the uniform-temperature mixed slurry region. Both of these thermocouples show a steadily increasing temperature after early 1998, as a result of the growth of the insulating crust layer. This temperature levels out in mid-1999, partly in response to the initial level growth mitigation efforts in this tank.

The temperatures in SY-103, shown in Figure 4-9, change very little on the average between 1995 and 2000 as neither the ventilation flows nor the waste configuration changed in SY-103 during this period. The average convective layer temperature, as registered by TC12, decreased about 2 °F while maintaining about a 7 °F seasonal variation. Note that the GREs in early 1995, end of 1996 and the summer of 1997 produced a sudden drop in the temperature at TC4 in the nonconvective layer 81 in. off the tank bottom. The GRE in late 1996 also affected TC2 and TC12.

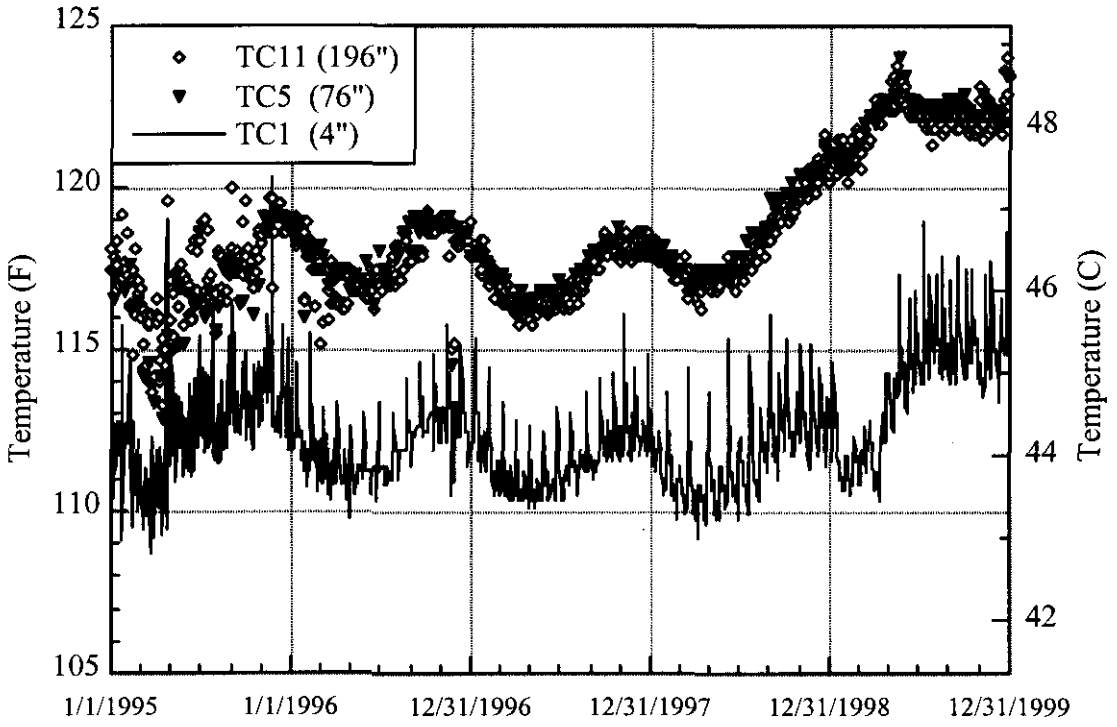

Figure 4-8. Tank 241-SY-101 Temperature History

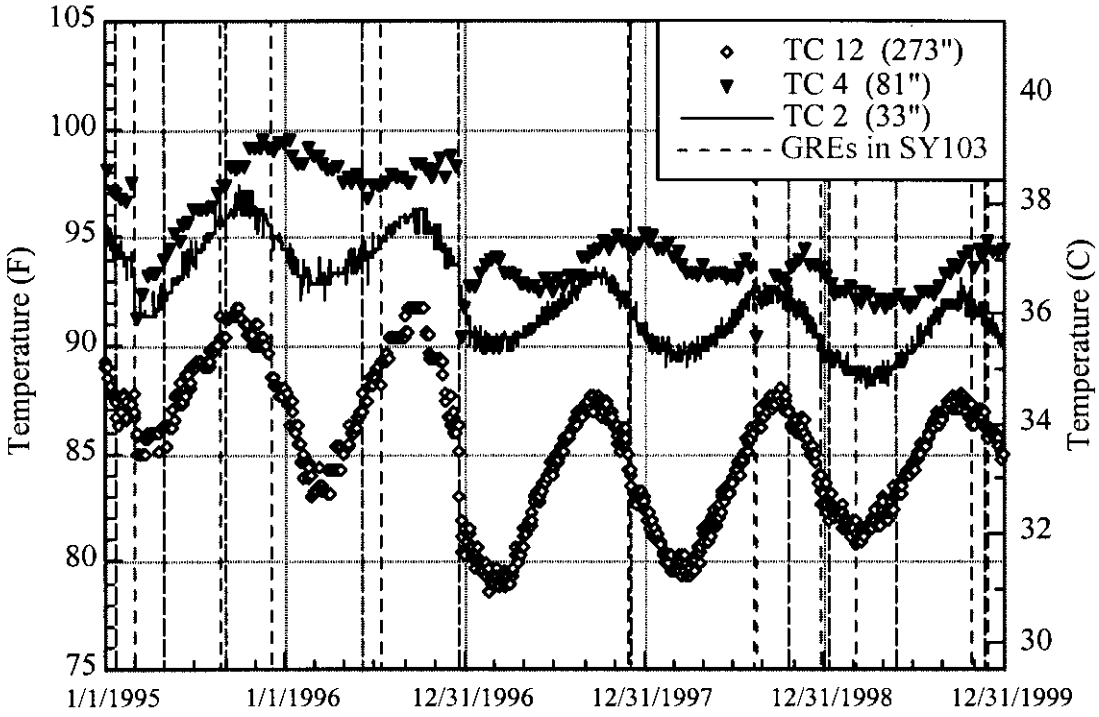

Figure 4-9. Tank 241-SY-103 Temperature History

4.3.3 Temperatures in the Concrete Pad Beneath the Tank

Instrumentation in the DSTs includes thermocouples to measure temperatures in the concrete dome, the outer tank wall, and the concrete pad beneath the inner steel shell. A total of 9 thermocouples are embedded approximately 2 in. below the surface of the 5.75-in. thick concrete pad just beneath the steel inner tank. The thermocouples are arranged in groups of 3, approximately 120-degrees apart, at radial distances of 4 ft, 21 ft, and 38 ft from the center of the tank. (Refer to drawings H-2-37751, H-2-3774, and H-14-020531 for details on all locations of all embedded thermocouples.) Concrete temperatures for SY-101 are recorded on its own DACS and they are read manually for SY-103. In AN-103, AN-104, AN-105, and AW-101, the SACS temperature data include one thermocouple at each radial location.

Figures 4-10 through 4-13 show the temperature response of the embedded thermocouples for these four tanks. In all cases, the temperatures in the concrete pad are somewhat lower than the waste temperature measured in the waste at 4 in. from the tank bottom (TC1). The concrete temperatures also show the expected dished distribution which is caused by the annulus inlet air entering directly beneath the center of the tank and flowing radially outward through cooling channels in the concrete.

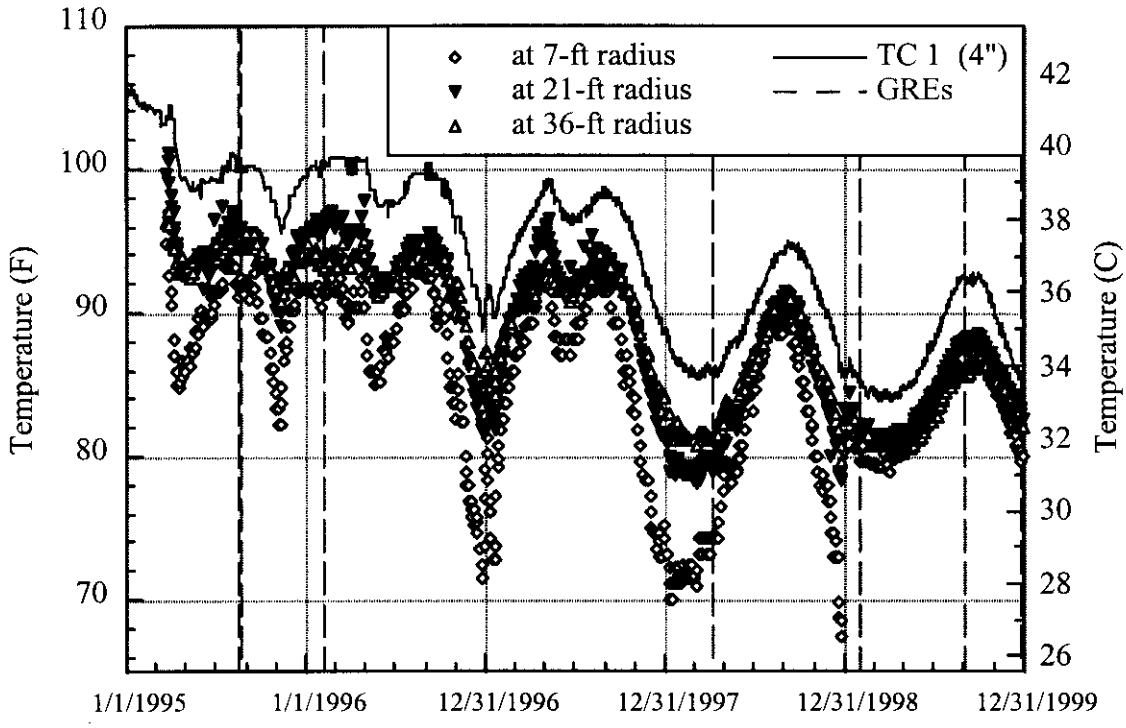

Figure 4-10. Concrete Temperatures beneath Tank 241-AN-103

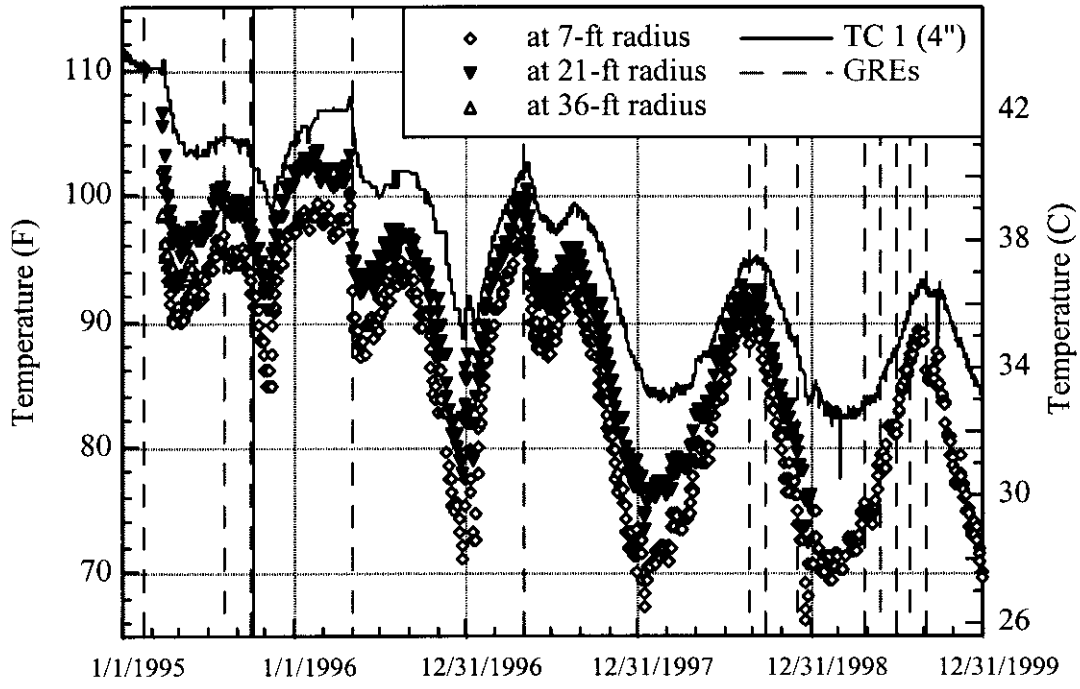

Figure 4-11. Concrete Temperatures beneath Tank 241-AN-104

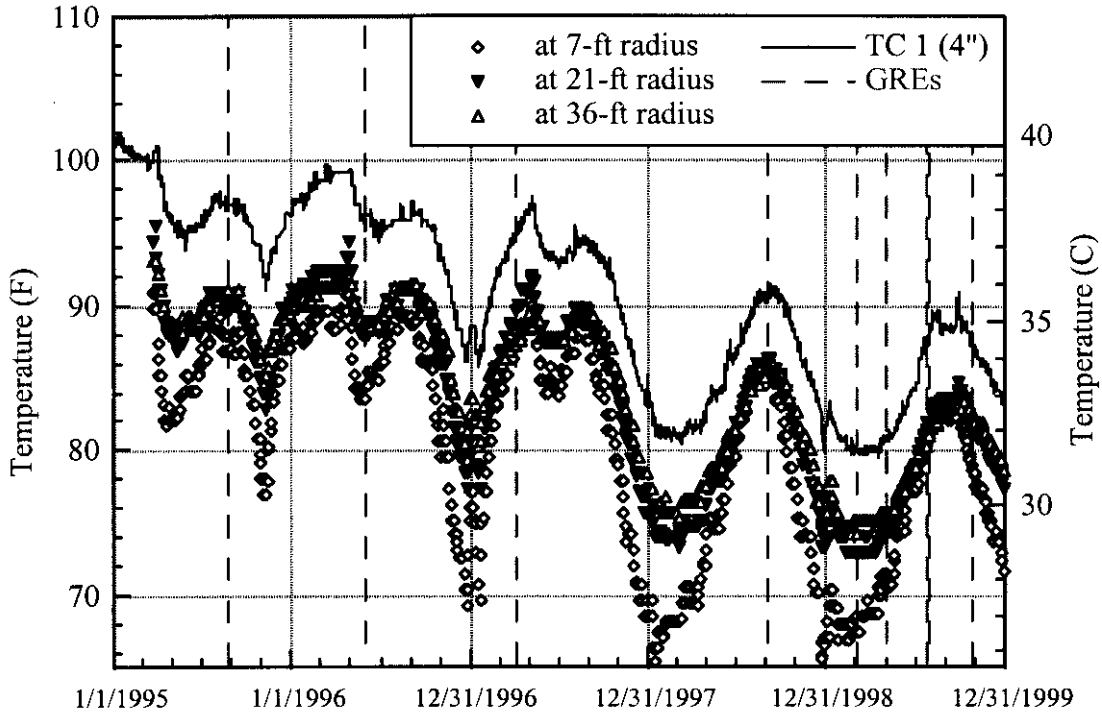

Figure 4-12. Concrete Temperatures beneath Tank 241-AN-105

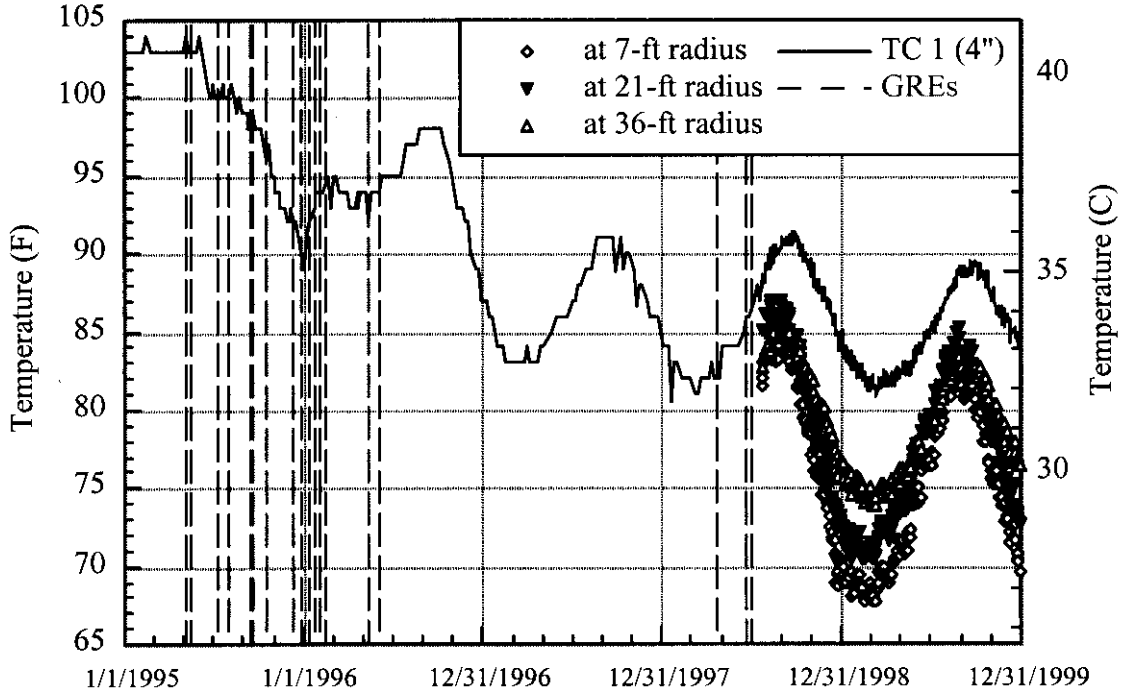

Figure 4-13. Concrete Temperatures beneath Tank 241-AW-101

The thermocouple at the 7-ft radius consistently shows the lowest value of the three measurements. The thermocouples at the 21-ft radius and the 36-ft radius generally show essentially the same value. When the annulus ventilation rate is decreased significantly for any reason, the temperature at the 21-ft radius rises above that at the 36-ft radius, creating the familiar "doughnut shaped" distribution seen in the waste in the DSTs. During the winter months, however, the enhanced heat transfer due to the lower temperature of the incoming air results in significantly lower temperatures at the 21-ft radius, compared to the 36-ft radius.

4.4 SUMMARY OF TANK THERMAL BEHAVIOR

Taking the convective layer temperature as most representative of the overall waste thermal state, temperatures in the FGWL tanks except SY-101 and SY-103 have decreased by 8 to 10 °F (4 to 6 K) in the 5-year period. Temperatures in SY-103 have changed only about 4 °F and hardly at all since 1996. SY-101 increased about 7 °F (4 K) because of crust growth. Since then, of course, transfer and back-dilution have reduced the temperature to 90 to 95 °F (Mahoney et al. 2000). This relatively small decrease in temperature appears to have had a pronounced effect on gas generation and release behavior as will be discussed in Sections 6.0 and 8.0.

The temperature histories indicate that GREs affect the waste around the thermocouple trees very infrequently. Two GREs appear to have disturbed the waste locally near the middle layer of the tank in AN-105, three in SY-103, and one in AN-104 during the 5-year period. No GREs caused detectable temperature changes in AN-103 or AW-101. A check of the more recent MIT thermocouple histories revealed no GRE influence. One must conclude that GREs are very local disturbances, and do not result in global movement of the waste.

5.0 WASTE CONFIGURATION AND PROPERTIES

The typical waste configuration in tanks subject to buoyant displacement includes a convective liquid layer overlying a layer of nonconvective mud-like material. In most cases, a floating crust layer also lies above the convective layer. The dimensions, characteristics, and properties of each layer must be understood to evaluate the flammable gas hazard in the FGWL DSTs. A variety of in-situ measurement and monitoring methods are available to determine the thickness and properties of each layer. Also, after several years of observation, changes in layer dimensions and retained gas volume or, in most cases, lack of significant change, are also known.

This section focuses on the dimensions and overall characteristics of each of the major divisions of the waste configuration. Section 5.1 depicts how the waste configuration is derived from temperature profiles, changes in cable tension plots from the ball rheometer, and information from neutron and gamma scans. Section 5.2 discusses the characteristics and properties of the major waste layers, and Section 5.3 summarizes the density and rheology measurements obtained with the ball rheometer. Section 5.4 describes the changes in waste configuration based on changes in the temperature profiles, waste level, and neutron and gamma logs.

5.1 DETERMINING WASTE LAYER BOUNDARIES

A simplified model for DST waste configuration is shown in Figure 5-1. The thickness of each of these layers can be estimated from temperature profiles and changes in cable tension with depth in the ball rheometer data. Layer boundaries can also be detected in many cases from neutron and gamma logs through the MITs. Each of these methods is discussed in Sections 5.1.1 through 5.1.3, below. Section 5.1.4 gives a summary of the waste configuration in each tank.

5.1.1 Layer Dimensions from Waste Temperature Profiles

The temperature profiles from the MITs and thermocouple trees provide a measurement of the height of the nonconvective layer and, prior to the advent of the small-bore neutron/gamma probe, the only available measurement of the thickness of the floating crust layer. Because the temperature gradient is parabolic in a nonconvective, heat-generating region and uniform in a convective region, the boundary can be located where the uniform and parabolic temperature profiles intersect. This is usually accomplished by visually interpreting a graph. The uncertainty is usually assigned as half the distance between temperature measurements, though it may be higher if the transition is indistinct or lower if it is particularly clear.

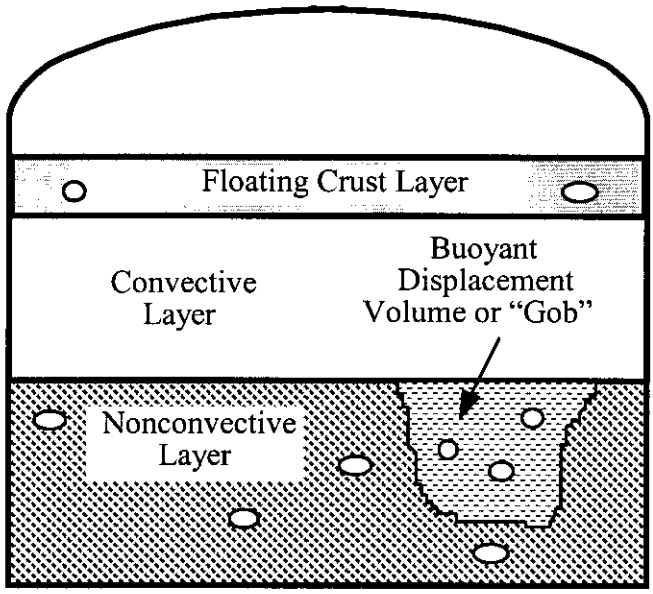

Figure 5-1. Waste Configuration for a Typical Double-Shell Tank Experiencing Buoyant Displacement Gas Release Events

For example, consider the segment of the temperature profile from the MIT validation probe near the top the nonconvective layer from SY-103, as shown in Figure 5-2. The nonconvective layer height is taken as the intersection of straight lines extending the convective and nonconvective segments of the temperature profile. This profile is quite distinct, and the total uncertainty band spans only three measurements, or 30 cm (12 in.). We take this band to represent four standard deviations ($\pm 2\sigma$). Thus, the plot is interpreted to give a nonconvective layer height of 325 ± 7 cm (128 ± 3 in.) where one standard deviation is 7 cm (3 in.).

The thickness of the floating crust layer is estimated in a similar way. Figure 5-3 shows a segment of the MIT validation probe temperature profile through the crust. The upper and lower surfaces are located the same way as the top of the nonconvective layer, and each has its own uncertainty band. The crust thickness is simply the difference between the two elevations. The uncertainty in the thickness is taken as the square root of the sum of the squares of the uncertainties of the boundary elevations. For SY-103, that is 58 ± 13 cm.

The temperature profiles shown in these two examples represent only a single location; a potentially large but unknown uncertainty exists in assuming that they represent the entire tank. For estimating the crust thickness, the MIT validation probe is the only measurement available, and we have no information on the potential spatial variation. For the nonconvective layer height, however, we can use the ball rheometer cable tension for a second, very precise measurement.

We chose not to make estimates of layer thickness from the temperature profiles of the old thermocouple trees because they have a very high uncertainty due to wide spaces between thermocouples. The temperature profile from the standard MIT thermocouples is not used because the thermocouples are in the same location as the validation probe.

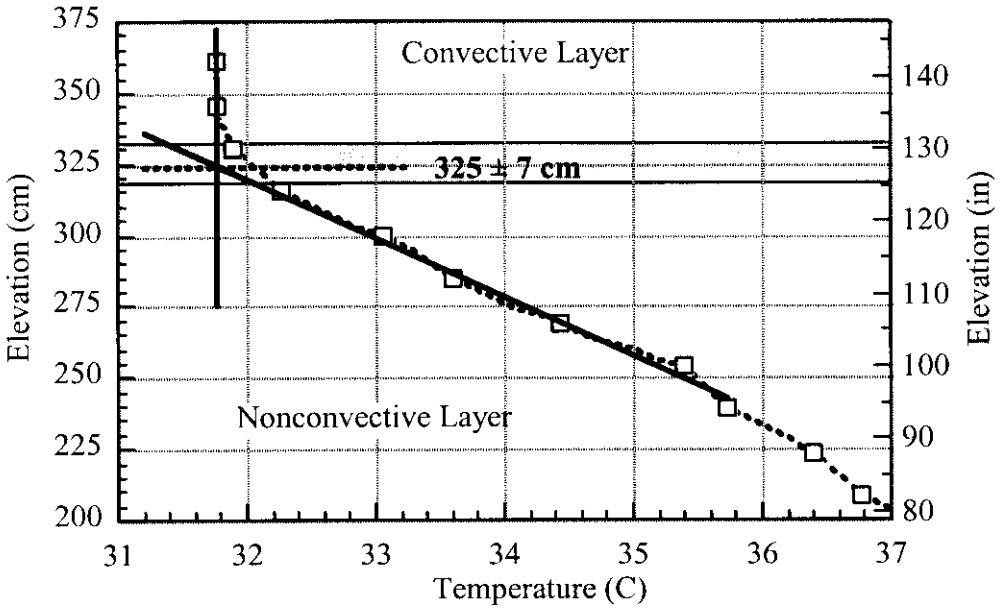

Figure 5-2. Temperature Profile at Top of Nonconvective Layer in Tank 241-SY-103

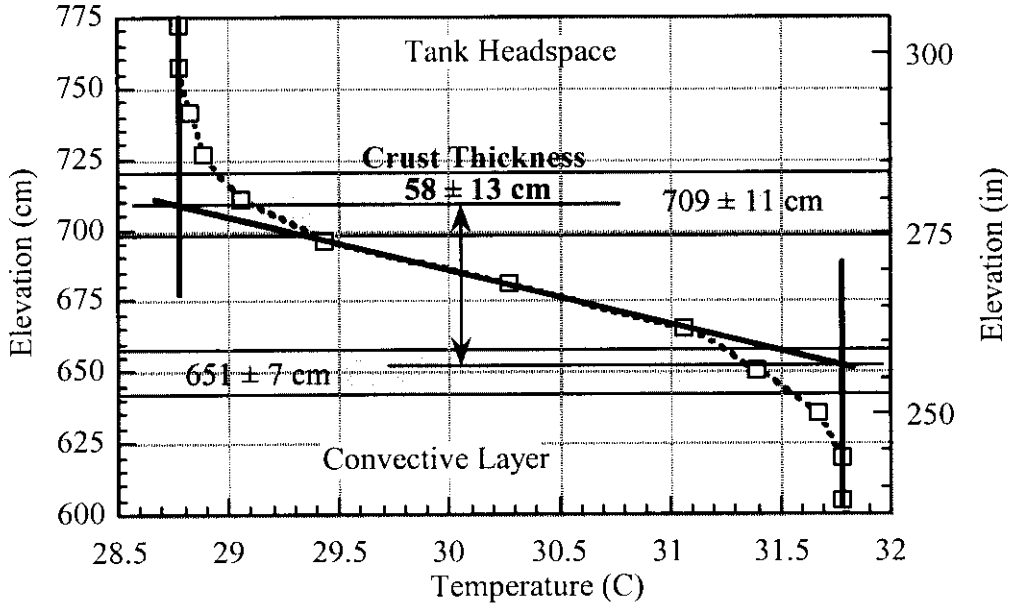

Figure 5-3. Temperature Profile Through the Crust Layer in Tank 241-SY-103

Temperature profiles for all six tanks (using 1997 data for AW-101, 1993 and 1994 data for SY-101, and 1996 data for the other tanks) are shown in Figure 5-4 for a visual comparison of the nonconvective layer depth and (in some tanks) crust thickness. The temperature profile for SY-101 just prior to Event I is shown for comparison to the other tanks currently exhibiting gas

releases. All profiles except the SY-101 pre-pump profile were recorded with the MIT validation probe.

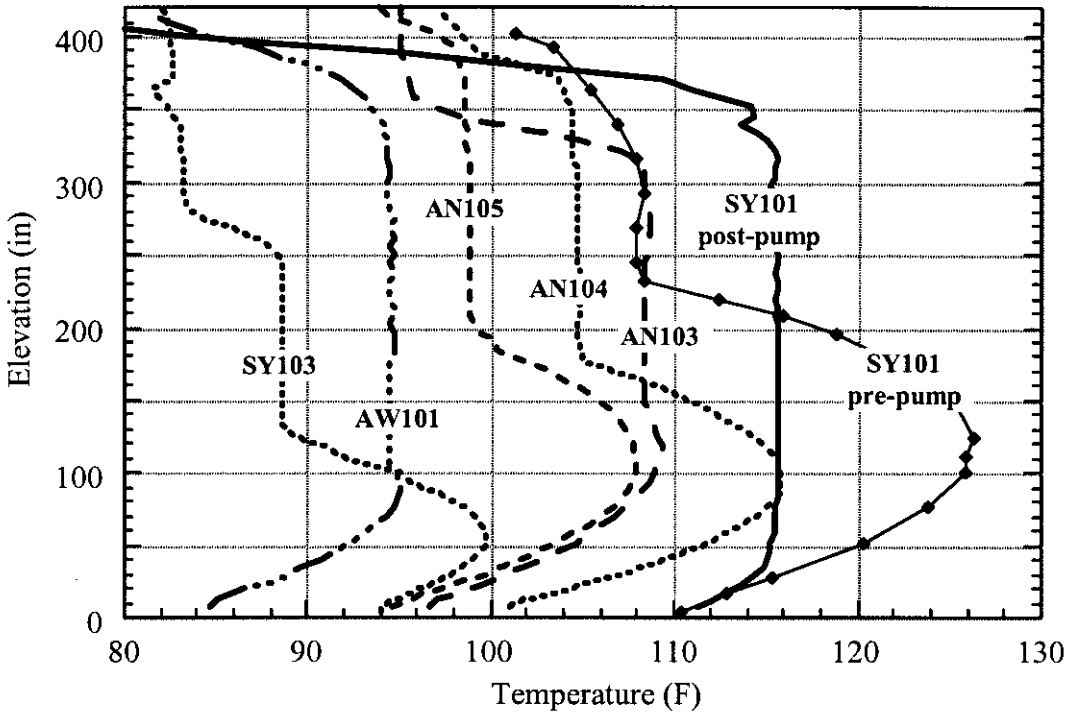

Figure 5-4. Temperature Profiles from All Six Double-Shell Tanks

5.1.2 Layer Boundaries from Ball Rheometer Data

The ball rheometer locates the liquid level and the top of the nonconvective layer in each riser to within one ball radius (4.6 cm, 1.8 in.). Passage of the ball through the liquid surface is taken to be the midpoint of the decrease in tension due to increasing buoyancy as the ball submerges. This occurs at approximately the same elevation in both risers. Figure 5-5 shows that the transition occurred at 705 ± 5 cm (278 ± 2 in.) below home position in AN-105. This equates to an elevation of 1041.8 ± 5 cm (410.2 ± 2 in.) above the tank bottom, which compares very closely to the waste level of 1041 ± 5 cm (410 ± 2 in.) measured by the ENRAF™ gauge on that day.

The interface between the convective and nonconvective layers is determined the same way as the liquid level. The cable tension begins to decrease as the ball passes into material with increasing viscosity, density, and yield strength. Interface passage is taken as the point at which tension begins to decrease from the constant value observed in the convective layer. This is illustrated for AN-105 in Figure 5-6. In this tank, the top of the nonconvective layer is 50 cm (20 in.) higher under Riser 16B than under Riser 1B.

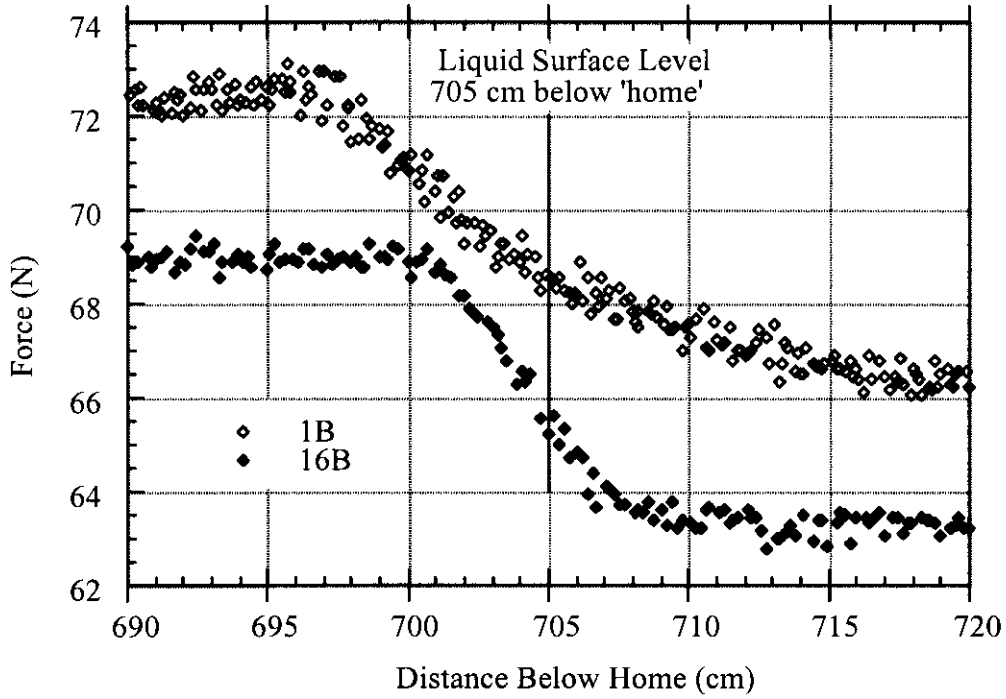

Figure 5-5. Liquid Level Passage in Tank 241-AN-105

5.1.3 Information from Neutron and Gamma Logs

A small-bore neutron and gamma probe has been developed to operate inside the tube designed for the MIT validation probe. The neutron count measured by the probe indicates the concentration of hydrogen atoms surrounding the probe. Thus, the neutron log is essentially a measure of the relative fraction of water, which is a surrogate for liquid waste. A low neutron count may indicate the presence of gas or a high solids volume fraction. A high neutron count would indicate a dilute region. The neutron probe is quite sensitive at high gas fractions (20 to 50% void) but does not discriminate low gas fractions very well.

The gamma count indicates the relative amount of cesium-137 which is the main gamma source in the waste. Since cesium is quite soluble, the gamma count is also a surrogate for liquid. A low gamma count also indicates either gas or a high solids fraction. However, unlike the neutron log, a dilute solution containing less dissolved cesium also produces a low gamma count. The gamma response is more linear than that of the neutron probe, but a sharp definition of layer boundaries still requires a large difference in liquid content.

Neutron and gamma logs were made in the two MITs in SY-101 approximately every week since early February 1999. With the high void fraction at the base of the crust layer and moderate void fraction elsewhere in the crust, the neutron and gamma logs gave very good information about the detailed structure of the crust. This is illustrated by plots of the neutron and gamma logs obtained December 28, 1999, in MIT 17B shown in Figures 5-7 and 5-8. These data have been

smoothed by using a weighted least-squares technique to remove random fluctuations. The actual data are shown as small dots to give some sense of the scatter in the raw data.

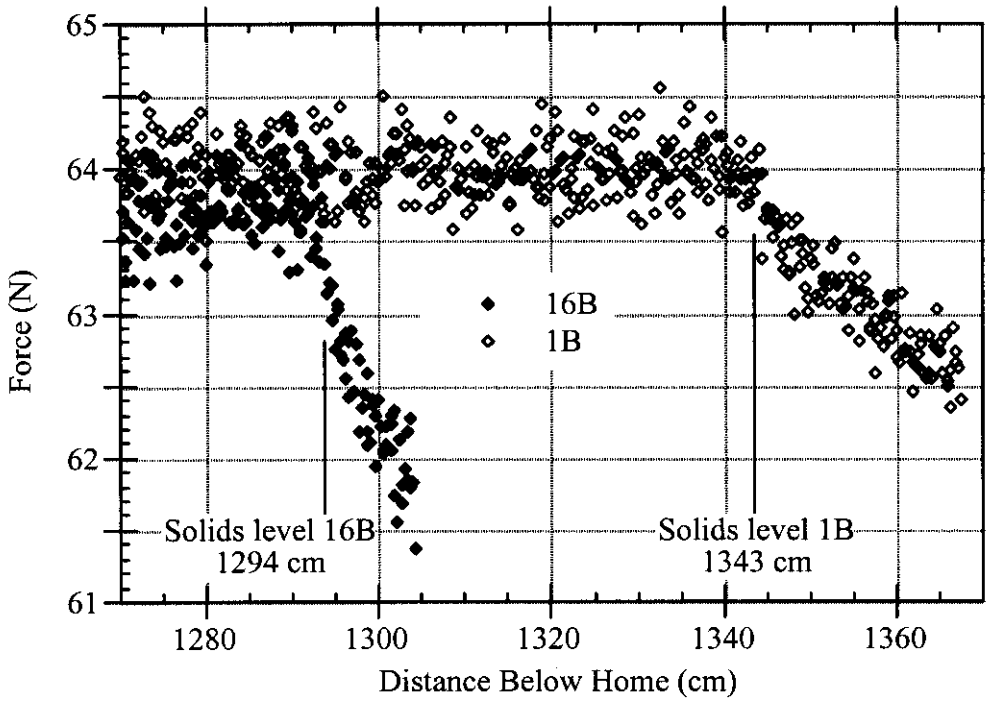

Figure 5-6. Nonconvective Layer Entry in Tank 241-AN-105

These logs were taken about one week after the first transfer and back dilution campaign. The thick crust is still intact but the upper 25 to 38 cm (10 to 15 in.) have been dissolved and the slurry under the crust has been diluted slightly with a small water addition at the 250-cm (100-in.) level. Both logs show the high-gas bubble slurry region at the crust base. The gamma log probably provides somewhat better definition of this layer. In either case, the crust base is assumed to be at the midpoint of the region where the count sharply decreases from the uniform value in the mixed slurry below. The uncertainty is estimated as one quarter of the total elevation difference of this region. For the neutron log the uncertainty is about ± 8 cm (± 3 in.) and about ± 5 cm (± 2 in.) for the gamma log.

Though data from the neutron/gamma probe was very useful in tracking the behavior of the crust layer in SY-101, it is not so useful in the other tanks. Except for AN-103 and AW-101, the crust layers are generally quite thin and have a relatively low void fraction compared to SY-101. The nonconvective layers of all the tanks have a much lower void fraction that is difficult to detect with these devices. Nevertheless, in combination with temperature profiles and other data, the neutron/gamma data provide confirmatory evidence of the location and characteristics of the crust and nonconvective layers of these tanks.

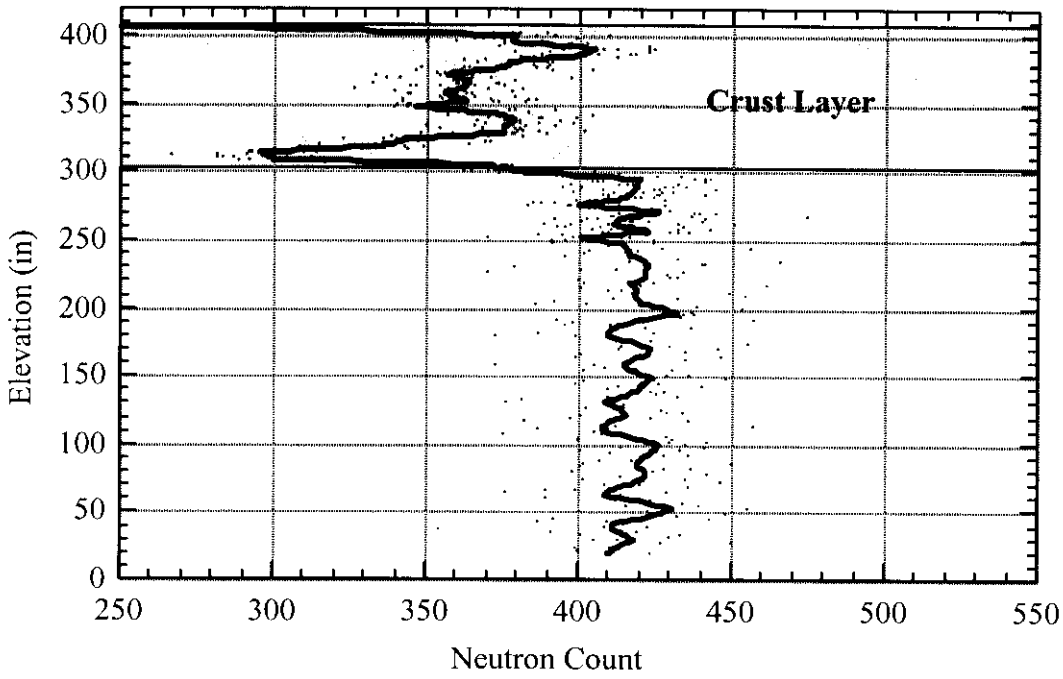

Figure 5-7. Tank 241-SY-101 Neutron Log from December 28, 1999

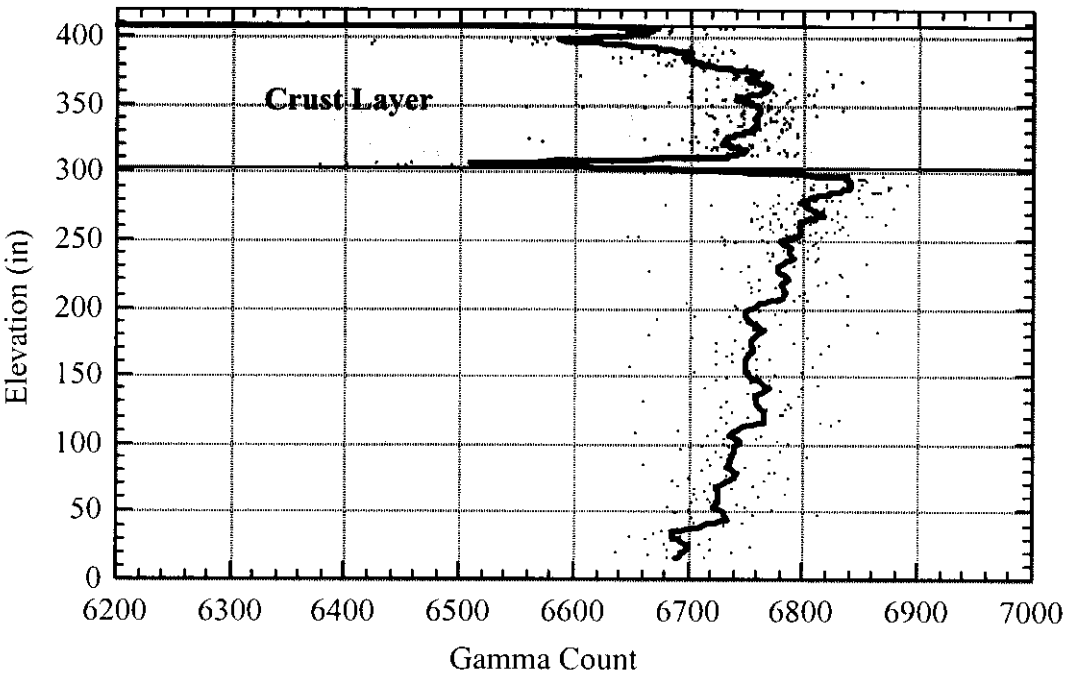

Figure 5-8. Tank 241-SY-101 Gamma Log from December 28, 1999

5.1.4 Summary of Waste Layer Dimensions

Table 5-1 contains a summary of the waste configurations for all tanks determined from the ball rheometer data and temperature profiles from the same time period. Possible changes to the waste configuration in the three years since then are postulated in Section 5.4.

Table 5-1. Summary of Waste Layer Dimensions

Item	AN-103	AN-104	AN-105	AW-101	SY-101[a]	SY-101[b]	SY-103
Waste Surface Level (cm)							
Riser	2A	2A	2A	2A	1C	1C	2A
ENRAF™	**884 ± 3**	**979 ± 3**	**1041 ± 3**	**1040 ± 3**	**1048 ± 5**	**1019 ± 3**	**691 ± 3**
Crust Thickness (cm)							
Riser	15A	15A	15A	15A	(est.)	17B/C	17B
MIT v.p.	**89 ± 16**	**41 ± 7**	**45 ± 10**	**80 ± 20**	**80 ± 30**	**100 ± 30**	**58 ± 13**
Nonconvective Layer Height (cm)							
Riser	15A	15A	15A	15A	17B		17B
MIT v.p.	375 ± 8	452 ± 8	490 ± 20	320 ± 10	600 ± 10		325 ± 7
Riser	16B	16B	16B	13A			22A
Ball Rheo.	386 ± 5	372 ± 5	405 ± 5	278 ± 5			329 ± 5
Riser	1B	1B	1B	1C			17C
Ball Rheo.	374 ± 5	412 ± 5	455 ± 5	259 ± 5			320 ± 5
Average	**378 ± 7**	**410 ± 40**	**450 ± 40**	**286 ± 30**		**N/A**	**325 ± 5**

Notes:

(a) SY-101 conditions just before Event I, June 26, 1993.

(b) SY-101 conditions during VFI deployment after about 1 year of mixing.

5.2 CHARACTERISTICS AND PROPERTIES OF THE MAIN WASTE LAYERS

The waste layers have very different physical properties (density, gas fraction, yield strength). In-situ measurements with the ball rheometer (Stewart et al. 1996a) indicate that the convective layer is a Newtonian fluid, while the nonconvective layer is a shear rate-dependent material with a finite yield strength (viscoplastic) and is able to retain gas that is generated in the waste. The floating crust layer consists of the same material as the nonconvective layer but contains a higher gas fraction and is somewhat stronger based on experience with the crust in SY-101 (Rassat et al. 2000).

This section provides a general description of each layer, highlighting the salient features and behavior. Section 5.2.1 covers the floating crust layer; Section 5.2.2 discusses the convective liquid; and Section 5.2.3 describes the characteristics of the nonconvective layer.

5.2.1 Floating Solids (Crust) Layer

Video of the waste surface (Meyer et al. 1997), core sample extrusions, and observations during waste-penetrating operations (e.g., installing a thermocouple tree, removing sludge weights, etc.) demonstrate the universal existence of a substantial layer of floating solids in tanks that have buoyant displacement gas releases. The appearance of a hard, broken upper surface gives rise to the term "crust" to describe this layer.

The processes of crust formation are not well understood but are probably more mechanical and thermodynamic than chemical. The crust is likely an accumulation of bubble-particle agglomerates that break free from the nonconvective layer. This behavior has been observed in laboratory waste samples.[6] Some of the nonconvective waste that rises during buoyant displacement GREs undoubtedly helps maintain the crust layer as well. Since the temperature in the crust decreases with elevation, further growth occurs by precipitation of solids whose solubility decreases with cooling.

Each tank (except SY-101) appears to have a characteristic crust thickness that does not change over the years. There is evidence in AW-101 that a decrease in temperature caused the crust layer to thicken at the expense of the nonconvective layer (see Section 5.4.4). This suggests that the equilibrium state of the crust with the convective layer on which it floats is a complex balance between the temperature-dependent solubility of the component species and the processes that dissipate the heat generated in the waste. See Kubic and Beloussov (1999) for a discussion of possible thermal-solubility interactions in the crust.

If the assumed crust creation mechanism is correct, gas is constantly being supplied to the base of the crust (as well as being generated by radiolysis and chemical reactions within it). To maintain the observed equilibrium, the gas must migrate through the crust at about the same rate as it is supplied. At the same time, in SY-101 before 1998, most of the gas released below the crust in mixer pump runs passed through the crust with relative ease. This shows that the crust is not a continuous barrier and that some kind of "fast" passages exist that allow gas to pass through it easily (Rassat et al. 1999). The above-described concept of the crust layer is illustrated in Figure 5-9.

Observations from recent core samples indicate that the submerged portion of the crust consists of the essentially same kind of material as the upper portion of the nonconvective layer. The extrusion photographs from the few recent DST core samples that included crust material show that the crust and nonconvective layer have a very similar appearance (Meyer et al. 1997). Laboratory analysis confirms that the composition of the two layers is virtually the same (Herting et al. 1992; Jo 1997; Wilkins 1997; Baldwin et al. 1995). At the same time, the single RGS measurement from the crust of AN-103 indicates a void fraction of about 0.16, which is only a little above the estimated neutral buoyancy value and of the same magnitude as the peak void fraction in the nonconvective layer. The void fraction measured in the SY-101 crust was much higher, ranging from over 0.5 at the base to about 0.2 in the top third (Stewart et al. 1998; Mahoney et al. 1999).

[6] Observed in chemical simulants by Dr. Steve Agnew, Los Alamos National Laboratory, and in actual waste by Dr. Dan Herting, PHMC.

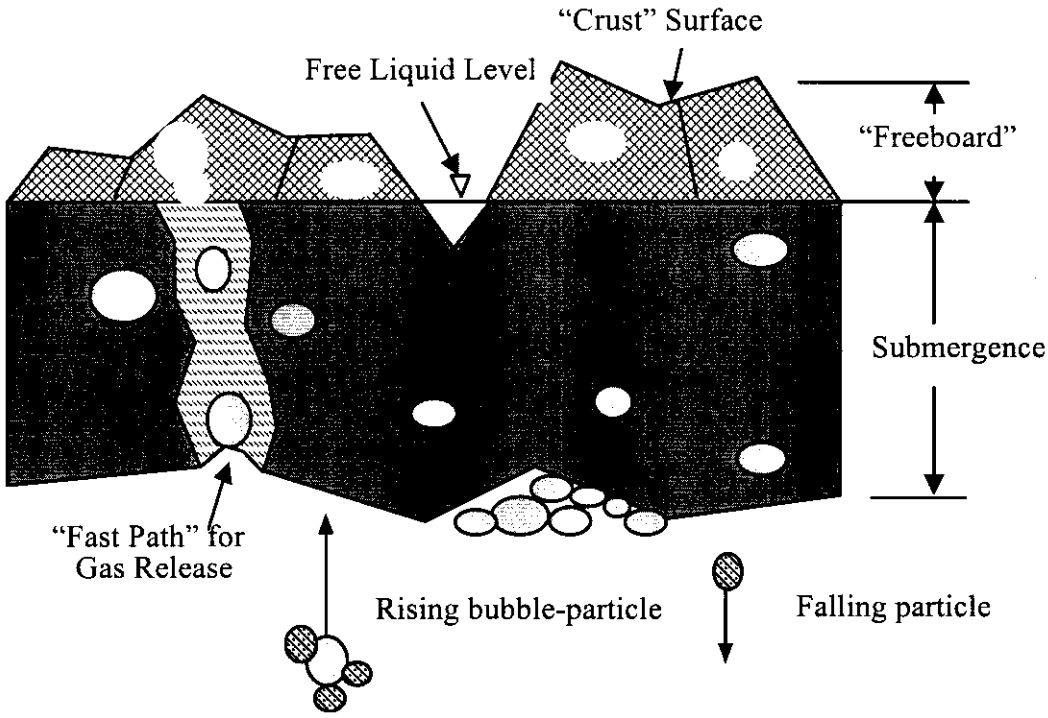

Figure 5-9. Illustration of Salient Features of the Crust Layer

Various crust-disturbing activities in SY-101, including the VFI runs have provided qualitative data from which the strength of each portion can be estimated. Coupled with void fraction measurements and data from the neutron and gamma logs, a detailed picture of the SY-101 crust was constructed as illustrated in Figure 5-10. Because of its high void fraction and the resulting buoyant forces supporting the freeboard, compaction forces are much higher in the crust than in the nonconvective layer. This creates a much higher yield stress in the crust that ranges from <100 Pa at the base to ~3,000 Pa near the top. It is not known how closely the much thinner crust layers in the other tanks may follow this conceptual model but physics dictate a higher void fraction and somewhat higher yield stress than the nonconvective layer.

Consistent with these observations and measurements, we assume that the crust consists of nonconvective layer material floating at slightly above neutral buoyancy such that a large fraction of its thickness is submerged below the free liquid surface. The submergence fraction determines how much the crust void fraction exceeds the neutral buoyancy value. We assume gas in the waste below the liquid surface is retained as bubbles that displace the liquid-solid matrix, as in the nonconvective layer:.

In the "freeboard" above the liquid level, we assume that the bubble structure is maintained though the gas they contained is replaced with air. The material between the bubbles is assumed to have the same porosity as the submerged waste, but most of the liquid has drained away and occupies only a fraction of the porosity. The submerged crust material is relatively weak, like the nonconvective layer, and the potentially stronger, brittle material on the exposed surface is assumed to be thin and/or fractured such that the bulk of the crust layer is not supported in any way by attachment to the tank wall.

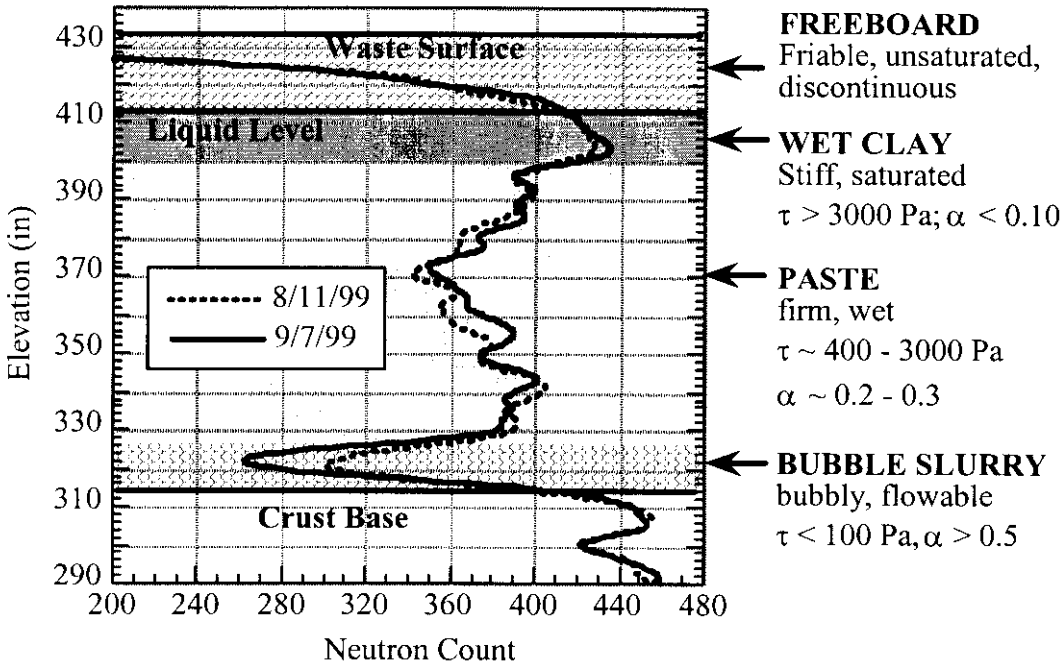

Figure 5-10. Tank 241-SY-101 Crust Dimensions and Properties

Since the crust is floating, it can be modeled using the simple buoyancy principle. Using Archimedes' principle, the crust submergence depth and "freeboard" height can be related to the average crust void fraction and material densities. This model was extended to include the effects of dilution and dissolution to predict the behavior of the SY-101 crust during transfer and back dilution. The details of the model are given in Stewart et al. (1999).

Knowing the crust freeboard height, one can estimate the average crust void fraction. In SY-101 the freeboard height was assumed to be the difference between the two level instruments since one had been flushed often, dissolving a depression in the crust down to the liquid level, and the other had not, thus measuring the elevation of the upper crust surface. In July 1998 the difference between the levels in SY-101 was about 30 cm (12 in.). Assuming that this difference was the freeboard, only 70 to 75% of the crust was submerged (of a total thickness of 100 to120 cm [40 to 50 in.]) at that time. The buoyancy model gives a void fraction of 0.3 to 0.4 for these conditions, which matches the 0.31 void fraction measured in mid-crust with the VFI measurements (Stewart et al. 1998). At the time of the earlier VFI measurements in 1994–1995, the difference between the levels was about 10 cm (4 in.). This is a 90% submergence for a crust thickness of 100 cm (40 in.) and indicates a much lower void fraction of 0.19, more consistent with the measurement in the AN-103 crust.

There are no similar data from which to estimate the submergence fraction in other tanks. Therefore, we somewhat arbitrarily set the submergence fraction to the 0.96 which is required for the buoyancy model to match the measured crust void fraction in AN-103, which is probably

more representative of the other tanks than SY-101. This value of submergence gives reasonable crust void fractions, from 0.11 to 0.14, slightly in excess of the neutral buoyancy values.

5.2.2 Convective Liquid Layer

As its title implies, the convective layer is a liquid in which thermal convection dominates. Properties of this layer are uniform due to the constant convective mixing. It has a relatively low viscosity and behaves essentially as a Newtonian fluid. Except for the few particles that occasionally fall from the crust and the small bubbles or bubble-particle combinations that rise from the non-convective layer, it is "clear" liquid. However, immediately after a GRE that has disturbed the nonconvective layer significantly, a much higher solids fraction could be expected. In SY-101, mixer pump operation kept most of the solids suspended in a mixed slurry with a solids volume fraction of 10 to 12%. When extruded, core samples of this material appeared entirely solid due to precipitation of additional solids on cooling.

The liquid is saturated or near saturation with dissolved sodium salts and has a relatively high density ranging from 1,400 to 1,600 kg/m^3. In some tanks core samples of this layer show a small amount of white solids that have precipitated from the saturated solution as it cooled to hot-cell temperatures. Cesium-137, the main gamma producer in the waste, is soluble and resides mainly in the liquid. Therefore, the convective layer has about the same gas generation and heat loading per unit volume as the nonconvective layer.

5.2.3 Nonconvective Layer

The nonconvective layer contains solid particles that have precipitated out of the solution as the waste cooled. As the name implies, the settled solids have a yield stress that inhibits convection. In-situ ball rheometer measurements show that the yield stress increases approximately linearly with depth from zero at the top surface to 200 to 300 Pa at the bottom. Particle sizes are generally in the few-micron range. When the solids are disturbed, settling is very slow.[7] The solid particles are relatively loosely packed with volume fractions ranging from 0.2 to 0.3. This makes the density 1,600 to 1,700 kg/m^3, only slightly greater than that of the convective layer.

The small particle size and limited lithostatic load dictate that gas retention is in the form of bubbles that displace the particles rather than occupying the interstitial pores between particles. The bubble size distribution is dominated by the few millimeter range though bubbles on the order of a centimeter have been observed in core extrusions (Meyer et al. 1997).

As will be described in detail in Section 7.1, the FGWL DSTs experience buoyant displacement gas releases when a portion or "gob" of the nonconvective layer accumulates sufficient gas to become buoyant. Buoyant displacements involve only a small portion of the nonconvective layer. Based on the measured gas release volumes and the neutral buoyancy void fractions computed from the layer densities, the diameter of a typical gob is only a few meters. Some of

[7] In SY-101, significant settling was still occurring a month after mixer pump operation was terminated April 2, 2000.

the larger releases might involve two or three gobs over a period of an hour or more (Barker et al. 1999). The large releases in SY-101 involved four to six gobs within a few minutes.

Since a buoyant displacement severely disturbs the waste in the vicinity of the buoyant gob(s), and buoyant displacements occur at the rate of one or more per year, the nonconvective layer is in a constant state of flux. Some areas of the tank contain almost enough gas to go buoyant while others have relatively little gas after having just experienced a buoyant displacement release. The rest of the waste resides in all states in between.

The configuration and properties of the nonconvective layer, therefore, can be considered to represent a dynamic steady state. This means that samples or measurements from several risers may be quite different, the collection of these data is just as representative of the tank as another set from another selection of risers or from the same set at a different time. Another way to describe the situation is that occurrence of a GRE shortly before or after a measurement or sample in no way invalidates the data since GREs are an important feature of the waste.

5.3 WASTE DENSITY AND RHEOLOGY

The physical properties of the waste that are most important for characterization and modeling are the density, yield stress, and viscosity. The density is a measure of the overall concentration of the salt solution; the difference between the density of the supernatant liquid and that of the nonconvective layer determines the neutral buoyancy void fraction. The yield stress determines how large a bubble can be held in the nonconvective layer, and the viscosity determines how the waste moves. These properties, particularly yield stress and viscosity, may vary considerably with elevation, though some tanks show trends in density as well. It is important to consider these trends when modeling the gas retention and release behavior of the waste.

Section 5.3.1 gives the density profiles for each tank; Section 5.3.2 deals with the rheology of the nonconvective layer; and Section 5.3.3 summarizes the average properties for each tank.

5.3.1 Density Profiles

Figures 5-11 through 5-16 give the density profiles for the six DSTs on the FGWL. The horizontal dashed line on the plots represents the average height of the top of the nonconvective layer. The two vertical lines with the corresponding numbers indicate the average densities (in g/mL) of the convective and nonconvective layers. For all the tanks except SY-101, the densities in the convective layer were measured with the ball rheometer, and the nonconvective layer densities were taken from core sample data.[8] In SY-101 (Figure 5-15) the density profile was measured with the ball rheometer for conditions one year after the waste had been mixed by the pump. The average densities in the convective and nonconvective layers before mixing are also shown. The nonconvective layer densities for SY-103 are composites of several cores, and the elevation shown is arbitrary.

[8] Data were retrieved online from the Hanford TWINS-3 database.

In tanks AN-104, AN-105, and AW-101, the densities show no definite trends with elevation but appear to vary more or less randomly. The convective layer densities in SY-103 (Figure 5-16) decrease with elevation from 1.52 g/mL at the bottom of the layer to 1.43 g/mL at the top. This would suggest a stable density gradient that should inhibit convection. But this is not consistent with the uniform temperature profile (see Figure 5-4), which can exist only in a convective fluid. The convective layer in AN-103 (Figure 5-11) also shows a stable density stratification with a uniform temperature profile. At this time, we attribute the density trend to waste disturbance during the ball rheometer testing.

The close correlation of the AN-103 density profile with the void fraction and yield stress trends is unique (compare with Figure 5-22). Apparently because this tank has not had large GREs to disrupt the waste, the retained gas has gradually displaced liquid so that the gas-free density of the highest void region nears that of the solid particles (2.3 to 2.6 g/mL). This density profile closely matches the appearance of the core extrusions in that the cores from the tank bottom appear almost runny while those toward the middle of the nonconvective layer appear much dryer (Meyer et al. 1997). It is interesting that the neutral buoyancy void fraction is 21% for a density of 1.93 g/mL with the liquid density at 1.53 g/mL. This prevents AN-103 from experiencing a large buoyant displacement for a long time, even though the average void fraction is approaching the neutral buoyancy value calculated from the average densities.

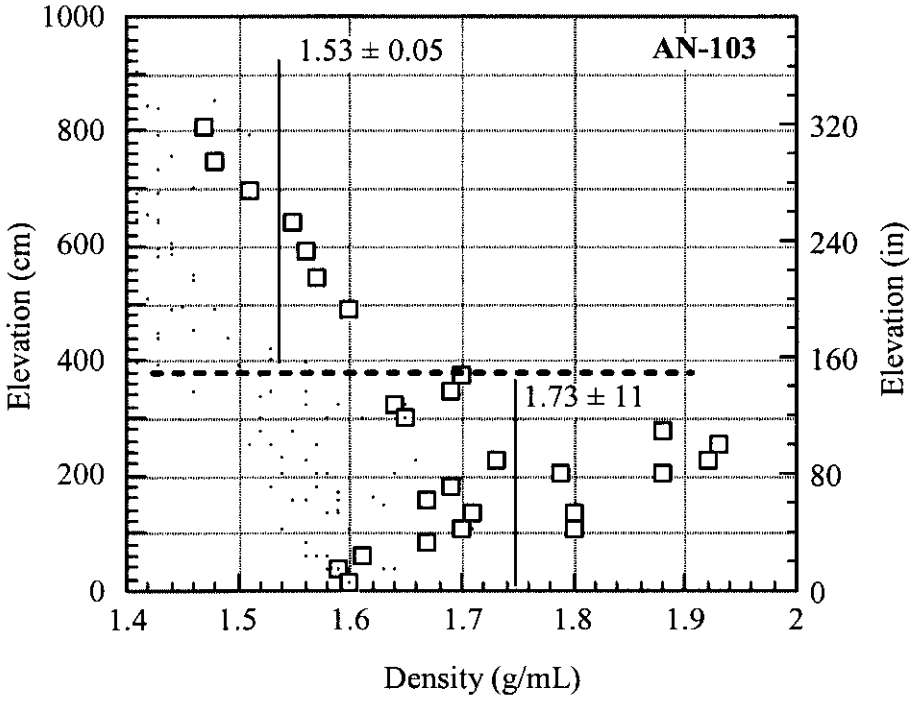

Figure 5-11. Tank 241-AN-103 Density Profile

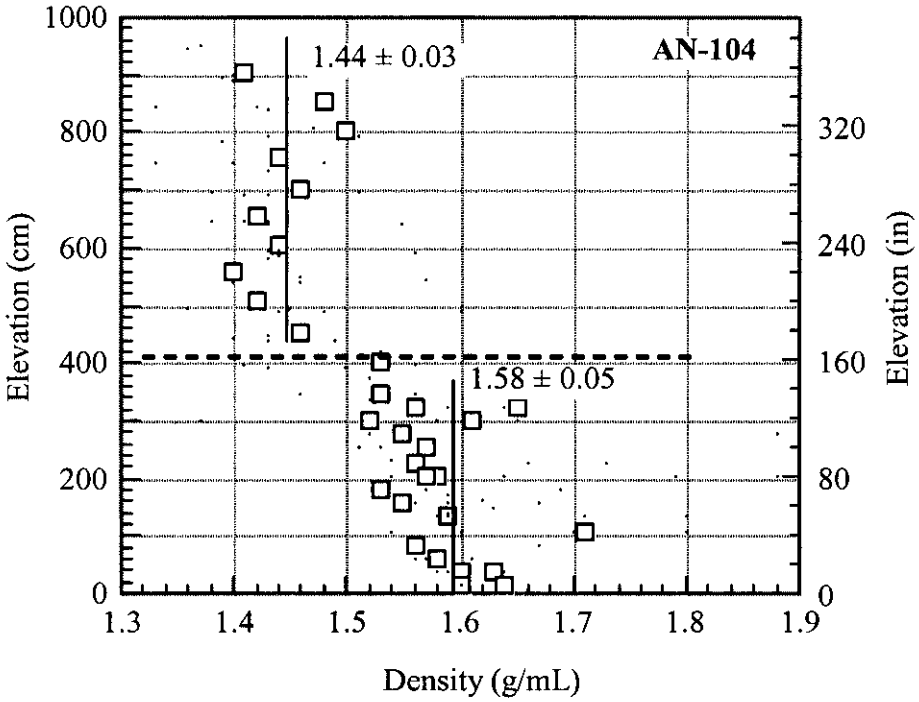

Figure 5-12. Tank 241-AN-104 Density Profile

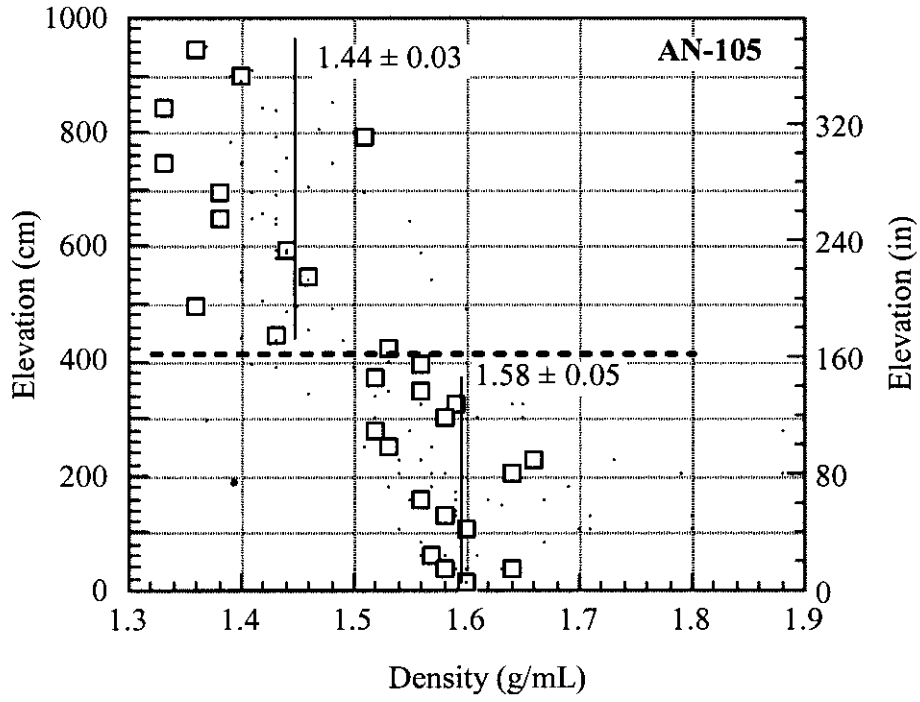

Figure 5-13. Tank 241-AN-105 Density Profile

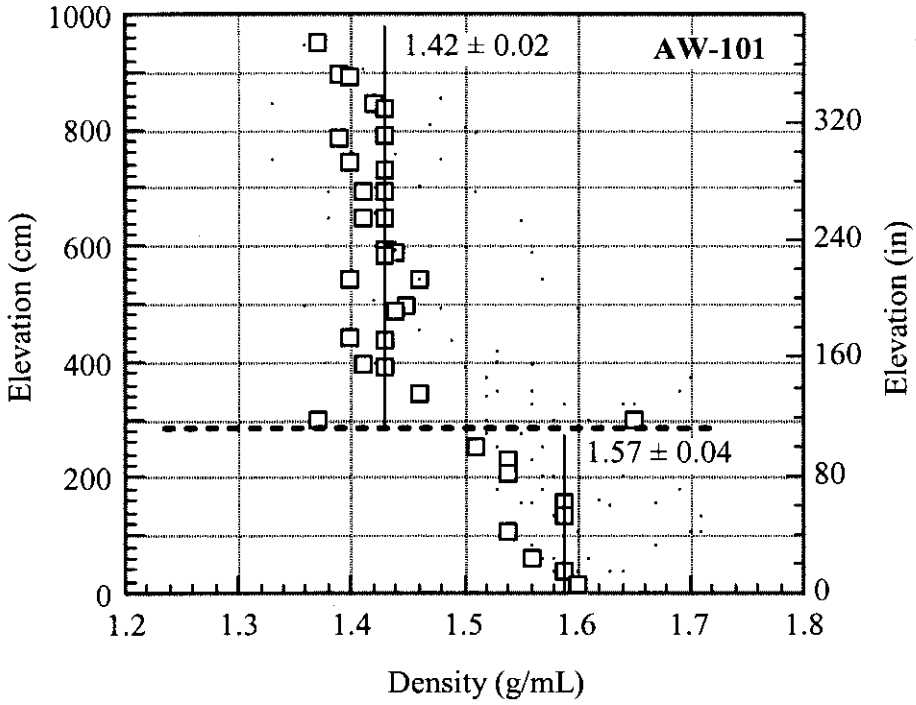

Figure 5-14. Tank 241-AW-101 Density Profile

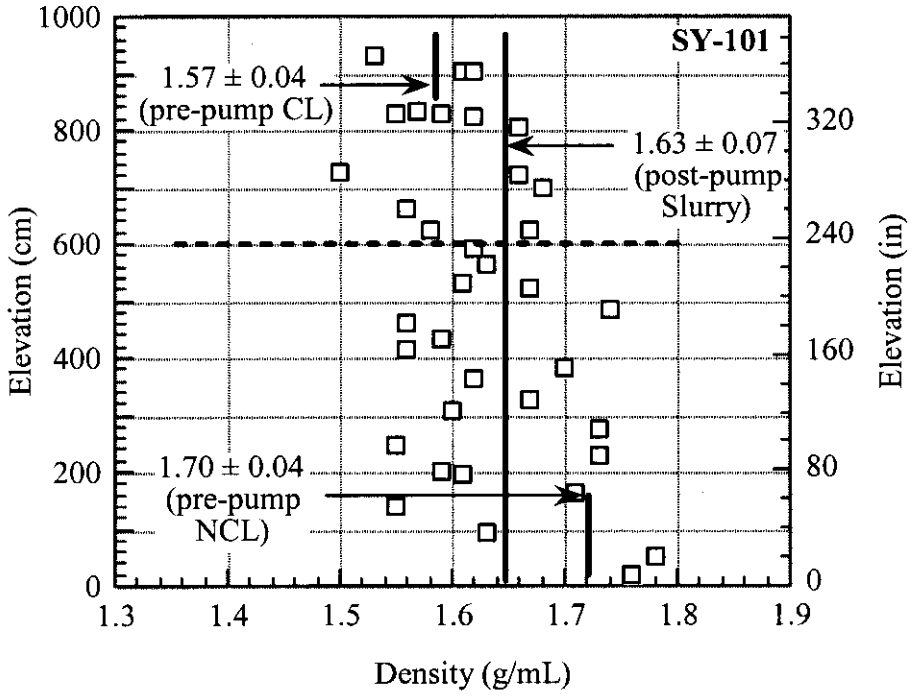

Figure 5-15. Tank 241-SY-101 Density Profile

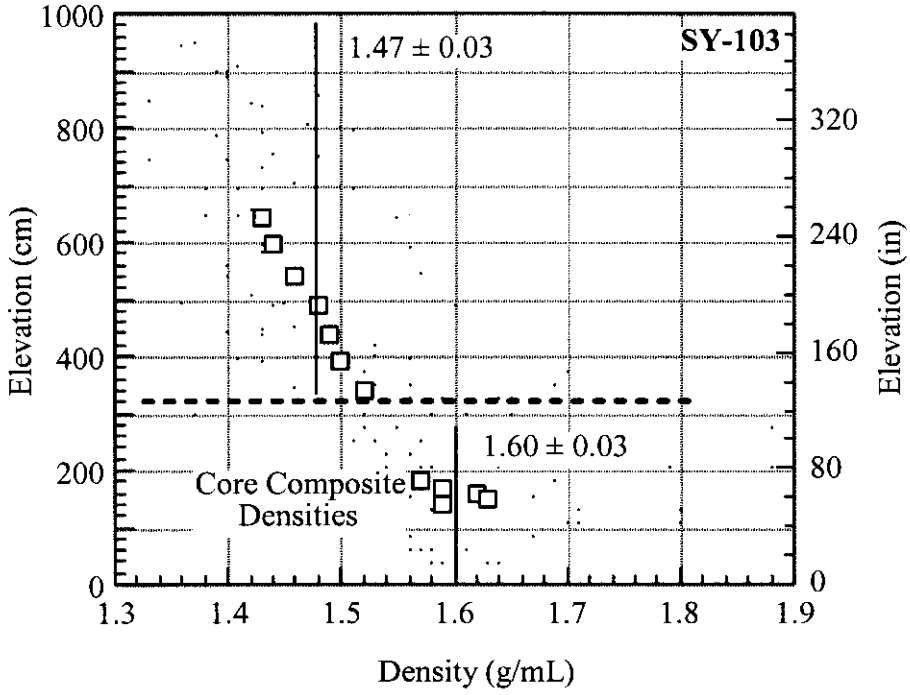

Figure 5-16. Tank 241-SY-103 Density Profile

5.3.2 Rheology of the Nonconvective Layer

The yield stress and apparent viscosity for the nonconvective layer derived from ball rheometer data are discussed in this section. Ex-situ rheological measurements performed on waste samples in the hot cell have consistently given much higher yield stresses and viscosities than are shown here and are not believed to be representative of in-situ conditions (see, for example, Herting et al. 1992). Yield stresses estimated from visual interpretation of core extrusion data generally match those obtained with the ball rheometer (Gauglitz and Aiken 1997). The convective layer is not discussed because its viscosity is generally estimated to be on the order of 5 to 20 cP, which is below what can be measured with the ball rheometer.

Figures 5-17 through 5-21 show the apparent viscosity and yield stress in the nonconvective layer measured on the first pass through the waste in each riser in AN-103, AN-104, AN-105, AW-101 and SY-103, respectively.[9] The apparent viscosities were normalized to a uniform ball speed of 0.1 cm/s. The yield stress was extrapolated to the minimum ball elevation even though it cannot be derived from the tension-versus-speed data within several ball diameters of a barrier.

The yield stress and viscosity increased approximately linearly from essentially zero at the top of the nonconvective layer to a maximum just before the ball stopped at the top of the stationary

[9] The apparent viscosity is defined as the ratio of the shear stress divided by the strain rate. It includes the effect of yield stress in a viscoplastic material.

layer. However, the slope of the yield stress versus depth varies widely from tank to tank and even from riser to riser within a tank. As discussed in Section 2.3.4, the slope is much more uniform if normalized to the thickness of the nonconvective layer above the stationary layer. The yield stress profiles follow roughly the same trends in both risers in AN-103, AN-105, and SY-103, while the two risers in AN-104 and AW-101 differ. Relatively recent GREs are a possible, but not provable, explanation.

The yield stress profiles correlate roughly with gas fraction where the void fraction increases with depth. But it is unclear whether the higher yield stress retains more gas or the higher gas fraction expels water that increases the yield stress. The correlation of yield stress with gas fraction is illustrated for AN-103, SY-103, and AN-104 in Figures 5-22, 5-23, and 5-24, respectively. Note that the yield stress data represent the region directly under the riser while the gas fraction measurements were taken at two or three angles on a radius of about 2.5 ft from the riser centerline.

In AN-103 (Figure 5-22), the void and yield stress profiles qualitatively match quite well in Riser 16B while only the trends agree in Riser 1B. Tank 241-SY-103 (Figure 5-23) shows a similar correlation. The profiles correspond closely in Riser 22A but only approximately in Riser 17C. Tank 241-AN-105 and 241-AW-101 comparisons are qualitatively similar. On the other hand, the profiles in both risers of AN-104 appear to fit one another well.

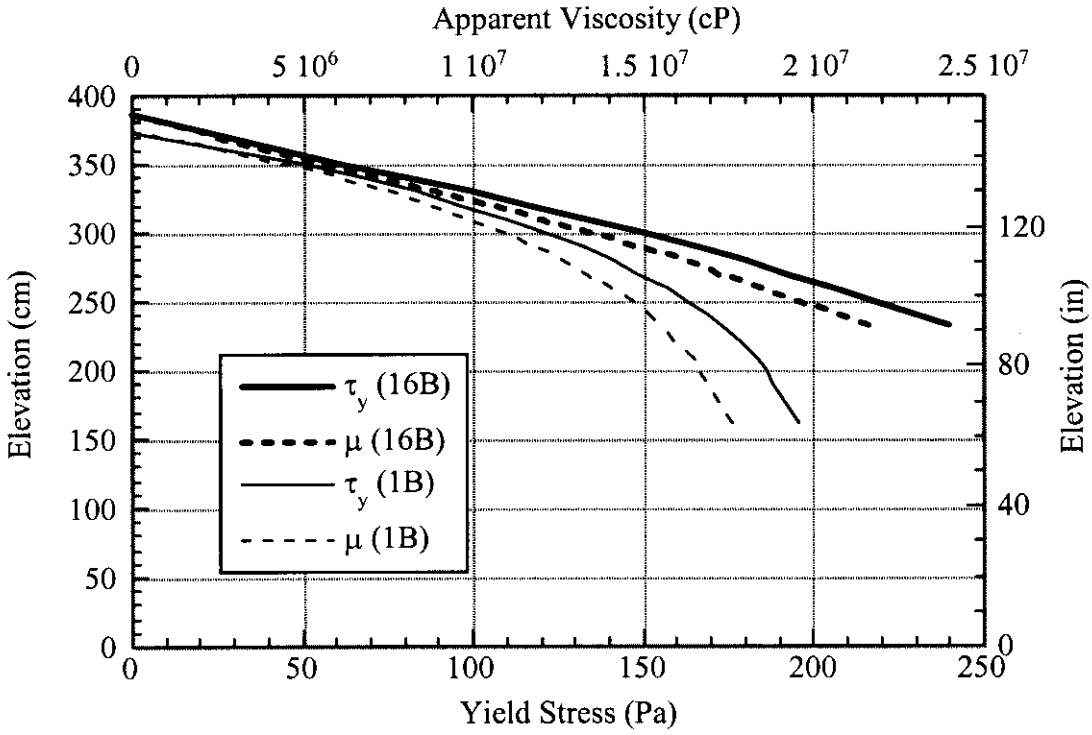

Figure 5-17. Apparent Viscosity and Yield Stress: Tank 241-AN-103

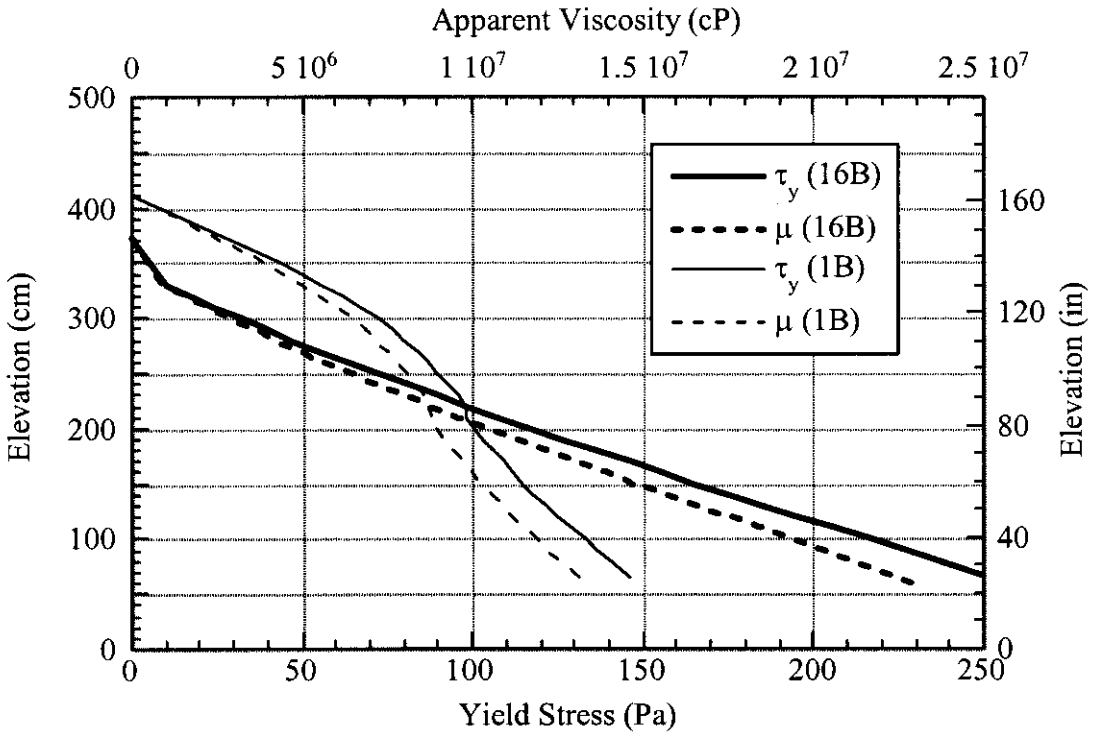

Figure 5-18. Apparent Viscosity and Yield Stress: Tank 241-AN-104

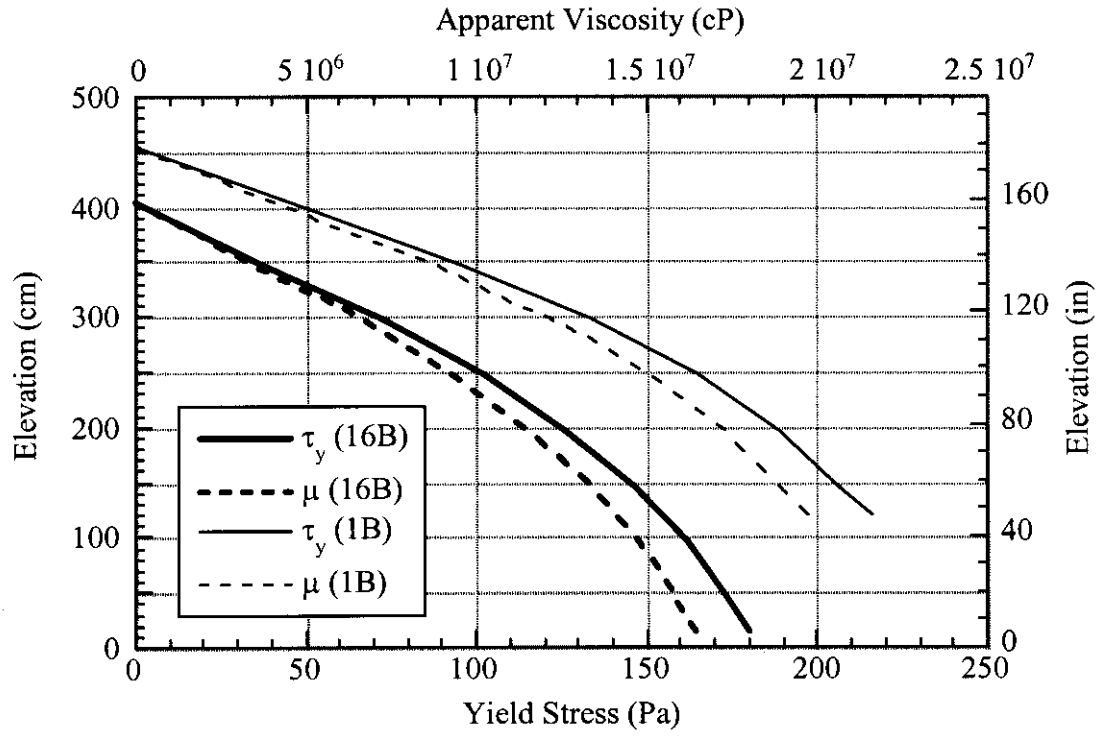

Figure 5-19. Apparent Viscosity and Yield Stress: Tank 241-AN-105

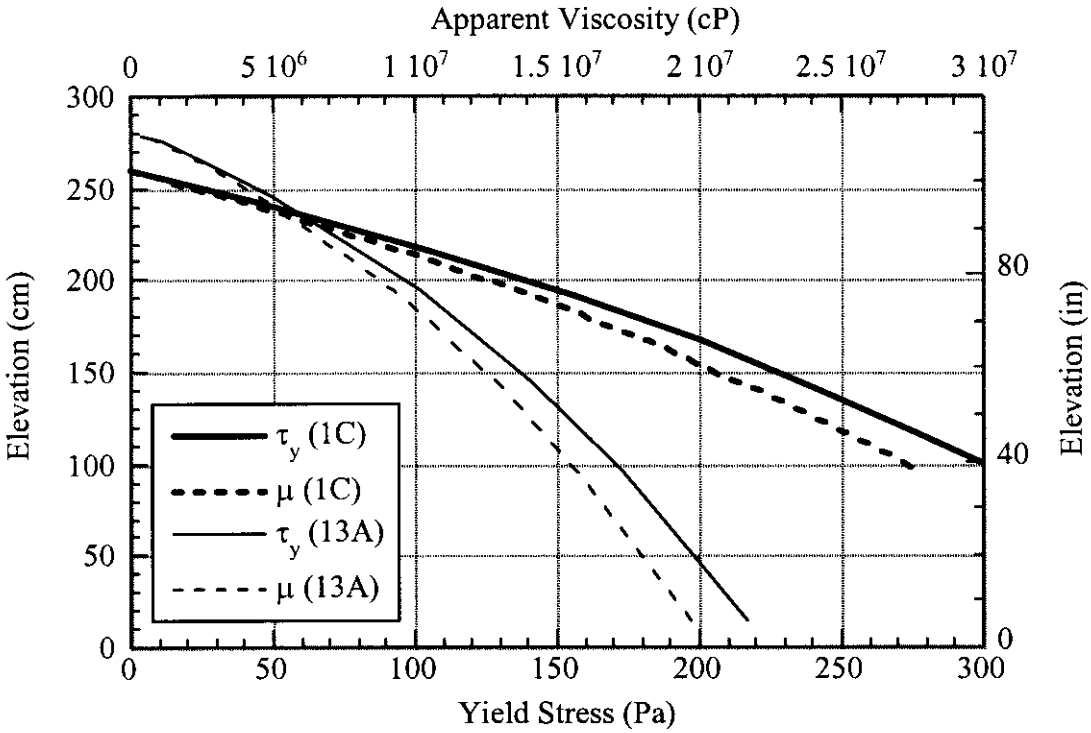

Figure 5-20. Apparent Viscosity and Yield Stress: Tank 241-AW-101

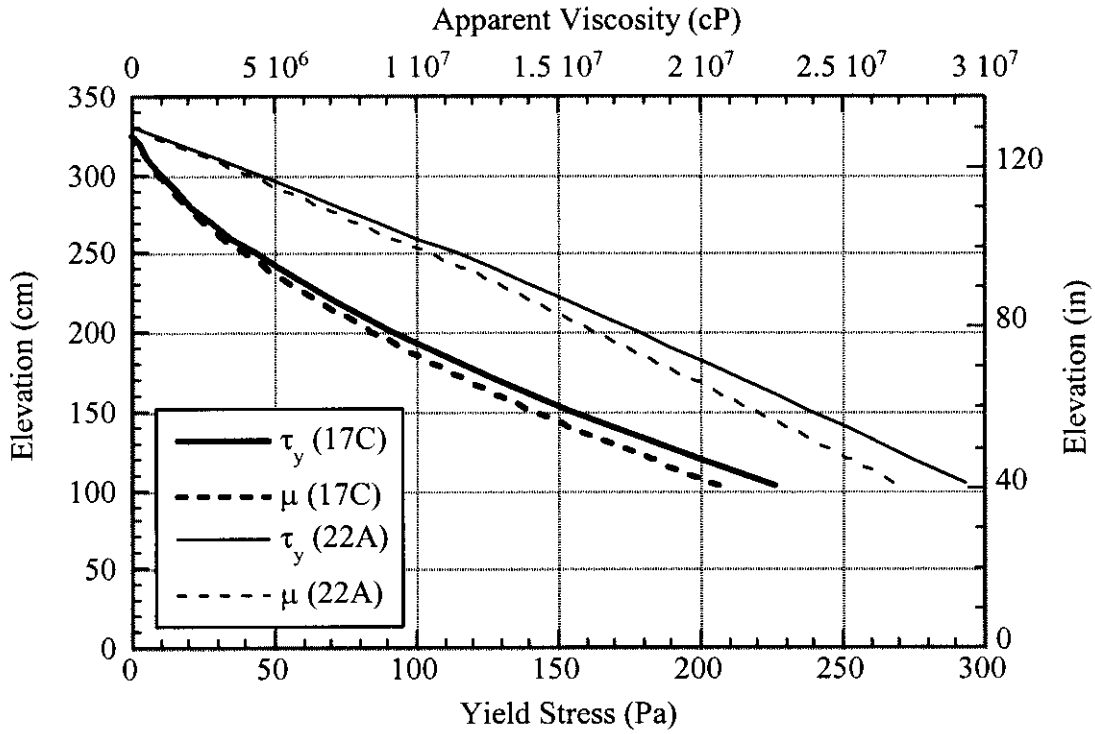

Figure 5-21. Apparent Viscosity and Yield Stress: Tank 241-SY-103

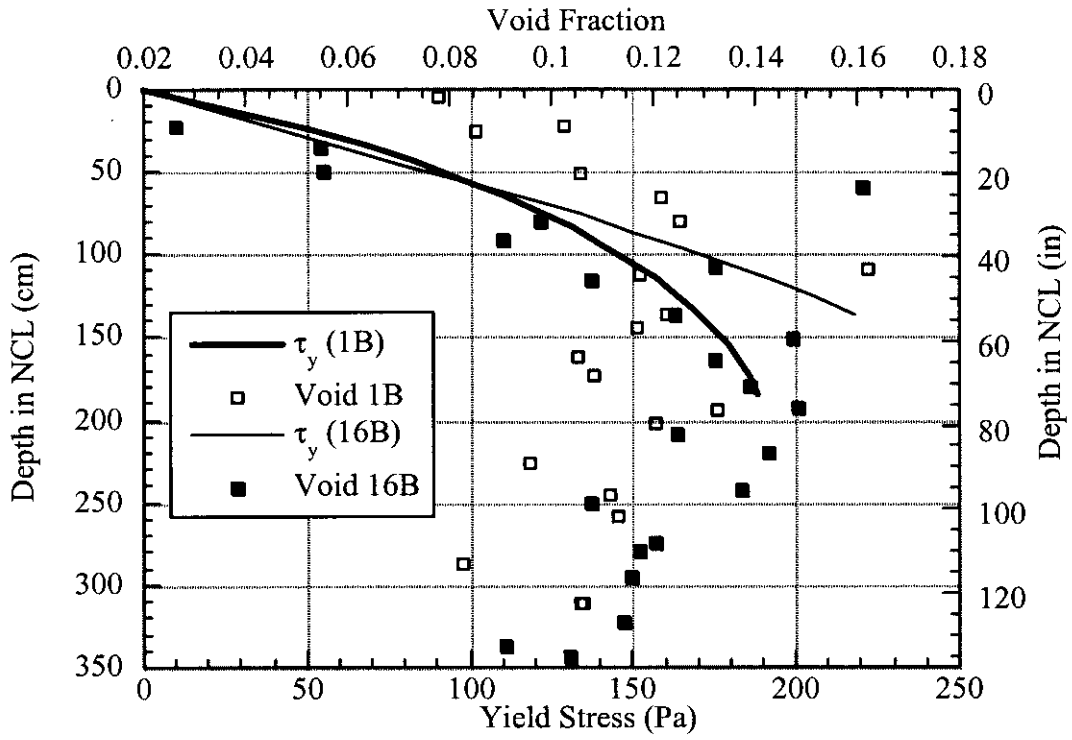

Figure 5-22. Gas Fraction and Yield Stress Profiles in Tank 241-AN-103

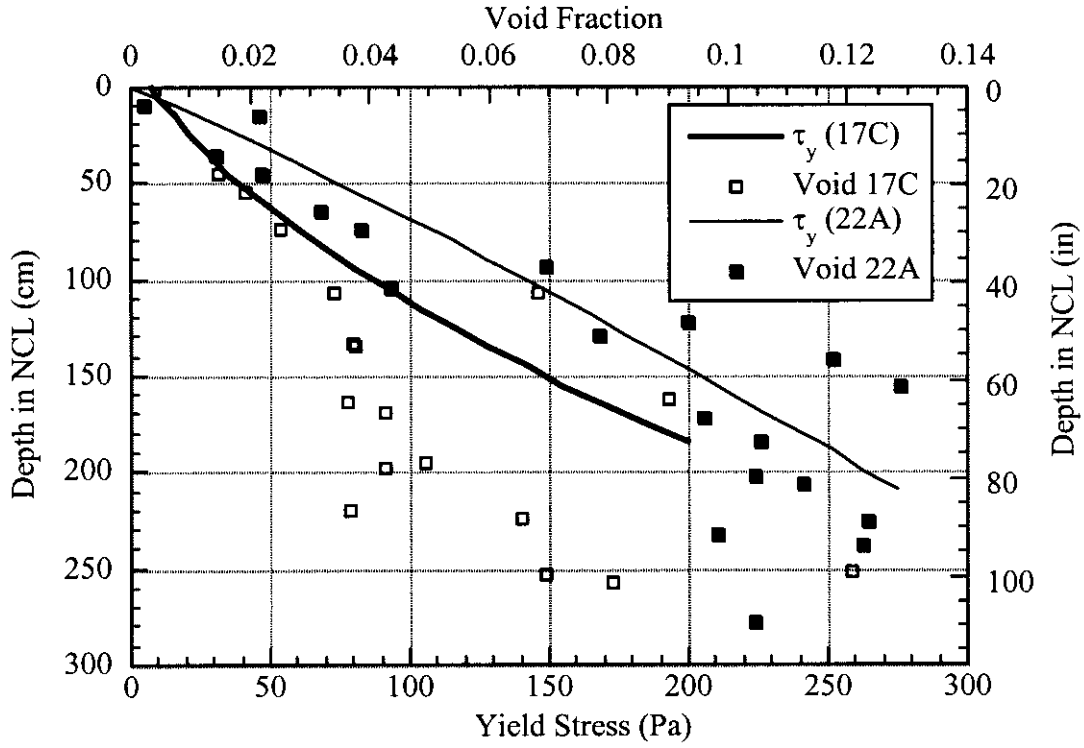

Figure 5-23. Gas Fraction and Yield Stress Profiles in Tank 241-SY-103

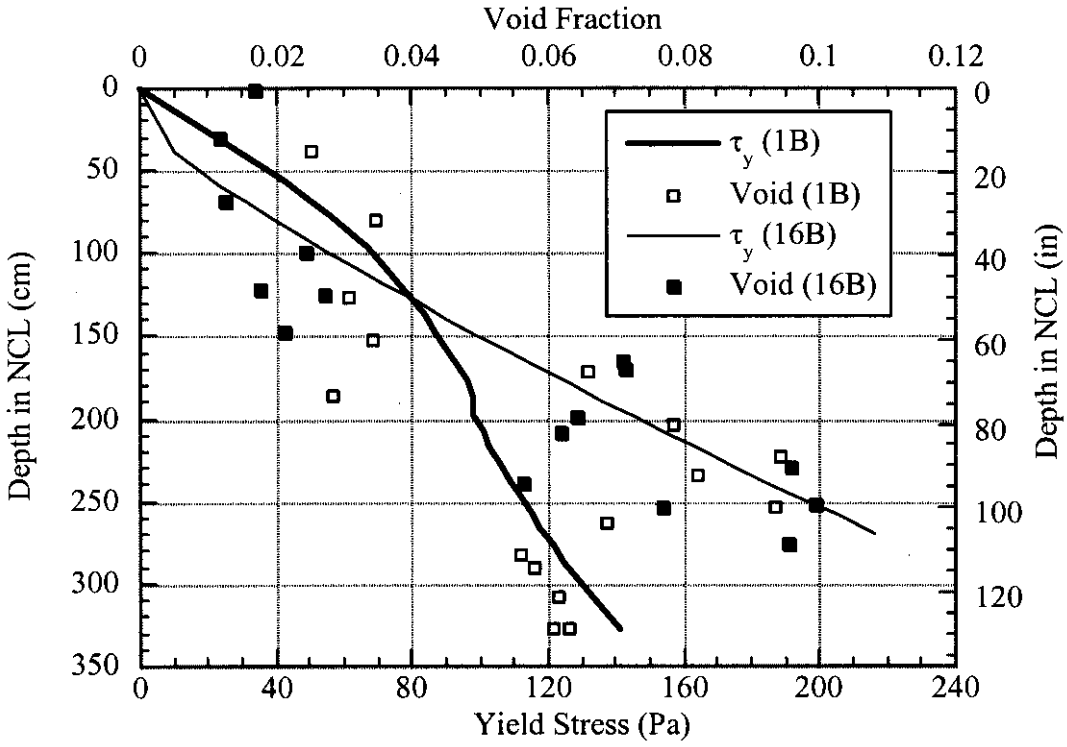

Figure 5-24. Gas Fraction and Yield Stress Profiles in Tank 241-AN-104

The regular jet pump mixing since December 1993 made the bulk of SY-101 waste a well-mixed slurry that contained very little gas. Though its properties were approximately uniform from just below the crust to near the bottom of the tank, the slurry was in a continual flux. Solids were suspended by thrice-weekly, 25-minute pump runs and settled out between them. Small bubbles were freed by the pump jet each run. A nonconvective layer of loosely settled solids over a meter deep formed soon after a pump run.

The viscosity of the mixed slurry was actually lower than the ball rheometer was designed to measure. In fact, the cumulative drag on the tether cable during the tests was several times greater than the drag on the ball, making it difficult to interpret the measurements. Nevertheless, the data seem to indicate that the mixed slurry was a non-Newtonian, shear-thinning fluid. The best fit to the data gave a viscosity of about 1000 cP with an uncertainty of about a factor of 2. These results are plotted in Figure 5-25.

The ball was able to penetrate the loosely settled layer to within about 15 cm (approximately 6 in.) of the bottom of the tank in Riser 4A. The material near the bottom showed shear-thickening behavior, a very small yield stress of about 20 Pa (0.004 psi), and an average viscosity of about 20,000 cP. The yield strength profile is plotted in Figure 5-26.

The above data no longer represents the waste in SY-101 because of the transfer and back dilutions performed from December 1999 to March 2000. However, it might provide a qualitative illustration of how the waste in the other tanks would behave if subjected to mixing.

Since the solids concentration was higher in SY-101 prior to dilution, the density, viscosity, and yield stress of a mixed slurry in the other tanks would probably be significantly lower.

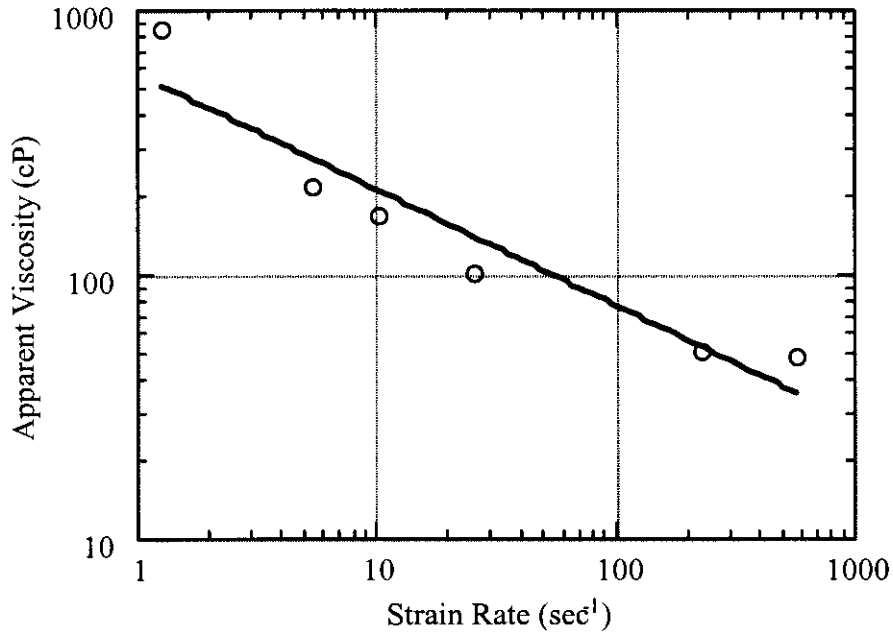

Figure 5-25. Apparent Viscosity of Tank 241-SY-101 Mixed Slurry

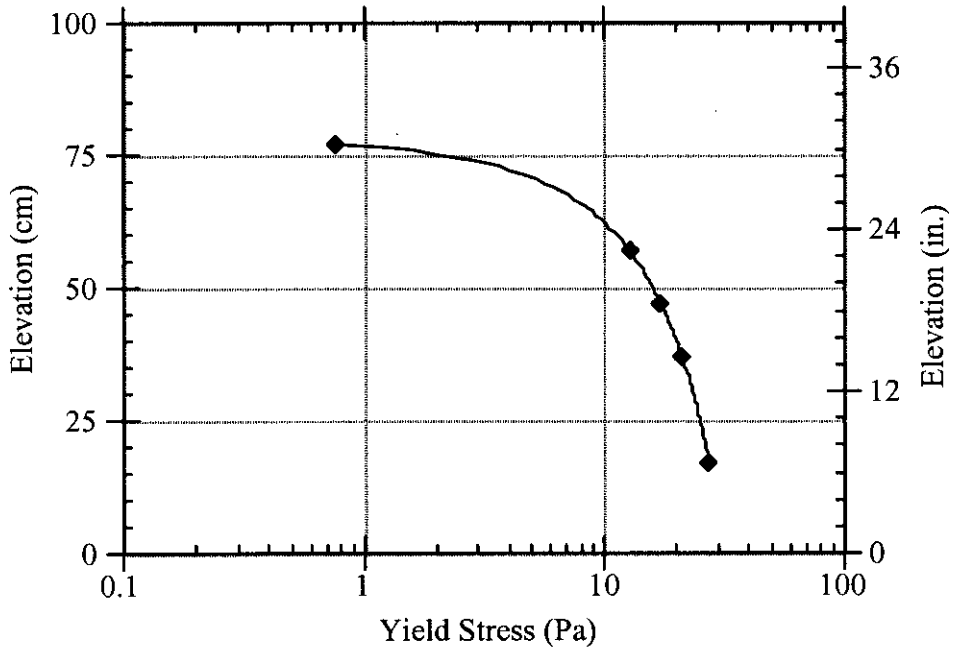

Figure 5-26. Yield Stress of the Loosely Settled Solids in Tank 241-SY-101 Riser 4A

5.4 CHANGES IN WASTE CONFIGURATION WITH TIME

Waste configuration, (i.e., layer dimensions and gas distribution), is determined from a variety of measurements. These include temperature profiles, void fraction profiles measured with the VFI, data obtained by the ball rheometer, neutron and gamma scans, and core samples, including RGS analyses. For the DST FGWL tanks, core samples and RGS analyses were obtained in 1996 in AN-103, AN-104, AN-105, and AW-101. Ball rheometer and VFI measurements were performed in all FGWL DSTs in 1995 and 1996. Information on waste properties, waste configuration, and retained gas volume derived from analyses using these measurements, which were obtained four or more years ago, must be evaluated and possibly revised based on observed changes in the tank conditions since then.

Several sources of data are available to evaluate these changes. Temperatures and waste levels are recorded at least daily, and detailed temperature profiles from validation probe runs in the MITs have been made quarterly in SY-101, approximately every six months in SY-103, and in 1996, 1999, and 2000 in the other tanks. Gas release events, that can locally affect the nonconvective layer depth, have been recorded since 1995-96 from headspace gas monitoring data. Neutron and gamma scans are made using the new small-diameter probe which is operated inside the MITs have been obtained approximately monthly in SY-101 since February 1999 and in the other tanks since January 2000.

The GREs were detected as rapid increases in the headspace hydrogen concentration. A GRE would temporarily reduce the depth of the nonconvective layer and possibly increase the crust thickness, if some of the waste remained buoyant. However, except for the historic large releases in SY-101, those in the other five DSTs are very local based on the evidence of the nonconvective layer temperature histories. Only in the most active tanks like AN-105 and SY-103 might changes in the waste configuration due to GREs be detectable. The gas release behavior of most of the FGWL DSTs has also changed. Prior to 1998, GREs tended to be larger and infrequent. In 1998 the pattern appears to have changed to smaller, much more frequent releases (see Section 8). This suggests that GREs have had little effect on waste configuration in the last few years.

The recent information obtained from neutron and gamma scans provides additional insight into the current waste configuration. The neutron count rate is proportional to the concentration of hydrogen, and, therefore, correlates strongly with the amount of water present. However, it is also non-linear, and only large decreases in water content (e.g., due to presence of gas) can be detected in the neutron profile. The gamma count is proportional to the concentration of Cs-137, the primary gamma emitter, present. Since most Cs-137 is dissolved in the liquid, the gamma count correlates with the volume fraction and concentration of liquid waste. Neutron data plotted here have been adjusted to a calibration reference, normalized to the maximum count for a given profile, and smoothed with a weighted least-squares curve-fit to facilitate comparison between different scans. Raw gamma data are smoothed similarly but not normalized. Measurements with these probes show considerable scatter within a scan and instrument drift between scans, which tends to hinder interpretation of trends when only the raw data is plotted.

With the exception of SY-101, the waste configurations in the DST FGWL tanks have changed very little in the past five years. The changes in SY-101 waste configuration are the result of mixer pump operation, the level-growth phenomenon, and the subsequent transfer and back-dilution operations. This is well documented elsewhere, and will only briefly summarized here. For details, see Allemann et al. (1994), Brewster et al. (1995), Stewart et al. (1998), Raymond (1999), and Mahoney et al. (2000). No waste has been added or removed from the other FGWL DSTs, and they have shown no major changes in surface level.

Waste temperatures have shown a slow steady decline since 1995-96, partly due to the natural decay in radio-nuclear heat load, but primarily because of increased headspace and annulus ventilation flow rates. From March 1995 to early 1996 both of the two annulus ventilation fans in the AN and AW farms were made fully operational. As these farms had been operating with only one fan, this doubled the annulus ventilation flow to AN-103, AN-104, AN-105, and AW-101. In mid-1996 inlet flow controllers were installed in the AW tanks that provided a minimum 100 cfm primary ventilation flow. The AN tanks got flow controllers by early 1997. The combination of doubling the annulus ventilation flow and insuring 100 cfm headspace ventilation greatly increased the heat dissipation rates in these tanks causing the waste to begin cooling. The concurrent changes in waste level and gas release behavior are believed to be related mostly to this temperature decrease. However, except for the possible crust growth in AN-103 and AW-101, the temperature decreases have not affected the waste configurations.

The following sections discuss the waste configuration history of each of the FGWL tanks and the significance of any changes that have been observed since 1995/1996.

5.4.1 Tank 241-AN-103 Waste Configuration History

The surface level in AN-103 since 1995 is shown in Figure 5-27, along with the occurrence of GREs, as indicated by the headspace hydrogen concentration data. The net change in surface level between January 1995 and January 2000 is a rise of only about 2 cm. However, the level has been approximately constant except for seasonal variation since about January 1998. This indicates the retained gas volume has not changed recently. There does not appear to be a correlation between GREs and level change in this tank, which suggests that the waste configuration is not influenced by GREs.

Figure 5-28 shows temperature profiles from Validation Probe runs in AN-103 in 1996, 1999, and 2000. The temperature profiles show a temperature decrease of 10 to 15 °F in the approximately four-year interval. Some of this difference is merely seasonal, since the 1996 profile was obtained in August, when ambient air temperatures generally peak above 100 °F, while the 1999 profile was obtained in March, with the peak air temperature at 60 °F. Based on the waste temperature history for this tank (see Section 4.2), the temperature of the middle of the nonconvective layer decreased only about 5 °F during this period.

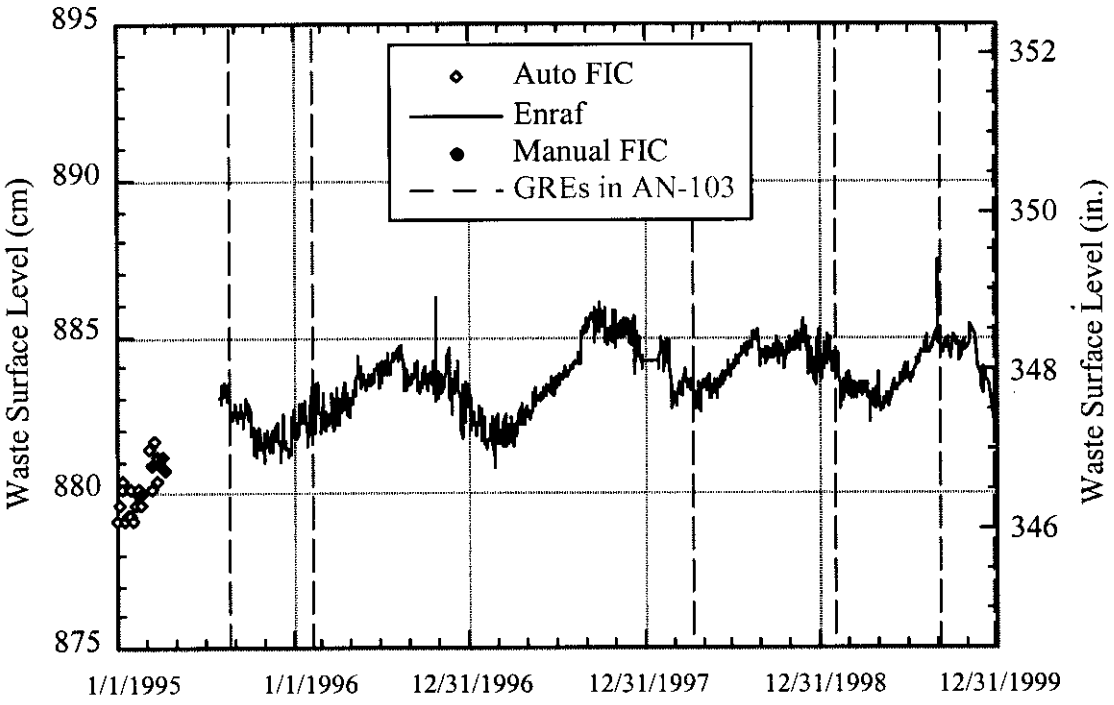

Figure 5-27. Tank 241-AN-103 Level and Gas Release Event History

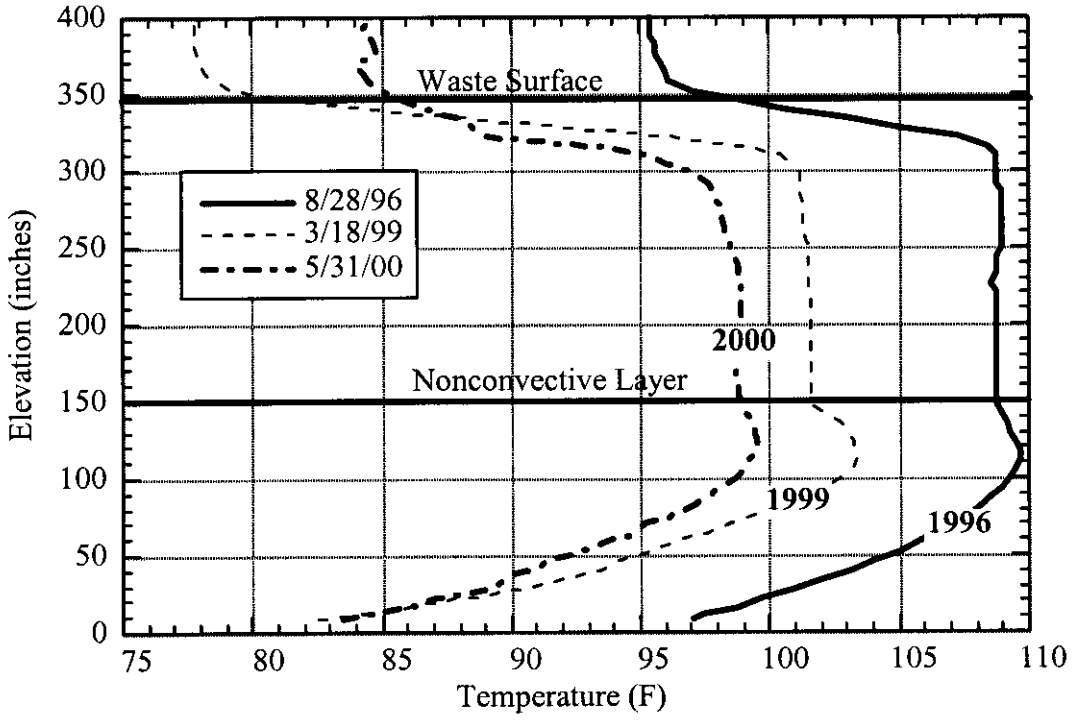

Figure 5-28. Tank 241-AN-103 Temperature Profile Change from 1996 to 2000

The change in shape of the temperature profile in the nonconvective layer in 1999 is probably due to the increased annulus and headspace ventilation flow rates. The profile obtained May 31, 2000, shows continued cooling, to the same boundary temperature. The height of the nonconvective layer has not changed significantly. However, the crust thickness may have increased by as much as 12 in. (30 cm) since 1996. At the same time, the interface between convective layer and the crust base is not as sharp as in the prior years. A region where convection is inhibited appears to have developed from the base of the crust down to about 250 in (635 cm). A similar process is occurring in AW-101 (see Section 5.4.4).

Neutron and gamma profiles, which have been obtained monthly since January 2000, are shown in Figures 5-29 and 5-30, respectively. The void fraction profile from VFI and RGS data (see Figure 7-5) shows that the highest void fraction was in the region from 60 to 100 in. (152 to 254 cm). The neutron profiles indicate that the water content of the nonconvective layer decreases more or less linearly with depth down to about 50 in. (127 cm) where it increases slightly. The gamma profiles in Figure 5-30 follow the void fraction quite closely with a lower gamma count at approximately the elevation as the maximum void fraction. This interpretation is further supported by the 1996 core extrusion video of nonconvective layer samples for this tank that showed a "dryer" appearance where the void fraction was highest (Meyer et al. 1997). Neither the gamma nor neutron profiles shows a marked change in the configuration of the crust layer that is significant within their respective variability.

These comparisons are consistent with the temperature profiles and suggest that neither the thickness of nor the void profile in the nonconvective layer has changed significantly since the VFI measurements were taken. However, the thickness and/or the properties of the crust layer may be changing as evidenced by the temperature profile. Future validation probe runs will be necessary to characterize whatever changes are occurring.

5.4.2 Tank 241-AN-104 Waste Configuration History

The surface level in AN-104 since 1995 is shown in Figure 5-31, along with the occurrence of GREs, as indicated by the headspace hydrogen concentration data. The waste level has dropped about 5 cm (2 in.) from mid-1996 to 2000, which indicates a reduction of about 740 ft^3 (21 m^3) of gas volume in-situ. Also, from August 1998 onward, gas releases are much smaller, with peaks of only a few hundred ppm (see Section 8.6). This is consistent with the level breaks associated with the GREs. In the earlier events, there was usually a sharp level drop or rise (on the order of 0.5 to 1.0 cm) at the time of the event. After 1998, however, level change does not appear to correlate with GREs. Instead, the level change seems to be a gradual more or less continuous decrease with fluctuations following seasonal changes. The waste configuration is not likely to have been influenced by GREs.

Figure 5-32 shows temperature profiles from Validation Probe runs in AN-104 in 1996, 1999, and 2000. The waste temperature has decreased 12 to 15 °F, which matches the decrease shown in the detailed waste temperature history for this tank (see Section 4.3). Seasonal variations aside, comparison of the change in the profile from 1999 to 2000 with that between 1999 and 1996 suggest that the rate of cooling has been essentially constant since 1996.

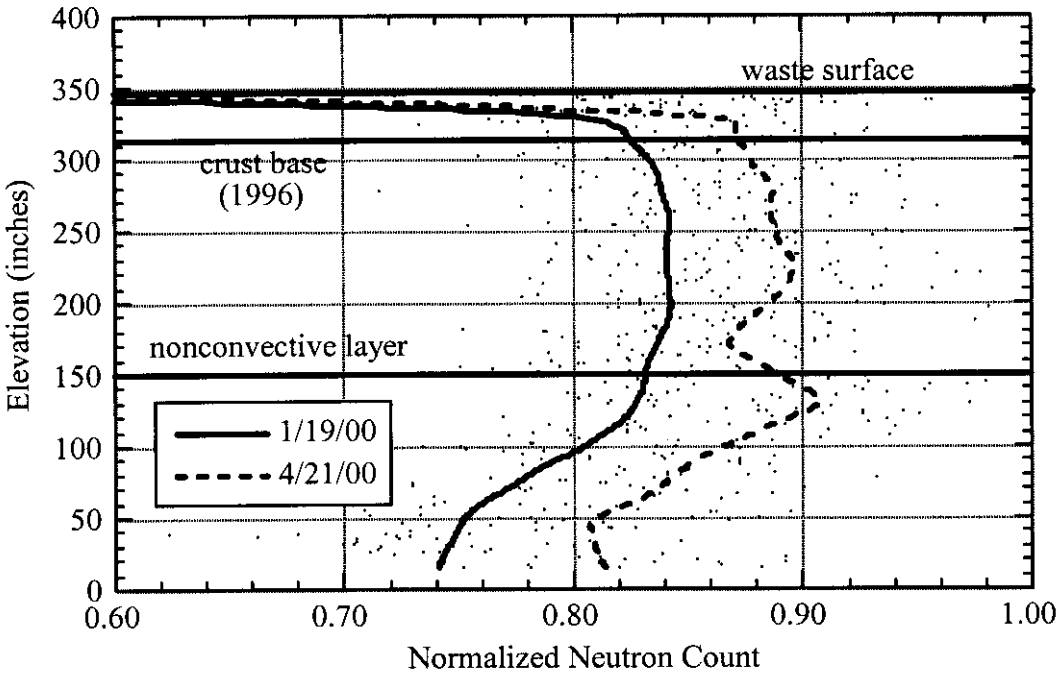

Figure 5-29. Tank 241-AN-103 Normalized Neutron Profiles

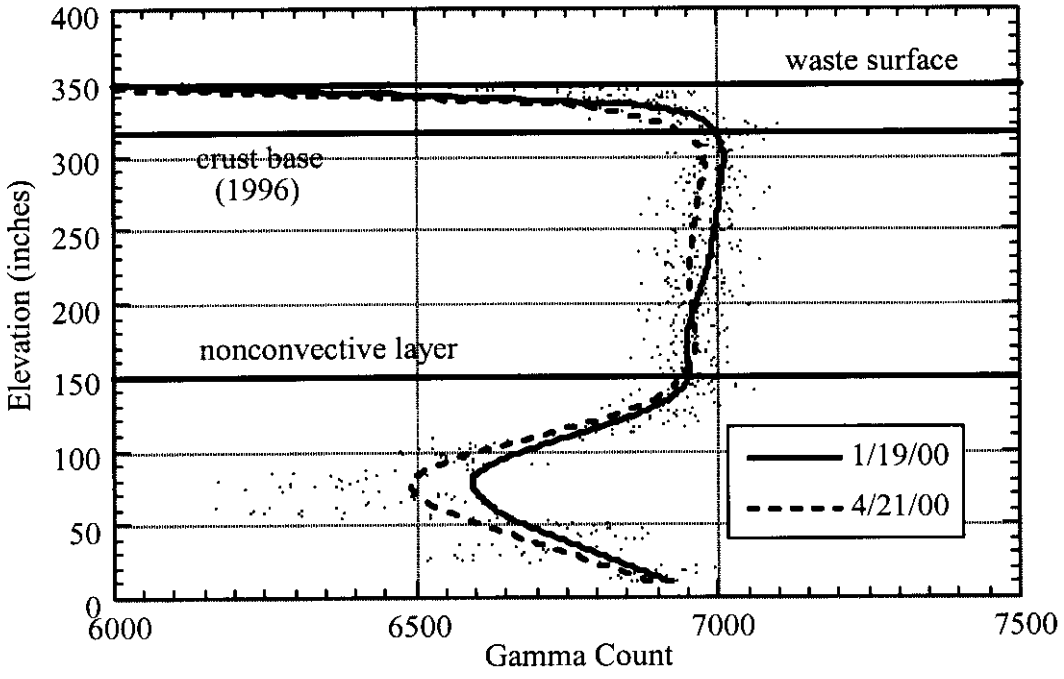

Figure 5-30. Tank 241-AN-103 Gamma Profiles

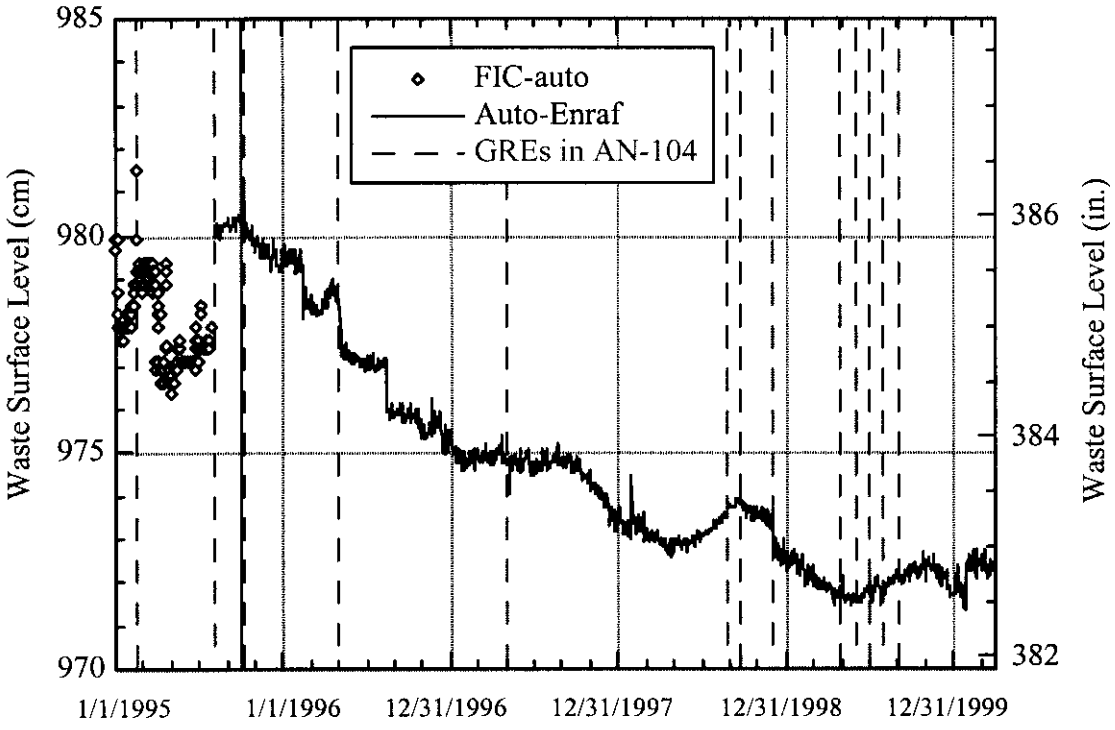

Figure 5-31. Tank 241-AN-104 Level and Gas Release Event History

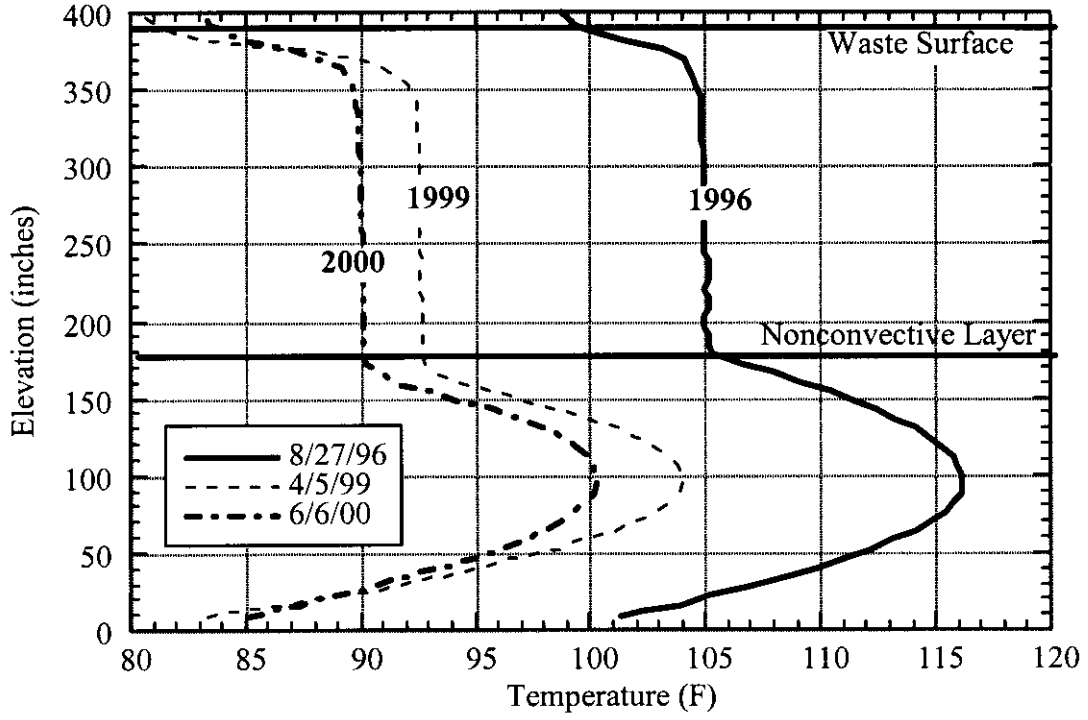

Figure 5-32. Tank 241-AN-104 Temperature Profile Change from 1996 to 1999

The shape of the temperature profile obtained in 2000 indicates that the depth of the nonconvective layer and the crust base elevation have both decreased slightly since 1996. Since the decreases of about the same magnitude as the waste level drop, this may be a reflection of the decrease in the volume of gas retained in the nonconvective layer. The change might also be the effect of a local rather than global drop in the nonconvective layer due to a gas release event (or events) between 1996 and 2000. However, the last GRE that had a detectable effect on level (Figure 5-31) or temperatures in the nonconvective layer (Figure 4-4) was April 1996. Since the 1996 temperature profile was obtained in August 1996, we conclude that the small difference in the 1999 and 2000 temperature profiles are not due to GREs.

Void fraction measurements obtained in 1996 in AN-104 using the VFI and RGS (see Figure 7-6) indicate that most of the retained gas in the tank lies relatively deep in the nonconvective layer compared to that in AN-103. The void fraction appears to increase almost linearly from essentially zero from the top of the nonconvective layer at 160 in. to about 0.17 at the bottom. The observed level changes over the period and the changes in the temperature profile suggest that the total retained gas volume has decreased somewhat, but the constant shape of the temperature profile in the nonconvective layer suggests that the void distribution has not changed significantly.

Figure 5-33 shows profiles obtained from recent neutron scans. The neutron profiles for January and February are reasonably consistent, but markedly different from the April profile for unknown reasons. All three neutron profiles indicate that the convective layer contains less water than the nonconvective layer, which is not physically possible. This may be the result of waste adhering to the MIT exterior as is apparently the case with AN-105 (as discussed in Section 5.4.3). However, the neutron profiles show a decreasing count below about 75 in. which is consistent with the increasing void fraction in this region.

Figure 5-34 presents gamma profiles for January, February, and April 2000. Normalized values are shown instead of raw data because of the great differences in average gamma count between profiles. Average counts were approximately 7,300, 6,500, and 18,000 for the three scans. Because of this wide variability between scans, these data are of questionable value. However, the January and February scans are at least consistent with the neutron data in showing a decreasing liquid content with depth in the nonconvective layer in the region of maximum void fraction.

Taken all together, the evidence from level, temperature, and neutron/gamma scans suggests that no major changes have occurred in AN-104 other than a small decrease in gas volume consistent with level and temperature decreases over the last four years.

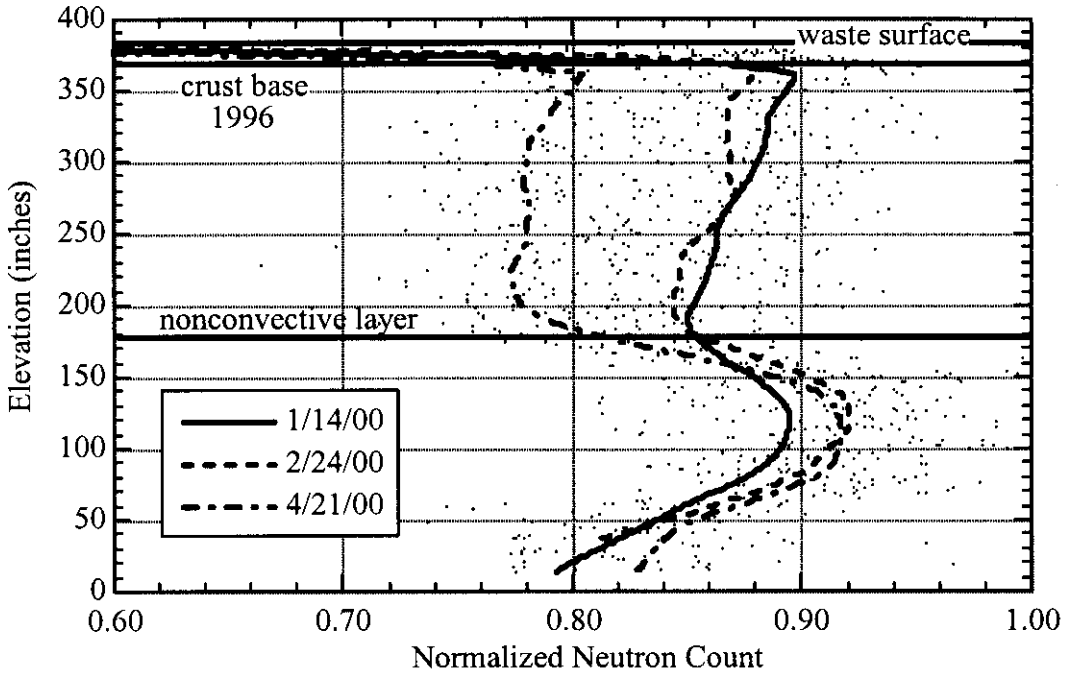

Figure 5-33. Tank 241-AN-104 Normalized Neutron Profiles

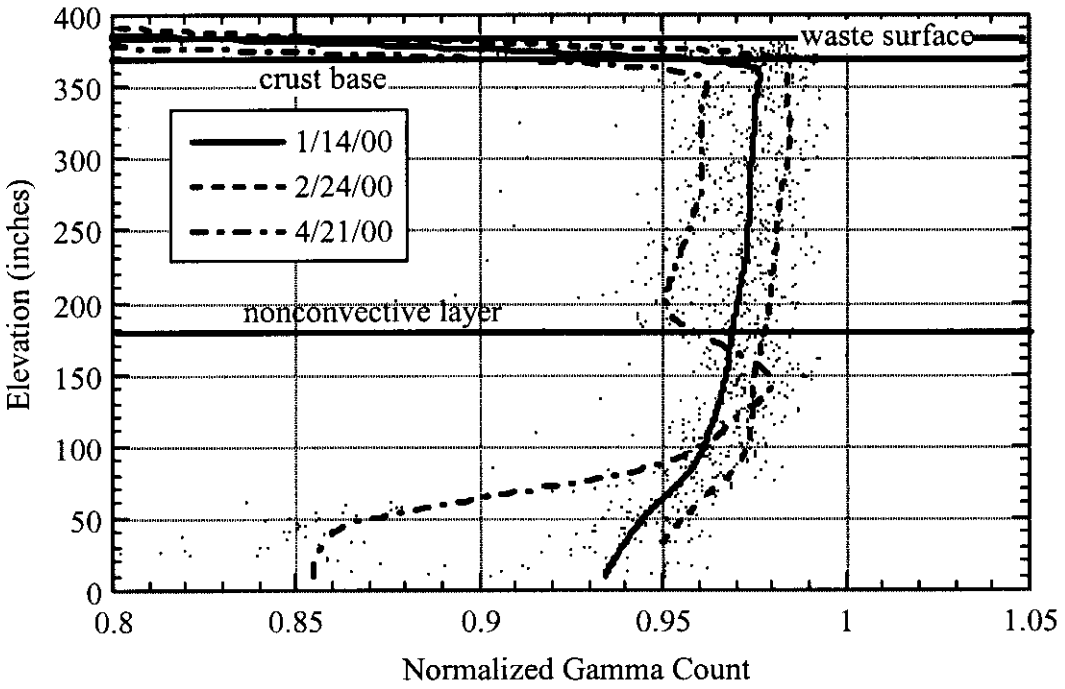

Figure 5-34. Tank 241-AN-104 (Normalized) Gamma Profiles

5.4.3 Tank 241-AN-105 Waste Configuration History

The surface level in AN-105 since 1995 is shown in Figure 5-35, along with the occurrence of GREs, as indicated by the headspace hydrogen concentration data. There has been a net level drop of approximately 3 cm (1.2 in.) since January 1, 1995, which indicates a decrease in the in-situ gas volume of 440 ft^3. Of the 13 GREs during this period, the four largest ones (August 1995, June 1996, April 1997, and July 1999) were accompanied by significant level drops. Approximately equal level rises can be identified prior to three of them. One of these rises in May 1999 was also accompanied by a small release. The mechanisms behind this behavior are not known. For the smaller releases, there does not appear to be a strong correlation between level change and GREs. However, some affects of the larger GREs on waste configuration might be expected in this tank.

Figure 5-36 shows temperature profiles from Validation Probe runs in AN-105 in 1996, 1999, and 2000. The general shape of the temperature profile measured with the Validation Probe has not changed significantly in the past four years. None of the GREs since 1996 have affected the waste in the vicinity of the MIT. There has been an overall temperature decrease of about 10 °F, consistent with the detailed waste temperature history for this tank (see Section 4.3).

The shape of the temperature profile in the nonconvective layer (below about 210 in.) for the profile obtained in 1999 indicates that the depth of this layer has decreased very slightly since 1996. This appears to be part of the overall surface level drop seen in Figure 5-35, since it is of about the same magnitude, and is probably due primarily to a decrease in the gas volume. As with AN-104, the void fraction measurements obtained in 1996 in AN-105 using the VFI and RGS (see Figure 7-7) show that most of the gas in the tank is stored relatively deep in the nonconvective layer. The observed level changes over the period, and the lack of change in the shape of the temperature profile suggest that the void volume has decreased somewhat, but the void profile is probably similar to the 1996 measurements.

Figures 5-37 and 5-38 show plots of profiles obtained from recent neutron and gamma scans of the tank. The neutron profiles are particularly difficult to reconcile with the temperature or void profiles or the neutron scans of the other tanks. On the surface, the data appear to indicate a very low liquid fraction (or high gas fraction) throughout the convective layer, which is contrary to the basic understanding of the waste configuration.

However, AN-105 and, to some extent, AN-104 may have an unusual propensity for waste to deposit on and adhere to steel surfaces. Thus, the low neutron count may be a result of a thick layer of crystalline solids with a relatively low liquid content covering the MIT pipe in the convective layer. Apparently this layer disappears in the nonconvective layer. The main evidence for this phenomenon is observation of a very large encrustation of waste around a sludge weight (a small spherical metal weight attached to a cable) that was pulled out of the tank in 1996. A video frame captured during the extraction is shown in Figure 5-39. Based on visual comparison of the waste ball and the barely visible 1/8-in. diameter cable above it, the ball's diameter was more than 12 in. (30 cm).

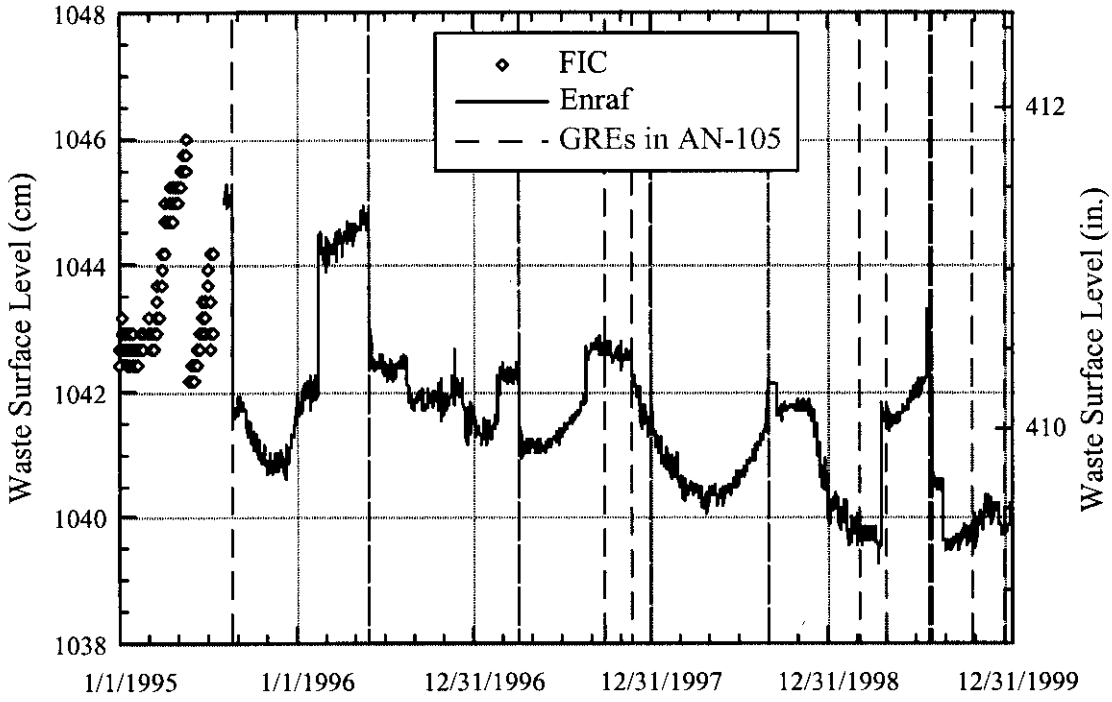

Figure 5-35. Tank 241-AN-105 Level and Gas Release Event History

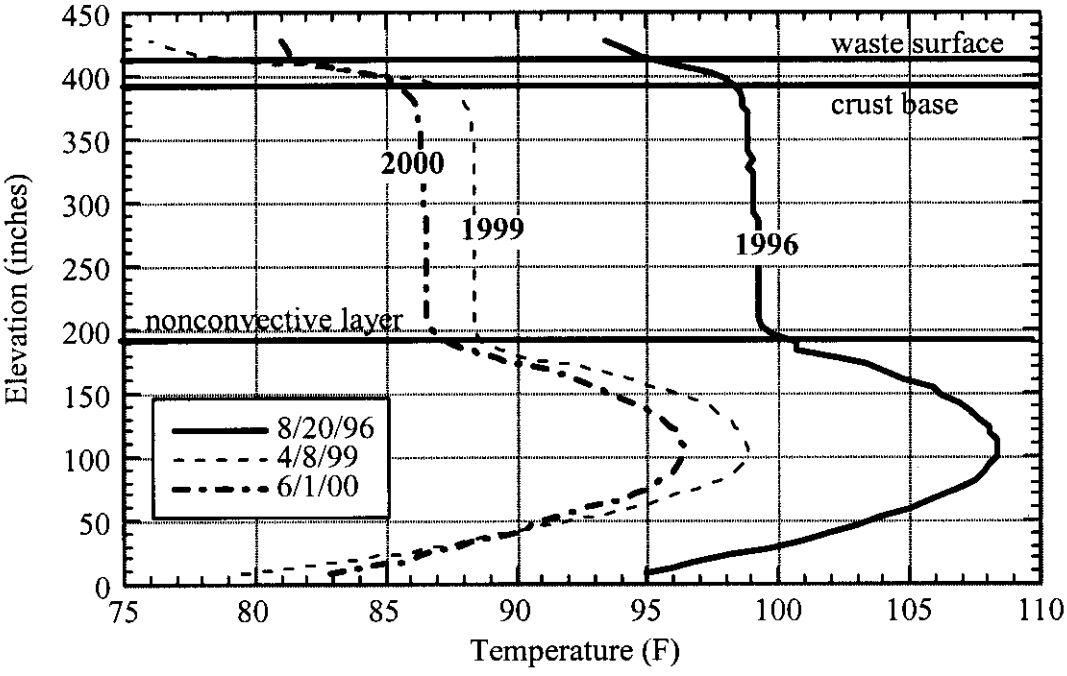

Figure 5-36. Tank 241-AN-105 Temperature Profile Change from 1996 to 1999

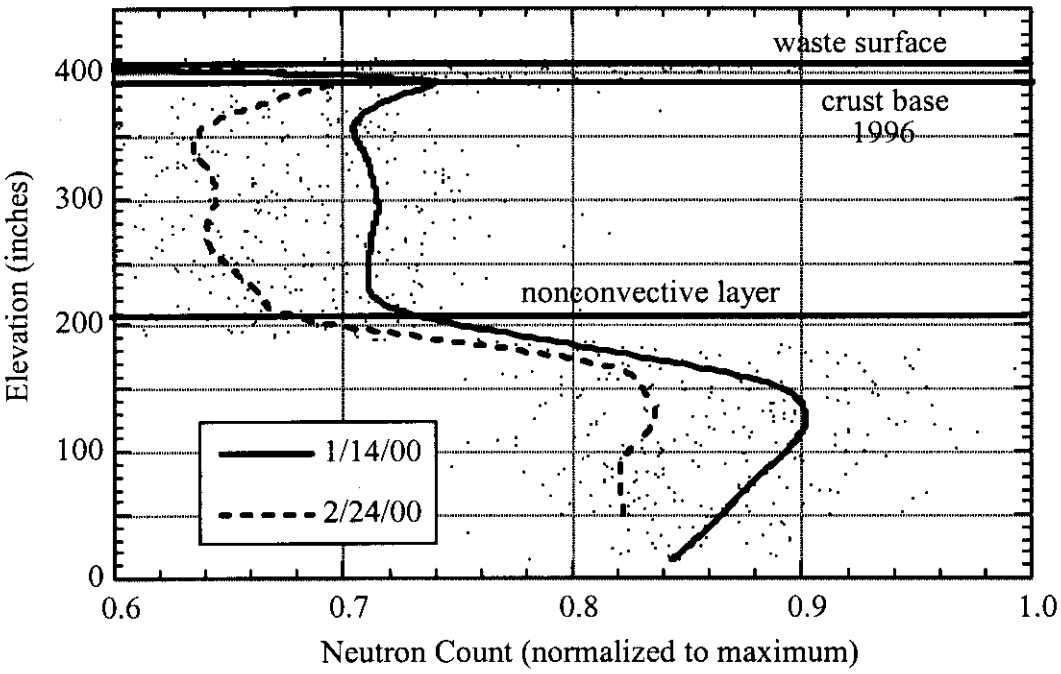

Figure 5-37. Tank 241-AN-105 Normalized Neutron Profiles

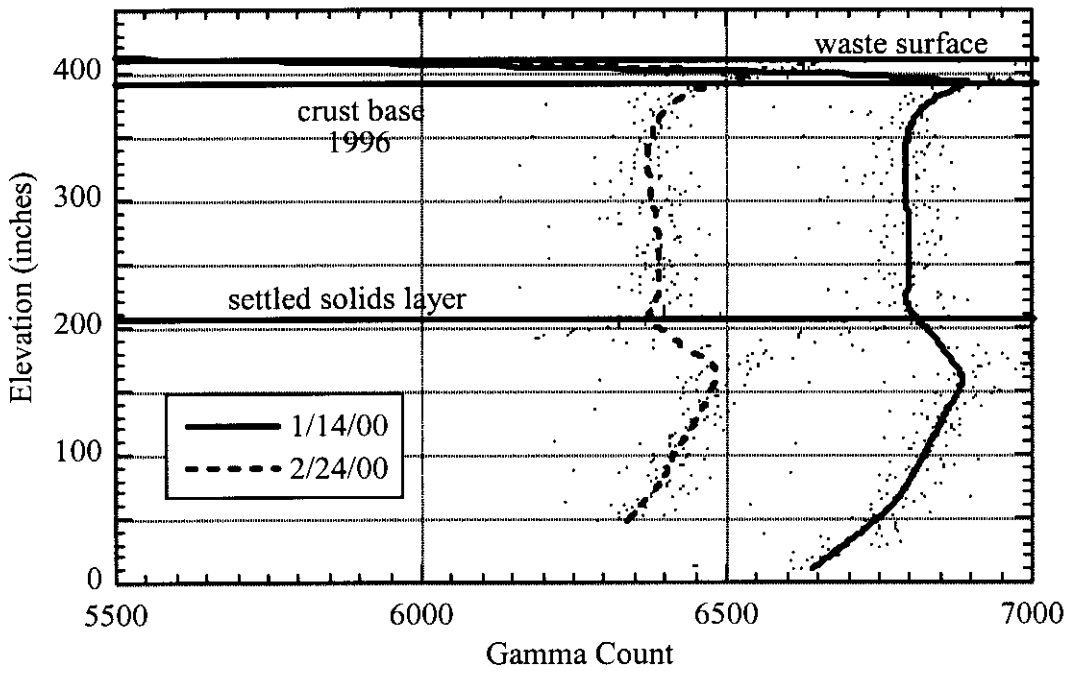

Figure 5-38. Tank 241-AN-105 Gamma Profiles

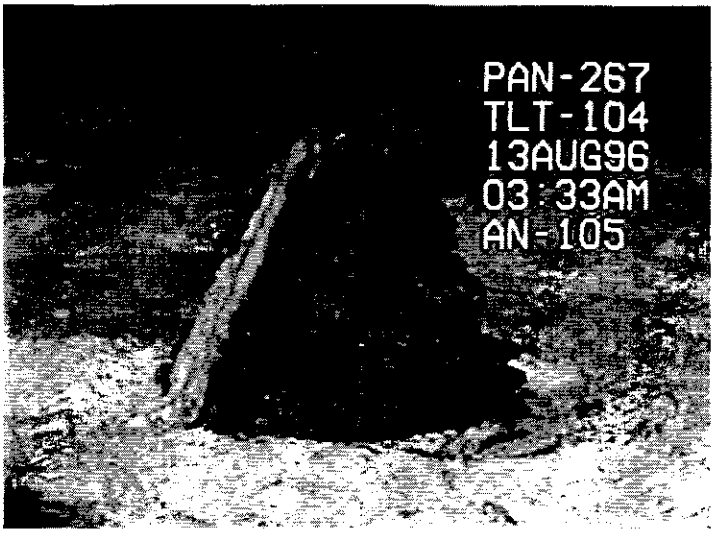

Figure 5-39. Sludge Weight Extraction from Tank 241-AN-105

Because of what appears to be an anomalous waste deposit on the MIT, the neutron and gamma scans are of questionable value in investigating the waste configuration. Assuming that the data is valid in the lower part of the nonconvective layer, the decreasing neutron and gamma counts below 150 in. is consistent with the void distribution and suggests that the void distribution has not changed significantly.

The waste in AN-105 has cooled by about 8 to 10 °F overall and, based on the waste level history, the retained gas volume has decreased slightly. The increased frequency of GREs, from about one very large release per year in previous years to six releases in 1999 (four of them quite small, and only two moderately large ones) suggests that the ability of the waste to retain gas has decreased. The temperature profiles also show that the waste configuration has not changed significantly in the last four years.

5.4.4 Tank 241-AW-101 Waste Configuration History

The surface level in AW-101 since 1995 is shown in Figure 5-40, along with the occurrence of GREs, as indicated by the headspace hydrogen concentration data. The waste level has remained approximately constant after a 1-in. decrease from late 1996 to early 1997. The GRE frequency was fairly high, at 6 to 8 per year, until about mid 1996. These were relatively large releases, with peak hydrogen concentrations ranging from 1,000 to 6,000 ppm. There were no releases from mid-1996 to early 1998. Three GREs occurred in 1998 and one in April 2000. All were quite small (less than 500 ppm peak hydrogen concentration). None occurred in 1999. Level change and GREs might generally be considered essentially independent in this tank.

Figure 5-41 shows temperature profiles from validation probe runs in AW-101 in 1997, 1999, and 2000. The temperature has decreased by about 5 °F during this period, consistent with the waste temperature history (see Section 4.4). The change in shape of the temperature profile in the nonconvective layer indicates that the top of the nonconvective layer rose by 10 to 12 in. (25

to 30 cm) between 1997 and 1999, while the waste surface rose less than half an inch (1.3 cm). At the same time, the thickness of the conductive part of the crust decreased by as much as 20 in. (51 cm) while a thickening layer of inhibited convection developed from the base of the crust down to 225 in. to 250 in. (572 to 635 cm). It appears that the lower 20 in. (51 cm) of the crust may have separated from the main mass. About half of this material fell to the top of the nonconvective layer while the rest may be loosely suspended in the upper half of the convective layer.

This process is apparently still developing in AW-101. A similar, but less conspicuous phenomenon can be discerned in the AN-103 temperature profiles (see Section 5.4.1). The temperature profile in SY-101 developed a similar shape in December 1998 and March 1999 prior to a crust "rearrangement" event in April and May 1999 during which the crust thickness increased by about a meter (Rassat et al. 2000). It is unclear whether this kind of crust thickening process will occur in AN-103 or AW-101 as their crusts are not regularly supplied with small gas bubbles as a result of mixing, as had occurred in SY-101. Validation probe runs should be made and the data analyzed after several more months to determine where the process may end.

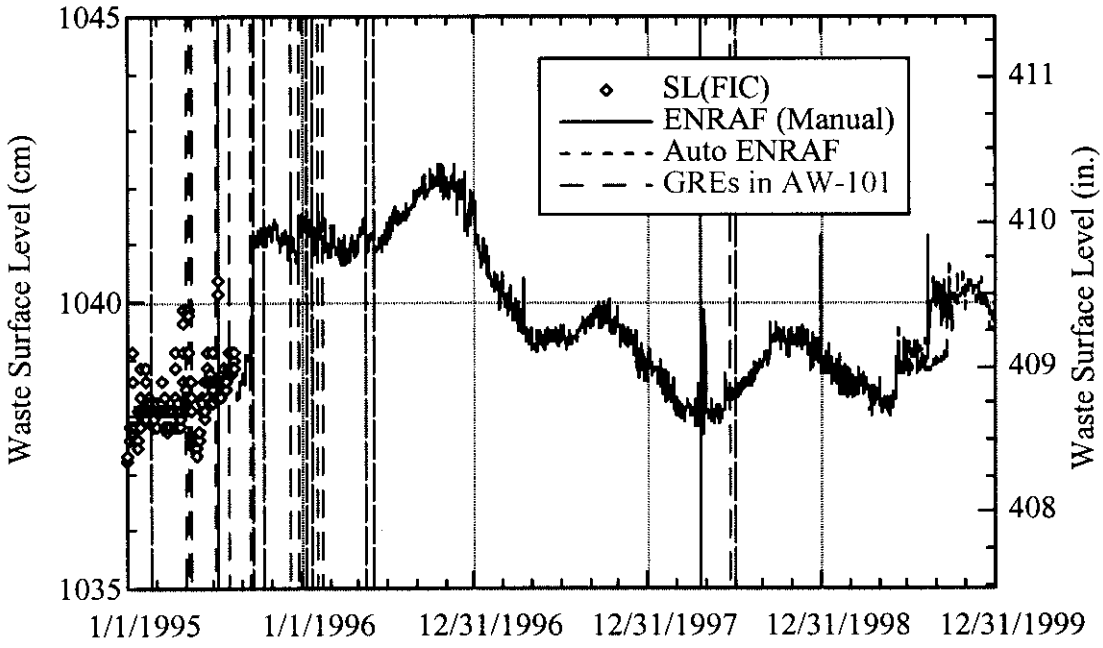

Figure 5-40. Tank 241-AW-101 Level and Gas Release Event History

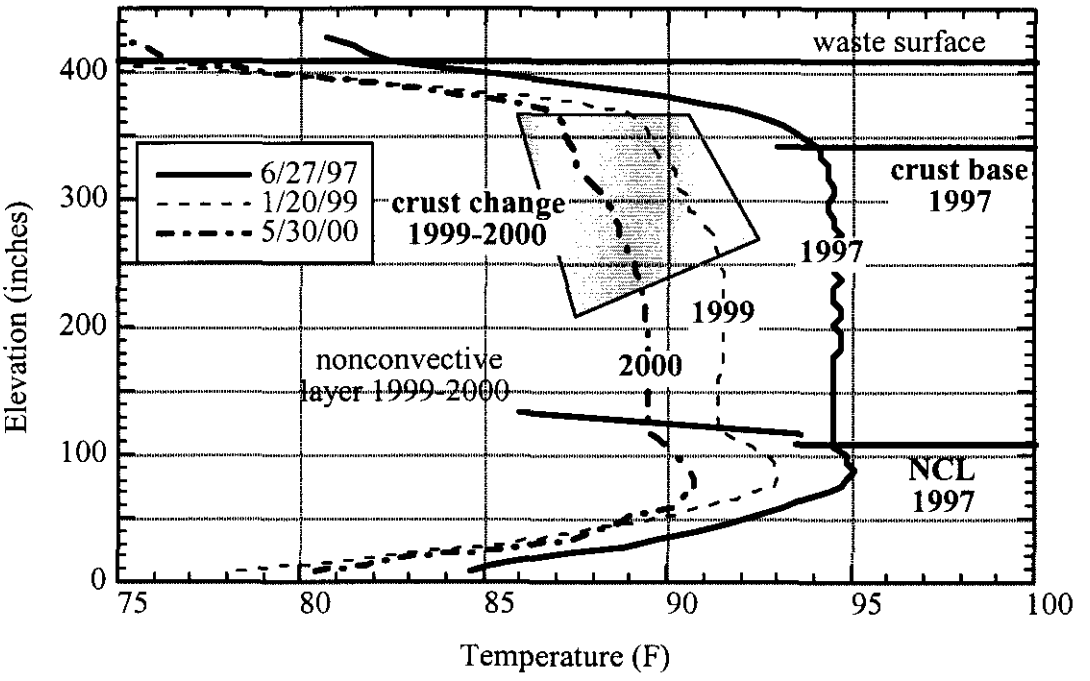

Figure 5-41. Tank 241-AW-101 Temperature Profile Change from 1997 to 2000

Void fraction measurements obtained in 1996 with the VFI and RGS (see Figure 7-4) show that most of the retained gas in the tank is relatively deep in the nonconvective layer with the maximum void fraction at about 40 in. (201 cm). This is consistent with the neutron and gamma scans shown in Figure 5-42 and 5-43. The neutron profiles in Figure 5-42 show a relatively high liquid fraction in the nonconvective layer, down to about 30 in. (76 cm). Below that point, the neutron count (particularly the April 20 profile) tapers off rather abruptly. The gamma profiles in Figure 5-43 show a steeper decrease in count with depth in the nonconvective layer. This suggests that the nonconvective layer has a relatively high liquid fraction, while the gas fraction does increase approximately linearly with depth.

The waste in AW-101 has cooled by about 5 °F overall during the past five years while the waste level has not changed significantly. However, the temperature profiles indicate that the crust thickness has decreased by about 20 in. (51 cm) from 1997 to 2000 while the nonconvective layer grew 10 to 12 in. (25 to30 cm). At the same time, the convective layer developed a region of less efficient convection below the crust. The observed crust behavior, the increasingly long periods of time between GREs, and the much lower volume of recent release events indicates a change in waste configuration and properties, even though the constant level indicates that the waste is not retaining gas. As the temperature profile is similar to that seen in SY-101 prior to a crust growth episode, these developments bear watching.

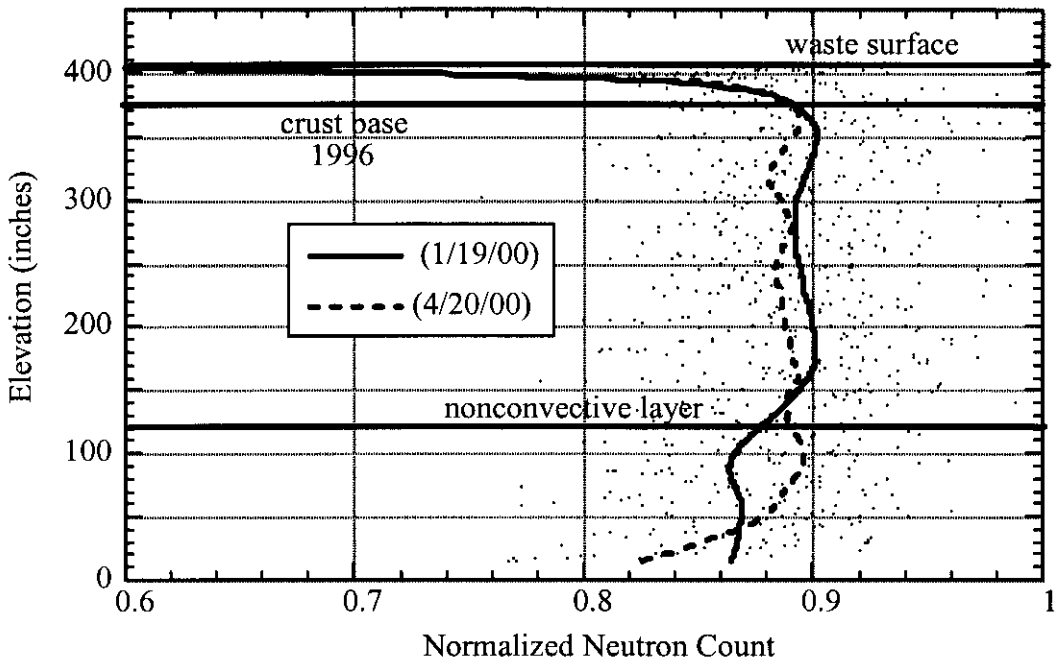

Figure 5-42. Tank 241-AW-101 Normalized Neutron Profiles

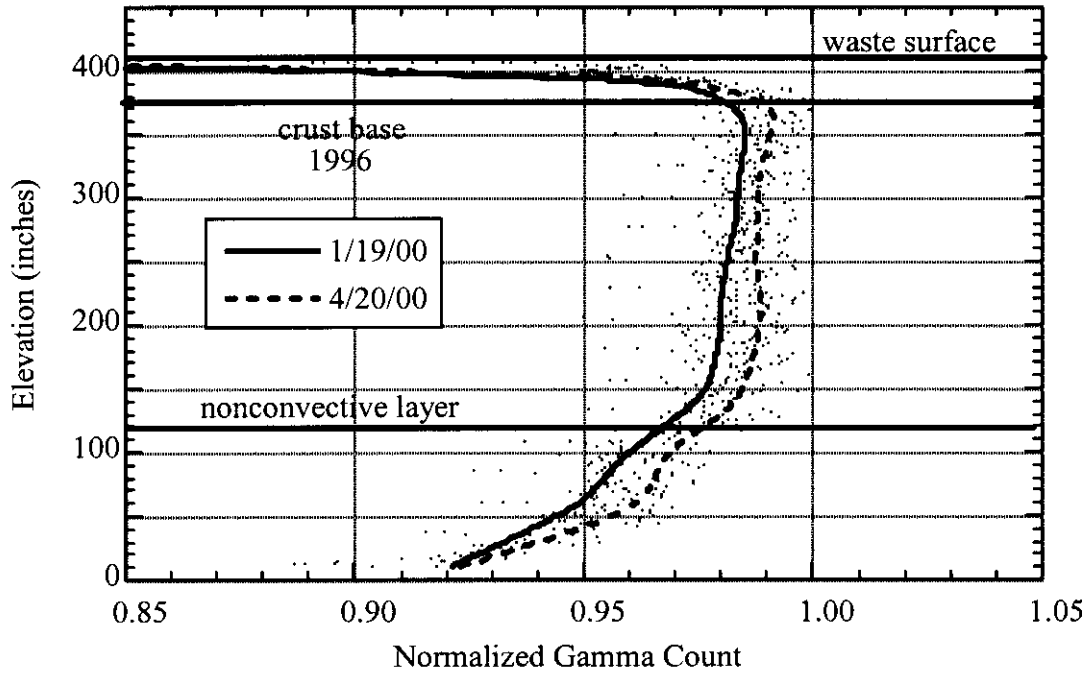

Figure 5-43. Tank 241-AW-101 Normalized Gamma Profiles

5.4.5 Tank 241-SY-101 Waste Configuration History

Because of the notoriety attendant on this tank's behavior, it has received far more attention than the other FGWL tanks. As a result, there is considerably more information on the waste configuration than in other tanks that are already well documented. Full treatment of the history of SY-101 is available in greater detail in Babad et al. (1992), Stewart et al. (1994), Brewster et al. (1995), Raymond (1998), Mahoney et al. (2000), and Johnson et al. (2000). Also, see the more recent quarterly reviews of SY-101 data by Conner and Koreski (1998, 1999a, b, c, and d). Only a brief overview of the waste configuration history for this tank is presented here.

The surface level in SY-101 since 1990 is shown in Figure 5-44, along with the occurrence of GREs. These events were quite regular and quite large, relative to the other FGWL DSTs, until installation of the mixer pump in July 1993. For about three years after that, the surface level was essentially constant then the crust growth trend began to be visible in early 1996, and continued at an accelerating rate until late 1999, when waste transfer and back-dilution operations were initiated. Note that the ENRAF™ level gauge in Riser 1A has been taken to indicate the top surface of the crust while the ENRAF™ in Riser 1C shows approximately the free liquid level since it was frequently flushed with water.

Figure 5-45 shows typical temperature profiles from each stage of the tank's history. The January 1993 profile was recorded a few days before a major GRE and shows the deep nonconvective layer. The mixer pump mobilized these solids and kept the nonconvective layer from forming except for a shallow layer of loosely settled particles that were disturbed each time the pump was run. This resulted in the more uniform temperature profiles seen in the 1996 and 1999 data. The changing shape of the upper portion temperature profiles in these plots show the dramatic increase in crust thickness between 1996 and 1999.

Void fractions were measured with the VFI in 1994-95 (see Figure 7-2) and again in 1998 with RGS void measurements also performed in 1998 and 1999 (Mahoney et al. 1999). Mixer pump operation kept the void fractions in the mixed portion of the tank at essentially zero. In 1994-1995 a thin layer of relatively high void fraction waste was found on the tank bottom but this material had been excavated before the 1998 data. High void fractions (above 50%) were found in the crust layer with the RGS that showed that crust growth included a significant gas volume increase.

Neutron and gamma scans have been run approximately every two weeks in this tank since February 1999. Neutron profiles in Riser 17B before and after transfer and back dilution are compared in Figure 5-46 and the gamma profile comparison is shown in Figure 5-47. These comparisons clearly show the effect of the transfer and back-dilution on the waste configuration. The 1999 neutron profile clearly shows the thick crust and high-void layer at its base. There is no evidence of a crust in June 2000, and the average count is higher, consistent with a higher water content from dilution. The thick crust layer is also clearly visible in the 1999 gamma profile but not in 2000. The ~120-in. (305 cm) nonconvective layer that formed after April 2, 2000, when mixing ceased is also clearly visible. These and other data show that gas retention in SY-101 has been remediated.

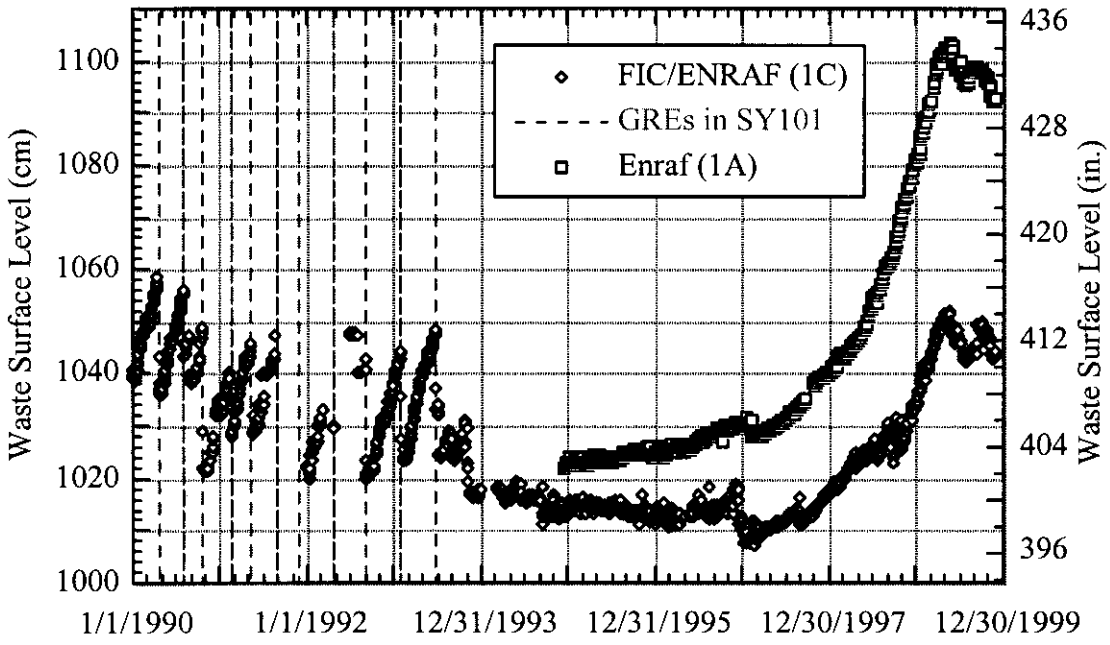

Figure 5-44. Tank 241-SY-101 Level and Gas Release Event History

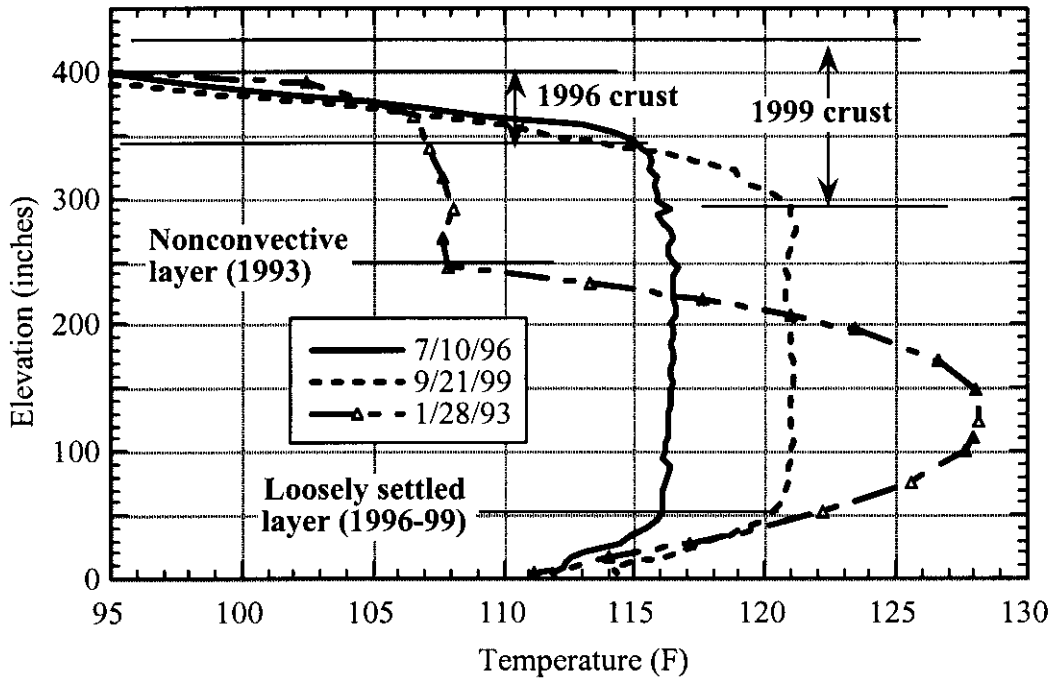

Figure 5-45. Riser 17B Temperature Profile Change from 1993 to 1999

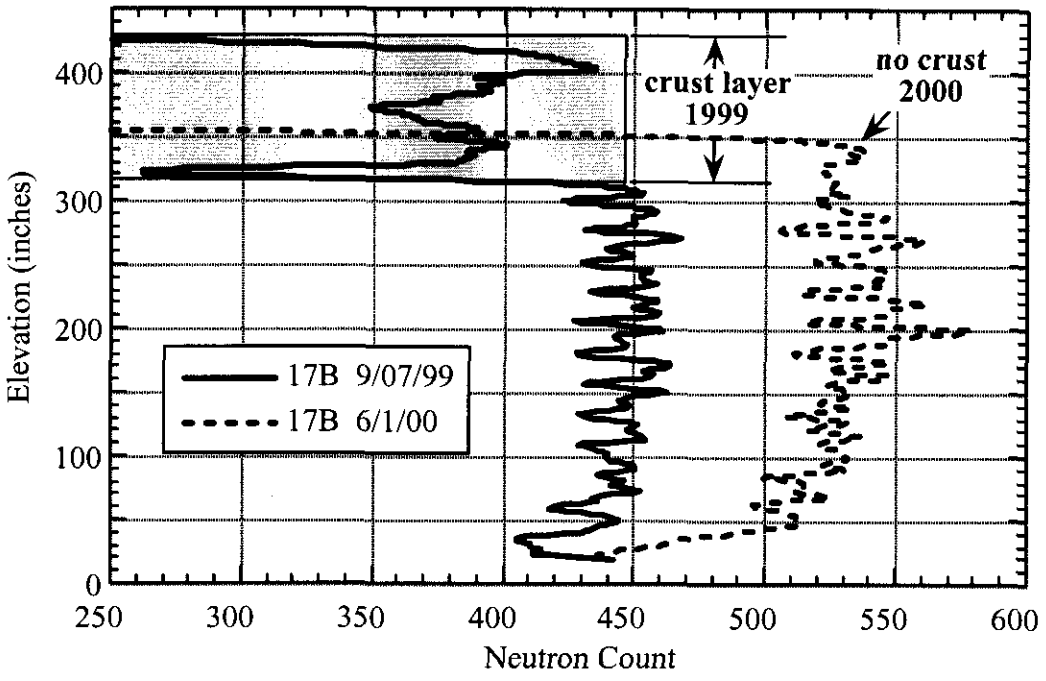

Figure 5-46. Tank 241-SY-101 Neutron Profile Comparison

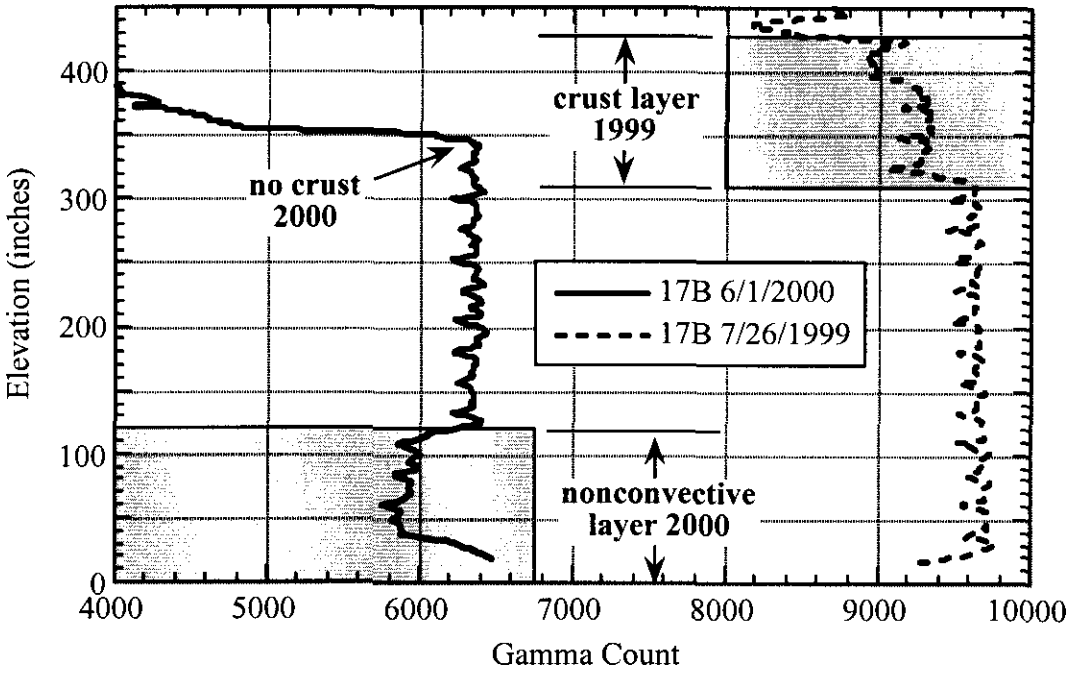

Figure 5-47. Tank 241-SY-101 Gamma Profile Comparison

5.4.6 Tank 241-SY-103 Waste Configuration History

The surface level in SY-103 since 1995 is shown in Figure 5-48, along with the occurrence of GREs, as indicated by the headspace hydrogen concentration data. The peak hydrogen concentration is generally a few thousand ppm. The surface level between January 1995 and January 2000 has decreased on the average only 2 to 3 cm (~1 in.), but the level changes associated with individual GREs range from 2 cm to as much as 9 cm. In this tank, GREs are almost always associated with a distinct level drop. Unlike the other tanks, the ventilation rates have not changed. Thus the waste temperature has not decreased and the GRE behavior has not changed in any major way over the last four years. With significant GREs still occurring, detectable changes in waste configuration should be expected in this tank.

Figures 5-49 and 5-50 show temperature profiles in SY-103 obtained each October and April, respectively, since 1996.[10] The temperature profiles for SY-103 appear to be much more dynamic than those of the other FGWL DSTs discussed above. This may be only because there are more of them, but it may also be due to the size and frequency of GREs in this tank. The depth of the non-convective layer changes from year to year. This layer was about 100 in. thick in April 1996, but had grown to approximately 150 in. (381 cm) by April 1997. In April 1998 it had dropped back to about 120 in. (305 cm). The most recent profile, obtained in March 2000, shows the top of the non-convective layer at about 130 in.

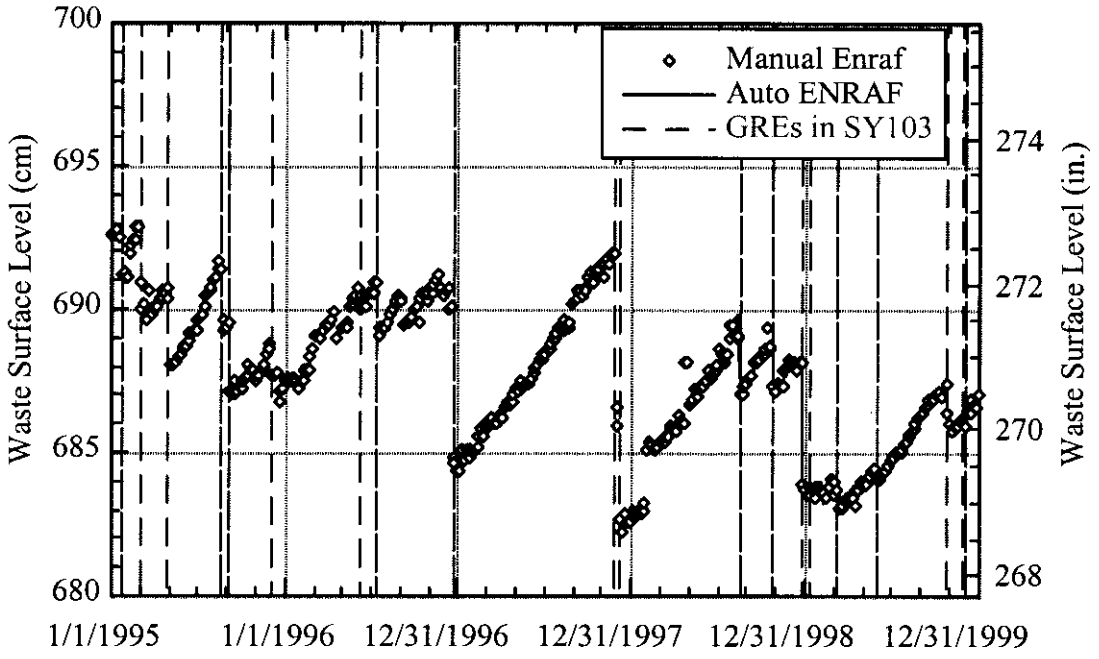

Figure 5-48. Tank 241-SY-103 Level and Gas Release Event History

[10] The profile for April 1999 is not shown because the recorded elevations appeared to be anomalously high, implying a waste level about two feet higher than recorded by the ENRAF™ gauge.

The waste temperatures show similar erratic behavior from 1996 to the present but the average has held relatively constant. The overall temperature dropped by about 4 to 5 °F at the end of December 1996 when the thermocouples were connected to the TMACS system and re-calibrated (a major GRE occurred at the same time which affected temperatures through the nonconvective layer). However, as shown in Figure 5-49, the October convective layer temperatures stayed within 1 °F from 1997 through 1999. In Figure 5-50, the April convective layer temperature variation was within about 2 °F. The peak non-convective layer temperature shows a net decline of up to 5 °F overall. The waste temperature history for this tank (see Section 4.2) is consistent with these profiles.

Void profile data obtained in 1995 in SY-103 using the VFI (see Figure 7-3) show a distinct difference between the void profile at the two risers where the measurements were made. The void in the vicinity of Riser 22A is generally higher in the waste with a peak at about 70 in. (178 cm) At Riser 17C the void is found lower in the tank with the highest void fraction near the bottom. No GREs were observed in the month between the two measurements, but an event that dropped the crust by about 2 cm occurred within two months prior to the first measurement. The differences between the two profiles may be the result of the GRE occurring at one location but not the other. This might illustrate the void fraction changes before and after a GRE with the Riser 22A data representing "pre-GRE" state and Riser 17C the "post-GRE" condition.

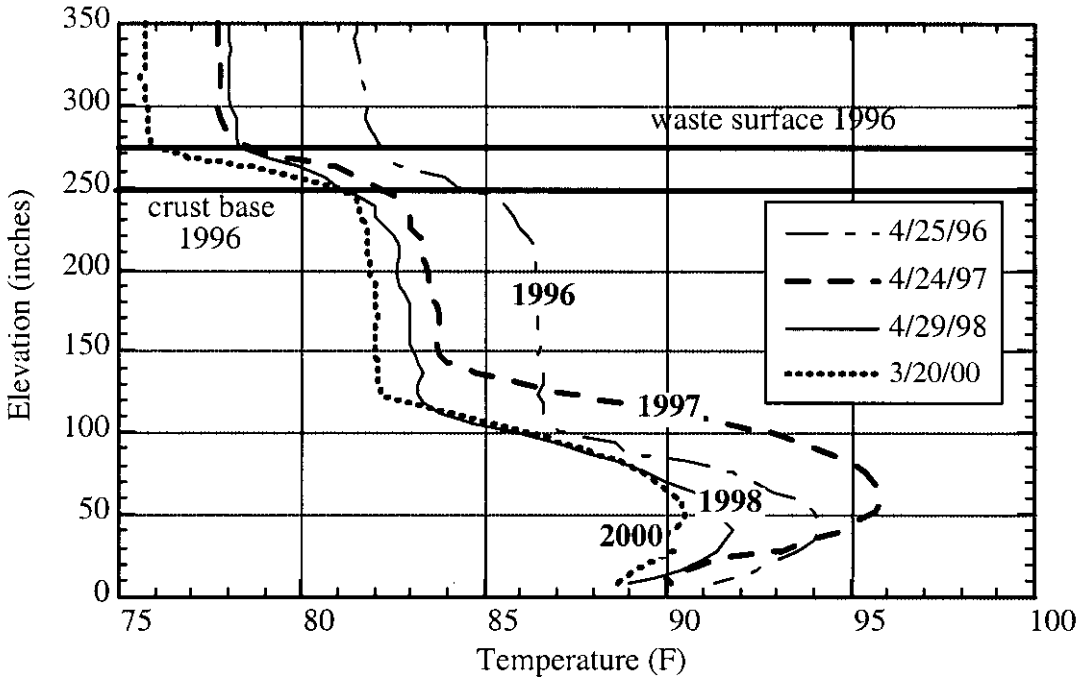

Figure 5-49. Tank 241-SY-103 Spring Temperature Profiles from 1996 to 2000

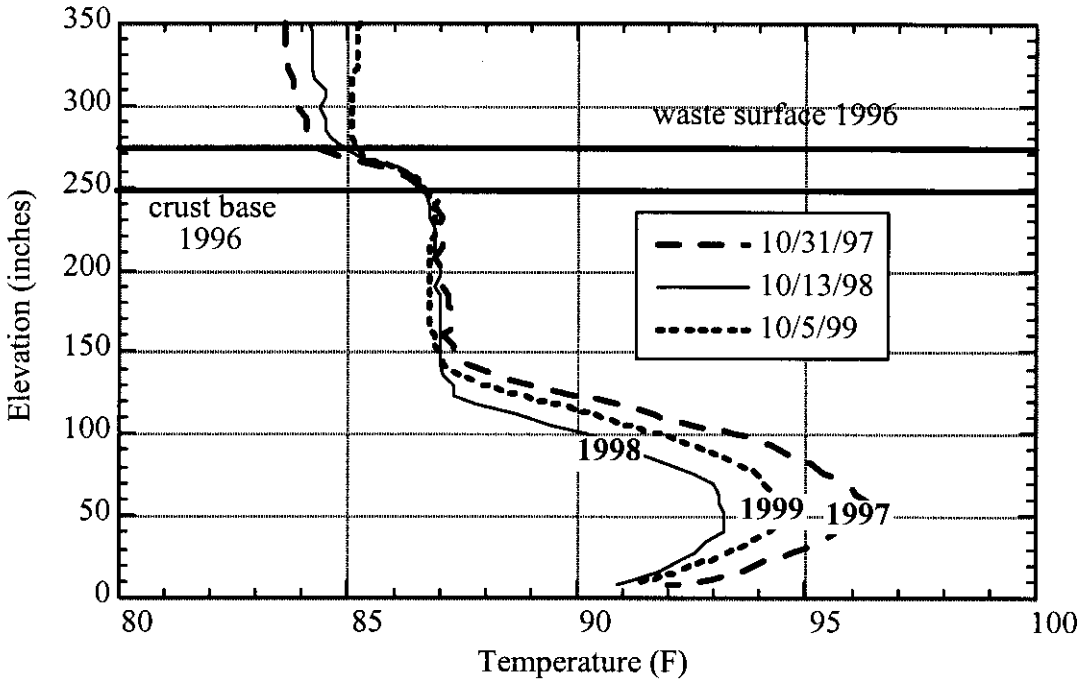

Figure 5-50. Tank 241-SY-103 Fall Temperature Profiles from 1997 to 1999

The level change with GREs and the year-to-year differences in the temperature profiles suggest that the void distribution in the waste has been similarly dynamic from 1995 to the present. However, the lack of major change in waste level or average temperature imply that the total gas volume has not changed significantly.

The neutron and gamma profiles for January and April, 2000, are shown in Figures 5-51 and 5-52. The neutron profile is relatively uniform down to about 60 inches, where the count suddenly begins a steep, linear decrease. This trend might be more consistent with the "post-GRE" void profile with the gas low in the waste. The gamma profile shows a decreasing count with depth all the way through the nonconvective layer with an inflection between 60 and 80 in. Either the "pre-GRE" or "post-GRE" void distribution might be consistent with this profile.

The measurements presented above show that the waste configuration in SY-103 is a dynamic one. Significant GREs have continued to occur from 1995 through 2000 that affect the waste level and temperatures as well as the depth of the nonconvective layer. However, neither the waste level nor the average temperature have changed significantly in this tank during the period so the changes in the various parameters represent oscillation about a steady base line.

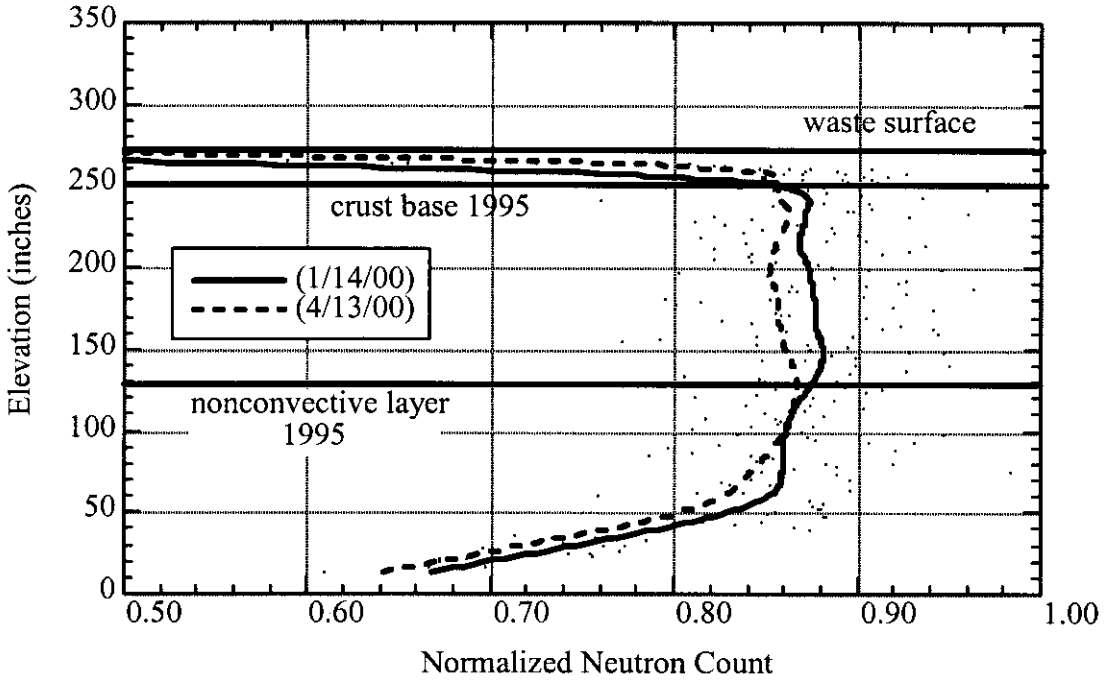

Figure 5-51. Tank 241-SY-103 (Normalized) Neutron Profiles

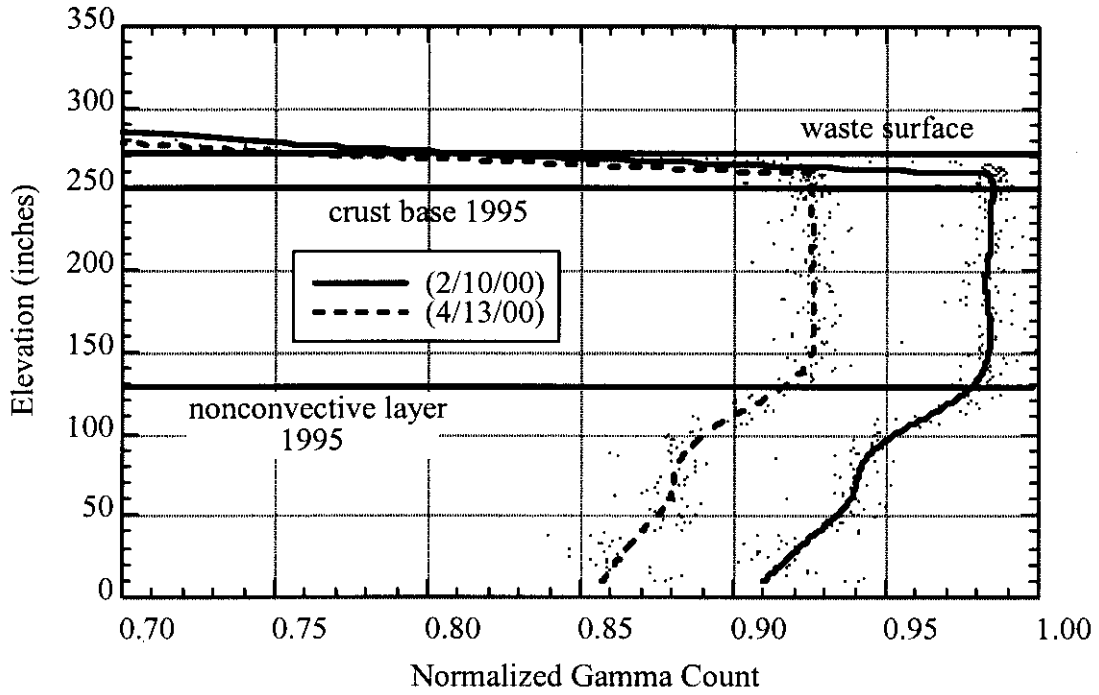

Figure 5-52. Tank 241-SY-103 (Normalized) Gamma Profile

This page intentionally left blank.

6.0 GAS GENERATION AND COMPOSITION

Gas generation rate is a key parameter in determining whether a tank will experience buoyant displacement gas releases in the DSTs (Meyer and Wells 2000). If such GREs occur, the gas generation rate is also in important factor in determining their frequency. Results of laboratory experiments reveal the effects of changes in dose rate, chemical composition and temperature. This knowledge allows future states to be predicted and creation of hazardous tanks to be avoided.

The composition of the gas generated, stored, and released from the waste must be known to determine whether the tank headspace can become flammable following a gas release. While gas generation tests can provide insight on trends in composition, the data most representative of gas composition that is actually released is provided by in-situ measurements. Steady-state headspace gas composition measurements also provide some information but are affected by transport processes and do not represent the bulk of the stored gas. The steady-state headspace concentration ratios (e.g., H_2/N_2O) are also quite variable and do not typically match the in-situ gas concentrations or those derived from laboratory gas generation tests.

This section summarizes the available gas composition measurements as well as gas generation data. Section 6.1 summarizes in-situ gas composition measurements with the RGS, and Section 6.2 covers headspace gas composition measurements. Section 6.3 discusses the results of laboratory gas generation tests on DST wastes, and Section 6.4 covers field gas generation data. Section 6.5 summarizes the gas generation and composition issue.

6.1 RETAINED GAS COMPOSITION MEASUREMENTS

The released gas composition has been estimated from the headspace gas concentrations after large GREs in SY-101 (Sullivan 1995) and inferred from the ratios of steady-state headspace concentrations (Van Vleet 1996). Since 1996, measurements of the in-situ composition of the stored gas have been made with the RGS. The composition can also be inferred from laboratory gas generation tests that have been performed with waste samples from a few of the tanks. The gas compositions measured in the core sampling drill string are also of interest since a major source of the drill string gas is bubbles retained in the nonconvective waste. Gas compositions obtained with the RGS are presented in Section 6.1.1, and compositions determined from gas release data or laboratory gas generation tests are summarized in Section 6.1.2. Drill string gas compositions are given in Section 6.1.3.

6.1.1 Retained Gas Sampler Gas Compositions

The composition of free (undissolved) gas measured within the waste is considered to be the best representation of the composition of the gas released in buoyant displacement events (Barker et al. 1999). The RGS is the only instrument in use that provides in-situ waste gas composition directly. These measurements are available for AN-103, AN-104, AN-105, AW-101, and most

recently for SY-101 (Mahoney 2000). The gas compositions measured by the RGS in the DSTs are summarized in Table 6-1.

A salient feature of these data is that the hydrogen concentration is significantly lower and the nitrogen concentration is significantly higher in the convective liquid than in the nonconvective layer. The nitrous oxide concentration is also typically somewhat lower in the liquid except in AN-103. However, the total amount of gas in the convective layer is also very small, therefore, its concentration is unimportant to the total flammability of the tank.

Table 6-1. Retained Gas Sampler Gas Compositions (mol%)

Tank Layer	Hydrogen	Nitrogen	Nitrous Oxide	Ammonia	Methane	Other Gases
AN-103 NCL	61 ± 8	33 ± 4	4 ± 0.6	< 1	< 1	< 1
AN-103 CL	19 ± 12	70 ± 62	8 ± 5	< 1	1.4 ± 1	1.4 ± 0.6
AN-103 Crust [a]	62 ± 6	29 ± 3	7 ± 1	1.4 ± 0.6	< 1	< 1
AN-104 NCL	45 ± 7	29 ± 5	23 ± 4	< 1	< 1	< 1
AN-104 CL	25 ± 13	56 ± 49	14 ± 8	< 1	1.9 ± 1.3	2.6 ± 1.4
AN-105 NCL	60 ± 5	24 ± 4	14 ± 2	< 1	< 1	< 1
AN-105 CL	25 ± 12	58 ± 42	11 ± 6	< 1	1.4 ± 0.9	3 ± 2
AW-101 NCL	32 ± 3	56 ± 6	7 ± 1	< 1	1.7 ± 0.2	3 ± 0.5
AW-101 CL	26 ± 9	67 ± 32	2 ± 1	< 1	1.0 ± 0.4	3 ± 2
SY-101 Slurry	30 ± 9	37 ± 13	25 ± 7	6 ± 2	1.4 ± 0.5	1.3 ± 0.5
SY-101 Crust [b]	34 ± 4	28 ± 5	20 ± 2	18 ± 5	< 1	< 1

Notes:

(a) From only one crust sample in AN-103.
(b) From several crust samples obtained at different elevations and locations in SY-101.

6.1.2 Other Estimates of Retained Gas Composition

The waste gas compositions in SY-101 prior to mixing was derived from the values given in the mixer pump safety assessment (Sullivan 1995). The composition in the safety assessment represents the released gas, including the ammonia co-released from the liquid by evaporation, not the waste gas. The waste gas concentrations are derived by reducing the ammonia concentration from the reported 11% to 6%, which is the estimated ammonia concentration in the bubbles, and normalizing the other species accordingly. The uncertainties are computed as the difference between the "conservative estimate" and "best estimate" values given in the safety assessment. These concentrations and those of the other tanks estimated by means other than RGS samples are given in Table 6-2.

The gas composition in SY-101 has not changed significantly in the six years since the mixer pump halted the large gas releases. There has been a steady, nearly linear decline in the headspace concentration of nitrous oxide (Conner and Koreski 1999a). However, the RGS results from late 1998 given in Table 6-1 reveal only a slightly lower N_2O concentration in the mixed slurry balanced by a slightly higher nitrogen concentration. The ammonia concentration

also compares well with that estimated from the gas releases. The crust layer in SY-101 prior to remediation was much higher in hydrogen and ammonia than the slurry layer with correspondingly less nitrogen and nitrous oxide. The gas composition could be expected to change after the recent dilution and cooling of the waste. The gas generation rate is approximately an order of magnitude lower (Kirch et al. 2000).

No RGS samples are available for SY-103, and its gas releases are not large enough to estimate the retained gas composition from the post-release headspace concentrations. In the past, SY-103 was assumed to have the same gas composition as SY-101 because it contained similar waste though at a much lower temperature. Gas generation tests on actual waste samples have provided a better estimate of the gas composition in this tank (Bryan et al. 1996). Gas compositions based on generation rates extrapolated to in-tank conditions are also given for AW-101 (King and Bryan 1999) and AN-105 (Person 1998) for comparison with RGS results (see Section 6.3 for details).

Generation rates are provided only for hydrogen, nitrous oxide, and nitrogen at tank conditions. The fraction of each of these gases in the waste is assumed to be proportional to these generation rates. Concentrations of ammonia and other gases must be estimated by other methods. The ammonia concentrations in SY-103 are assumed to be negligible as indicated by the yield from the gas generation tests performed at the lowest temperature. The ammonia concentration for AW-101 and AN-105 is assumed negligible as indicated by the RGS. The AN-105 gas concentrations compare quite closely to RGS values while those derived from generation rates in AW-101 are far higher in hydrogen than found by the RGS.

Table 6-2. Non-Retained Gas Sampler Gas Compositions Estimates (mol%)

Tank Layer	Hydrogen	Nitrogen	Nitrous Oxide	Ammonia	Methane
AN-105 [a]	58	15	26	-	< 1
AW-101 [a]	79	8	13	-	< 1
SY-103 [a]	54	31	14	-	1.2
SY-101 [b]	30	35	26	6	< 1

Notes:

(a) Based on gas generation rates assuming negligible ammonia.

(b) Based headspace measurements during gas releases with ammonia reduced to 6%

6.1.3 Gas Composition from Drill String Samples

Drill string samples are taken during tank waste core drilling operations primarily to ensure safe working conditions during core drilling. Under certain circumstances, these samples also provide data on gases retained in the tank waste. Siciliano (1998) provides a detailed description of the process of extracting, from this type of sample, data relevant to characterizing retained gases. These data provide approximate retained gas information on tanks not sampled using the more refined RGS method.

The drill string is the passageway through which core samplers are lowered into the waste and cores are retrieved. Vapors or gases that are released from the waste during the drilling are contained in the headspace of the drill string. During the tank waste coring operation, hazardous gas monitoring is employed to verify that hazardous gases in the drill string are below specified safety limits. When the limits are exceeded, a grab sample may be collected for later laboratory analysis. In addition, the drill string headspace may be purged with argon or N_2 or air may be admitted to the drill string. Thus, subsequent grab samples can contain residual purge gas or air, which complicates the interpretation of the results. The sample containers sometimes also contained residual helium from their preparation.

The samples were analyzed using mass spectrometry at the Pacific Northwest National Laboratory (PNNL) Analytical Chemistry Laboratory. Because O_2, argon, and helium are not produced in the waste, the measured amounts of these gases were assumed to be residuals from either the sample container preparation or drill string purging, and used to correct for air/purge gas contamination. Siciliano (1998) provides the details of data correction. Table 6-3 lists the drill string samples collected in the FGWL DSTs and the concentrations of the primary gases in each sample. Ammonia is not listed because, as in the case of SHMS grab samples, the sampling methods and devices did not allow this species to be properly measured.

Table 6-3. Adjusted Gas Analysis Data from Drill String Samples

Tank	H_2 (mol%)	CH_4 (mol%)	N_2 (mol%)	N_2O (mol%)	Other (mol%)
AN-103	48	0.2	47	5	0.3
AN-104	33	0.9	54	11	0.6
AW-101	25	-	73	2	-

6.2 HEADSPACE GAS COMPOSITION MEASUREMENT

The concentration of a waste gas in a tank headspace at any time is a function of the concentration of the gas at some initial time, the rate of gas release by the waste, ventilation rate, and the degree of mixing in the headspace. To the extent that the gas release and ventilation rates are constant, the concentrations of waste gases will approach constant (steady-state) values.

One limitation of headspace composition measurements is that headspace gas concentrations are inherently based on the rates of gas release from the waste surface and may not be representative of the retained gases within the waste. Gases that are soluble in the aqueous waste are transported to the waste surface via diffusion and convection in the aqueous phase, where they may be released by evaporation into the headspace. Less soluble gases are not efficiently transported by this mechanism and tend to accumulate as bubbles trapped in the waste.

Headspace gas composition data have been obtained in the FGWL DSTs by "grab" samples that are routinely collected using SHMS and are given below. Gas samples have also been collected from SSTs using SUMMA[11] canisters and sorbent traps which are not discussed in this report.

Gas grab samples are routinely collected from the SHMS cabinets for laboratory analysis. Grab samples are also collected automatically when a high-level alarm is activated by a monitoring instrument. A description of the sampling system and the analytical method is given by McCain (1999). The SHMS grab samples have been analyzed for permanent gases by mass spectrometry at the PNNL 325 Laboratory. Table 6-4 lists the SHMS grab sample results for the FGWL DSTs (McCain 1999). The H_2 averages include the reported detection limits, when no H_2 was detected in the sample. The average H_2 to N_2O ratio includes only samples for which both H_2 and N_2O concentrations were above detection limits.

Boldface type has been used to indicate that the maximum reported H_2 concentrations in AN-103, AN-104, AN-105, AW-101, and SY-103 are each associated with a gas release event, and were collected automatically by a high-level alarm. All of these measured hydrogen concentrations are well below the LFL of hydrogen at 40,000 ppmv in air.

Table 6-4. Standard Hydrogen Monitoring System Cabinet Grab Sample Data

Tank	Number of H_2 Samples	Average H_2 (ppmv)	Average H_2/N_2O	Maximum H_2 (ppmv)
AN-103	62	44	11	**800**
AN-104	57	27	6.2	**154**
AN-105	35	476	5.3	**10,700**
AW-101	39	426	43	**2,980**
SY-101	9	14	0.9	22
SY-103	56	229	2.0	**1,810**

6.3 LABORATORY GAS GENERATION STUDIES

Gas generation rates have been measured on a variety of chemical simulants and on Hanford waste core samples. An excellent summary and interpretation of the results obtained through 1996 is given by Pederson and Bryan (1996). Besides samples from a number of SSTs, DST wastes tested include AN-105 core composites (Person 1998), convective layer samples from AW-101 (Bryan and King 1998) and SY-103 (Bryan et al. 1996), and a core composite sample from SY-101 (Person 1996).

Laboratory gas generation tests are performed in a hot cell (222-S Laboratory or the PNNL 325 Building hot cell facility) by measuring the volume of gas produced in a given time by a small waste sample in a small sealed vessel. These tests are particularly challenging because the gas generation rates are very low under tank conditions and the time required to obtain a measurable volume of gas is prohibitively long. To get around the problem, gas generation rates

[11] SUMMA is a trademark of Moletrics, Inc., Cleveland, Ohio.

are accelerated by increasing the temperature above 60 °C. Similarly, self-irradiation dose rate in a small sample is much lower than in the tank, and powerful external gamma sources are used (in PNNL tests) to increase the radiolytic gas production sufficiently to be measured with reasonable accuracy.

The gas generation rates at elevated temperatures without external irradiation are extrapolated back to tank conditions assuming the standard Arrhenius behavior,

$$Q_T = Ae^{-E_a/RT} \tag{6-1}$$

where Q_T is the thermal gas generation rate (mol/kg-d),
A is the pre-exponential constant (mol/kg-d),
E_a is the activation energy (kJ/mol),
R is the gas constant (0.008314 kJ/mol-K), and
T is the temperature (K).
A and E_a are determined fitting Equation 6-1 to the measured gas generation rates.

Similarly, comparing the gas generation rates at several temperatures with and without external irradiation, assuming that radiolytic gas generation is independent of temperature, provides a "G-value" from which the radiolytic contribution can be calculated as

$$Q_R = 2.488(10^{-8})GR \tag{6-2}$$

where Q_R is the radiolytic gas generation rate,
G is the "G-value" in molecules/100 ev and
R is the dose rate (R/h).

Q_R is determined by subtracting the thermal component calculated by Equation 6-1 from the measured total generation rate with external irradiation.

The results of hot cell gas generation tests on wastes from SY-101, SY-103, AW-101, and AN-105 are summarized in separate subsections below.

6.3.1 Tank 241-SY-101 Gas Generation Tests

Person (1996) performed gas generation tests on a core composite sample taken shortly after large gas release events in SY-101 in 1990-1991. The tests were run over a temperature range of approximately 65 to 100 °C with a cover gas of helium or a mixture of 30% oxygen and 70% helium. Additional tests were performed on a sample diluted 0.54:1 (diluent to original sample) with 2.5 M NaOH solution.

The results are summarized in Table 6-5. Dilution at 0.54:1 should have reduced the species concentration to 0.65 (1/1.54) of their original concentrations. Based on prior simulant studies (Ashby et al. 1994, Delegard 1980), this dilution should have reduced the gas generation rate to about $(0.65)^2$ or 0.42 of the undiluted rate. The observed reduction in gas generation was about

0.55. While this result is comparable with theory within experimental error, the difference might also be due to higher solution concentrations created by solids dissolution.

Table 6-5. Tank 241-SY-101 Experimental Gas Generation Rates

Waste	Temperature (°C)	Cover Gas	Rate (mol/kg-d)
Undiluted	100	He	4.9 (10^{-4})
Diluted [(a)]	65	He	1.1 (10^{-5})
Diluted [(a)]	100	He	3.0 (10^{-4})
Undiluted	70	0.3 O_2, 0.7 He	1.4 - 3.4 (10^{-4})
Undiluted	90 - 100	0.3 O_2, 0.7 He	1.5 - 2 (10^{-3})

Notes:
(a) Dilution was 0.54:1 (dilutent:original waste) with 2.5 M NaOH

The composition of the generated gas is given in Table 6-6. In both diluted and undiluted waste samples, nitrous oxide was produced in concentrations about double that of hydrogen at both 65 °C and 100 °C. The in-tank concentrations given in the LANL safety assessment (Sullivan 1995) that were determined from headspace concentrations during large gas releases were substantially different. The hydrogen, nitrogen, and ammonia concentrations are higher and the nitrous oxide concentration is much lower. In-situ measurements in the slurry below the crust with the RGS after mixing (Mahoney 2000) show a composition comparable to those determined during large releases. The lower hydrogen concentration found by Person (1996) are probably due to a much higher temperature and lower irradiation dose rate than found in-tank. Both conditions indicate a much larger contribution from radiolysis which favors hydrogen production over thermal reactions which favor production of nitrogenous gases.

Table 6-6. Gas Composition from Tank 241-SY-101 Waste

Sample	$[H_2]$	$[N_2O]$	$[N_2]$	$[NH_3]$	$[CH_4]$
Test Data					
Undiluted, 100 °C	0.22	0.43	0.27	0.02	0.05
Diluted, 100 °C	0.22	0.49	0.22	0.01	0.05
Diluted, 65 °C	0.22	0.48	0.25	0.01	0.01
Undiluted, 100 °C, O_2 cover	0.38	0.32	0.21	0.05	0.04
Other Measurements					
Headspace during GRE	0.29	0.24	0.33	0.11	0.004
RGS mixed slurry	0.30	0.25	0.38	0.04	0.014
RGS crust layer	0.37	0.22	0.30	0.09	0.006

When oxygen was added to the cover gas, hydrogen production was enhanced while that of nitrous oxide and nitrogen were not substantially affected. This resulted in approximately equal concentrations of hydrogen and nitrous oxide in the cover gas. The oxygen in the cover gas was

also partially consumed. This effect is generally consistent with the behavior observed in simulant studies by Barefield et al. (1996), Camaioni et al. (1995, 1996), and Meisel et al. (1993). It has also been mentioned as an explanation for higher hydrogen concentrations in the floating crust layer whose surface is exposed to the air in the tank headspace [RGS measurements reported by Mahoney et al. (1999) showed 32 to 40% hydrogen in the SY-101 crust layer]. However, the low diffusion rate of dissolved oxygen in the waste precludes atmospheric oxygen from having a measurable effect below the waste surface.

6.3.2 Tank 241-SY-103 Gas Generation Tests

Gas generation tests on a convective liquid layer sample from SY-103 were performed by Bryan et al. (1996) for temperatures from 60 to 120 °C with both self irradiation and irradiation by a 5,300 R/h gamma source. The self-irradiation dose for the sample was 119 R/h while the actual in-tank dose was calculated to be 444 R/h, about 75% of which derives from Cs-137 gamma decay.

The thermal gas generation rate was found to follow standard Arrhenius behavior (Equation 6-1), and the radiolytic gas generation rate was observed to be essentially independent of temperature. Pre-exponential factors and activation energies for the Arrhenius equation for thermal generation of hydrogen, nitrogen, nitrous oxide, and the total gas generation are given in Table 6-7 (Bryan and Pederson 1996). The table also shows the G-values for radiolytic gas generation. A comparison of the total thermal gas generation rates for SY-101 (Section 6.3.1) and SY-103 is shown in Figure 6-1. The undiluted SY-101 waste has statistically the same thermal gas generation rate as does SY-103 at 100 °C.

When the parameter values in Table 6-7 are used to extrapolate down to a tank temperature of 32 °C and a radiation dose of 444 R/h, the total gas generation rate is predicted to be 2 (10-^{6}) mol/kg-d. This compares quite well to the rate measured by Wilkins (1995) of 2.3 (10^{-6}) mol/kg-d.

Table 6-7. Gas Generation Parameters in Tank 241-SY-103 Convective Waste

Gas	Thermal		Radiolytic
	A (mol/kg-d)	E_a (kJ/mol)	G (molecule/100 ev)
Hydrogen	9.5 E +8	90 ± 9	0.14 ± 0.02
Nitrogen	3.2 E +7	80 ± 8	0.53 ± 0.06
Nitrous Oxide	4.5 E +12	116 ± 9	0.033 ± 0.009
Total	1.0 E +10	94 ± 6	0.8 ± 0.07

The gas compositions measured in the self-irradiated tests (estimated at 119 R/h) are shown for the five temperatures in Table 6-8. The nitrous oxide concentration increases steadily with

temperature while the nitrogen concentration decreases in roughly the same proportion. The hydrogen concentration initially decreases significantly from 60 °C to 90 °C and then increases slightly at the higher temperatures. Ammonia and methane are not detectable at 60 °C but their concentrations increase strongly with temperature with ammonia and methane reaching about 3% and 1%, respectively, at 120 °C.

Table 6-8. Gas Composition from Tank 241-SY-103 Waste

Sample (self-irradiated)	$[H_2]$	$[N_2O]$	$[N_2]$	$[NH_3]$	$[CH_4]$
60 °C	0.44	0.12	0.42	-	-
75 °C	0.29	0.24	0.44	0.002	-
90 °C	0.26	0.36	0.36	0.002	0.002
105 °C	0.30	0.38	0.28	0.01	0.003
120 °C	0.33	0.43	0.19	0.03	0.01
In-tank state, 32 °C, 444 R/h	0.54	0.14	0.31	-	0.012

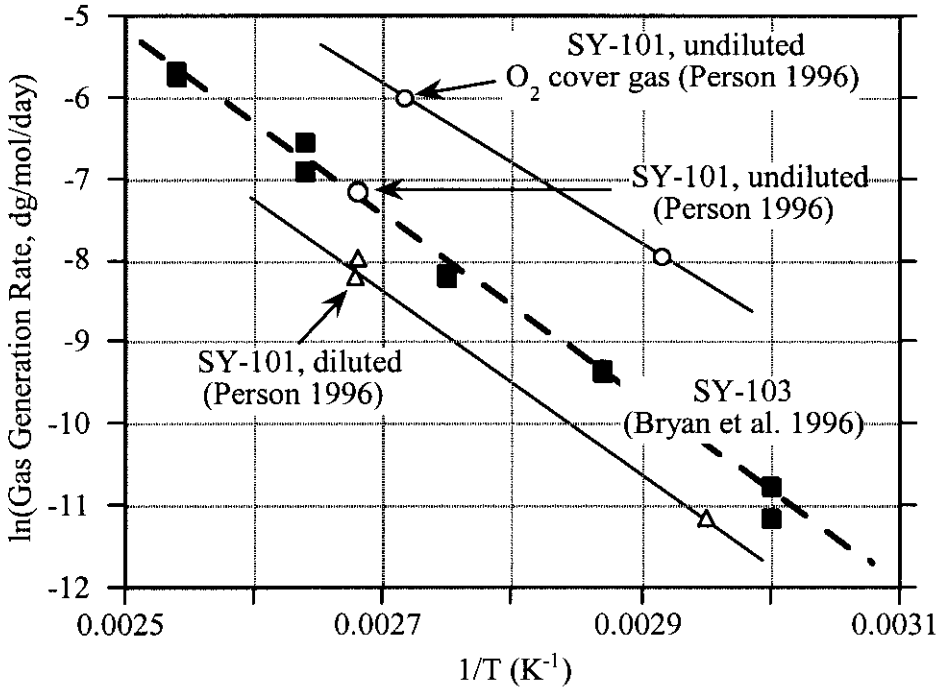

Figure 6-1. Comparison of Thermal Gas Generation in Tanks 241-SY-101 and 241-SY-103

6.3.3 Tank 241-AW-101 Gas Generation Tests

Two sets of gas generation rate measurements were conducted with samples of convective layer material from AW-101 (King and Bryan 1999). The first set used temperatures of 60, 90, and 120 °C with external irradiation of 37,000 R/h following basically the same procedure as used for SY-103 above.[12] The results of these tests indicated that the radiolytic G-values for some of the gases were temperature-dependent and raised the possibility they might also be dose-rate-dependent. Accordingly, the second set of tests used the same three temperatures but with an external irradiation dose of 3,564 R/h, about 10% of that applied in the original tests. For comparison, the self-dose was calculated to be 252 R/h in the test vessel and 786 R/h in the tank convective layer (642 R/h in the nonconvective layer).

The thermal and radiolytic gas generation parameters determined from the results of the high-dose irradiation tests (37,000 R/h) are listed in Table 6-9. G-values for radiolytic generation of hydrogen, nitrous oxide, and nitrogen are given for both 60 and 90 °C. The 60 °C values for hydrogen and nitrous oxide are close to those obtained in the SY-103 tests, but the $G(N_2)$ and all of the 90 °C values are quite different. The negative G-values for nitrogen and nitrous oxide at 90 °C indicate that irradiation actually reduced the generation rate of the gas. No satisfactory explanation for this behavior has yet been proposed. The temperature-independence of $G(CH_4)$ suggests that the explanation is in the area of complex chemistry rather than experimental procedure.

Table 6-9. Gas Generation Parameters in Tank 241-AW-101 Convective Waste (37,000 R/h Tests)

Gas	Thermal		Radiolytic G (molecule/100 ev)	
	A (mol/kg-d)	E_a (kJ/mol)	60 °C	90 °C
Hydrogen	7.1 E +10	100 ± 3	0.10	0.36
Nitrogen	4.7 E +13	126 ± 15	0.011	-0.04
Nitrous Oxide	3.0 E +14	131 ± 20	0.019	-0.08
Methane	3.3 E +14	138 ± 6	0.0011	0.0015

The G-values at 60 °C developed from low- and high-dose-rate test results are compared in Table 6-10. Both $G(H_2)$ and $G(CH_4)$ are lower at the high dose while $G(N_2O)$ increases. The $G(N_2)$ is essentially dose-independent. When the hydrogen generation parameters are used to extrapolate to tank conditions of 786 R/h and 37 °C, the predicted hydrogen generation rate is 10.8 scfd. This is a factor of 2 to 3 higher than the hydrogen generation rates measured from headspace hydrogen concentration and ventilation rate.

The gas composition of the gas generated varied significantly with temperature as shown in Table 6-11. The hydrogen concentration in the self-irradiated tests decreased from 80% at 60 °C

[12] Bryan, S. A., and C. M. King, 1998, *Thermal and Radiolytic Gas Generation from Tank 241-AW-101 Waste: Status Report.* PNNL letter report TWS98.39, April 1998.

to 55% at 90 and 120 °C with corresponding increases in nitrogen and nitrous oxide. The high-dose irradiated samples showed the hydrogen concentration increasing from 77% at 60 °C to over 90% at 90 °C and then decreasing to about 66% at 120 °C. The hydrogen concentration in the low-dose samples decreased from 85% at 60 °C to about 82% at 90 °C and 55% at 120 °C. These concentrations differ widely those recorded by the RGS (Mahoney 2000). The RGS samples had a much lower hydrogen concentration and much higher nitrogen fraction. This is contrary to expectations that the lower temperature and higher in-tank radiation dose should produce a higher hydrogen concentration than the high-temperature thermal-only tests.

Table 6-10. Comparison of G-values at 60 °C for Tank 241-AW-101 Convective Waste

Gas	Radiolytic G (molecule/100 ev)	
	3,564 R/h	37,000 R/h
Hydrogen	0.21	0.10
Nitrogen	0.012	0.011
Nitrous Oxide	0.01	0.019
Methane	0.0015	0.0011

Table 6-11. Gas Concentrations from Tank 241-AW-101 Waste

Sample	$[H_2]$	$[N_2O]$	$[N_2]$	$[CH_4]$
Test Data				
60 °C, thermal only	0.80	0.09	0.07	0.01
90 °C, thermal only	0.53	0.27	0.17	0.02
120 °C, thermal only	0.52	0.26	0.17	0.04
60 °C, 3,564 R/h irradiation	0.85	0.07	0.06	0.01
90 °C, 3,564 R/h irradiation	0.82	0.06	0.08	0.03
120 °C, 3,564 R/h irradiation	0.55	0.22	0.16	0.06
60 °C, 37,000 R/h irradiation	0.77	0.14	0.08	0.01
90 °C, 37,000 R/h irradiation	0.92	0.03	0.03	0.01
120 °C, 37,000 R/h irradiation	0.66	0.12	0.14	0.07
Other Measurements				
RGS nonconvective layer	0.32	0.08	0.55	0.02

6.3.4 Tank 241-AN-105 Gas Generation Tests

Gas generation from a sample of convective material from AN-105 was studied by Person (1998). Temperatures were varied from 35 to 100 °C. Both helium and 30% oxygen and helium were used as the cover gas. The thermal generation rates followed standard Arrhenius behavior. The gas generation parameters developed from the data are listed in Table 6-12. Note that the

G-values were determined from the deviation of the 35 °C tests from Arrhenius behavior due to self-irradiation, not by additional external irradiation.

The generated gas composition is consistent with that measured in the nonconvective layer with the RGS (Mahoney 2000) as shown in Table 6-13. Hydrogen concentrations matched most closely with 59% from the RGS and 58% in the generated gas at predicted tank conditions which closely matches the test results at 35 °C. The relative amounts of nitrogen and nitrous oxide were reversed, however. As in the SY-101 tests (Person 1996), the presence of oxygen in the cover gas greatly accelerated the production of hydrogen.

Table 6-12. Gas Generation Parameters in Tank 241-AN-105 Convective Waste

Gas	Thermal		Radiolytic
	A (mol/kg-d)	E_a (kJ/mol)	G (molecule/100 ev)
Hydrogen	1.84 E +8	87 ± 4	0.064
Nitrogen	6.6 E +14	135 ± 8	0.029
Nitrous Oxide	8.0 E +10	107 ± 9	0.042
Total	1.25 E +10	97 ± 4	0.16

Table 6-13. Gas Concentrations from Tank 241-AN-105 Waste

Sample	$[H_2]$	$[N_2O]$	$[N_2]$	$[NH_3]$	$[CH_4]$
Test Data					
35 °C	0.57	0.25	0.08	0.10	-
60 °C	0.66	0.20	0.06	0.06	0.003
80 °C	0.68	0.23	0.09	-	0.01
100 °C	0.45	0.30	0.21	0.007	0.017
93 °C, 30% O_2 cover gas	0.93	0.03	0.01	-	0.02
Predicted at in-tank state	0.58	0.26	0.15	-	0.004
Other Measurements					
RGS nonconvective layer	0.59	0.15	0.24	0.006	0.007

The hydrogen generation rate for the entire tank was calculated to be 8.2 scfd. This is about double the measured hydrogen release rate from AN-105 of 4.4 scfd reported by Hu (2000). Section 6.4, which follows next, gives release rates from 10 scfd in 1996 down to 4 scfd in 1999.

6.4 FIELD MEASUREMENTS OF GAS GENERATION RATES

Gas generation rates are estimated by integrating the product of dome space hydrogen concentration data and the ventilation flow rate. If the net gas accumulation is negligible as indicated by the waste level histories, the total released gas is equal to the volume of gas generated. Gas chromatographs (GCs) were installed in AN-104 in late 1995 and in AN-105 and

AW-101 in early 1996. The GCs are calibrated regularly, and the sensor error is typically less than 10% of the reading. Improved ventilation flow controllers were installed in the tanks in mid-1995. Gas generation rates are not calculated for AN-103 and SY-103, since they do not have GCs and no reliable measure of absolute hydrogen concentration is available.

The total gas release volume per year is determined by

$$V = \sum_{i=1}^{n} \frac{\Delta t_i V_R GC_i \times 10^{-6}}{[H_2]} \qquad (6\text{-}3)$$

where n is the number of samples for the year,
Δt_i is the sampling interval of the GC data (typically six to ten minutes),
V_R is the assumed ventilation rate (100 cfm average),
GC_i is the GC headspace hydrogen concentration reading in ppm at a given time step, and
$[H_2]$ is the hydrogen concentration in the waste gas.

Mahoney et al. (1999) gives hydrogen concentrations as 0.44 for AN-104, 0.61 for AN-105, and 0.32 for AW-101 as determined with the RGS. Periods of missing GC data were dealt with by computing the average hydrogen concentration in the dome space for a year and applying that value during the down time.

The average GC readings, calculated total gas generation per year, and daily hydrogen generation rates are given in Table 6-14. These rates compare well with the field-estimated steady-state hydrogen generation rates determined by Hu (2000) which are based on data from 1998 and 1999, Table 6-15. The differences in the results are easily explained by total generation (includes gas release events) versus steady-state generation and different ventilation flow rates.

Note that the yearly GC average includes gas release events. As a result, the instrument down times are accounted for with dome space hydrogen concentrations which may be higher the than baseline. However, due to the extended periods (up to 172 consecutive days) of instrument failure, it is expected that at least minor release events would have occurred during these periods, making the higher than baseline averages reasonable. For those years with instrument failures of less than 57 consecutive days, the over-estimation of gas generation is only about 10% of the total generation, so the effect is minimal compared to the overall uncertainty in the calculation.

The relatively high gas generation in AN-105 for 1996 is attributable to the large GRE on May 30, 1996. This event is 2.3 times the average volume releases in AN-105, and the gas release during the three days after the event accounts for over 3000 ft^3 of the total release for the year. The GC average for this year is computed without this release as it is so atypical.

Table 6-14. Estimated Gas Generation Rates for Tanks 241-AN-104, 241-AN-105, and 241-AW-101

Tank	Year	GC Average [H_2] (ppm)	Total Generation (scf/year)	Hydrogen Generation Rate (scfd)
AN-104	96	44.7	5284	6.4
	97	29.7	3494	4.2
	98	17.8	2070	2.5
	99	17.1	2099	2.5
AN-105	96	36.9*	6492	10.8
	97	33.9	2977	5.0
	98	31.9	2798	4.7
	99	27	2387	4.0
AW-101	96	42.9	7122	6.2
	97	32.6	5374	4.7
	98	28.7	4641	4.1
	99	22	3677	3.2

* Does not include GRE on 5/30/96

Table 6-15. Field-Estimated Hydrogen Generation Rates (Hu 2000)

Tank	Hydrogen Generation Rate (scfd)
AN-103	6.8
AN-104	3.7
AN-105	4.4
AW-101	3.6
SY-103	5.1
SY-101	35.1

The gas generation in each tank decreased exponentially from 1996 to 1999 as shown in Figure 6-2. As discussed in Section 4.2, the waste temperatures decreased by approximately 10° F over this time period. The empirical hydrogen generation rate model of Hu (2000) predicts a reduction of the gas generation rate of 33% in AN-104 and AN-105 and 32% in AW-101 for a waste temperature decrease of 10° F. These results are tabulated in Table 6-16, along with the decrease in measured generation rates from Table 6-14. Given the large GC down times in AN-105 and AW-101 during 1996, the exceptionally large release in AN-105 on May 30, 1996, and the inclusion of the release events as compared to the steady-state estimation of the empirical model, the results compare well, most notably to the decreases from 1997 to 1999.

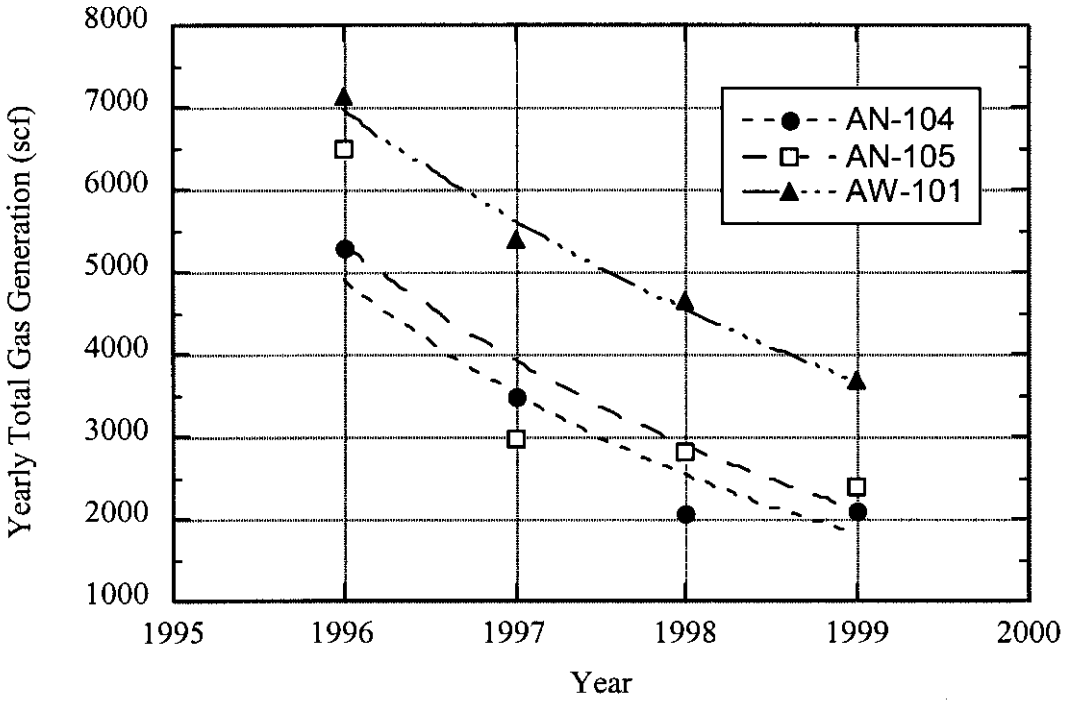

Figure 6-2. Total Gas Generation Per Year

Table 6-16. Percentage Decrease in Generation Rates

Tank	Decrease Predicted by Hu (2000) Model (%)	Decrease in Measured Rates (%)	
	1996 to 1999	1996 to 1999	1997 to 1999
AN-104	33	60	40
AN-105	33	63	20
AW-101	32	48	32

In summary, a decrease in the gas generation rate, as determined from the hydrogen release data, has been observed for tanks AN-104, AN-105, and AW-101. The magnitude of this decrease corresponds with the decrease in the average waste temperatures. Since the waste temperature trend in AN-103, the same order of gas generation decrease is expected in that tank. The generation rate in SY-103 should not have changed significantly since the temperature has remained relatively constant.

6.5 SUMMARY OF GAS GENERATION AND COMPOSITION

The preponderance of data relating to gas generation and composition for the six DSTs considered in this report are consistent in general though not in all specifics. Gas composition generally favors hydrogen at low temperatures and nitrogenous gases at higher temperatures. In all the DSTs considered here, three gasses, hydrogen, nitrogen, and nitrous oxide, dominate the retained gas composition. Methane is also present at a 1 to 2% level. Only SY-101 had an appreciable concentration of ammonia.

The total gas generation rate is clearly a strong function of temperature though the effect decreases at low temperatures, radiolysis becomes dominant. The strong dependence of gas generation on temperature is demonstrated by the significant decrease in the observed gas release rate in AN-104, AN-105, and AW-101 (the release rate in AN-103 almost certainly decreased also but data are insufficient to quantify it) corresponding to temperature decreases of 3 to 5 °C.

The radiolytic gas generation rate has been shown to be independent of temperature in at least one tank (SY-103) and is probably temperature independent in two others (SY-101 and AN-105) though it cannot be proven with the available data. In one tank (AW-101), the radiolytic generation rate was found to depend on both temperature and dose rate (wastes from two SSTs also showed temperature-dependent radiolysis). The gas generation rates determined from laboratory data were generally consistent with field release rate observations except for AW-101 whose field data show a much lower release rate. Retained gas compositions also generally agree with in-situ measurements with the RGS, again except for AW-101 where the RGS showed a much lower hydrogen fraction.

Overall, we believe the available gas generation and composition data provide a sound, if not totally precise, basis for both evaluating the current flammable gas hazard in the DSTs and predicting the future state of the tanks as conditions change.

7.0 GAS RETENTION AND DISTRIBUTION

The volume of gas that a tank can store and the potential for a large, sudden gas release depends on the waste configuration and properties. The tanks of greatest concern are those with the deepest layer of settled solids under a deep layer of supernatant liquid. A good understanding of how gas is retained in the waste and the important mechanisms for its release is required to manage the existing hazard and to prevent new hazards from being created in the future. Almost ten years of tank monitoring, in-situ measurements, analyses and laboratory experiments have shown that the physical characteristics of the waste are the dominant factor in determining tank behavior.

This section describes the gas retention characteristics of the five FGWL DSTs. Section 7.1 summarizes the currently understood theory of gas retention in these tanks, and Section 7.2 outlines the results of laboratory gas retention tests that have been performed on actual waste samples from these tanks. Section 7.3 gives the void fraction distributions of measurements performed with the VFI and RGS in 1995 and 1996. Section 7.4 presents the results of integrating the void data to obtain the total gas inventory of the tanks and the changes in retained gas volume that have occurred since the measurements were made. Section 7.5 summarizes the gas retention behavior of the five tanks.

7.1 GAS RETENTION THEORY

The gaseous species are initially generated in the waste as molecules in solution in the liquid. Except for ammonia, the gases are not very soluble in concentrated salt solutions. Therefore, after a slight super-saturation develops, most of the gas that is generated comes out of solution as bubbles. Bubbles, which contain the most flammable of the gases and are readily releasable, are the most important mode of gas retention concerning flammability.

In the five FGWL DSTs, gas bubbles are retained in the nonconvective layer primarily by the strength of the surrounding waste. With the relatively weak waste and small bubbles found in the DSTs, surface tension pulls bubbles into an approximately spherical shape though they may be ellipsoidal or similarly distorted from truly spherical. A bubble can grow only until its buoyancy exceeds the ability of the waste to hold it in place. The maximum bubble size can be estimated by a balance of the buoyant force and the restraining force of the waste at its yield stress. The limiting diameter is expressed as

$$D_b < \frac{6\tau_y}{\rho_{NCL} g} \qquad (7\text{-}1)$$

where ρ_{NCL} is the bulk degassed nonconvective layer density,
τ_y is the yield stress, and
g is the acceleration of gravity.

The maximum round bubble diameter in typical DST nonconvective layer is 1 to 3 cm. This size is quite consistent with observations in waste though the average bubble has a diameter of a few millimeters. At the same time, a bubble can be approximately spherical only when the forces defining its surface are dominated by surface tension. Otherwise the bubble grows into the weakest part of the waste surrounding it and assumes an irregular dendritic shape. From a simple scaling of the relative importance of strength to surface tension, the maximum diameter of round bubbles before they begin to assume a dendritic shape is given by

$$D_b < \frac{\sigma}{\tau_y} \tag{7-2}$$

where σ is the surface tension which is estimated to be on the order of 0.08 to 0.10 N/m in these tanks (Norton and Pederson 1996).

Equation 7-2 dictates that a 1 mm diameter bubble will be round if the yield stress is less than about 100 Pa. Nearer the tank bottom, where the yield stress may exceed 300 Pa, larger bubbles are likely to assume an irregular shape.

Gas can accumulate until a portion of the nonconvective layer becomes buoyant with respect to the liquid above it. At that point the buoyant section rises to the surface and releases a large fraction of its gas as will be discussed in Section 8. The average gas fraction in a tank is, therefore, limited to that required for neutral buoyancy. The neutral buoyancy gas fraction is a function of the convective and nonconvective layer densities, ρ_{CL} and ρ_{NCL}, and is given by:

$$\alpha_{NB} = 1 - \frac{\rho_{CL}}{\rho_{NCL}} \tag{7-3}$$

In order to predict whether a tank can retain sufficient gas to become buoyant, it has been postulated that bubbles are not held stationary in the waste but migrate very slowly as if through a very viscous fluid. With the assumption that the viscosity increases linearly with depth in the nonconvective layer as does the yield stress, the simultaneous solution of the bubble number and mass conservation equations expresses the void distribution as a parabola with a maximum at the midpoint of the layer (Meyer and Wells 2000). This shape matches the measured void distributions reasonably well (see Section 7.3). The profile is given by

$$\alpha(\eta) = \frac{C_B}{\rho_{NCL}} \left(\frac{GT}{p_{NCL}} \right)^{\frac{1}{3}} H_{NCL}^2 \eta(1-\eta) \tag{7-4}$$

where T is the average waste temperature,
p_{NCL} is the average pressure in the retained gas,
G is the volumetric gas generation rate,
H_{NCL} is the depth of the nonconvective layer and $\eta = z/H_{NCL}$.

If the average gas fraction predicted by Equation 7-4 exceeds the neutral buoyancy gas fraction from Equation 7-3, a buoyant displacement gas release can occur. The coefficient C_B is adjusted to ensure that the tanks currently exhibiting buoyant displacements are predicted to exceed neutral buoyancy.

7.2 GAS RETENTION TEST RESULTS

Much of our understanding of gas bubble retention in waste is based on the results of extensive bubble retention tests with various simulants including Bentonite and Kaolin clay, sand and glass beads (Gauglitz et al. 1994, 1995, 1996). Gas was generated in the simulant using yeast and sugar to generate CO_2, hydrogen peroxide to generate oxygen by decomposition, and by depressurizing the test section to evolve previously dissolved CO_2 or ammonia (Rassat and Gauglitz 1995).

Gas retention tests with actual waste were performed initially as part of a series of experiments to investigate the effects of dilution on waste properties of SY-101 and SY-103 (Bredt et al. 1995; Bredt and Tingey 1996). The success of these tests led to further work using similar test apparatus and procedures with undiluted samples of waste from SY-103, AW-101, and AN-103 and several SSTs (Gauglitz et al. 1996; Rassat et al. 1997).

Most of the experiments in actual waste and the early simulant tests focused on bubbles in a settled solids layer beneath a liquid layer modeling the typical DST configuration. In this situation gas retention in the solids layer can lead to gas releases with the appearance of a buoyant displacement on a small scale. In some cases the bubbles exceeded the maximum size and simply disengaged from the solids. Some experiments removed the supernatant liquid to prevent buoyant displacements and allow the gas fraction to exceed neutral buoyancy. Typical results include the height of the waste column versus time, maximum gas fraction (computed from change in height) before large gas releases, and photographs of the bubble configuration and the gas release process.

The tank waste experiments were all conducted with approximately the same method that differed slightly in concept with that used in simulants. Transparent test vessels about 1-in. in diameter were filled to a given level with waste and suspended solids allowed to settle out. The samples were then exposed to a high-intensity gamma source to generate a small volume of gas in the settled solids layer by the same processes occurring naturally in the waste. To control the void fraction in the gas retention tests, this initial gas was expanded by depressurizing the sample vessels at a controlled rate over hours or even days. In all cases, the equivalent gas generation rate during expansion was necessarily much faster than that occurring in the tanks.

The results of gas retention tests are summarized in separate subsections for each tank below.

7.2.1 Gas Retention Tests in Tank 241-SY-101

Tank 241-SY-101 waste was the first to undergo gas retention tests as part of a dilution study. Refer to Bredt et al. (1995) for details. The waste was a whole-tank composite made up of archived waste from 1991 core samples. Dilutions of 0.5:1, 0.75:1, 1:1, and 3:1 (volume of

diluent to original waste) were prepared using 2M NaOH. One undiluted waste sample was also included in gas retention tests.

After 27 days of irradiation with a 2,500 R/h gamma source, the five samples were depressurized to 22 in. of mercury over about one minute. The bubbles formed were round, and no dendritic bubbles were seen. Nonconvective layer growth occurred in all except the 3:1 dilution, and bubbles were seen escaping from the solids in all the samples. A "rollover"-like event was observed in the undiluted samples and the 0.5:1 and 0.75:1 dilutions.

The solids level in the undiluted sample grew by 17% and remained there for about one minute before the solid-gas mixture rose to the surface. The 0.5:1 sample grew as vacuum was applied and, before full vacuum, at 10% growth, about 60% of the solids-gas mixture rose to the surface. The settled solids in the 0.75:1 sample grew past neutral buoyancy, separated from the vessel walls as a single mass, and rose to the surface where the expansion was measured as 8%. The solids level in the 1:1 dilution grew by 18% as vacuum was applied. Before full vacuum, bubbles 2 to 3 mm in diameter were released from the solids without the appearance of a "rollover." This gas release continued for about 10 minutes. No solids growth was seen in the 3:1 dilution as bubbles were released from the settled solids.

Based on the appearance of "rollovers" with dilutions up to 0.75:1, the authors concluded that a dilution of 1:1 would prevent gas retention in SY-101. The dilution of 0.8:1 at the end of the remediation sequence appears to have confirmed this conclusion (Mahoney et al. 2000).

7.2.2 Gas Retention Tests in Tank 241-SY-103

As in the above SY-101 experiments, the SY-103 gas retention tests were performed in October 1995 as part of a dilution study and were conducted similarly (Bredt and Tingey 1996). The waste was taken from non-convective layer segments 10 to 14 of core 62 obtained in August 1994. Dilutions of 0.5:1, 0.75:1, 1:1, and 3:1 (volume of diluent to original waste) were prepared with 2 M NaOH solution. All dilutions except 3:1 were prepared in duplicate for a total of nine samples. The samples were exposed to a 8,200 R/h gamma source for 34 days prior to testing.

Gas was generated in the samples by depressurizing them to 22 in. of mercury in one or two minutes. The waste behaved similarly to the SY-101 tests except that the appearance of "rollovers" occurred only in the undiluted sample and the 0.5:1 dilution. Dilutions of 0.75:1 and higher released bubbles without disturbing the solids. Thus, a 0.75:1 or greater dilution was considered sufficient to prevent gas retention in SY-103.

When vacuum was applied, the solids level in the two undiluted samples increased by 16% and 19%. The latter sample remained at maximum level for about one minute before releasing gas in a "rollover." The sample that rose 16% had a very shallow supernate layer (10% by volume). During depressurization, most of this supernate was observed to percolate down into the solids-gas mixture preventing a later "rollover." The two 0.5:1 samples experienced a "rollover" at 9% and 13% solids growth with most of the solids-gas mixture rising to the surface. The solids in the 0.75:1 samples raised by 8% and 9% during depressurization. Bubbles 2 to 3 mm in

diameter were released from the solids one at a time with minimal disturbance to the solids layer, and no "rollover" occurred. The 1:1 dilution samples behaved similarly after growth of 7% and 9%. The 3:1 sample did not grow but released small 0.5-mm bubbles from the solids.

Two more samples were tested in April 1996 using a slightly different procedure (Gauglitz et al. 1996). A nonconvective layer composite and a whole tank composite were used. The supernate depth was only 0.2 cm, 4% of the waste column in the nonconvective composite while the whole-tank composite had about 3.6 cm or 25% supernatant. The samples were irradiated with a 37,000 R/h gamma source for four days prior to depressurization. The final pressure was much lower than the earlier tests and reduced much more slowly. The depressurization was conducted in a series of steps reaching 13 mm Hg in 60 to 90 minutes. Bubbles generated by the depressurization were essentially round and less than 1 mm in diameter.

The supernate depth in the nonconvective layer composite was not sufficient to allow a "rollover," and gas retention reached about 30%, far above the buoyancy point of 19%. After reaching this maximum gas fraction, the small amount of supernate was observed to infiltrate the surface of the settled solids, eroding it to provide a release path for individual bubbles. Eventually over half the retained gas was released in this way.

In the whole-tank composite sample, a "rollover"-like event was clearly observed. This occurred at 9.2% void, slightly lower than the 12% predicted neutral buoyancy void fraction. Prior to the rollover, some individual bubbles released at the liquid-settled solids interface. At maximum gas retention, a large cloud of bubbly waste rose suddenly into the supernate layer, indicative of a buoyancy-induced "rollover."

The measured maximum void fractions compared to the void fraction predicted for buoyancy for the four undiluted samples are shown in Figure 7-1. It is apparent from the figure that the thickness of the supernatant liquid layer affects both the magnitude of the maximum retention and the mechanism of gas release (rollover or bubble disengagement). Additional, larger scale buoyant displacement tests were later performed with simulants that confirmed this assertion (Stewart et al. 1996b) and led to development of a model for the minimum depth of supernate required for gas release by buoyant displacement (Meyer et al. 1997; Meyer and Wells 2000).

7.2.3 Gas Retention Tests in Tanks 241-AN-103 and 241-AW-101

The gas retention experiments for these two tanks were conducted in 1997 as part of a single task and are discussed together in this section. Composite waste samples were prepared from core material obtained in 1996. The experimental procedure was similar to that used in the SY-103 tests.

Two composites were made for AW-101: one from the upper portion of the nonconvective layer and one from the bottom two segments. Two samples of each of the composites (four total samples) were prepared with settled solids depth about 25 cm (10 in.) and supernate depth of about 2 cm (0.8 in.) except for the second sample of the second composite which had a solids depth of about 18 cm (7 in.) with only 0.1 cm (0.04 in.) of supernate.

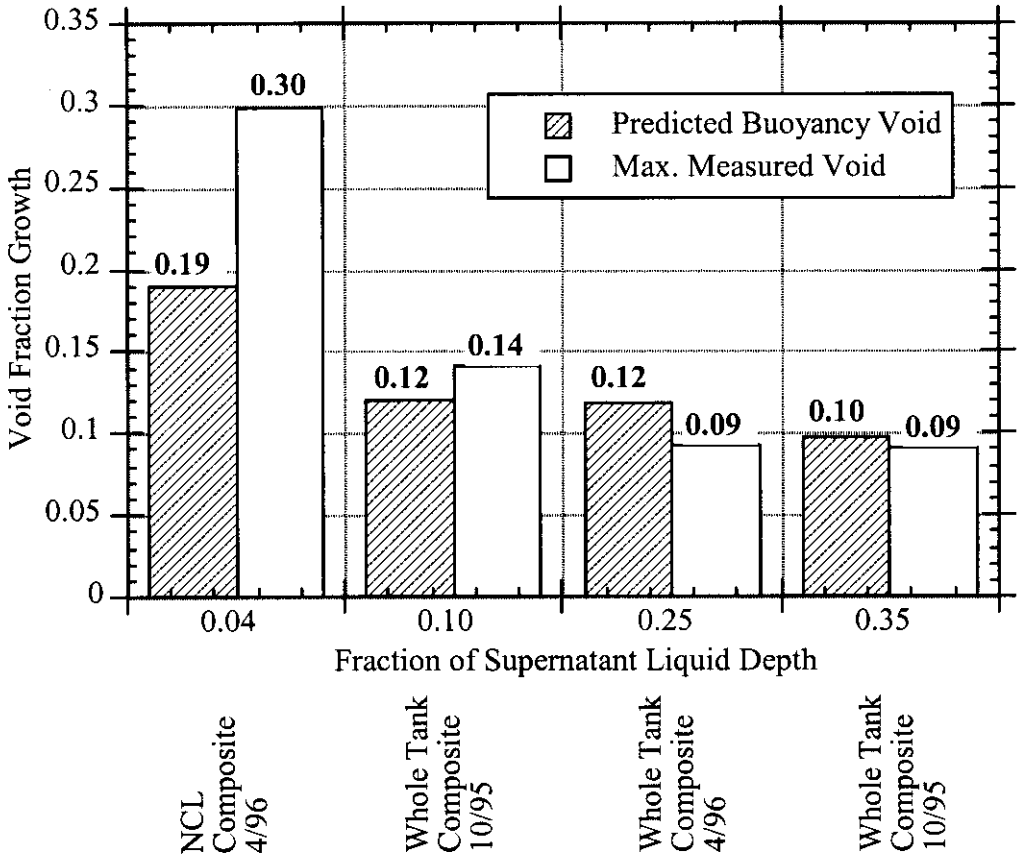

Figure 7-1. Void Fractions in Tank 241-SY-103 Gas Retention Tests

Waste representing AN-103 was obtained as spent samples from the RGS extractor from the upper portion of the nonconvective layer. Drainable liquid collected from core extrusion was added. Four samples were prepared with settled solids depth of 9 to 10 cm (3.5 to 4 in.) and supernate depths of 3 to 5 cm (1.2 to 2 in.) except for one with 7 cm (2.75 in.) of solids and only 0.1 cm (0.04 in.) of supernate.

The samples were irradiated with a 76,000 R/h source for four days. This gave initial gas fractions of 0.02 to 0.03. Depressurization was more precisely controlled in these tests, and longer depressurization periods from 2 hours to 24 hours were used. Bubbles formed in the process were usually round initially but tended to be slightly distorted at 1 mm diameter or larger.

All of the tests in both AW-101 and AN-103 waste samples reached much higher void fractions than the predicted buoyancy point. The measured growth in the three AW-101 samples with supernate was about 19% while the neutral buoyancy void was only 9%. The sample without supernate reached 22% void growth. The AN-103 samples with supernate reached a measured

growth of about 30% while the expected growth at buoyancy was only 15%. The sample without supernate grew by 37%.

The duration of the experiment had little effect on the maximum void but the gas release behavior was different in the long-duration tests. In AW-101 waste samples, distinct buoyant "rollovers" were seen only in the shortest (2-hour) tests. Gas release appeared to be by bubble disengagement in the longer tests. But the gas release rate after maximum void growth was most rapid in the slowest (1-day) tests. In the AN-103 tests, the shorter tests showed a slightly higher maximum void growth, but more gas release activity was seen prior to peak void in the longer (4-day) test. However, because the sample was not as homogeneous, this difference cannot be attributed conclusively to test duration.

The effect of waste strength in the small sample vessel was proposed as the explanation of the void growth above the predicted buoyancy point. Calculations indicated that a yield stress of only 9 to 20 Pa could explain the high void fraction. The reason that the void growth in SY-101 and SY-103 samples did not exceed buoyancy significantly may have been a lower yield stress resulting from their shear history. These samples had been liquified in a blender at shear rates estimated at 500 s^{-1} while great care was taken to disturb the AW-101 and AN-103 samples as little as possible.

Stable foams were observed on top of the supernate in the AN-103 experiments. Once the solids layer became buoyant, the bubbly mass formed a froth that continued to expand with further depressurization. This may explain why these two tanks have a much thicker crust layer than the others (except SY-101). Anomalously high gas fractions up to 90% void were seen near the vessel walls. This wall void phenomenon, which was observed to a lesser extent in the AW-101 tests and hardly at all in SY-103 waste, appeared to be caused by direct attachment of bubbles to the vessel walls. This may also have contributed to the high void growth.

7.2.4 Summary of Gas Retention Tests

While the effects of the necessarily small scale of these experiments make it difficult to apply the results to full-scale tank behavior, the experiments provided valuable insights on the general mechanisms of gas retention and release. Bulk buoyancy gas release mechanism, supernate infiltration, and individual bubble disengagement were observed in the tests. In many cases buoyant phenomena began to occur at about the same void growth predicted from the layer densities via Equation 7-1. Bubble size prior to release was observed in all cases to be on the order of 1 mm or less. Some novel gas retention phenomena were also observed, including the wall foaming in AN-103 waste and the stable froths in both AN-103 and AW-101 samples. Finally, the overall bubble configuration in all of these tests, including those with SST waste not discussed here, were consistent with the bubble retention theory developed earlier based on simulant studies.

7.3 VOID FRACTION INSTRUMENT AND RETAINED GAS SAMPLER VOID FRACTION MEASUREMENTS

Retention of relatively insoluble gases in the form of bubbles is the most important in terms of flammability (Stewart 2000). Bubbles can comprise large volumes and can potentially be released quickly. A large mass of soluble gas (almost entirely ammonia) can also be retained dissolved in the liquid, but it is not very flammable and exists in high concentrations in only a few tanks. It has not proven to be a flammability issue even in those.

The primary measure of gas retention is the average gas volume fraction in the waste, which is also commonly referred to as the "void fraction." The average void fraction has been determined from local void fraction data measured with the VFI and RGS in the six FGWL DSTs. Except for the few tanks with a thick crust layer (AN-103, AW-101, and SY-101 prior to remediation), gas is retained mainly in the nonconvective layer. The settled solids have a yield stress that increases from zero at the upper surface to 200 to 300 Pa at the tank bottom (see Sections 2.4 and 5.2). This strength is enough to hold bubbles up to about a centimeter in diameter (Gauglitz et al. 1996).

Because waste configuration in DSTs is subject to buoyant displacement gas release, the bulk or average void fraction in the nonconvective layer is limited to approximately the neutral buoyancy condition. The neutral buoyancy void fraction ranges from 0.09 to 0.12 for DSTs on the FGWL. Note that the average void fraction, not the local void fraction, determines whether a buoyant displacement can occur. Cumulative buoyancy is computed by integrating the void fraction from the top down. It is normal for a region of the nonconvective layer where the local void exceeds neutral buoyancy to lie beneath one with much lower void fraction.

Plots of the local void fractions measured by the VFI and RGS in 1995-1996 are shown in Figures 7-2 through 7-7. The plot legends show each traverse of the VFI in each riser and each riser of an RGS core sample. Thus "1B - 1" indicates the first traverse of the VFI in Riser 1B while "RGS 7B" denotes RGS data from Riser 7B.

An obvious feature of many of the plots is that the shape of the void profiles differ significantly between risers. SY-103, Figure 7-3, is probably the best example. While both profiles have similar maximum void fractions, that of Riser 17C occurs at a lower elevation. The higher void fractions were at higher elevations in Riser 22A. This is consistent with the theory that buoyant displacements occur in discrete gobs that are more or less independent of each other. A parallel observation is the considerable temporal variation in nonconvective layer height over the past several years revealed by the temperature profiles in this tank, presumably due to recurrent BD GREs (see Section 5.1). AW-101 shows a similar but less distinct difference between profiles in Risers 13A and 1C (Figure 7-4). In AN-105, the VFI void profiles are similar but the RGS data from Riser 12A shows a much higher void. In contrast AN-103 and AN-104, with fewer, smaller BD GREs, show more uniform profiles (Figures 7-5 and 7-6).

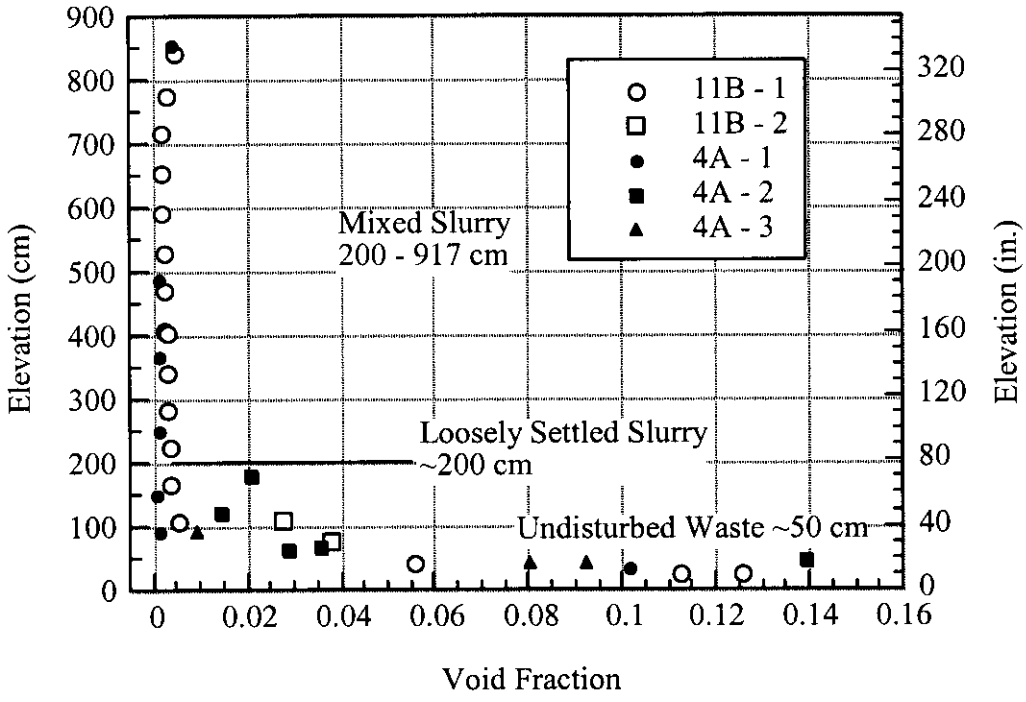

Figure 7-2. Tank 241-SY-101 Void Profile (1994-1995 Data)

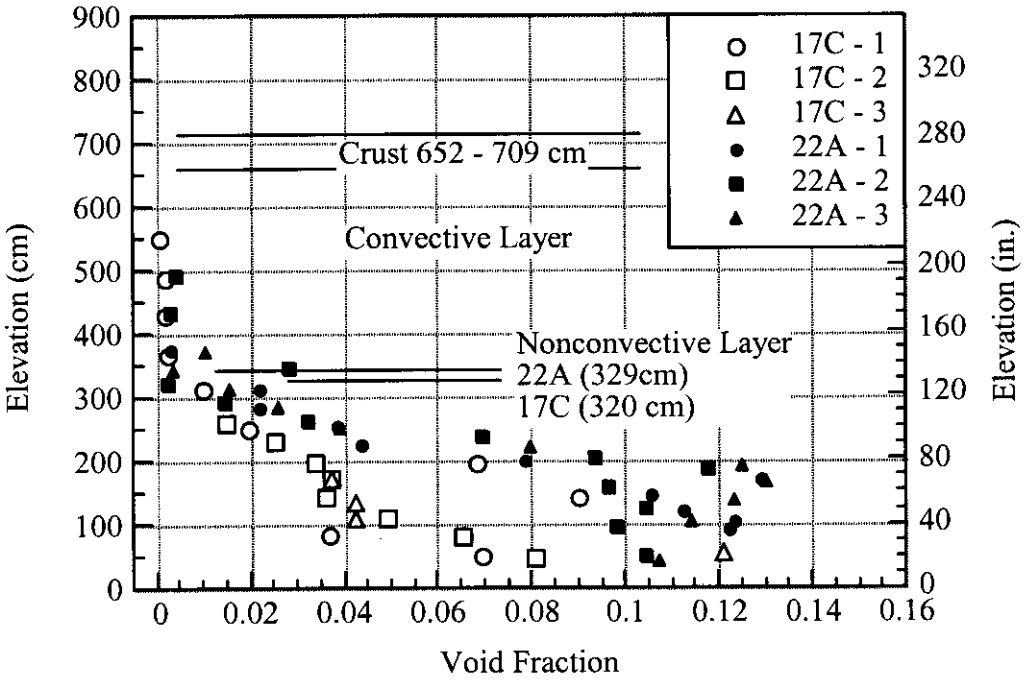

Figure 7-3. Tank 241-SY-103 Void Profile

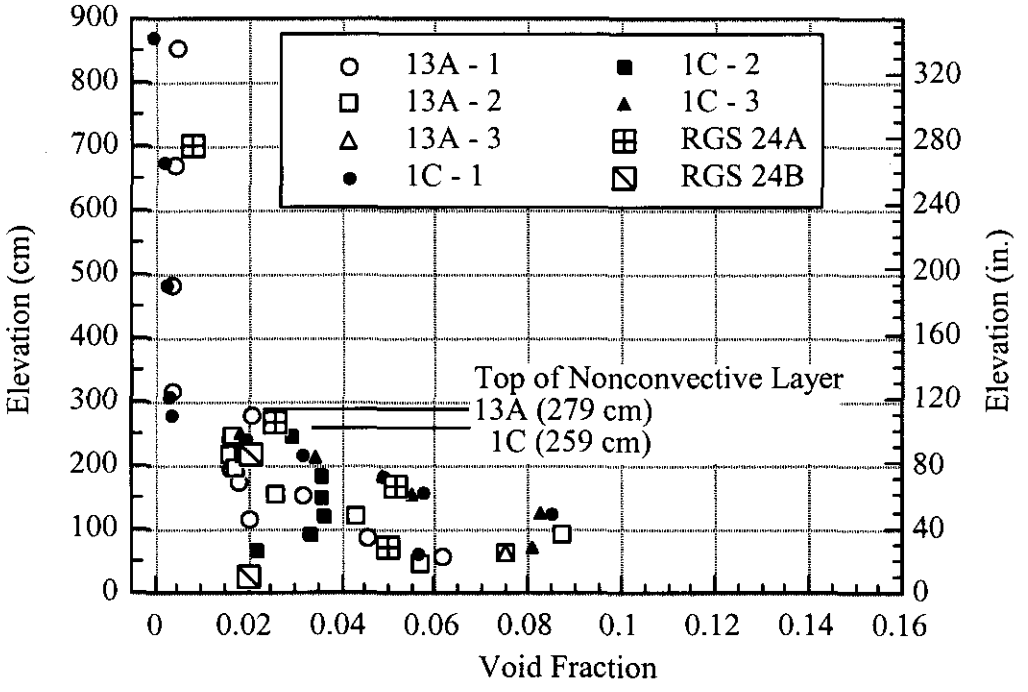

Figure 7-4. Tank 241-AW-101 Void Profile

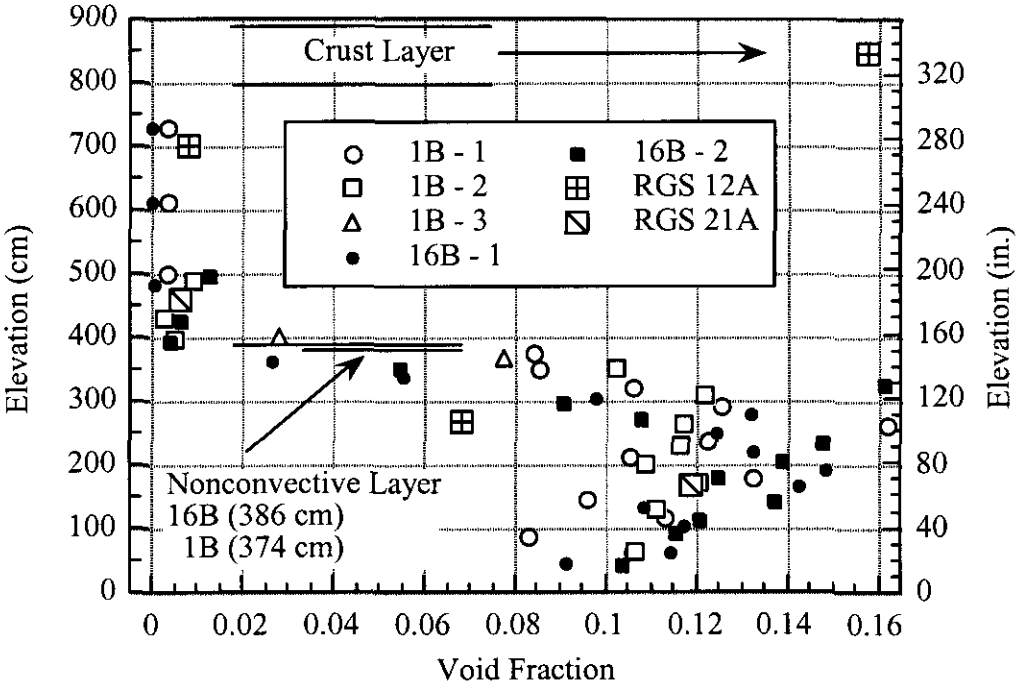

Figure 7-5. Tank 241-AN-103 Void Profile

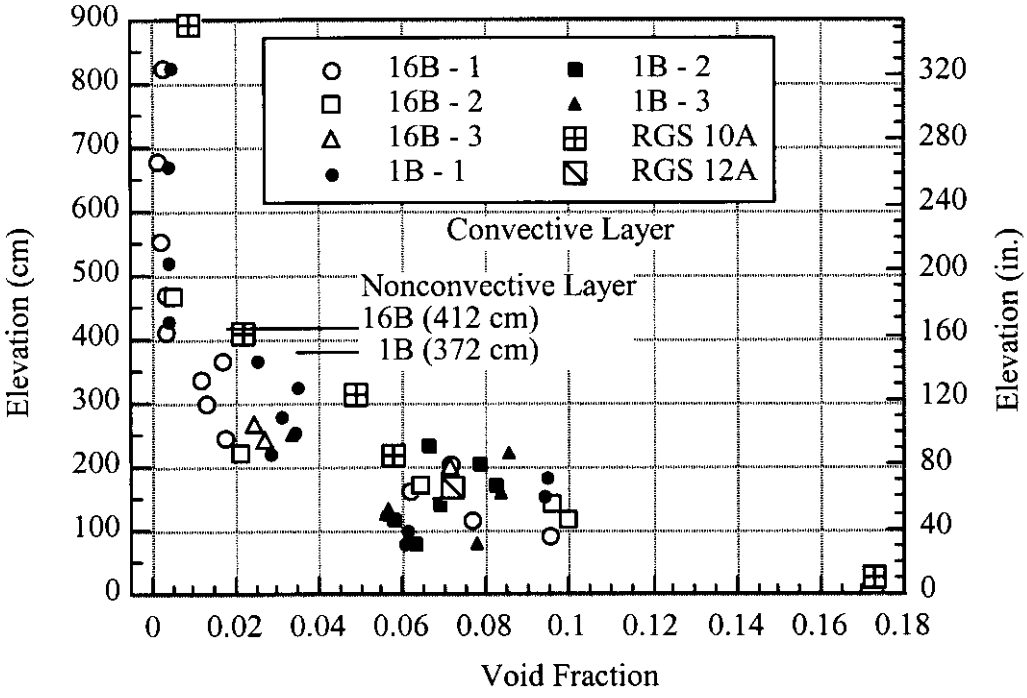

Figure 7-6. Tank 241-AN-104 Void Profile

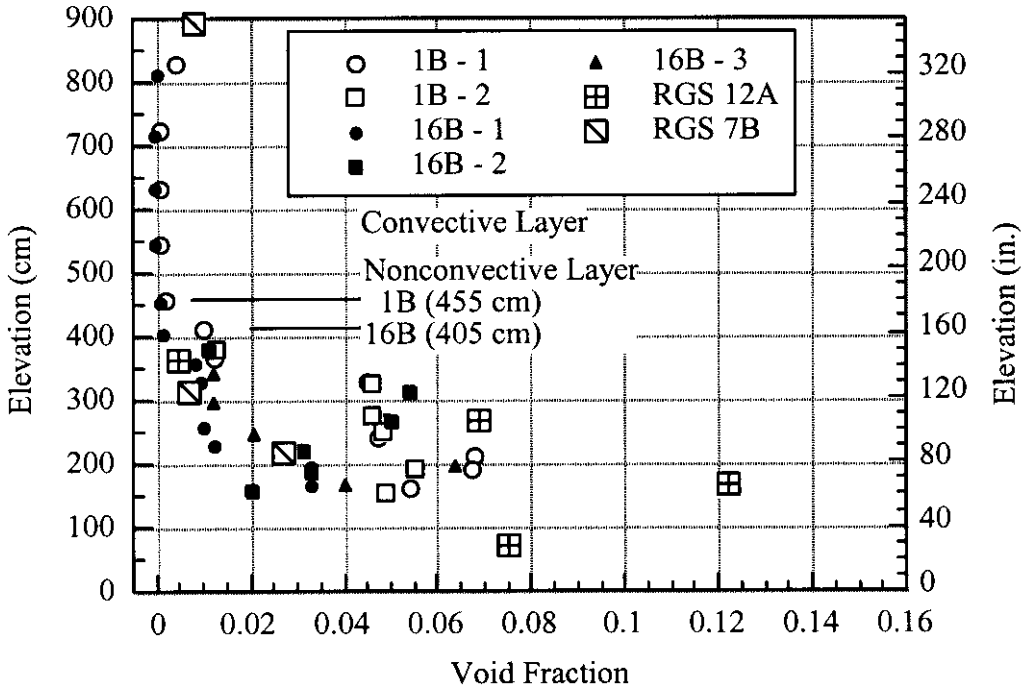

Figure 7-7. Tank 241-AN-105 Void Profile

7.4 RETAINED GAS INVENTORY

Gas retention is the precursor to every gas release, whether spontaneous or induced and the waste in almost every tank retains some flammable gas. Most tanks accumulate gas until they reach some equilibrium between background release and generation. But, in the five FGWL DSTs, some of the gas accumulates in the waste until it is released suddenly in BD GREs. The retained gas inventory helps determine the potential for larger-than-normal spontaneous or induced gas releases and establishes a reference for the relative size of historic BD GREs.

The average void fraction and retained gas volume has been determined from local void fraction data obtained with the VFI and RGS in the six FGWL DSTs that was shown in Section 7.3. The retained gas volume can also be estimated from the correlation of waste level changes to barometric pressure fluctuations. Changes in gas volume since the local void measurements were made can be determined from changes in surface level.

This section summarizes the gas volumes and other quantities of interest calculated from VFI and RGS measurements, from barometric pressure effects, and surface level changes. Section 7.4.1 presents a summary of the void fractions, gas volumes, and other computed quantities in the six DSTs on the FGWL. Gas volumes calculated using the BPE model are discussed in Section 7.4.2, and changes in gas volume estimated from the surface level changes since the VFI measurements are given in Section 7.4.3.

7.4.1 Retained Gas Volumes Calculated from Void Fraction Instrument and Retained Gas Sampler Data

The data reduction model and uncertainty calculation procedure are described in Appendix A. Table 7-1 gives layer thicknesses and densities and the calculated void fractions and gas volumes for all six tanks using the combined VFI and RGS data set. All uncertainties in the table represent one standard deviation. The data given for SY-101 represent conditions and void measurements made in 1994–1995. Later data are not shown because essentially the entire retained gas volume in this tank has been released by transfer and dilution (see Section 1.3).

Given the average void fraction, α_i, in a layer i (e.g., crust, convective layer or non-convective layer), the in-situ gas volume held in the layer is calculated by

$$V_i = \alpha_i A H_i \tag{7-5}$$

where H_i is the layer thickness and
A is the tank area.

The gas volume corrected to standard temperature and pressure is then given by

$$\hat{V}_i = V_i \frac{p_i}{\hat{p}} \frac{\hat{T}}{T_i} \tag{7-6}$$

where p_i and T_i are the average pressure and temperature in the layer, respectively, and $\hat{p}$ and $\hat{T}$ are standard atmospheric pressure and temperature, respectively.

Specific considerations and equations for each layer are given in Appendix A and referenced in the nomenclature below.

Table 7-1. Best Estimate Retained Gas Volume Summary, Retained Gas Sampler (RGS) and Void Fraction Instrument (VFI) Data

	AN-103	AN-104	AN-105	AW-101	SY-101[a,b]	SY-103[b]
Input Data						
1. Waste Level (cm)	884±3	979±3	1041±3	1040±3	1019±5	691±3
2. Dome Vol. (m^3)	1712±20	1323±18	1066±21	1070±30	1159±22	2503±13
3. CL Den. (kg/m^3)	1530±50	1440±30	1400±60	1420±20	1620±60	1470±30
4. NC Den. (kg/m^3)	1730±110	1580±50	1580±40	1570±40	1700±40	1600±30
5. CL Thickness (cm)	417±18	526±41	546±43	674±37	717±38	308±14
6. NC Thickness (cm)	378±7	412±40	450±42	286±30	200±22	325±5
7. Crust Thickness (cm)	89±16	41±7	45±10	80±20	102±30	58±13
Crust Layer (Gas volume calculation is independent of VFI and RGS data)						
8. Submerged Fraction	0.96±0.02	0.96±0.02	0.96±0.02	0.96±0.04	0.91±0.05	0.96±0.02
9. Void (%)	15±6	12±4	14±5	13±4	19±6	11±3
10. In-situ Vol. (m^3)	52±22	19±7	25±10	40±15	72±32	25±9
11. Eff. Pres. Ratio	1.02±0.01	0.99±0.01	0.99±0.01	1.02±0.01	1.06±0.02	1.03±0.01
12. Std. Vol. (m^3)	53±23	19±7	25±10	41±15	76±31	26±9
Convective Layer						
13. Mean Void (%)	0.5±0.1	0.4±0.1	0.2±0.1	0.3±0.1	0.3±0.03	0.7±0.3
14. In-situ Vol. (m^3)	8±2	9±2	4±2	10±2	9±1	9±4
15. Eff. Pres. Ratio	1.36±0.04	1.35±0.04	1.38±0.09	1.51±0.06	1.63±0.05	1.28±0.06
16. Std. Vol. (m^3)	11±3	12±2	6±2	15±3	15±2	11±4
Nonconvective Layer						
17. Mean Void (%)	11.0±0.7	6.6±0.8	4.4±0.9	3.8±0.4	5.7±0.7	7.0±1.9
18. In-situ Vol.(m^3)	170±10	110±12	80±16	45±5	46±5	93±25
19. Eff. Pres. Ratio	1.93±0.03	2.07±0.03	2.13±0.05	2.17±0.02	2.26±0.05	1.74±0.02
20. Std. Vol. (m^3)	329±22	230±23	170±33	97±11	104±12	160±42
Whole Tank						
21. In-situ Vol. (m^3)	231±24	138±14	110±19	95±16	127±28	127±27
22. Eff. Pres. Ratio	1.71±0.07	1.88±0.05	1.84±0.10	1.63±0.10	1.53±0.10	1.56±0.05
23. Std. Vol. (m^3)	393±32	259±24	202±34	153±19	195±30	198±43
24. Degassed Level (cm)	842±4	952±4	1021±5	1029±3	988±10	668±7

Notes:

(a) SY-101 data conditions as of 1994-95 with mixer pump operation.

(b) SY-101 and SY-103 void fractions derived from VFI data only.

Nomenclature for Table 7-1

Input Data

1. Waste Level—level measured at approximately the time of the VFI measurements
2. Dome Vol. (m^3)—volume of the headspace above the waste level
3. CL Den. (kg/m^3)—mean convective layer density determined from ball rheometer measurements
4. NC Den. (kg/m^3)—mean nonconvective layer density determined from core samples
5. CL Thickness (cm)—thickness of the convective layer from the bottom of the crust to the top of the nonconvective layer (Equation A-14)
6. NC Thickness (cm)—thickness of the nonconvective layer determined from averaging indications from the ball rheometer, temperature profiles (MIT only), and core samples, as available.
7. Crust Thickness (cm)—crust thickness as determined from MIT validation probe temperature profiles, core samples, or other indications

Crust Layer

8. Submerged Fraction—fraction of crust estimated submerged below the free liquid level
9. Void Fraction—gas volume fraction required to float the crust Equation A-19
10. In-situ Vol. (m^3)—gas volume at local pressure and temperature (Equation A-21)
11. Eff. Pres. Ratio—factor required to convert in-situ volume to standard pressure and temperature; includes both temperature and pressure correction (Equations A-8 and A-20)
12. Std. Vol. (m^3)—stored gas volume at standard pressure and temperature (Equation A-22).

Convective Layer

13. Mean Void (%)—average gas volume fraction computed from VFI and RGS data using the statistical model described in Section A.2. Only VFI data are available for SY-101 and SY-103
14. In-Situ Vol. (m^3)—gas volume at local pressure and temperature (Equation A-16)
15. Eff. Pres. Ratio—factor required to convert in-situ volume to standard pressure and temperature. Includes both temperature and pressure correction (Equations A-8 and A-15)
16. Std. Vol. (m^3)—stored gas volume at standard pressure and temperature (Equation A-17)

Nonconvective Layer

17. Mean Void (%)—see #13.
18. In-Situ Vol. (m^3)—gas volume at the local pressure and temperature (Equation A-10)
19. Eff. Pres. Ratio—factor required to convert in-situ volume to standard pressure and temperature; includes both temperature and pressure correction (Equations A-8, A-9, and A-13)
20. Std. Vol. (m^3)—stored gas volume at standard pressure and temperature (Equation A-11)

Whole Tank

21. In-Situ Vol. (m^3) —sum of in-situ volume of crust, convective, and nonconvective layers (Equation A-23)
22. Eff. Pres. Ratio—the overall effective pressure ratio for the entire tank is equal to the standard volume divided by the in-situ volume (Equation A-25)
23. Std. Vol. (m^3)—sum of the standard volumes of crust, convective, and nonconvective layers (Equation A-24)
24. Degassed Level (cm)—the waste level (see #1) less the nonconvective layer in-situ volume (see #18) divided by tank area (Equation A-26).

7.4.2 Gas Volume Estimated from Barometric Pressure Effects

In-situ measurements of local void fraction provide a relatively accurate estimate of a tank's retained gas volume. However, it is not practical to operate the VFI or RGS each time the gas volume is needed. Fortunately, an alternative method is available for estimating stored gas volume based on the response of the waste surface level to fluctuations in barometric pressure due to compression and expansion of stored gas. This model is referred to as the Barometric Pressure Effect (BPE) model. A detailed derivation of the BPE model is given in Appendix B. The BPE in-situ gas volume is calculated by

$$V_G = -A p_{BPE} \frac{dL}{dp_0} \tag{7-7}$$

where the effective pressure for barometric pressure response is defined by

$$\frac{1}{p_{BPE}} = \sum_{i=1}^{N} \left[\frac{f_i}{p_i} \right] \tag{7-8}$$

and f_i is the fraction of the total in-situ gas stored in layer i:

$$f_i = \frac{A \alpha_i H_i}{V_G} \tag{7-9}$$

The BPE model can be used at any time without prior knowledge of the gas volume, but it requires sensitive and frequent level measurements over some period of time to determine the in-situ gas volume accurately. It also requires an estimate of the vertical distribution of gas. Nevertheless, the BPE model remains the only non-intrusive, independent means available to assess the total stored gas volume. The uncertainty of the BPE model may be ± 30 to 50% of the in-situ volume.

The BPE model should provide good estimates of stored gas volume in the DSTs. Surface level readings from highly sensitive ENRAF™ buoyancy gauges have now been recorded long enough to obtain very good correlations of level with barometric pressure changes. At the same time,

VFI operation has provided a detailed measurement of the gas distribution as well as an independent calculation of the in-situ gas volume. Therefore, the BPE estimates of in-situ gas volume in these tanks should be the most accurate possible.

In Table 7-2, the BPE volume estimates are compared with those calculated from the VFI/RGS results. The BPE estimates use the measured barometric pressure response with the effective pressure and pressure ratio calculated from the gas distribution derived in the VFI and RGS data using Equation B-12.[13] No reliable barometric pressure response could be obtained from SY-101 because of the regular disturbance of mixer pump operation, so it is not shown in the table.

The difference between the BPE and VFI/RGS estimates of in-situ and standard volumes is within the uncertainty of the BPE method. The uncertainty for the BPE result is significantly larger than for the VFI calculation. However, except for SY-103 it is still an acceptable 25 to 40% of the mean. In these tanks, gas releases do not influence estimates of stored gas volume by either VFI measurement or BPE calculation because the typical release volumes are less than the uncertainty of the inventory estimate.

Table 7-2. Measured and Barometric Pressure Effect Gas Volume Estimates in Double-Shell Tanks

	AN-103	AN-104	AN-105	AW-101	SY-103
Values derived from VFI/RGS data (see Table 7-1)					
In-situ volume (m^3)	231 ± 24	138 ± 14	110 ± 19	95 ± 16	127 ± 27
Standard volume (m^3)	393 ± 32	259 ± 24	202 ± 34	153 ± 19	198 ± 43
P_{EFF} for BPE (atm) [(a)]	1.67 ± 0.09	1.84 ± 0.7	1.73 ± 0.12	1.49 ± 0.1	1.53 ± 0.06
Volumes derived from BPE model with measured dL/dP					
Measured dL/dP (cm/kPa)	-0.39 ± 0.11	-0.15 ± 0.05	-0.15 ± 0.05	-0.16 ± 0.05	-0.14 ± 0.11
In-situ volume (m^3)	268 ± 76	116 ± 38	105 ● 36	100 ± 31	91 ± 70
VFI/RGS - BPE (m^3)	-37	22	5	-5	36
Standard volume (m^3)	463 ± 133	218 ± 72	133 ± 67	162 ± 51	142 ± 109
VFI/RGS - BPE (m^3)	-70	41	9	-9	56

Notes:

(a) Effective pressure for the BPE model is calculated differently from the effective pressure for the standard volume. See Equation B-12.

The BPE model was also applied to dL/dP correlations obtained from level and meteorological data from 1998. The in-situ gas volume was calculated assuming the effective pressure value that was calculated from the gas distribution measured by the VFI. The results, shown in Table 7-3, indicate that the BPE has too high an uncertainty to distinguish small changes in gas volume. In fact, the BPE calculation shows an increase in gas content in AN-103, AN-104, and AW-101 where level and temperature changes show a decrease as discussed in the next section.

[13] Barometric pressure response values were calculated by Paul Whitney, PNNL, from ENRAF™ data recorded over all of 1996. The values for SY-103 include 1995 data as well.

7.4.3 Change in Retained Gas Volume Based on Level

Because the five-year period since measurements were made is long compared with the typical time between GREs, and because the gas release volume is usually a small fraction of the gas inventory, the gas volume is not expected to change significantly. Tank 241-SY-101 is the exception due to level growth phenomenon and recent remediation program. For a detailed discussion of the changes in gas volume in that tank, see Mahoney et al. (2000). In the other five tanks, the waste level can be taken as the primary indicator of gas inventory. The BPE method applied to 1995 and 1998 provides additional insight on the changes.

Table 7-3. Change in Retained Gas Volume Based on Barometric Pressure Effect Model

	AN-103	AN-104	AN-105	AW-101	SY-103
dL/dP for 1995 (cm/kPa)	-0.39 ± 0.11	-0.15 ± 0.05	-0.15 ± 0.05	-0.16 ± 0.05	-0.14 ± 0.11
P_{eff} (dL/dP) from VFI (atm)	1.67 ± 0.09	1.84 ± 0.7	1.73 ± 0.12	1.49 ± 0.1	1.53 ± 0.06
In-situ BPE vol. 1995 (m^3)	268 ± 76	116 ± 38	105 ± 36	100 ± 31	91 ± 70
dL/dP for 1998 (cm/kPa)	-0.40 ± 0.07	-0.17 ± 0.05	-0.14 ± 0.09	-0.17 ± 0.08	-0.14 ± 0.11
In-situ BPE vol. 1998 (m^3)	273 ± 53	130 ± 40	96 ± 65	101 ± 50	85 ± 70
In-situ BPE vol. chg. (m^3)	**8 ± 90**	**15 ± 60**	**-8 ± 75**	**2 ± 60**	**-5 ± 100**

The change in both in-situ and standard gas volumes based on level and temperature changes are summarized in Table 7-4. Current gas volumes are computed by adding the change indicated by the waste level to the volumes calculated from VFI and RGS data in Section 7.3 and correcting for changes in temperature. The effect of evaporation of water is neglected due to the presence of a crust and the high salt content of these tanks.

The gas volume in all five tanks has decreased slightly, but only one tank has changed significantly with respect to the uncertainty of the initial volume. Tank 241-AN-104 has lost about 29 m^3 of in-situ gas inventory. Tank 241-SY-103 has lost about 16 m^3 but this is less than the uncertainty in the volume. Including the effect of temperature changes but assuming the same effective pressure as determined from VFI data, AN-104 lost 61 scm, 23% of its initial total gas inventory at one atm.

7.5 SUMMARY OF GAS RETENTION

In-situ measurements of local gas fraction made in 1995-1996 with the VFI and RGS provided data from which the total retained gas volume of each tank could be estimated with fair accuracy. While the data showed significant variation in gas content at different locations, the overall consistency of VFI and RGS data and confirmation of the total gas volume with the BPE method show that the data adequately represents the dynamic state of the tanks.

Table 7-4. Change in Retained Gas Volume Based on Level and Temperature

	AN-103	AN-104	AN-105	AW-101	SY-103
In-situ vol. via VFI/RGS (m^3)	231 ± 24	138 ± 14	110 ± 19	95 ± 16	127 ± 27
Level at VFI (cm)	884 ± 3	979 ± 3	1041 ± 3	1040 ± 3	691 ± 3
Level 1/1/00 (cm)	883 ± 3	972 ● 3	1040 ± 3	1040 ± 3	687 ± 3
Level change (cm)	-1 ± 0.5	-7 ± 0.5	-1 ± 0.5	0 ± 0.5	-4 ± 0.5
In-situ vol. change (m^3)	**-4 ± 2**	**-29 ± 2**	**-4 ± 2**	**0 ± 2**	**-16 ± 2**
In-situ vol. 1/1/00 (m^3)	226 ± 24	110 ± 14	106 ± 19	95 ± 16	111 ± 27
Std. vol. via VFI/RGS (m^3)	393 ± 32	259 ± 24	202 ± 34	153 ± 19	198 ± 43
Temp. at VFI (°K)	313 ± 2	316 ± 2	311 ± 2	313 ± 2	309 ± 2
Temp. 1/1/00 (°K)	307 ± 2	309 ± 2	306 ± 2	305 ± 2	304 ± 2
P_{eff} from VFI (atm)	1.71 ± 0.07	1.88 ± 0.05	1.84 ± 0.10	1.63 ± 0.10	1.56 ± 0.05
Std. vol. 1/1/00 (m^3)	375 ± 43	198 ± 25	189 ± 35	148 ± 26	167 ± 41
Std. vol. change (m^3)	**-18 ± 54**	**-61 ± 35**	**-13 ± 49**	**-5 ± 32**	**-31 ± 60**

The gas retention characteristics of the FGWL DSTs is similar in that they retain most of their gas below the 100-in. (254-cm) elevation in the nonconvective layer and that the total gas volume has not changed significantly in the last four years. However, the volume of gas varies widely. Tank 241-AN-103 has by far the largest volume at almost 400 scm. This approximates the gas stored in SY-101 prior to its historic large releases and is almost four times that of AW-101 that holds just under 100 scm. The other three tanks, AN-104, AN-105, and SY-103 have approximately equal gas volumes at 110 to 140 scm. As will be shown in Section 8.0, the average gas release volumes from these tanks are only 10 to 15% of the total gas volume retained in the non-convective layer.

Each tank holds a significant gas volume in its floating crust layer. Tank 241-AN-103 has the thickest crust (excluding SY-101 prior to dilution) that stores the most gas, over 50 scm. However, AW-101's crust retains over 40 scm which is the largest fraction of the tank total. The other tanks store from 20 to 26 scm in their crust layer.

8.0 SPONTANEOUS AND INDUCED GAS RELEASE BEHAVIOR

Buoyant displacement GREs are the primary flammable gas hazard because steady-state gas concentrations are insignificant. The gas release history of the DSTs is of great importance in assessing the hazard. Also, marked changes in gas release behavior have occurred over the last four years. GREs have generally become much smaller and, in some cases fewer. This has altered the overall picture of the FGWL DSTs, and the reasons for the change must be understood to avoid reversing the trend in the future.

Most of the gas generated in the waste is released to the tank headspace in a gradual, essentially steady manner. But the FGWL DSTs store a portion of the gas that is occasionally released in sudden, episodic buoyant displacements (Meyer et al. 1997). A GRE is characterized by a sudden increase in measured headspace hydrogen concentration from the steady-state level followed by a more gradual decrease back to the steady-state concentration. The gas release may be accompanied by a drop in waste level, which indicates that the waste volume decreased because of the release of gas. However, because volumes are small and gas release is generally slow, the correlation between level drop and GRE is very weak in most tanks. Therefore, headspace hydrogen concentration is the only practical method to identify and quantify releases.

Section 8.1 discusses the methods used to quantify gas releases and the limitations associated with these methods. Occurrence of induced gas releases is discussed in Section 8.2, and the effect of barometric pressure changes on spontaneous releases is investigated in Section 8.3. The gas release histories and trends are described in Section 8.4, and an overall summary of gas release behavior and its evolution is given in Section 8.5

8.1 METHODS USED TO QUANTIFY GAS RELEASES

Three main methods have been developed to quantify gas releases during GREs, waste surface level drop analysis, headspace hydrogen concentration analysis, and exhaust hydrogen concentration integration. Waste surface level drop analysis was the only method available prior to SHMS installation in 1994–1995 (see Section 2.2.1).[14] It is an indirect and imprecise indication of gas release with a detection limit on the order of 10 m^3. Except for SY-101, none of the GREs considered in this report are based on level drops.

Because of the relative imprecision of the waste surface level drop method, work has focused on analyzing headspace gas concentration data as they became available, starting in 1994–1995, to determine the magnitude of gas releases during GREs. Headspace hydrogen concentration analysis is a positive and direct measurement of integral gas release. It is extremely sensitive and does not require a knowledge of the ventilation rate but actually computes it. Nevertheless, this method has its own limitations, which are discussed in subsection 8.1.2.

[14] The large gas releases in SY-101 prior to mixing were also quantified by analyzing the dome pressure and ventilation rate. However this method cannot typically be applied to the much smaller gas releases in other tanks.

8.1.1 Waste Surface Level Drop Analysis

The waste surface level drop analysis method is not very useful because of the following factors:

1. Small GREs are difficult to detect. Detecting the GRE signature is more "art" than science. For example, the entire level evolution surrounding a GRE may occur over weeks and involve level rises as well as intermediate drops.
2. It has been found that there is no correlation between level drop and gas release volume in AN-103, AN-104, and AW-101.
3. Level instrument maintenance, including flushes and recalibration, or crust motion can appear to be GREs.
4. Determination of the level drop is open to interpretation. A specific time period or the maximum to minimum level could be used. There are also several instruments from which level drop data can be taken.

The GRE history for a typical tank prior to the mid-1990s must be derived from the waste level history, usually measured by an FIC contact probe or ENRAF™ buoyancy gauge (since about 1995). The manual tape or other devices are suitable for identifying, but not quantifying, some of the larger releases.

Large GREs are identified by a sudden level drop following a long period of steady level rise. The initial drop is usually followed by a slower decline to a minimum level several days or even a couple of weeks after the main event. Often there is an accelerated or even abrupt level rise just before the event. During a buoyant displacement event, the expansion of the gas in the rising gob will produce a level rise if it occurs slowly or if the gas is not released immediately. At the surface, gas is released until the gob returns to approximately neutral buoyancy at the surface. Then the gob may disintegrate, as pieces sink back to the bottom, compressing the gas that remains trapped. This final process produces the slower level decline that occurs days or even weeks after the actual release.

A formal procedure was developed by Whitney et al. (1996) that locates statistically significant breaks in the level history (rises or drops) that might indicate a GRE. Once the level breaks were identified, the waste level history had to be screened to weed out false positives resulting from occasional FIC flushes or spurious readings recorded in the operations log. The validated list of breaks in each tank then had to be evaluated one-by-one by inspecting the daily level data with a generous application of human judgment. Different analysts could record different sets of GREs. There was no doubt about the larger ones (e.g., SY-101 prior to mixing), but considerable doubt about the barely detectable drops in AN-103 and AW-101, for example.

However, no matter how carefully the level record was studied, the fact that many clear level drops show no evidence of gas release in the gas monitoring data and, conversely, many significant gas releases recorded by gas monitoring were not associated with a level break. For this reason, the level drop method has been discarded as a viable technique for evaluating GREs, except for the very largest.

Assuming an event sufficiently large to make the level drop method viable, the gas release is calculated from the difference between the peak waste level immediately before the drop and minimum the level even if it occurs several days later. From a comparison of the few level GREs in SY-101 where both gas data and level drops were available, the peak-to-minimum drop represents the total gas release while the level drop over the first 12 to 24 hours represents the prompt release responsible for the peak headspace hydrogen concentration.

The gas release is assumed to originate in the nonconvective layer because the convective layer contains essentially no gas, and the gas stored in the crust apparently does not participate heavily, as evidenced by the quick reestablishment of the crust layer in SY-101 even after large releases. The standard gas release volume is computed as

$$\hat{V}_{REL} = \Delta L_{GRE} A P_{NC} \tag{8-1}$$

where L_{GRE} is the level drop,
A is the tank area, and
P_{NC} is the average pressure ratio (includes both temperature and pressure effects) of the gas stored in the nonconvective layer.

8.1.2 Headspace Hydrogen Concentration Analysis Methods

Total gas release volumes can also be estimated using two methods that are based on the measured concentration of hydrogen gas in the headspace. The first provides the lower bound estimate and the second gives a best estimate based on integrated hydrogen concentration in the headspace. Both assume that the headspace is well-mixed. This assumption is usually valid after about one hour from the start of a GRE. Headspace hydrogen gas concentration data support the well-mixed assumption for the period after most of the gas has been released. Both also require a knowledge of the hydrogen fraction in the waste gas which must be obtained through waste sampling [e.g., RGS as described by Mahoney et al. (1999)].

8.1.2.1 Lower Bound Estimate

The total volume of gas released is determined using the following equation:

$$V_R = V_{HS} \frac{[H_2]_{Peak} - [H_2]_{Base}}{[H_2]_{Waste}} \tag{8-2}$$

where V_R is the total volume of gas released,
V_{HS} is the headspace volume,
$[H_2]_{Peak}$ is the peak measured hydrogen concentration in the headspace,
$[H_2]_{Base}$ is the measured baseline hydrogen concentration before the GRE, and
$[H_2]_{Waste}$ is the hydrogen fraction in the waste gas.

Application of this method yields only the lower bound of the volume of gas released because, assuming a well-mixed headspace and zero ventilation rate, no less than exactly the peak

hydrogen concentration times the headspace volume is required to achieve that concentration. That a larger release actually occurs is also evident because the ventilation actually reduces the peak measured concentration somewhat. Furthermore, release continues at a low rate long after the peak.

8.1.2.2 Hydrogen Release Model

An exponential model is postulated for the release rate that is given by Equation 8-3. The model hydrogen released rate, Q_{R0}, time constant, τ, and the ventilation rate, Q_V, are determined using the headspace hydrogen continuity equation, Equation 8-4, where $[H_2]$ is the headspace hydrogen concentration above the initial, background value. The constants are adjusted values to minimize the error between the calculated and measured hydrogen concentrations for all data points from the start of the GRE to some time after its peak. Finally, the total release volume is simply the hydrogen release volume divided by the hydrogen fraction in the waste via Equation 8-5.

$$Q_R = Q_{R0}\left(\frac{t-t_0}{\tau}\right)e^{-\frac{t-t_0}{\tau}} \tag{8-3}$$

$$V_{HS}\frac{d[H_2]}{dt} = Q_R - (Q_V + Q_R)[H_2] \tag{8-4}$$

$$V_R = \frac{\int_{t_0}^{\infty} Q_R\,dt}{[H_2]_{Waste}} = \frac{Q_{R0}\tau}{[H_2]_{Waste}} \tag{8-5}$$

Besides a well-mixed headspace, this method assumes that the inlet air ventilation rate, Q_V, is constant (but need not be known) over the GRE period, a reasonable assumption for positively ventilated tanks.

Examples of the results of applying this method are shown in Figures 8-1 through 8-4 for sample measured GREs in tanks SY-103 and AN-105. Notice the marked difference between the duration of the GRE and the time required for the concentration to return to the value before the GRE. To adequately model the releases in SY-103, two releases, one with a short time constant and another with a much longer time constant and lower base rate, were required to capture the unique long-term behavior.

Note that this method provides not only the release rate and volume but also the ventilation rate. This is especially valuable in analyzing releases prior to the installation of the constant flow controllers when the ventilation rate varied considerably.

8.1.2.3 Integrated Exhaust Hydrogen Concentration

The total hydrogen release over some time period can also be calculated directly as the integral of the product of ventilation rate and the hydrogen concentration in the ventilation exhaust above the initial background concentration. The integral is given by Equation 8-6 and an equivalent difference form by Equation 8-7.

$$V_R = \frac{1}{[H_2]_{Waste}} \int_{T_0}^{T_1} [H_2](t) Q_V(t) dt \tag{8-6}$$

$$V_R = \frac{1}{[H_2]_{Waste}} \sum_{i=1}^{N} \frac{1}{2} \{[H_2]_i Q_{Vi} + [H_2]_{i-1} Q_{Vi-1}\}(t_i - t_{i-1}) \tag{8-7}$$

where T_0 and T_1 are the start and end times of the release,
N is the number of data points between T_0 to T_1, and
t_i is the time of data point i.

This procedure requires that the ventilation rate be known from direct measurement (as in SY-101) or can be reasonably estimated and assumed constant. Most importantly, however, the model does not require the headspace to be well-mixed. Therefore, the technique is particularly useful for small or irregular releases where plume behavior is suspected or in other cases where the model release rate does not fit the data.

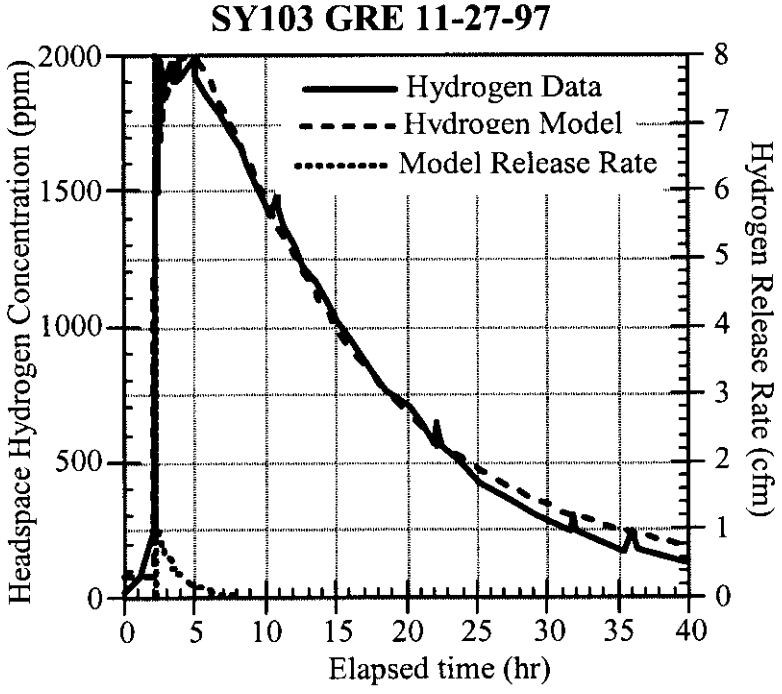

Figure 8-1. Gas Release Model Results for Tank 241-SY-103

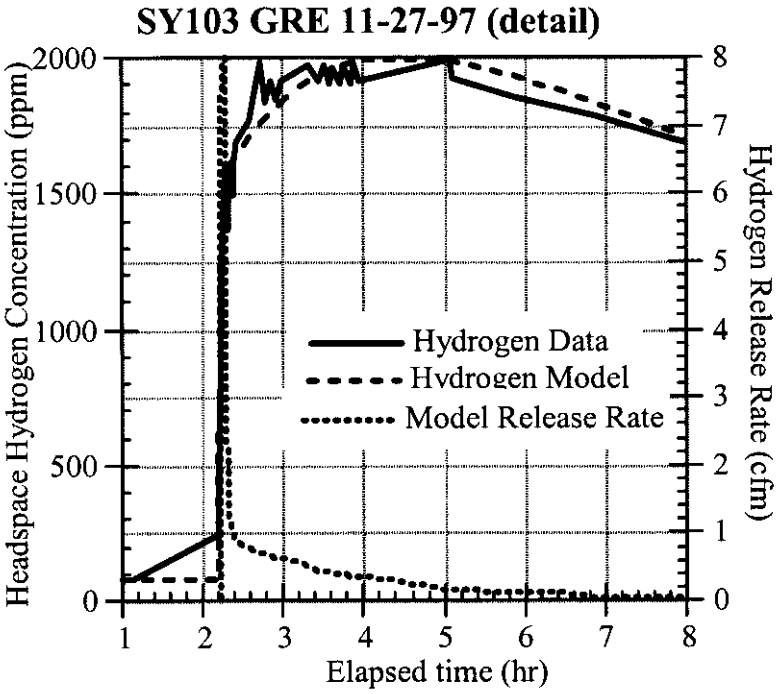

Figure 8-2. Initial Portion of Gas Release Model Results for Tank 241-SY-103

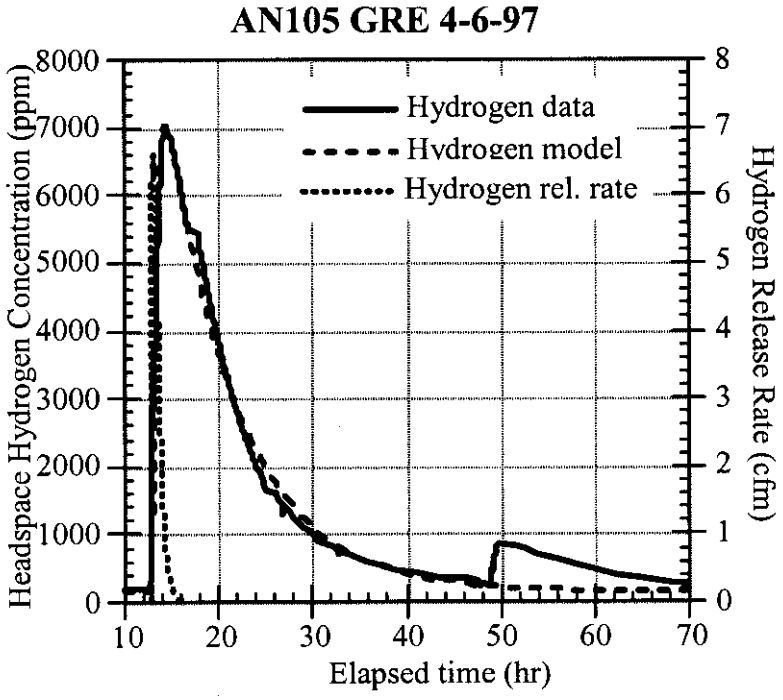

Figure 8-3. Gas Release Model Results for Tank 241-AN-105

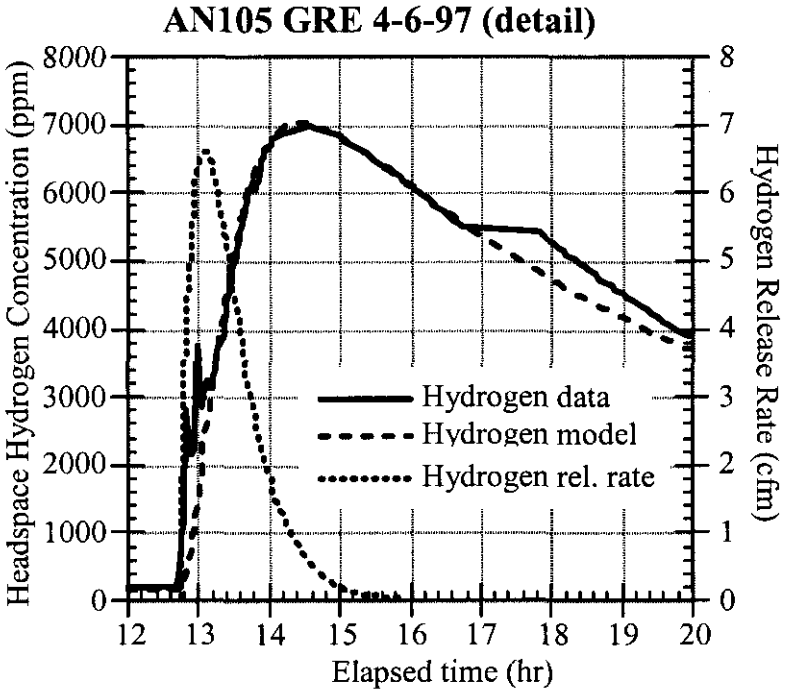

Figure 8-4. Initial Portion of Gas Release Model Results for Tank 241-AN-105

8.2 INDUCED GAS RELEASE EVENTS

Over the years many waste disturbing activities have been conducted in the Facility Group 1 tanks. In some cases the intent of these activities was to induce a gas release from the tank. The waste disturbing activities can be broken into two major groupings, locally waste disturbing activities such as sampling, lancing, ball rheometer, and VFI and globally waste disturbing activities such as transfers and mixer pump operation. The following discussion will be broken down along the lines of the two types of activities.

Locally Waste Disturbing Activities. During the 1980s, numerous attempts were made to induce gas release from tank SY-101 using a perforated lance with either steam or water as the motive fluid. These attempts were unsuccessful in inducing releases large enough to be detected by a level change in the tank. Review of the lance design has shown that the perforations were along most of the submerged length of the lance. This resulted in the steam or water being released into the upper region of the waste away from the main gas reservoir. Thus, in hindsight it is not surprising that little gas was released by this device.

During the 1990s, all the Facility Group 1 tanks were sampled with full-length core samplers. The core sampling consisted of penetrating the waste surface crust with a waste lance followed by inserting the ~ 3-inch diameter core sampler slowly into the waste until the tank bottom was reached. Sampling took from a couple days to over two months depending on equipment problems and the weather. In all cases at least two cores were taken in each sampling event. No significant gas release (surface level drop of 0.1 inch or greater or a SHMS reading of greater

than 1,000 ppm hydrogen) was observes for any of these events. Video monitoring of some of the sample events did show bubbling around the lance or sampler shaft, but insufficient gas was released to be detectable even by the SHMS monitors.

Each tank also was investigated using the Ball Rheometer and the VFI. The ball rheometer is a 4-in. diameter 16-lb ball attached to a cable, which is lowered and raised through the waste at varying speeds. The VFI has a 3-ft arm, which allows it to sweep an area 6-ft in diameter around the support shaft. The VFI is slowly lowered and raised through the waste with measurements taken about every six inches. Each tank was examined through at least two risers. During the course of the deployment of the ball rheometer and VFI in tank AW-101, significant gas releases were observed. This is the only known case of a significant gas release being induced by a locally waste disturbing action.

The VFI and ball rheometer testing activity apparently disturbed the waste sufficiently to trigger small gas releases. The hydrogen concentration history during this period is given in Figure 8-5. The first release occurred immediately after lancing through the crust in Riser 13A and must have come from the crust because the lance did not penetrate the nonconvective layer. The ball rheometer did not release any more gas in Riser 13A; neither did the subsequent lancing and testing in Riser 1C. The VFI also released gas. Looking closely at the timing of the gas release and VFI operation in Figure 8-6, the entire test series was completed in 13A, and the first pass was completed in Riser 1C before the hydrogen concentration began to increase.

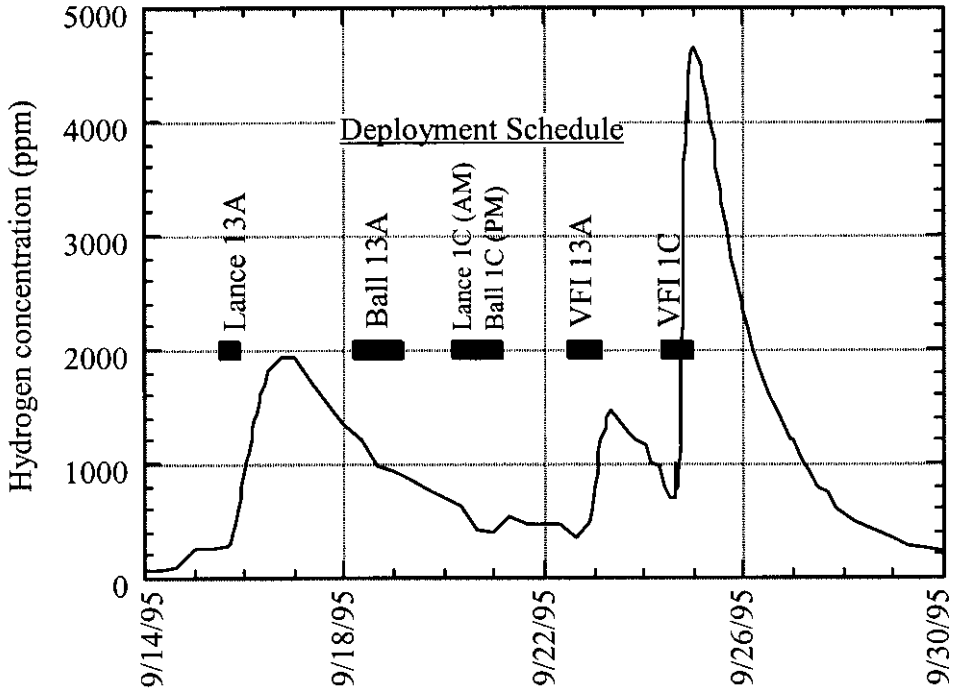

Figure 8-5. Hydrogen Concentration History in Tank 241-AW-101 During Void Fraction Instrument and Ball Rheometer Deployment

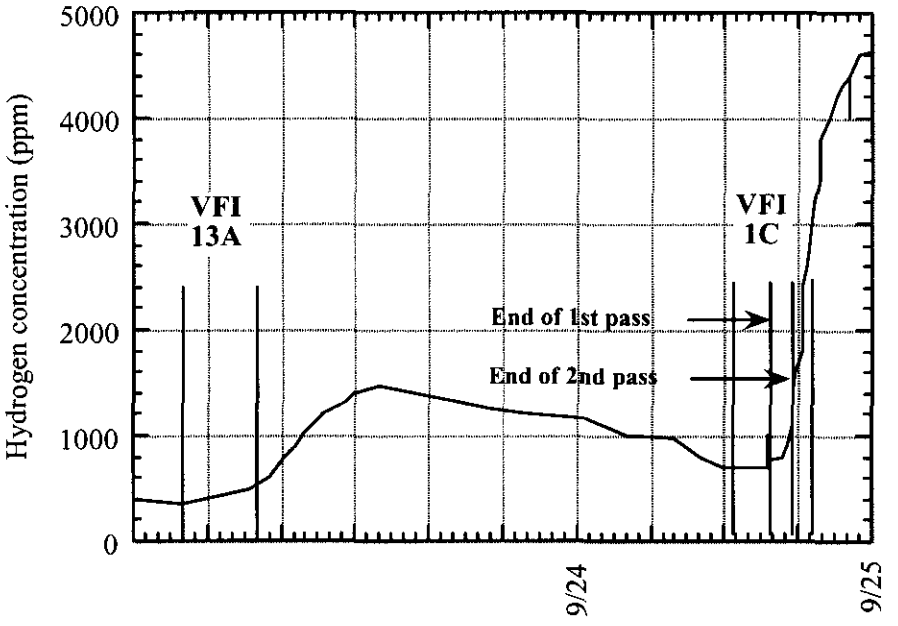

Figure 8-6. Sequence of Gas Release Compared with Void Fraction Instrument Deployment in Tank 241-AW-101

The computed release rate matching the dome concentration transient from September 22, 1995, through September 29, 1995, indicated that about 14.3 m^3 (503 scf) of hydrogen was released. Assuming 30% hydrogen concentration, the total gas release may have been as high as 47.7 m^3 (1670 scf). Additional gas may have been stored in the crust layer, as evidenced by the 2.5-cm (1-in.) waste level increase over this period.

Globally Waste Disturbing Activities. A globally waste disturbing activity is one which affects the majority of the waste in a tank. The two most common examples of globally waste disturbing activities are waste transfers between tanks and operation of a mixer pump. The Wyden Bill restrictions on transfers of waste into Watch List tanks and the lack of mixer pumps in the Facility Group 1 tanks restricts the available data to the mixer pump operation in SY-101 and the recent transfer of waste out of SY-101 and associated dilution with water following the transfer.

The data from mixer pump operation have been documented in a series of quarterly reports (see, for example, Conner 2000b). The mixer pump has prevented the formation of a deep nonconvective layer and effectively released retained gas from the shallow nonconvective layer that did form. It is believed that the gas release is proportional to the total volume of gas stored in the nonconvective layer and the power input from the pump. No analysis of the data has been made which would verify this belief or establish specific proportionality constants. However, in essentially all cases where the mixer pump was run a small but measurable release of gas was detected.

Approximately half of the waste in SY-101 was transferred to SY-102 in a series of three transfers between December 18, 1999, and March 23, 2000. During these transfers, the tank domespace was monitored for hydrogen. The maximum concentration observed was less than 1000 ppm indicating a small slow release associated with the removal of waste from the tank. During and following dilution with water, the tank was much more active in releasing gas with hydrogen concentration as high as 2000 ppm. The elevated hydrogen continues for some days after the water additions due to continuing dissolution of the solids in the water. For a detailed discussion of the observations from the transfer and dilution, see Mahoney et al. (2000). It should be noted that these transfers were from a well-mixed tank with a minimal nonconvective layer. If a thick nonconvective layer is formed with a significant gas inventory, it is likely that larger gas releases will be observed during transfer.

8.3 EFFECT OF BAROMETRIC PRESSURE CHANGES

In SSTs, small gas releases typically accompany deep atmospheric pressure decreases.[15] This suggests that large pressure fluctuations may also serve as a potential triggering mechanism for GREs in DSTs. Lowering pressure causes gas trapped in the nonconvective layer to expand, possibly enough to become buoyant.

This section investigates the occurrence of GREs in the FGWL DSTs (excluding SY-101) over the past several years compared with concurrent barometric pressure fluctuations to determine if a correlation exists. Section 8.3.1 provides the theoretical basis for the relationship. Section 8.3.2 lists the GREs that have been observed in gas monitoring data in the past five years and illustrates the identification method for the barometric pressure fluctuations that have occurred in the same period. The investigation is detailed in Section 8.3.3, and the results are summarized in Section 8.3.4.

8.3.1 Relation Between Gas Release Events and Barometric Pressure

The basis for considering the potential for barometric pressure fluctuations to cause GREs is the ideal gas law, which states that, for a given mass of gas at a constant temperature, the product of the pressure and the volume of the gas is constant, or

$$pV_G = \text{constant} \tag{8-8}$$

Differentiating Equation 8-8 with respect to the pressure yields

$$\frac{dV_G}{dp} = \frac{-V_G}{p} \tag{8-9}$$

[15] Reported monthly in informal "SHMS Reports" by D. J. McCain, CHG.

The gas volume fraction or void fraction is defined as

$$\alpha = \frac{V_G}{V_G + V_{NG}} \tag{8-10}$$

where V_{NG} is the volume of non-gas, liquid and solid waste.

The gas volume may then be expressed in terms of V_{NG} as

$$V_G = \frac{\alpha}{1-\alpha} V_{NG} \tag{8-11}$$

Substituting Equation 8-11 into Equation 8-12, the change in the void fraction in the nonconvective layer with a change in pressure can be determined to be

$$\frac{d\alpha}{\alpha(1-\alpha)} = -\frac{dp_s}{p_s} \tag{8-12}$$

where p_s is the average in-situ gas pressure, in atmospheres, defined by

$$p_s = \frac{1}{p_{SP}}\left[p_A + \rho_{CL} g\left(h_C + h_{CL} + \frac{h_{NCL}}{2} \right) \right] \tag{8-13}$$

where ρ_{CL} is the density of the convective layer,
P_{SP} is the standard atmospheric pressure and
p_A is the local barometric pressure, g is the acceleration due to gravity, and
h_C, h_{CL}, and h_{NCL} are the thickness of the crust, convective, and nonconvective layer respectively.

All terms in Equation 8-13 except for p_A are assumed constant on the time scale of barometric pressure fluctuations.

According to Equation 8-12, a pressure decrease causes the void fraction in the nonconvective layer to increase. An increase in void fraction also increases the thickness of the layer. However, an expansion due to increased gas content has no effect on pressure so the small change in layer thickness can be ignored. The pressure change required to make the average void fraction in the nonconvective layer equal to the neutral buoyancy void fraction (Equation 7-2) can then be computed for any given initial void fraction by integrating Equation 8-12. The result, solving for the pressure change, is

$$\frac{\Delta p_s}{p_s} = \frac{\Delta p_A}{p_s} = -\frac{1}{1-\alpha_0}\left(1 - \frac{\alpha_0}{\alpha_{NB}} \right) \tag{8-14}$$

where α_0 is the initial void fraction and
α_{NB} is the neutral buoyancy void fraction.

If α_{NB} is approximately equal to 0.1, a 5% pressure decrease would cause the necessary 5% change in void fraction to increase it from 0.095 to the neutral buoyancy point. As will be shown below, however, a change as large as 5% in barometric pressure is relatively rare.

8.3.2 Recorded Gas Release Events and Barometric Pressure Data

The date and peak headspace hydrogen concentration for gas release events recorded by headspace gas monitoring over the last five years for the five DSTs exhibiting GRE behavior are listed in Table 8-1 (McCain 1999). The decreasing trend in gas release volume, as evidenced by the decreasing headspace concentration is discussed in Section 8.4.

These GREs are all assumed to have occurred by buoyant displacement. The guidelines applied to identify the GREs from the gas release data of the tanks ensure that the releases are significant.[16] The total gas release volumes estimated from the table demonstrate that the size of the participating "gob" of waste in a majority of these events were comparable to that predicted by Meyer et al. (1997). Further, no distinct separation in release volume can be identified among the events which would indicate a different release mechanism.

The barometric pressure history was obtained from the Hanford Weather Station as hourly averages for 1994 through 1999. Local maxima and minima in the barometric pressure history were selected by visual examination to capture the significant pressure fluctuations from the mass of data. An example is shown in Figure 8-7.

8.3.3 Correlation of Gas Release Events with Pressure Changes

The magnitude of the barometric pressure changes prior to and during the identified GREs was determined from the visually identified maxima and minima. The number of GREs that occurred during a pressure decrease is 48 out of 78 events, or almost 62%. However, a pressure change some time prior to the event may also be its cause. If some GREs are in fact triggered by prior barometric pressure decreases, it is reasonable to impose a time lag from the onset of the GRE to the previous maximum or minimum (henceforth denoted as the prior peak) in the barometric pressure history so that the number of GREs coinciding with a pressure decrease is maximized.

Table 8-2 lists the frequency of GREs that occur within specific times after a prior barometric pressure peak. The largest count occurs for times from 1.4 to 2.8 days. The number of GREs coinciding with a pressure decrease is maximized to 53 out of 78 events (68%) when the time lag is set to 2.5 days.

[16] Personal communication with D. J. McCain, CHG, May 2000.

Table 8-1. Gas Release Events Summary

TANK GRE DATE	Max. [H_2] (ppm)	TANK GRE DATE	Max. [H_2] (ppm)	TANK GRE DATE	Max. [H_2] (ppm)
AN-103		**AW-101**		**SY-103**	
8/22/95	1600	10/1/94	5500	1/22/95	1090
4/11/98	960	10/4/94	6200	3/1/95	2230
2/1/99	900	10/21/94	2980	5/2/95	2940
9/4/99	1560	11/27/94	4900	8/23/95	1260
12/29/99	530	2/22/95	4600	9/6/95	1890
AN-104		5/8/95	1800	12/3/95	740
11/6/94	3000	5/17/95	1000	6/6/96	1090
2/16/95	2088	7/8/95	2000	7/14/96	2170
8/3/95	480	7/12/95	900	12/20/96	5110
10/2/95	3200	8/2/95	3300	11/27/97	2660
10/5/95	1000	9/15/95	1930	12/7/97	2060
10/8/95	5000	9/22/95	4660	8/15/98	1660
5/3/96	6109	10/16/95	1750	10/23/98	1140
5/1/97	3183	12/12/95	2110	12/25/98	3160
8/25/98	310	12/29/95	6000	1/10/99	690
9/26/98	310	1/13/96	1170	3/9/99	570
12/2/98	550	1/25/96	1830	5/30/99	950
4/26/99	135	2/5/96	3200	10/26/99	1020
6/1/99	151	2/14/96	940	11/26/99	600
7/2/99	249	5/14/96	1363	12/2/99	570
8/1/99	181	6/5/96	2511		
9/4/99	155	4/21/98	398		
AN-105		6/24/98	450		
8/21/95	17000	7/4/98	480		
5/30/96	14500				
4/5/97	6980				
9/25/97	950				
11/22/97	1030				
12/31/97	3940				
9/2/98	2280				
3/7/99	760				
5/2/99	182				
7/28/99	7100				
8/2/99	7620				
10/27/99	180				
12/31/99	186				

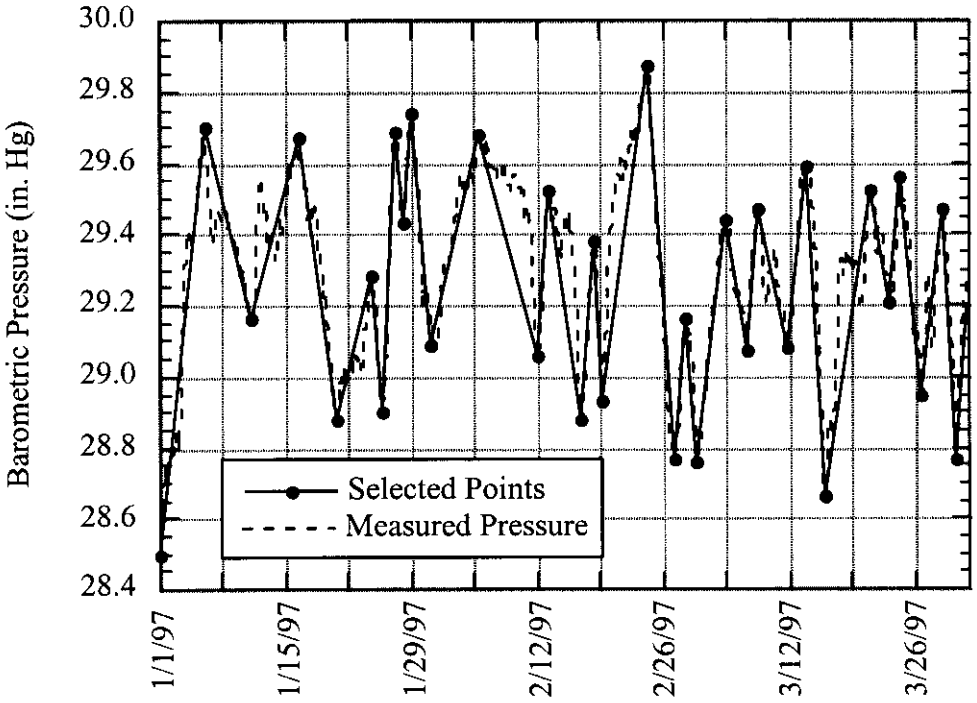

Figure 8-7. Barometric Pressure and Selected Maxima and Minima

Table 8-2. Frequency Table of the Time between Gas Release Events and the Prior Peak

Time to Prior Peak (days)	Count
1.4	23
2.8	25
4.2	16
5.6	7
7.0	4
8.4	0
9.8	1
More	2

Table 8-3 lists the frequency of GREs occurring during a given magnitude of barometric pressure decrease (no lag time). Pressure decreases of 0.005 to 0.035 atmospheres (atm) most often precede a GRE, with 43 of the 78 events occurring in this range. These pressure changes produce relatively small changes in the void fraction via Equation 8-14. In order for the barometric pressure decrease to be the "trigger" for a GRE, the initial void fraction of the participating portion of the nonconvective layer must already be close to the neutral buoyancy point. For the maximum observed pressure change of 0.054 atm to trigger a GRE, the initial void fraction must be within 5% of the neutral buoyancy void fraction. The typical preceding pressure decrease of 0.020 atm requires that the initial void fraction be within about 2.0% of

neutral buoyancy. These results suggest that barometric pressure fluctuations are only capable of triggering GREs that are already about to occur.

Table 8-3. Frequency of Preceding Pressure Changes Associated with Gas Release Events

Affecting Pressure Change (atm)	Count
-0.054	1
-0.044	1
-0.035	2
-0.025	9
-0.015	24
-0.005	10
0.005	0
0.015	14
More	17

The largest barometric pressure decreases typically occur in October through March as shown in Figure 8-8. If the occurrence of GREs is indeed a function of the barometric pressure, a similar periodic behavior in the number of GREs per month should be evident. The average magnitude of the positive and negative pressure fluctuations over five years (1995 to 1999) are given in Table 8-4 together with the GRE count (all five tanks are included; 1994 is neglected as its data set is incomplete). The number of GREs recorded per month are plotted in Figure 8-9. The largest number of events occur in October and December, and the majority of the events appear to occur in the latter half of the year.

Comparison of Figure 8-8 with Figure 8-9 and examination of the data in Table 8-4 does not show a strong correlation throughout the year. The quiescent period of the barometric pressure fluctuations; May through September, does not coincide with the "quiescent period" of GREs; January through April, for example. However, the large number of events in October through December coincides with large differences in the pressure fluctuations. In fact, for December, which has the largest number of GREs, the average difference between the positive and negative pressure fluctuations is also the largest. Note, however, that when the GRE data for SY-103 is removed, December is no longer the dominant month.

Several statistical techniques as well as Fourier analysis were applied to attempt to find periodic behavior in the GRE history or correlation with barometric pressure. This investigation is described in Appendix C. No significant periodicity or correlation with barometric pressure was found.

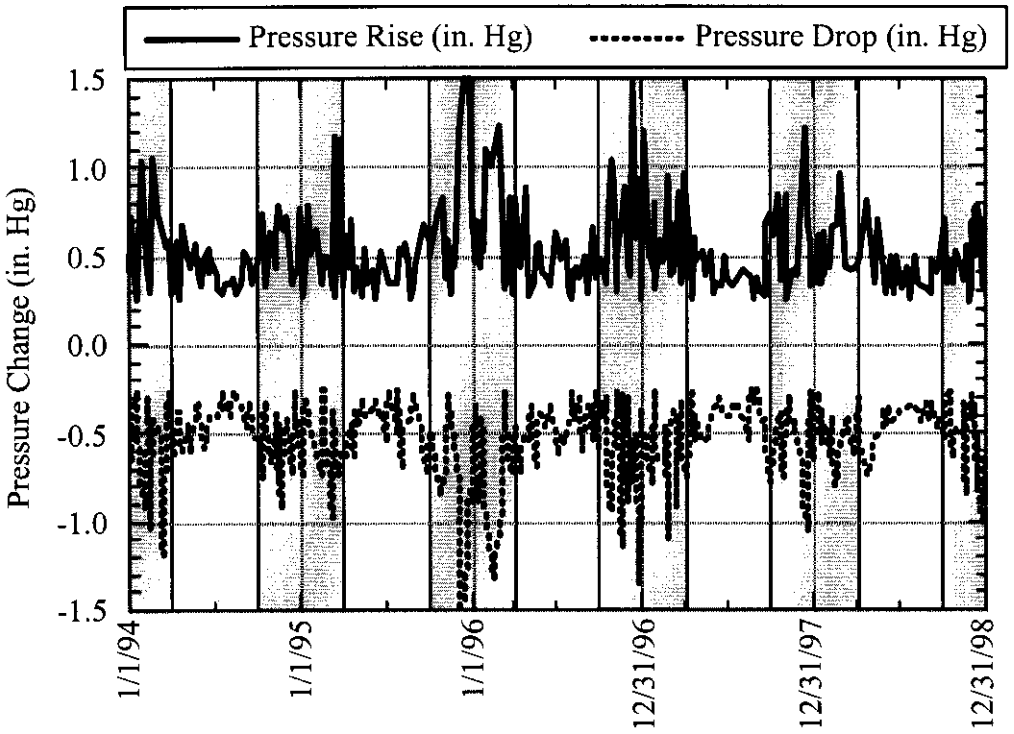

Figure 8-8. Barometric Pressure Fluctuations as a Function of Time

Table 8-4. Average Pressure Fluctuations and Gas Release Events Count per Month for 1995-1999

Month	Average Pressure Drop (atm)	Average Pressure Rise (atm)	GRE Count
January	-0.010	0.009	4
February	-0.011	0.010	5
March	-0.010	0.009	3
April	-0.008	0.010	4
May	-0.009	0.007	9
June	-0.008	0.005	4
July	-0.008	0.006	5
August	-0.008	0.005	9
September	-0.008	0.007	8
October	-0.008	0.010	7
November	-0.008	0.009	3
December	-0.011	0.013	11

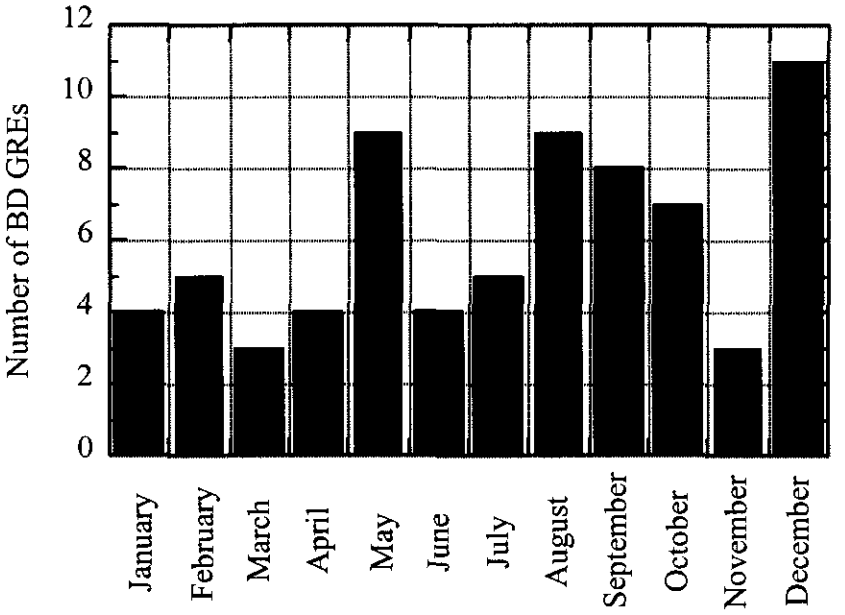

Figure 8-9. Gas Release Events per Month Summed for 1995 through 1999

As noted above, the annual quiescent period of the barometric pressure fluctuations does not coincide with the quiescent period of GREs, so no strong correlation is expected. There is, however, a period of larger pressure fluctuations that does coincide with higher GRE counts which does suggest a relation. As discussed in Meyer et al. (1997), a number of regions exist in the nonconvective layer of a given tank that participate in buoyant displacements, each in a varying state of "maturity" (i.e., retaining enough gas to become buoyant). Those regions which have most recently participated in a GRE will necessarily contain the least amount of gas, while other regions may be close to buoyancy. A possible sequence is that the larger pressure fluctuations trigger those regions that are most mature, after which, even with large pressure fluctuations, no other regions are sufficiently close to buoyancy to be triggered. Later on, as a gas generation and retention continue, GREs begin to occur independent of the pressure as these regions become buoyant. Increasing pressure fluctuations are then again able to trigger GREs as the cycle repeats. Therefore, correlation would not be equally identifiable throughout the year.

Periodic behavior may possibly be indicated in the GRE count over the 60 months (Appendix C). While the waste configuration in each of the tanks is similar, each GRE is independent, and the tanks are obviously disassociated from each other. As a result, it is unlikely that a periodic behavior would be observed for the combination of the GRE histories for the five independent tanks. Periodic behavior may, therefore, be indicative of a cyclic stimuli capable of affecting all the tanks in the same manner. Barometric pressure and temperature are the only cyclic inputs able to effect all of the tanks' behaviors in this fashion. The yearly temperature fluctuations affect the tank waste temperatures in a repeating cycle of typically less than 3 °F, with the highest temperatures in August and September (Sections 4.2 and 5.5). This temperature fluctuation causes a change in the gas generation rate of almost 12% over the year (as predicted by the empirical hydrogen generation rate model of Hu [2000]) and may contribute to GRE

behavior. Similar analysis to those described in Appendix C, however, even allowing for significant phase shifts, shows correlation coefficients an order of magnitude less than the weak coefficients determined in association with the barometric pressure. Periodic behavior may then in and of itself indicate a relation to the stimulus of barometric pressure. It must be emphasized that no definitive statistical evidence of periodic GRE behavior was identified.

Possible correlation between the barometric pressure and the total gas volume of the GRE was also investigated. A discussion of the magnitudes and trends of these gas releases is presented in Section 8.4. No evidence of a correlation was found.

8.3.4 Conclusions on the Effect Pressure on Gas Release Events

A majority (over 60%) of the identified GREs for tanks AN-103, AN-104, AN-105, AW-101, and SY-103 from 1994 to 1999 are found to be associated with a decrease in barometric pressure. Decreases in the barometric pressure increase the void fraction of the waste, which can cause regions already almost buoyant to become so. Even large barometric pressure swings, however, are capable of inducing buoyancy only in waste that is already within ~2% of neutral buoyancy, and GREs were therefore hastened only minimally by the barometric pressure changes. Further, while periods of large pressure fluctuations and numerous GREs do exist, no statistically significant association between barometric pressure and GREs was identified.

8.4 GAS RELEASE HISTORIES AND GAS RELEASE EVENT DISTRIBUTIONS

This section presents a summary of the GRE history for the FGWL DSTs from 1995 through 1999. There were 5 recorded GREs in AN-103 during this period, 15 in AN-104, and 13 in AN-105. Tank 241-AW-101 experienced 19 events, and 20 were recorded in SY-103. No GREs have occurred in SY-101 since the mixer pump was installed in 1993. However, the large releases from that tank from 1989 through 1993 are summarized to put the GREs in the other tanks in perspective. Except in SY-101, all GREs listed and discussed in this section are identified and quantified solely by headspace hydrogen concentration measurements and not by surface level drops. In SY-101, the lack of good gas monitoring data made it necessary to use level drop data to quantify release volumes for most GREs. Tank 241-SY-101 is the only tank where level drops were sufficiently large to be used in this way.

Table 8-5 lists the total number of GREs recorded in AN-103, AN-104, AN-105, AW-101, and SY-103 since January 1, 1995, and includes the peak headspace hydrogen concentration and the estimated release volume. An estimate of the release volume for all GREs was obtained from the peak hydrogen concentration for the release, using the *Lower Bound Estimate* method described in Section 8.1.2. The peak concentration values in Table 8-5 are selected from the data ignoring abrupt spikes to represent a well-mixed headspace, and these values were used in the calculation of the release volume. For some events, the peak concentration value recorded in McCain (1999) represents a plume or spike, and the values in Table 8-5 are somewhat lower. In such cases, McCain's value is noted in parentheses.

For events where the release approximated the typical pattern of a relatively sharp peak followed by an exponential decay, an estimate of the release volume was also calculated using the hydrogen release model developed for cases where the ventilation rate is not known (see Section 8.1.2, *Hydrogen Release Model*). Since the ventilation rate is known approximately for these tanks (after installation of the constant flow controllers in 1996), the release volume was also calculated directly, by integrating the product of the measured hydrogen concentration and ventilation rate over the duration of the event (see Section 8.1.2, *Integrated Exhaust Hydrogen Concentration*). A ventilation rate of 100 scfm was assumed unless the hydrogen release model fit the data well, in which case the vent flow rate calculated with that model was used. These entries are marked with an asterisk (*).

The values in Table 8-5 show that the values estimated from the peak hydrogen concentration generally provide a lower bound for the release volume associated with a given event. For well-behaved events, where the release is large enough that the headspace is effectively fully mixed and the concentration decays exponentially following the release, the model predictions and the exhaust integration estimates are in good agreement. Not all GREs conform to the model, however, and for some events, the release model tends to over-estimate the release volume. In very abrupt releases where the headspace is not well-mixed during the GRE, the model may under-estimate the release volume.

In general, the GRE volumes appear to decrease over time as illustrated in Figure 8-10. Some tanks also appear to be experiencing a decreasing GRE frequency compared to prior years, while others show an increase. There is a distinct scarcity of GREs in 1996 and 1997, with activity picking up again in 1998. Some tanks had no events at all in 1996 or 1997, but experienced multiple events in 1995 and in 1998. There is considerable variation in the release volume and frequency from tank to tank, but the trend line through this data shows a steady downward slope. SY-103 is the exception and appears to generally maintain a consistent GRE behavior.

The relationship between GRE size and frequency is illustrated by a histogram of the events from 1995 through 1999, shown in Figure 8-11. For consistency in this comparison, the release volumes estimated from the product of peak hydrogen concentration and headspace volume (shown in Table 8-5) were used to obtain the histogram. The data is divided into bins based on GRE size, and the histogram shows that the larger events are less frequent than the smaller events. The most frequent release volume for an event is from 1 to 5 m^3, with frequency tapering off with increasing release volume. The basic shape of the histogram is maintained when the data is grouped separately for 1995 to 1996 and 1997 to 1999, although there is a clear shift to smaller GRE volumes, as shown in Figures 8-12 and 8-13.

Table 8-5. Gas Release Event Summary in Flammable Gas Watch List Double-Shell Tanks Since January 1, 1995 (3 Sheets)

GRE date	peak [H_2] (ppm)	Estimated Total Release Vol. (m^3)		
		Peak [H_2] *V_{HS}	Release model	Exhaust integration
AN-103				
08/22/95	1600	4.6	4.1	4.8*
04/11/98	960	2.7		
02/01/99	900	2.6	1.5	4.1
09/04/99	1260	3.6	3.4	10.7
12/29/99	530	1.5	5.6	2.8
AN-104				
02/16/95	2088	6.4	7.1	
08/03/95	480	1.5		
10/02/95	3200	9.7	11.4	11.0*
10/05/95	1000	3.0		
10/08/95	1820 (5000)	5.6	5.0	6.4
05/03/96	6109	18.7	20.2	22.2*
05/01/97	2250 (3183)	6.9	7.5	7.0*
08/25/98	310	0.9		
09/26/98	310	0.9		
12/02/98	550	1.7	1.7	2.0
04/26/99	75 (135)	0.2	0.2	0.2
06/01/99	78.4 (151)	0.3	NA	0.3
07/02/99	249	0.8	0.7	1.3
08/01/99	181	0.5	NA	0.7
09/04/99	155	0.5	NA	0.5
AN-105				
08/21/95	17000	28.9		
05/30/96	14500	24.6	35.3	25.7*
04/05/97	6980	11.8	18.6	20.4
09/25/97	950	1.6	1.5	1.4
11/22/97	1030	1.7		
12/31/97	3940	6.6		
09/02/98	2280	3.8	18.9	7.4
03/07/99	760	1.3	1.3	2.8
05/02/99	182	0.3	1.0	0.8
07/28/99	7100	12.0	19.1	19.1
08/02/99	4900 (7620)	8.2	30.9	19.2
10/27/99	180	0.3	1.8	0.9
12/31/99	186	0.3	1.3	0.8

(xxxx) -- spike or plume peak [H_2] values from McCain (1999)

* Values adjusted to the vent flow calculated by the release model

Table 8.5. Gas Release Event Summary in Flammable Gas Watch List Double-Shell Tanks Since January 1, 1995 (3 Sheets)

GRE date	peak [H_2] (ppm)	Estimated Total Release Vol. (m^3)		
		Peak [H_2] *V_{HS}	Release model	Exhaust integration
AW-101				
02/22/95	4600	14.7	21.3	19.6*
05/08/95	1800	5.7	18.1	17.1*
05/17/95	1000	3.2		
07/08/95	2000	6.4		
07/12/95	900	2.9		
08/02/95	3300	10.5		
09/15/95	1930	6.2	24.9	23.1*
09/22/95	4660	14.9		
10/16/95	1750	5.6	8.5	6.6*
12/12/95	2110	6.7		
12/29/95	6000	19.2	27.7	22.9*
01/13/96	1170	3.7		
01/25/96	1830	5.8		
02/05/96	3200	10.2		
02/14/96	940	3.0		
05/14/96	1393	4.3	12.7	11.2
06/05/96	2511	8.0	16.7	14.3
04/21/98	398	1.3		
06/24/98	450	1.4		
07/04/98	480	1.5		
SY-101				(a)
4/19/90	35000	120		197
8/5/90	12000	41		114
10/24/90	47000	162		219
2/16/91	-			92
5/16/91	28000	96	168	153
8/27/91	-			126
12/4/91	53000	182		263
4/20/92	14800	51	145	131
9/3/92	51200	176		214
2/2/93	27400	94		197
6/26/93	34000	117	209	214

(a) SY-101 release volumes in this column computed from waste level drops

(xxxx) -- spike or plume peak [H_2] values from McCain (1999)

* Values adjusted to the vent flow calculated by the release model

Table 8.5. Gas Release Event Summary in Flammable Gas Watch List Double-Shell Tanks Since January 1, 1995 (3 Sheets)

GRE date	peak [H_2] (ppm)	Estimated Total Release Vol. (m^3)		
		Peak [H_2] *V_{HS}	Release model	Exhaust integration
SY-103				
01/22/95	1090	4.4	6.3	5.4*
03/01/95	2230	9.1	11.1	9.3*
05/02/95	1430 (2940)	5.8	6.1	5.5*
08/23/95	1260	5.1	4.6	5.6
09/06/95	1890	7.7	10.0	8.8
12/03/95	740	3.0		
06/06/96	1090	4.4	6.2	5.2*
07/14/96	2170	8.8	28.4	16.4*
12/20/96	5110	20.8	26.6	27.0*
11/27/97	1990 (2660)	10.8	11.7	13.2*
12/07/97	2060	8.4		
08/15/98	1660	6.7		
10/23/98	100 (1140)	0.4	1.7	0.6
12/25/98	2854 (3160)	11.7	23.2	16.3
01/10/99	690	2.8		
03/09/99	570	2.3		
05/30/99	950	3.9		
10/26/99	1020	4.1		
11/26/99	600	2.4		
12/02/99	570	2.3		

(xxxx) -- spike or plume peak [H_2] values from McCain (1999)

* Values adjusted to the vent flow calculated by the release model

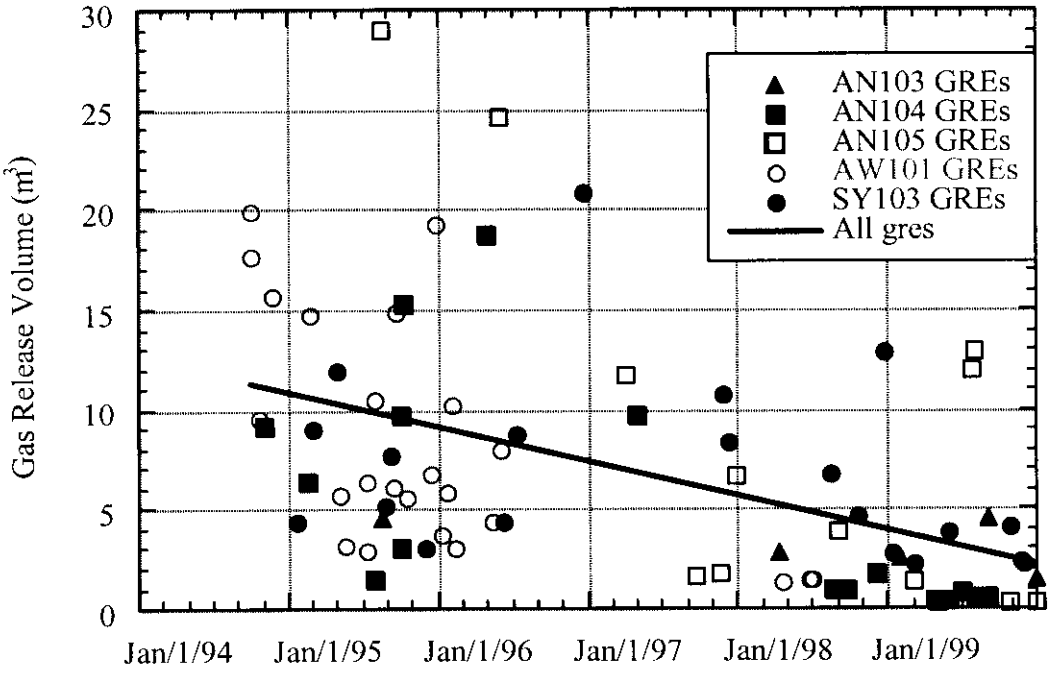

Figure 8-10. Gas Release Event Release Volume Over Time

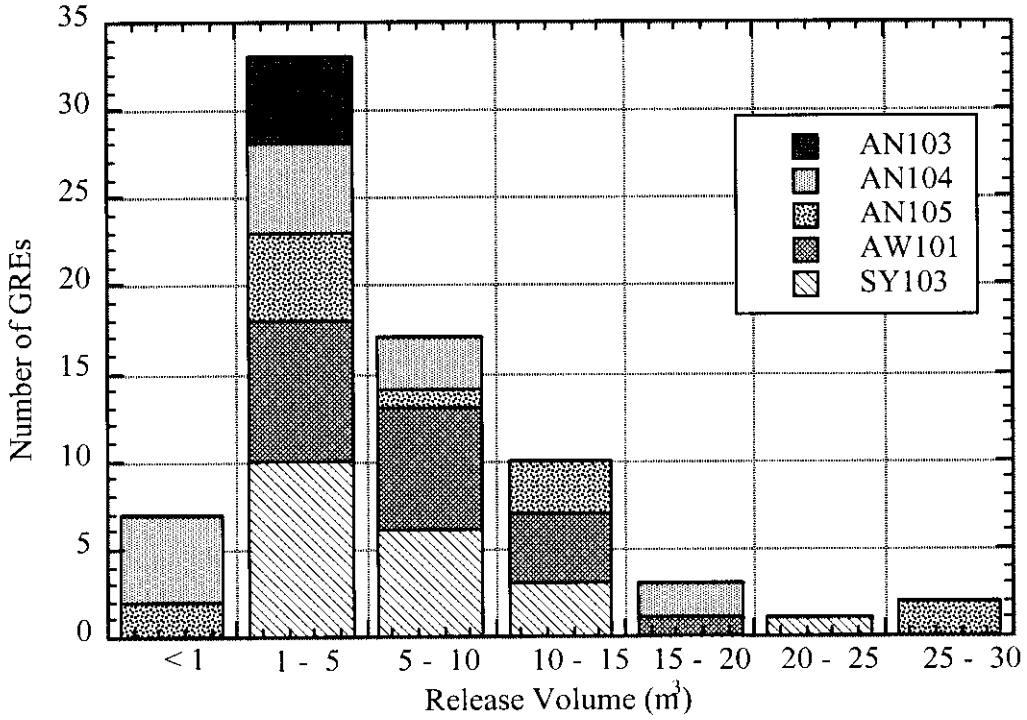

Figure 8-11. Histogram of Release Volume for Gas Release Events from 1995 to 1999

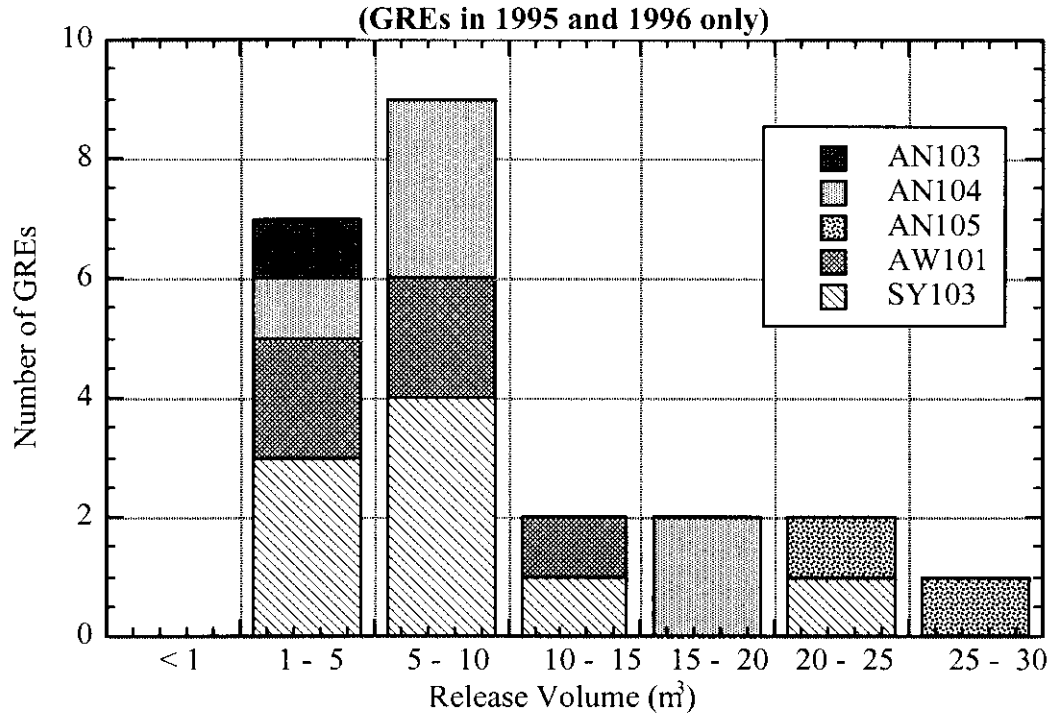

Figure 8-12. Histogram of Release Volume for Gas Release Events from 1995 to 1996

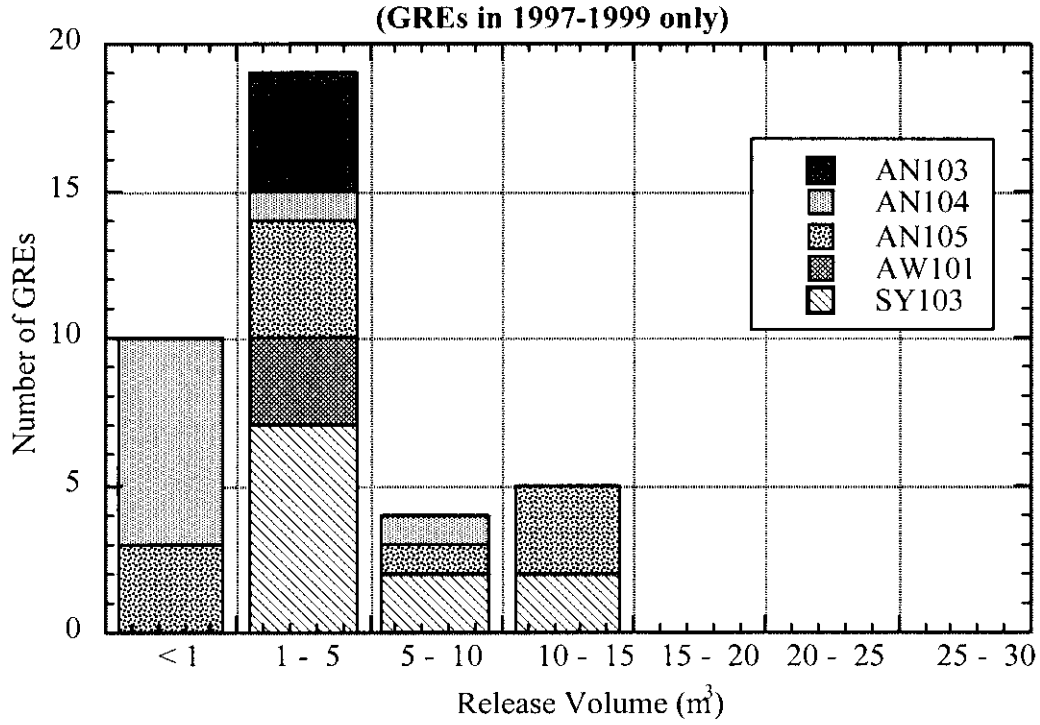

Figure 8-13. Histogram of Release Volume for Gas Release Events from 1997 to 1999

The unity of the overall pattern is particularly significant, since the tanks have very different GRE histories. This is evidence that the events are caused by the same physical processes, and the differences between tanks are due mainly to differences in waste properties and configuration. Table 8-6 summarizes the GRE count and range of sizes (computed as the product of peak [H_2] and headspace volume) for each tank. Relevant details on the individual behavior of the tanks are discussed in the following subsections.

Table 8-6. Gas Release Event Count and Average Gas Release Volume per Tank

Tank	GRE Count	Average Gas Release Volume (m^3)	Minimum Gas Release Volume (m^3)	Maximum Gas Release Volume (m^3)
AW-101	20	6.8	1.3	19.2
SY-103	20	6.8	2.3	20.8
AN-103	5	3.2	1.5	4.6
AN-104	15	4.7	0.4	18.7
AN-105	13	8.2	0.3	28.9

8.4.1 Gas Release History in Tank 241-AN-103

Only five events have been observed in AN-103 during the five-year period; one in 1995, one in 1998, and three in 1999. Despite the unequal intervals between the events, the estimated gas release volume was in each case very nearly the same and there are too few events to show a clear trend.

The general shape of the hydrogen concentration profiles for the events in this tank, shown in Figure 8-14, indicates that all of these events are quite similar. They consist of a sudden sharp increase in headspace hydrogen, followed by a slightly more gradual decrease back to the background release level. This suggests that the release is a sudden relatively rapid event, rather than a sustained release. Therefore, the method of estimating the total release from the peak concentration and ventilation rate should give a reasonable estimate of the total release volume for an event.

Five data points is a rather feeble reed on which to hang an interpretation of GRE behavior in this tank, which is unique among the other FGWL DSTs. The waste level and temperature histories of this tank suggest that its gas content and waste configuration have been quite stable over the five-year period (see Section 5.5.1). However, it also has an average void fraction close to neutral buoyancy. This suggests that the tank could either remain in the same configuration indefinitely, experiencing infrequent small GREs at irregular intervals, or that a very large release could eventually occur. Monitoring of this tank should give particular attention to any indication of changes in the void profile or gas volume.

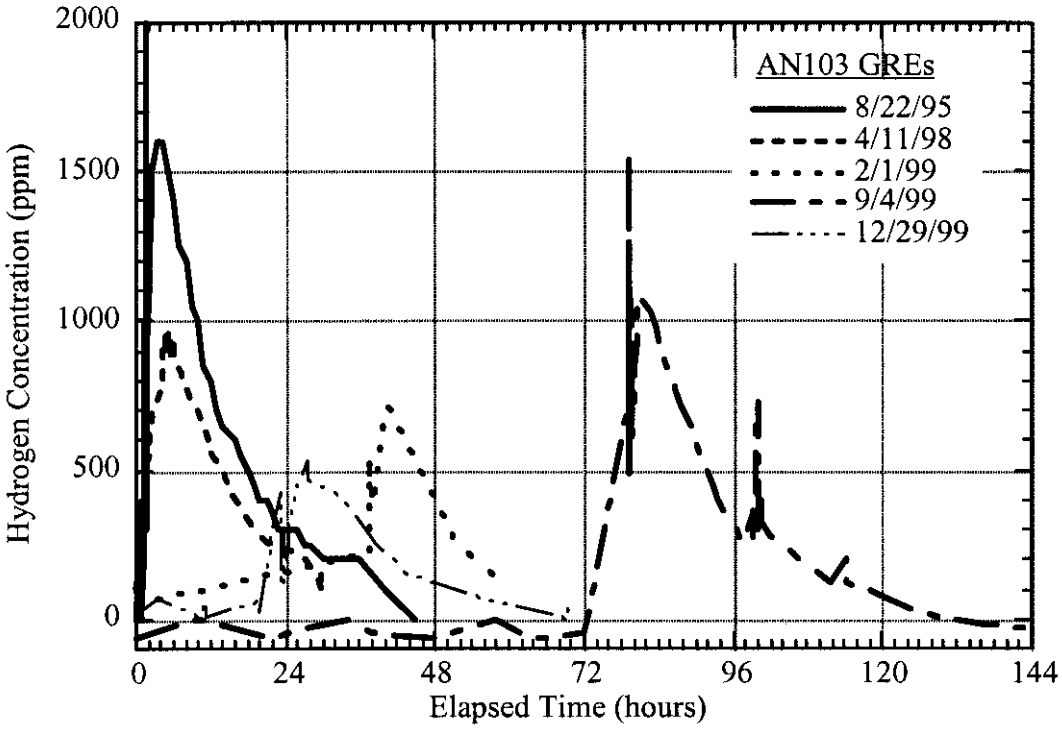

Figure 8-14. Hydrogen Concentration Profiles for Gas Release Events in Tank 241-AN-103

8.4.2 Gas Release History in Tank 241-AN-104

A total of 15 GREs have been observed in AN-104 since January 1, 1995, and the character of the events show some interesting changes during the interval. Figure 8-15 shows the GREs over time in this tank. A decreasing trend line is defined by a linear curve fit to the data. (Note that the approach to zero is an artifact of the linear fit.) Figure 8-16 illustrates the changing character of the GREs in this tank, showing a representative sample of events over the five-year interval. Prior to 1998, the events show a sharp peak, followed by an exponential decay. The events in 1999 have much lower peaks, and a much more gradual decay. This is shown more clearly by the plot for GREs in 1999 only, in Figure 8-17.

Five events were observed in this tank in 1995, ranging from small (3.1 m^3) to moderately large (15.2 m^3). Only one relatively large release (18.6 m^3) was observed in 1996. This single release was about half the total volume of all releases in the previous year. There was only one GRE observed in 1997, as well, (9.7 m^3); this one was smaller than the 1996 release, and also somewhat smaller than the largest release in 1995. The number of GREs observed in 1998 increased to three, but the release volumes were quite small, (0.9 to 1.6 m^3). In 1999, the number of GREs increased to six, but the volume of each release was even smaller (0.4 to 0.8 m^3), so that the total release for the six events in 1999 was less than that for the three events in 1998.

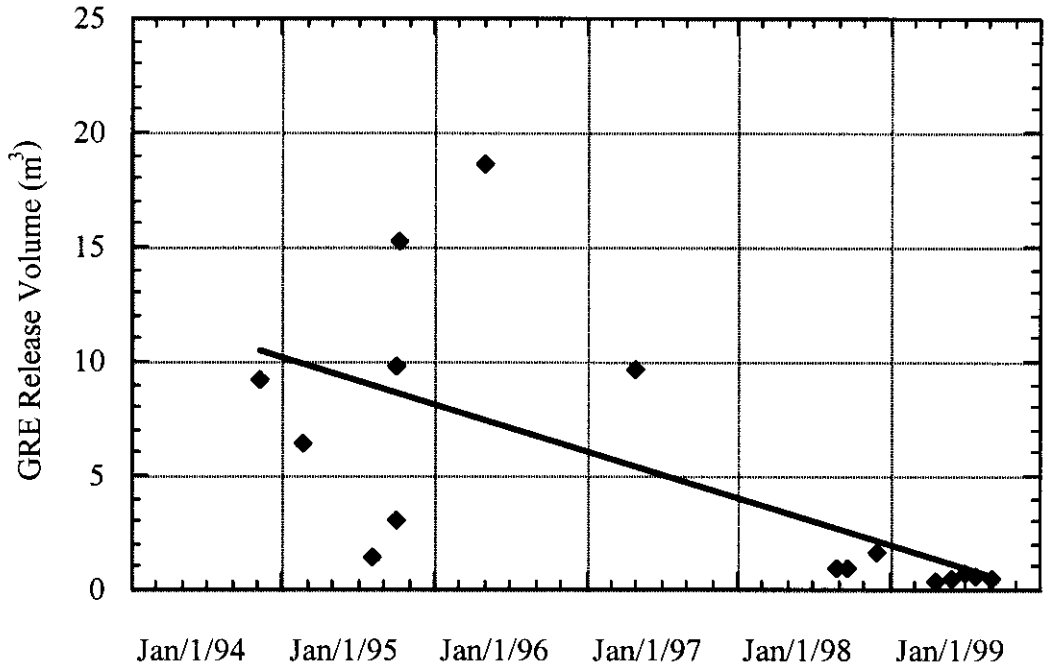

Figure 8-15. Gas Release Volume History for Tank 241-AN-104

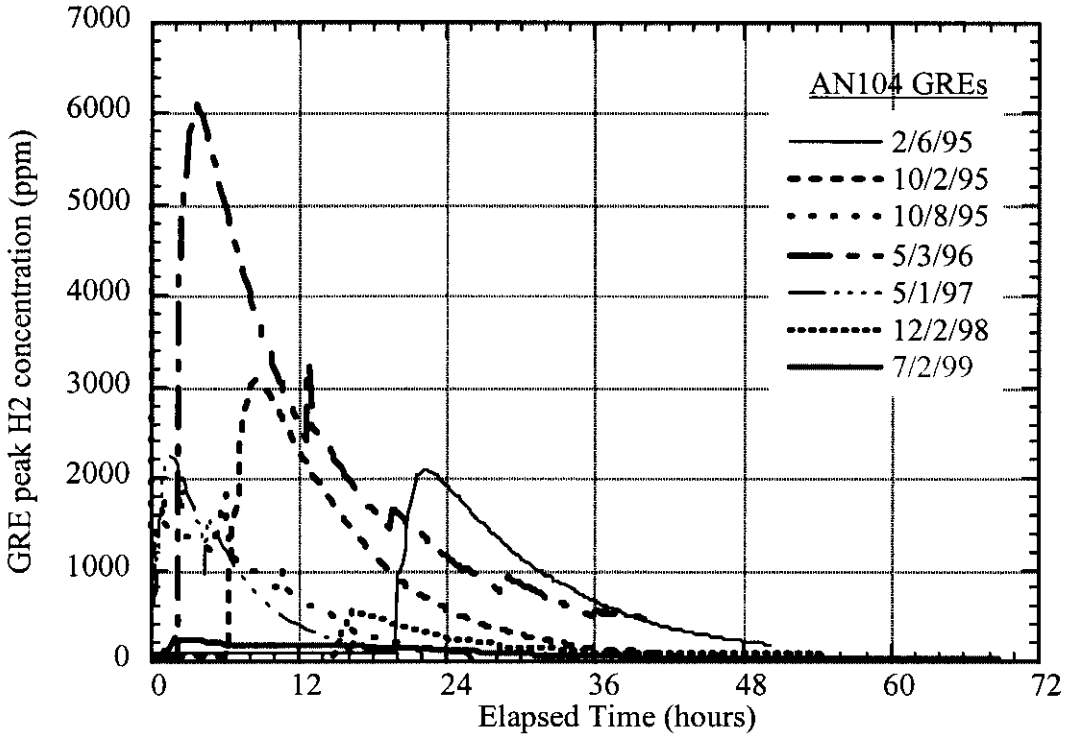

Figure 8-16. Representative Gas Release Events from 1995 to 1999 for Tank 241-AN-104

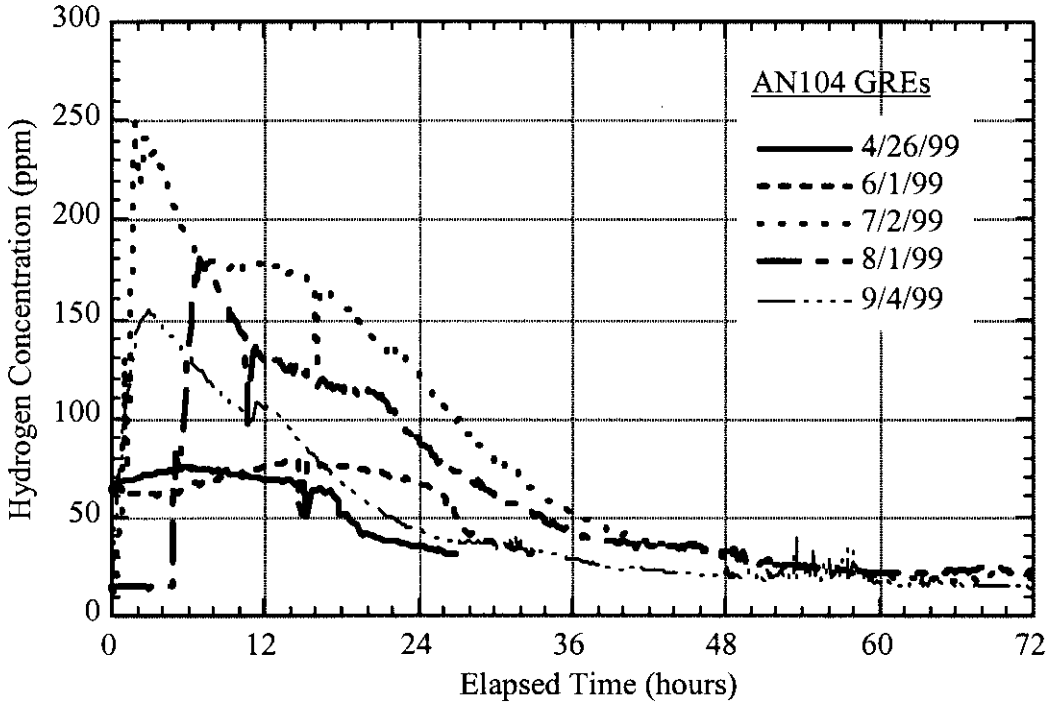

Figure 8-17. Gas Release Events in 1999 for Tank 241-AN-104

The total gas release volume from GREs in this tank has decreased remarkably over the past five years, from 35.8 m^3 in 1995, to 18.7 m^3 in 1996, to 9.7 m^3 in 1997, to 3.5 m^3 in 1998, to 2.6 m^3 in 1999. However, there is no evidence of gas accumulation in the waste (see the discussion in Section 5.5.2), nor has there been any significant increase in the background release rate for this tank. The available evidence suggests that the retained gas volume is not increasing in this tank, and the decreased volume of released gas represents a decrease in the gas generation in the tank due to a significant reduction in waste temperature.

8.4.3 Gas Release History in Tank 241-AN-105

A total of 13 GREs have been observed in AN-105 since January 1, 1995. Figure 8-18 shows the GREs in this tank over the five-year period, with a linear curve fit to the data. The release volume per event shows a steady decrease. (Note that the approach to zero is an artifact of the linear curve fit.) The events in this tank show a general trend of decreasing gas release volume for the individual GREs over time, but the frequency appears to be increasing. As a result, the total gas release volume per year has remained fairly constant over this period, at 28 m^3 in 1995, 25 m^3 in 1996, 22 m^3 in 1997 and 27 m^3 in 1999. (The one exception is in 1998, with a single small release totaling only about 3.8 m^3, but this appears to be mainly an artifact of imposing regular time divisions on the irregular intervals between events.)

Figures 8-19 and 8-20 of the gas concentration profiles during the GREs in AN-105 show that the character of the larger releases is markedly different from the smaller ones. The larger

releases in 1996 through 1999 show relatively sharp peak hydrogen concentrations, followed by an exponential decay. The smaller ones in 1999 have relatively mild peaks, with a very gradual rise and fall before and after the event.

8.4.4 Gas Release History in Tank 241-AW-101

A total of 20 GREs have been observed in AW-101 over the interval from 1995 through 1999. These events show a very marked change in distribution over time, as shown by the plot in Figure 8-21. Over half of the events (11 of the 20) occurred in 1995, only six occurred in 1996; there were no events at all in 1997, and only three small events in 1998. No events were recorded in 1999, although a relatively large event (on the order of 2082-ppm peak hydrogen concentration, with a release volume estimated at about 6.6 m^3) occurred on April 22, 2000.

A trend line interpolated for the data shows a gradual decrease in release volume per GRE over time. The total release due to GREs was approximately 96.1 m^3 in 1995. It decreased by more than half, to about 35.2 m^3 in 1996, and has been very close to zero since then, except for the three small releases (totaling about 4.2 m^3) in 1998, and the single release of approximately 6.6 m^3 in April 2000.

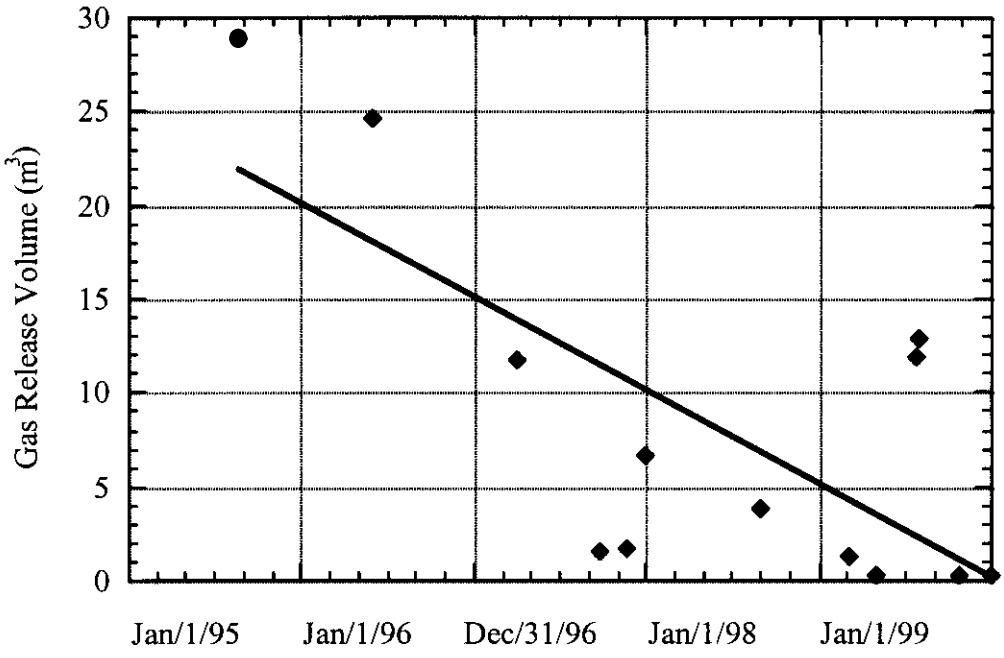

Figure 8-18. Gas Release Volume History for Tank 241-AN-105

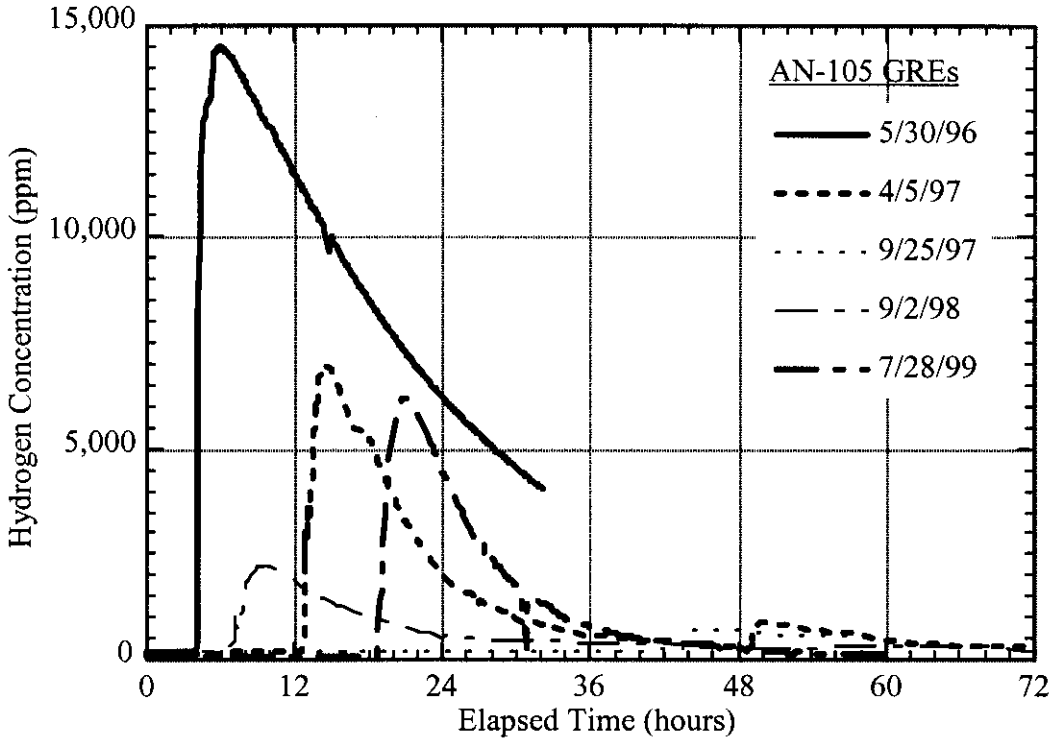

Figure 8-19. Hydrogen Concentration Profiles for Tank 241-AN-105 Gas Release Events in 1996 through 1998

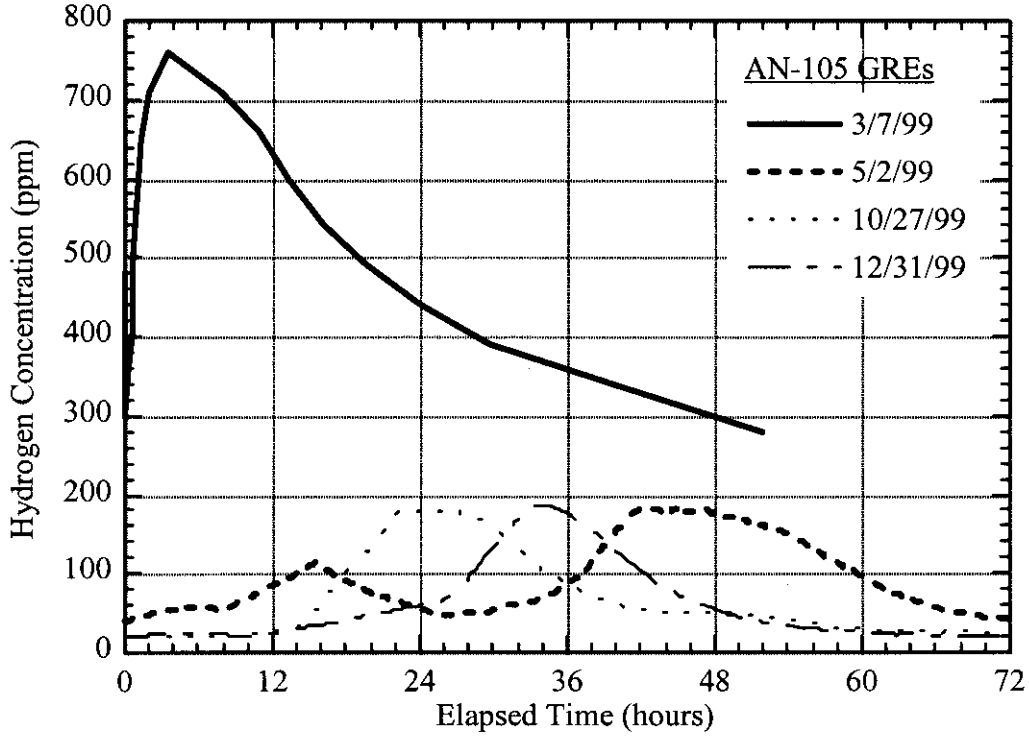

Figure 8-20. Hydrogen Concentration Profiles for Tank 241-AN-105 Gas Release Events in 1999

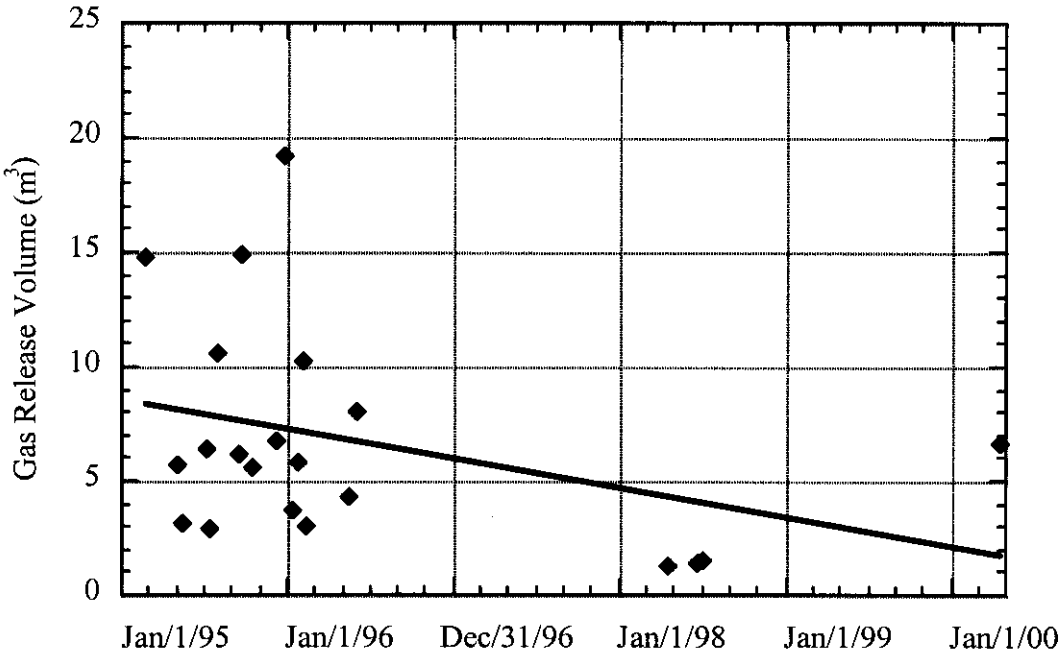

Figure 8-21. Gas Release Volume History for Tank 241-AW-101

Figure 8-22 illustrates the decreasing magnitude of the release events over time, showing the rise and fall of the headspace hydrogen concentration during representative GREs that occurred during the five-year period. This behavior, in conjunction with the evidence from temperature and level histories for the tank (refer to Section 5.5.4), suggests that gas retention is increasing in the waste. This may be in the form of a thickening bubble slurry layer below the crust, which is indicated by evidence from changes in the tank temperature profiles.

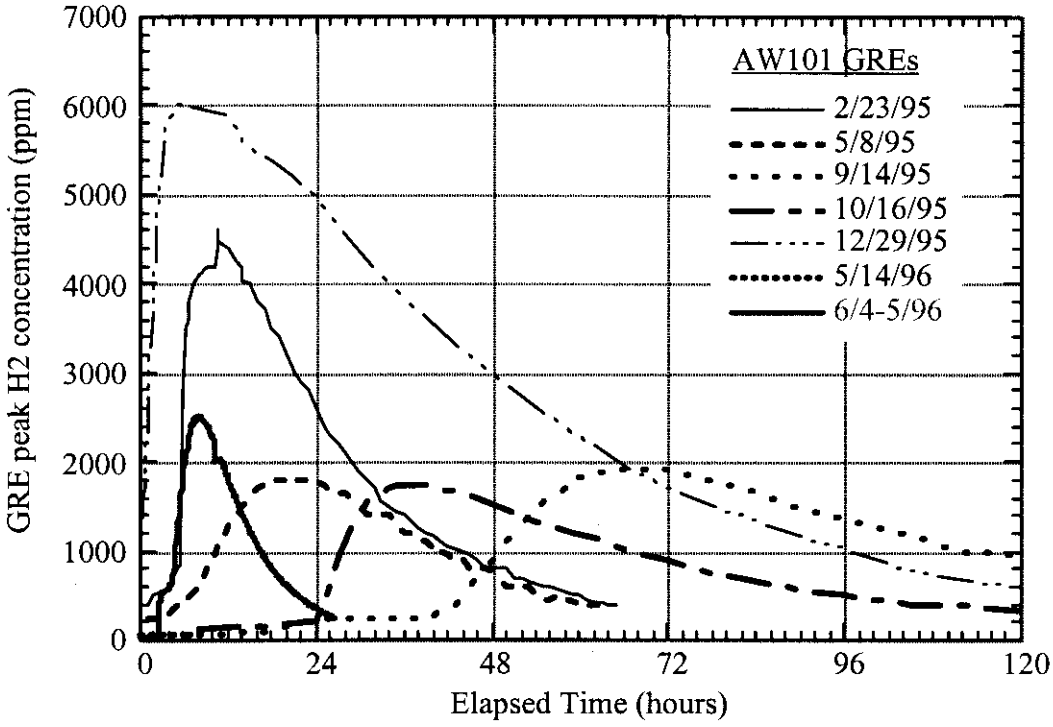

Figure 8-22. Representative Gas Release Events from 1995 through 1999 for Tank 241-AW-101

8.4.5 Gas Release History in Tank 241-SY-101

Gas release volumes are available for the events on May 16, 1991, August 27, 1991, and April 20, 1992 were determined from the Whittaker™ hydrogen monitoring system (Erhart 1991 and 1992; Wilkins 1992). The gas release volume for the event on June 26, 1993, was determined by integrating the GC hydrogen data (not available for prior events). The gas was assumed to be stored in the waste at 2.1 atm, and the hydrogen fraction of the released gas was assumed to be 0.3. The resulting computed waste level drops, together with the measured waste level drops from McCain (1999), are presented in Table 8-7. Re-examination of the level drops as determined by the auto FIC, manual FIC, manual tape, and manual radar is also given in the table as "New."

Given the uncertainties in the level data as exemplified by the glaring disparities between different level instruments, and the subjectivity in interpreting the data, the level drops determined by McCain (1999) and those labeled "New" in the table compare reasonably well with each other and with the level drops derived from gas monitoring data except for the events on September 3, 1992, and June 26, 1993. The manual radar during the event on September 3, 1992 shows extreme (4 in.) swings, and is, therefore, considered unsuitable. The three active waste level instruments for the June 26, 1993 event, the manual FIC, manual radar, and manual tape, tracked closely (level varied by 1.5 in between instruments) for the 26 days preceding the event. The manual radar and manual tape registered the same level change during the event and

correspond more closely to the drop calculated from the gas release. This suggests that the manual radar or the manual tape data are the best for representing this event.

The level drop derived from the lower bound gas release, which is computed as the product of the maximum hydrogen concentration (as given in McCain [1999]) and the headspace volume, corresponds closely with the prompt (< 24 hours) level drop for the majority of the events. This result is not surprising as the gas release signatures are typically a fairly abrupt peak followed by an exponential decay to the baseline release that continues longer than the time required for ventilation to clear the headspace. Additionally, the waste level usually does not reach its minimum until a few days after the event. This total level drop corresponds more closely to the total gas release computed by integrating the product of headspace concentration and vent rate. Also, this method is consistent with the integration method used for computing gas release volumes in the other DSTs.

In light of these factors, the difference in the waste level immediately prior to a GRE and the minimum afterwards probably best represents the total gas release. However, the prompt level drop (<24 hours) better represents the peak headspace concentration. The result of applying the level drops in the "New" column of Table 8-7 are shown in Table 8-8. The average historical gas release computed from Events E-I is 204 m^3.

8.4.6 Gas Release History in Tank 241-SY-103

A total of 20 GREs have been observed in SY-103 over the interval from 1995 through 1999. These events show an essentially constant distribution over time, as shown by the plot in Figure 8-23. A trend line through the data shows a very slight decrease in gas release volume per GRE. The number of GREs in any one year varied from 2 to 6, but the events display no clear trend of increasing or decreasing in frequency.

There appears to have been a slight decrease in the total GRE release volume per year over this five-year interval. The total release due to GREs was about 41.3 m^3 in 1995, 34.1 m^3 in 1996, 19.2 m^3 in 1997, 24.2 m^3 in 1998, and 17.9 m^3 in 1999. Figure 8-24 shows the hydrogen concentration profiles for a number of GREs in this tank over the five-year period. This plot shows that the character of the release varies somewhat from event-to-event, with some showing the typical sharp peak followed by an exponential decay, others peaking sharply but with a sustained high release rate followed by a gradual decay.

The waste temperature and level histories for SY-103 show considerable disturbance of the waste due to GREs (refer to Section 5.5.6). The level generally shows a distinct drop when the release occurs. The nonconvective layer also shows changes in height that can be attributed to the accumulation and release of gas. Unlike the behavior in other tanks, there is a definite relationship between gas release volume and the size of the level drop for a given GRE in SY-103.

Table 8-7. Waste Level Drop from Gas Release Events in Tank 241-SY-101

Date	Drop due to Gas Release (cm)	McCain (1999) Level Drop (cm)*	Drop from max. ppm (cm)	Initial Drop (cm)	New (cm)
4/19/90		23.6 [auto FIC]	15.4	15.2 [auto FIC]	22.9 [auto FIC]
8/5/90		13.2 [auto FIC]	5.2	10.2 [auto FIC]	13.2 [auto FIC]
10/24/90		25.4 [auto FIC]	21.0	22.1 [auto FIC]	25.4 [auto FIC]
2/16/91		12.7 [man. tape]	0.2	10.2 [man. FIC]	10.7 [man. FIC]
5/16/91	19.5	18.3 [auto FIC]	12.3	11.2 [auto FIC]	17.8 [auto FIC]
8/27/91	7.3	15.2 [man. tape/radar]	1.6	12.1 [man. tape]	14.6 [man. tape]
12/4/91		33 [?]	23.8	25.4 [man. tape]	30.5 [man. tape]
4/20/92	16.8	18.3 [man. radar]	6.4	10.2 [man. tape]	15.2 [man. tape]
9/3/92		33.5 [man. radar]	23.0	20.3 [man. FIC]	24.8 [man. FIC]
2/2/93		21.6 [man tape]	12.0	17.8 [man. tape]	22.9 [man. tape]
6/26/93	24.3	24.8 [man tape/radar]	15.0	15.2 [man. FIC]	24.8 [man. tape/radar]

Note: *source of measurement inferred by comparison to the data.

Table 8-8. Revised Gas Release Calculations

Event	Date	Peak [H_2] (ppm)	Level drop (cm)	Estimated Gas Release (m^3)		
				From Level Drop	Peak [H_2] *V_{HS}	Release model
	4/19/90	35000	22.9	197	120	
	8/5/90	12000	13.2	114	41	
A	10/24/90	47000	25.4	219	162	
B	2/16/91	-	10.7	92		
C	5/16/91	28000	17.8	153	96	168
D	8/27/91	-	14.6	126		
E	12/4/91	53000	30.5	263	182	
F	4/20/92	14800	15.2	131	51	145
G	9/3/92	51200	24.8	214	176	
H	2/2/93	27400	22.9	197	94	
I	6/26/93	34000	24.8	214	117	209

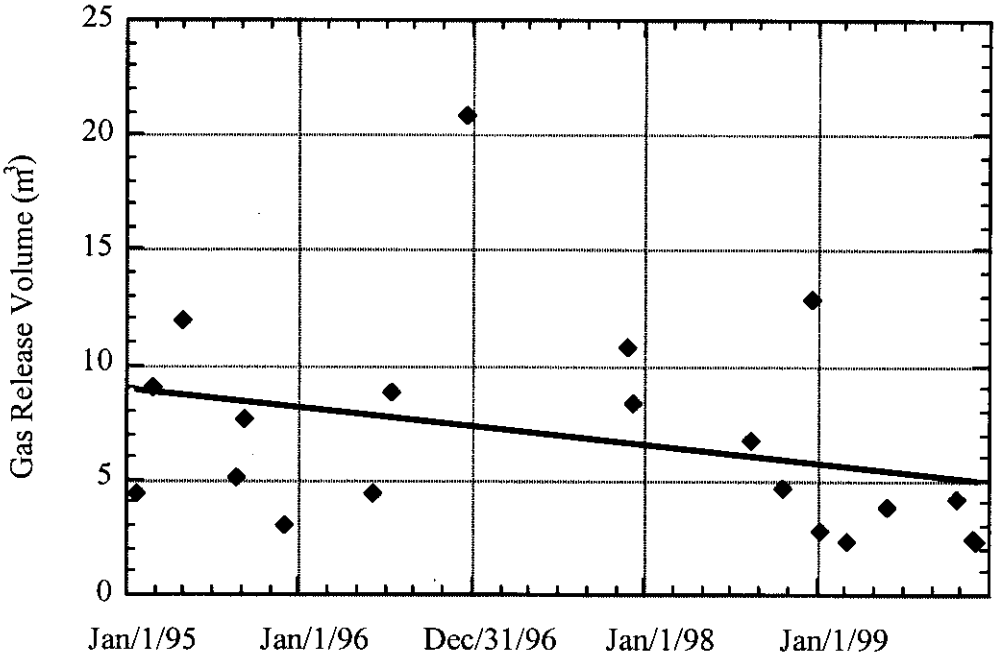

Figure 8-23. Gas Release Volume History for Tank 241-SY-103

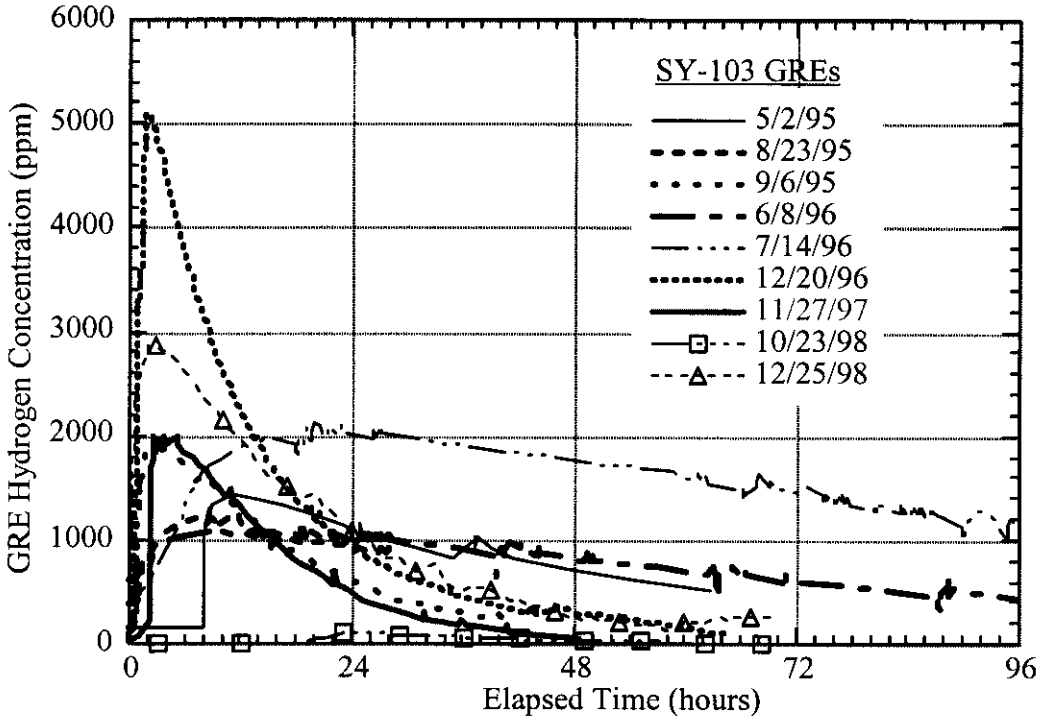

Figure 8-24. Representative Gas Release Events from 1995 through1999 for Tank 241-SY-103

This page intentionally left blank.

9.0 OVERALL SUMMARY AND CONCLUSIONS

Considering the preponderance of evidence from the data and analysis results presented in the preceding sections, the general condition of the five Facility Group 1 tanks can be summarized as follows:

- The waste configurations have not changed significantly since 1995 although AW-101 and AN-103 show a potential for future crust growth.
- The retained gas volume has decreased from a few percent (AW-101) to as much as 30% (AN-104) since 1995.
- The gas generation rate has decreased significantly since 1995 in four of the tanks (AN-103, AN-104, AN-105, and AW-101) consistent with a concurrent waste temperature decrease resulting from increased annulus and primary ventilation flows.
- Gas releases have become much smaller since 1995 in four of the tanks (AN-103, AN-104, AN-105, and AW-101) consistent with the decreased gas generation rate and waste temperature. SY-103 waste temperatures remained relatively constant and its gas release behavior has not changed significantly.
- The changes in gas generation, retention, and release behavior is generally consistent with our current understanding of the mechanisms involved.

Besides continuous monitoring of waste level and temperature, specific in-situ measurements have been performed to understand the properties of the waste. The ball rheometer and VFI were run in all five tanks plus SY-101 which revealed the yield stress profile, precise measurement of the nonconvective layer depth, and void fraction profile. The RGS was used in all of the tanks except SY-103, which provided a direct measurement of retained gas composition and the dissolved ammonia concentration. Laboratory gas generation tests were performed on SY-101, SY-103, AN-105, and AW-101 wastes from core samples, and gas retention tests were run on waste samples from SY-101, SY-103, AW-101, and AN-103. Recently, each tank has been logged with a small-bore neutron/gamma probe to confirm the waste configuration. Finally, the headspace hydrogen concentration has been continuously monitored in each tank from which the gas release volume and frequency has been determined. While none of these data sets are perfect or complete, the sum of the available information taken together forms a sound basis for understanding and predicting the waste behavior.

The most significant development in these tanks over the past five years has been a decrease in average waste temperature caused by increased headspace ventilation flow. The temperature change ranges from about 10 °F in AN-104 to possibly 2 °F in SY-103. Temperatures appear to have become more-or-less steady under the 2 to 4 °F seasonal variations during 1999. The gas generation rate has also decreased significantly since it is very sensitive to temperature. The waste level has remained constant or decreased slightly during this period. This indicates that no additional gas is being retained. The temperature profiles and neutron/gamma logs show the thickness of the crust and nonconvective layers have changed little, if at all, except in AN-103 and AW-101. In these tanks the crust appears to be in the process of becoming abruptly and

significantly thicker with some decrease in the depth of the nonconvective layer. Except in SY-103, the gas release volumes have also decreased significantly consistent with the reduced temperature and gas generation rate. While the current release frequency is now roughly the same as in 1995, there was a two-year hiatus in 1996-1997 during which far fewer GREs occurred in each tank except SY-103. In all cases the GREs have continued to be very local events with no effect on the tank-wide waste configuration.

This set of inter-related changes in tank conditions is consistent with and tends to validate our understanding of the gas generation, retention and release processes. The temperature change is a direct result of installation of inlet-flow controllers and bringing both annulus ventilation fans on line in the AN and AW farms. This increased the headspace vent flow to a nominal 100 scfm and doubled the annulus flow to about 200 scfm. The gas generation rate decreased significantly with the temperature, roughly in the same proportion as predicted by Hu's (2000) semi-empirical model. The decrease in GRE volume is consistent with the decrease in generation rate since the net gas retention or release rate is postulated to depend on the gas generation rate.

Based on these observations and the data on which they are based, the following conclusions can be made on the current and future state of the Facility Group 1 tanks:

- Three of the five tanks (AN-103, AN-104, and AN-105) contain more than enough flammable gas to make the headspace flammable if all of it were suddenly released. Since only a violent disturbance of the entire waste volume could create such a total release, this retained gas does not present an immediate hazard. However, future retrieval operations need to be planned carefully.
- Spontaneous gas releases are random (can be expected at any time) but are small and do not create a flammability hazard.
- The tanks do not present a serious flammable gas hazard, no new hazards have been identified in the data, and the observed trends are of decreasing hazard.

10.0 REFERENCES

Allemann, R. T., T. M. Burke, D. A. Reynolds, and D. E. Simpson, 1993, *Assessment of Gas Accumulation and Retention - Tank 241-SY-101*, WHC-EP-0576, Rev. 0, Westinghouse Hanford Company, Richland, Washington.

Allemann, R. T., Z. I. Antoniak, W. D. Chvala, L. E. Efferding, J. G. Fadeff, J. R. Friley, W. B. Gregory, J. D. Hudson, J. J. Irwin, N. W. Kirch, T. E. Michener, F. E. Panisko, C. W. Stewart, and B. M. Wise, 1994, *Mitigation of Tank 241-SY-101 by Pump Mixing: Results of Testing Phases A and B,* PNL-9423, Pacific Northwest Laboratory, Richland, Washington.

Antoniak, Z. I., 1993, *Historical Trends in Tank 241-SY-101 Waste Temperatures and Levels*, PNL-8880, Pacific Northwest Laboratory, Richland, Washington.

Ashby, E. C., A. Annis, E. K. Barefield, D. Boatright, R. Doctorovich, C. L. Liotta, H. M. Neumann, C. F. Yao, K. Zhang, and N. F. McDuffie, 1994, *Synthetic Waste Chemical Mechanism Studies*, WHC-EP-0823, Westinghouse Hanford Company, Richland, Washington.

Babad, H., J. L. Deichman, B. M. Johnson, D. K. Lemon, and D. M. Strachan, 1992, *Mitigation/Remediation Concepts for Hanford Site Flammable Gas Generating Waste Tanks*, WHC-EP-0516, Westinghouse Hanford Company, Richland, Washington.

Baldwin, J. H., L. C. Amato, and T. T. Tran, 1995, *Tank Characterization Report for Double-Shell Tank 241-AW-101*, WHC-SD-WM-ER-470, Westinghouse Hanford Company, Richland, Washington.

Barefield, E. K., D. Boatright, A. Desphande, R. Doctorovich, C. L. Liotta, H. M. Neumann, and S. Seymore, 1996, *Mechanisms of Gas Generation from Simulated SY Tank Farm Wastes: FY 1995 Progress Report*, PNL-11247, Pacific Northwest National Laboratory, Richland, Washington.

Barker, S. A., W. B. Barton, D. R. Bratzel, M. Epstein, P. A. Gauglitz, G. D. Johnson, S. N. Maruvada, C. E. Olson, M. L. Sauer, S. E. Slezak, C. W. Stewart, and J. Young, 1999, *Flammable Gas Safety Analysis Review,* SNL-000198, Sandia National Laboratory, Albuquerque, New Mexico.

Bredt, P. R., S. M. Tingey, and E. H. Shade, 1995, *The Effect of Dilution on the Gas Retention Behavior of Tank 241-SY-101*, PNL-10781, Pacific Northwest National Laboratory, Richland, Washington.

Bredt, P. R., and S. M. Tingey, 1996, *The Effect of Dilution on the Gas Retention Behavior of Tank 241-SY-103 Waste*, PNL-10893, Pacific Northwest National Laboratory, Richland, Washington.

Brewster, M. E., N. B. Gallagher, J. D. Hudson, and C. W. Stewart, 1995, *The Behavior, Quantity, and Location of Undissolved Gas in Tank 241-SY-101*, PNL-10681, Pacific Northwest Laboratory, Richland, Washington.

Bryan, S. A., and C. M. King, 1998, *Thermal and Radiolytic Gas Generation From Tank 241-AW-101 Waste: Status Report,* TWRS98.39, Pacific Northwest National Laboratory, Richland, Washington.

Bryan, S. A., and L. R. Pederson, 1996, *Thermal and Combined Thermal and Radiolytic Reactions Involving Nitrous Oxide, Hydrogen, Nitrogen, and Ammonia in the Gas Phase*, PNNL-10748, Pacific Northwest Laboratory, Richland, Washington.

Bryan, S. A., C. M. King, L. R. Pederson, S. V. Forbes, and R. L. Sell, 1996, *Gas Generation from Tank 241-SY-103 Waste*, PNNL-10978, Pacific Northwest National Laboratory, Richland, WA.

Camaioni, D. M., W. D. Samuels, S. A. Clauss, B. D. Lenihan, K. L. Wahl, J. A. Campbell, and W. J. Sahw, 1995, *FY95 Waste Aging Studies*, PNL-10794, Pacific Northwest National Laboratory, Richland, Washington.

Camaioni, D. M., W. D. Samuels, S. A. Clauss, B. D. Lenihan, K. L. Wahl, J. A. Campbell, and W. J. Sahw, 1996, *FY96 Waste Aging Studies*, PNL-11312, Pacific Northwest National Laboratory, Richland, Washington.

Cannon, N. S., 1996, *Retained Gas Sampler System Acceptance Test Report*, WHC-SD-WM-ATR-137, Rev. 1, Westinghouse Hanford Company, Richland, Washington.

Cannon, N. S., and R. C. Knight, 1995, *Retained Gas Sampler System Acceptance Test Report*, WHC-SD-WM-ATR-137, Westinghouse Hanford Company, Richland, Washington.

CHG, 2000, Tank Characterization Database, Internet at http://twins.pnl.gov:8001/TCD/main.html.

Conner, J. M., 2000a, *Inventory for Selected Constituents in Tank 241-SY-101 Waste Prior to December 1999 Transfers*, (Internal memorandum 74B50-00-061 to C. E. Anderson and W. B. Barton, June 19), CH2M HILL Hanford Group, Inc., Richland, Washington.

Conner, J. M., 2000b, *Quarterly Review of 241-SY-101 Data: January – March, 2000,* RPP-6332, CH2M HILL Hanford Group, Inc., Richland, Washington.

Conner, J. M., and G. M. Koreski, 1998, *Quarterly Review of 241-SY-101 Data: October - December, 1998*, HNF-4039, Rev. 0, Lockheed Martin Hanford Corp., Richland, Washington.

Conner, J. M., and G. M. Koreski, 1999a, *Quarterly Review of 241-SY-101 Data: January - March, 1999*, HNF-4511, Rev. 0, Lockheed Martin Hanford Corp., Richland, Washington.

Conner, J. M., and G. M. Koreski, 1999b, *Quarterly Review of 241-SY-101 Data: April - June, 1999*, HNF-5029, Rev. 0, Lockheed Martin Hanford Corp., Richland, Washington.

Conner, J. M., and G. M. Koreski, 1999c, *Quarterly Review of 241-SY-101 Data: July - September, 1999*, HNF-5265, Rev. 0, Lockheed Martin Hanford Corp., Richland, Washington.

Conner, J. M., and G. M. Koreski, 1999d, *Quarterly Review of 241-SY-101 Data: October - December, 1999*, RPP-5869, Rev. 0, Lockheed Martin Hanford Corp., Richland, Washington.

Delegard, C. H., 1980, *Laboratory Studies of Complexed Waste Slurry Volume Growth in Tank 241-SY-101*, RHO-LD-124, Rockwell Hanford Operations, Richland, Washington.

DeLorenzo, D. S., A. T. DiCenso, D. B. Hiller, K. W. Johnson, J. H. Rutherford, D. J. Smith, and B. C. Simpson, 1994, *Tank Characterization Reference Guide*, WHC-SD-WM-TI-648, Rev. 0, Westinghouse Hanford Company, Richland, Washington.

Erhart, M. F., 1991, *Evaluation of May 1991 Tank 241-SY-101 Gas-Release Event*, WHC-SD-WM-PE-044, Rev. 0, Westinghouse Hanford Company, Richland, Washington.

Erhart, M. F., 1992, *Evaluation of August 1992 Tank 241-SY-101 Gas-Release Event*, WHC-SD-WM-PE-045, Rev. 1, Westinghouse Hanford Company, Richland, Washington.

Estey, S. D., 2000, *Process Control Plan for Tank 241-SY-101 Surface Level Rise Remediation*, HNF-4264, Rev 3-B, Lockheed Martin Hanford Corp., Richland, Washington.

Gauglitz, P. A., L. A. Mahoney, D. P. Mendoza, and M. C. Miller, 1994, *Mechanisms of Gas Bubble Retention*, PNL-10120, Pacific Northwest National Laboratory, Richland, Washington.

Gauglitz, P. A., S. D. Rassat, M. R. Powell, R. R. Shah, and L. A. Mahoney, 1995, *Gas Bubble Retention and Its Effects on Waste Properties: Retention Mechanisms, Viscosity, and Tensile and Shear Strengths*, PNL-10740, Pacific Northwest National Laboratory, Richland, Washington.

Gauglitz, P. A., S. D. Rassat, P. R. Bredt, J. H. Konynenbelt, J. M. Tingey, and D. P. Mendoza, 1996, *Mechanisms of Gas Bubble Retention and Release: Results for Hanford Waste Tanks 241-S-102 and 241-SY-103 and Single-Shell Tank Simulants*, PNNL-11298, Pacific Northwest National Laboratory, Richland, Washington.

Gauglitz, P. A., and J. T. Aikin, 1997, *Waste Behavior During Horizontal Extrusion: Effect of Waste Strength for Bentonite and Kaolin/Ludox Simulants and Strength Estimates for Wastes from Hanford Waste Tanks 241-SY-103, AW-101, AN-103, and S-102*, PNNL-11706, Pacific Northwest Laboratory, Richland, Washington.

Herting, D. L., 1997, *Results of Dilution Studies with Waste from Tank 241-AN-105*, HNF-SD-WM-DTR-046, Rev. 0, Fluor Daniel Hanford, Inc., Richland, Washington.

Herting, D. L., 1998, *Results of Dilution Studies with Waste from Tank 241-AN-104*, HNF-3352, Rev. 0, Fluor Daniel Hanford, Inc., Richland, Washington.

Herting, D. L., D. B. Bechtold, B. E. Hey, B. D. Keele, L. Jensen, and T. L. Welsh, 1992, *Laboratory Characterization of Samples Taken in December 1991 (Window E) from Hanford Waste Tank 241-SY-101*, WHC-SD-WM-DTR-026, Rev. 0, Westinghouse Hanford Company, Richland Washington.

Herting, D. L., J. F. O'Rourke, D. W. Edmonson, J. W. Chenault, and J. C. Person, 1999, *Results of Dilution Studies with Waste from Tank-AW-101*, HNF-4964, Rev. 0, Fluor Daniel Hanford, Inc., Richland, Washington.

Hodgson, K. M., R. P. Anantatmuly, S. A. Barker, K. D. Fowler, J. D. Hopkins, J. A. Lechelt, D. A. Reynolds, D. C. Hedengren, R. E. Stout, and R. T. Winward, 1996, *Evaluation of Hanford Tanks for Trapped Gas*, WHC-SD-WM-ER-526, Rev. 1D, Westinghouse Hanford Company, Richland, Washington.

Hopkins, J. D., 1995, *Methodology for Flammable Gas Evaluations*, WHC-SD-WM-TI-724, Westinghouse Hanford Company, Richland, Washington.

Hu, T. A., 2000, *Empirical Rate Equation Model and Rate Calculations of Hydrogen Generation for Hanford Tank Waste*, HNF-3851, Rev. 0A, Lockheed Martin Hanford Corp., Richland, Washington.

Jo, J., 1997, *Tank Characterization Report for Double-Shell Tank 241-AN-105*, HNF-SD-WM-ER-678, Rev. 0, Lockheed Martin Hanford Corp., Richland, Washington.

Johnson, G. D., 1997, *Strategy for Resolution of the Flammable Gas Safety Issue*, HNF-SD-WM-ER-680, Rev. 0, DE&S Hanford, Richland, Washington.

Johnson, G. D., N. W. Kirch, W. B. Barton, C. W. Stewart, and B. E. Wells, 2000, *Evaluation of Hanford High-Level Waste Tank 241-SY-101*, RPP-6517, Rev. 0, CH2M HILL Hanford Group, Inc., Richland, Washington.

King, C. M., and S. A. Bryan, 1999, *Thermal and Radiolytic Gas Generation Tests on Material from Tanks 241-U-103, 241-AW-101, 241-S-106, and 241-S-102: Status Report*, PNNL-12181, Pacific Northwest National Laboratory, Richland, Washington.

Kirch, N. W., C. W. Stewart and J. M. Grigsby, 2000, *Remediation of Crust Growth and Buoyant Displacement Gas Release Event Behavior in Tank 241-SY-101*, RPP-6754, CH2M HILL Hanford Group, Inc., Richland, Washington.

Kubic, W. L., and A. V. Beloussov, 1999, *Dilution to Eliminate and Prevent Crust Formation in Tank 241-SY-101*, LA-UR-99-3770, Los Alamos National Laboratory, Los Alamos, New Mexico.

Kufahl, M. A., and D. C. Hedengren, 2000, *Hydrogen Generation Rate Model Calculation Input Data*, RPP-6069, Rev. 0, CH2M HILL Hanford Group, Inc., Richland, Washington.

Lentsch, J. W., 1992, *Tank 101-SY Flammable Gas Mitigation Test Project Plan*, WHC-EP-550, Rev. 0, Westinghouse Hanford Company, Richland, Washington.

Liu, J., L. R. Pederson, and L. Q. Wang, 1995, *Solid-Phase Characterization in Flammable-Gas-Tank Sludges by Electron Microscopy*, PNL-10723, Pacific Northwest National Laboratory, Richland, Washington.

Mahoney, L. A., 2000, *Ammonia Results Review for Retained Gas Sampling,* PNNL-13317, Pacific Northwest National Laboratory, Richland, Washington.

Mahoney, L. A., Z. I. Antoniak, and J. M. Bates, 1997, *Composition and Quantities of Retained Gas Measured in Hanford Waste Tanks 241-U-103, S-106, BY-101, and BY-109,* PNNL-11777, Pacific Northwest National Laboratory, Richland, Washington.

Mahoney, L. A., Z. I. Antoniak, J. M. Bates, and M. E. Dahl, 1999, *Retained Gas Sampling Results for the Flammable Gas Program*, PNNL-13000, Pacific Northwest National Laboratory, Richland, Washington.

Mahoney, L. A., Z. I. Antoniak, W. B. Barton, J. M. Conner, N. W. Kirch, C. W. Stewart, and B. E. Wells, 2000, *Results of Waste Transfer and Back-Dilution in Tanks 241-SY-101 and 241-SY-102*, PNNL-13267, Pacific Northwest National Laboratory, Richland, Washington.

McCain, D. J., 1999, *Results of Vapor Space Monitoring of Flammable Gas Watch List Tanks,* HNF-SD-WM-TI-797, Rev. 4, Fluor Daniel Hanford, Inc., Richland, Washington.

Meisel, D., C. D. Jonah, S. Kapoor, M. S. Matheson, and M. C. Sauer, 1993, *Radiolytic and Radiolytically Induced Generation of Gases from Synthetic Wastes,* ANL-93/43, Argonne National Laboratory, Argonne, Illinois.

Meyer, P. A., M. E. Brewster, S. A. Bryan, G. Chen, L. R. Pederson, C. W. Stewart, and G. Terrones, 1997. *Gas Retention and Release Behavior in Hanford Double-Shell Waste Tanks*, PNNL-11536, Rev.1, Pacific Northwest National Laboratory, Richland, Washington.

Meyer, P. A., and B. E. Wells, 2000, *Understanding Gas Release Events in Hanford Double-Shell Tanks,* Proceedings of Waste Management 2000, February 27 - March 2, 2000, Tucson, Arizona.

Norton, J. D., and L. R. Pederson, 1994, *Ammonia in Simulated Hanford Double-Shell Tank Wastes: Solubility and Effects on Surface Tension*, PNL-10173, Pacific Northwest Laboratory, Richland, Washington.

Norton, J. D., and L. R. Pederson, 1996, *Solubilities of Gases in Simulated Tank 241-SY-101 Wastes*, PNL-10785, Pacific Northwest National Laboratory, Richland, Washington.

Pederson, L. R., and S. A. Bryan, 1996, *Status and Integration of Studies of Gas Generation in Hanford Wastes*, PNNL-11297, Pacific Northwest National Laboratory, Richland, Washington.

Person, J. C., 1999, *Dilution Studies of Tank 241-SY-101 Waste*, Preliminary Report. 82100-99-015, Numatec Hanford Company, Richland, Washington.

Person, J. C., 1996, *Effects of Oxygen Cover Gas and NaOH Dilution on Gas Generation in Tank 241-SY-101 Waste*, WHC-SD-WM-DTR-043, Rev. 0, Westinghouse Hanford Company, Richland, Washington.

Person, J. C., 1998, *Gas Generation in Tank 241-AN-105 Waste With and Without Oxygen Reactions*, HNF-2038, Rev.0, Numatec Hanford Corporation, Richland, Washington.

Peurrung, L. M., L. A. Mahoney, C. W. Stewart, P. A. Gauglitz, L. R. Pederson, S. A. Bryan, and C. L. Shepard, 1998, *Flammable Gas Issues in Double-Contained Receiver Tanks*, PNNL-11836, Rev. 1, Pacific Northwest National Laboratory, Richland, Washington.

Prignano, A. L., 1988, *Tank 103-SY Dissolution Study – Results of Physical Measurements*, 12712-PCL88-011, Westinghouse Hanford Company, Richland, Washington.

Public Law 101-510, 1990, "Safety Measures for Waste Tanks at Hanford Nuclear Reservation," Section 3137 of *National Defense Authorization Act for Fiscal Year 1991.*

Rassat, S. D., and P. A. Gauglitz, 1995, *Bubble Retention in Synthetic Sludge: Testing of Alternative Gas Retention Apparatus*, PNL-10661, Pacific Northwest Laboratory, Richland, Washington.

Rassat, S. D., P. A. Gauglitz, P. R. Bredt, L. A. Mahoney, S. V. Forbes, and S. M. Tingey, 1997, *Mechanisms of Gas Retention and Release: Experimental Results for Hanford Waste Tanks 241-AW-101 and 241-AN-103*, PNNL-11642, Pacific Northwest National Laboratory, Richland, Washington.

Rassat, S. D., P. A. Gauglitz, S. M. Caley, L. A. Mahoney, and D. P. Mendoza, 1999, *A Discussion of SY-101 Crust Gas Retention and Release Mechanisms*, PNNL-12092, Pacific Northwest National Laboratory, Richland, Washington.

Rassat, S. D., C. W. Stewart, B. E. Wells, W. L. Kuhn, Z. I. Antoniak, J. M. Cuta, K. P. Recknagle, G. Terrones, V. V. Viswanathan, J. H. Sukamto, and D. P. Mendoza, 2000, *Dynamics of Crust Dissolution and Gas Release in Tank 241-SY-101*, PNNL-13112, Pacific Northwest National Laboratory, Richland, Washington.

Raymond, R. E., 1998, *Tank 231-SY-101 Surface Level Rise Remediation Options and Evaluation*, HNF-3705, Rev. 1, Fluor Daniel Hanford, Inc., Richland, Washington.

Raymond, R. E., 1999, *Tank 241-SY-101 Surface Level Rise Remediation Project Plan*, HNF-3834, Rev. 0, Lockheed Martin Hanford Corp., Richland, Washington.

Ryan, G. W., 2000, *Tank 241-SY-101 Safety Basis for Remediation Activities and Operations Before Closure of the Unreviewed Safety Question on Waste Surface Change*, HNF-3737, Rev. 1A, Fluor Daniel Northwest, Richland, Washington.

Schneider, T. C., 1996, *Standard-D Hydrogen Monitoring System Design Description*, WHC-SD-WM-SDD-059, Rev. 0, Westinghouse Hanford Company, Richland, Washington.

Schofield, J. S., 1996, *Sample Recovery Measurement Parameters*, (Internal Memorandum 75210-016-95-4, to Distribution, June 24), Westinghouse Hanford Company, Richland, Washington.

Shekarriz, A., 1994, *Retained Gas Sampler Visualization Guide*, PNL-10138, Pacific Northwest National Laboratory, Richland, Washington.

Shekarriz, A., D. R. Rector, L. A. Mahoney, M. A. Chieda, J. M. Bates, R. E. Bauer, N. S. Cannon, B. E. Hey, C. G. Linschooten, F. J. Reitz, and E. R. Siciliano, 1997, *Composition and Quantities of Retained Bas Measured in Hanford Waste Tanks 241-AW-101, A-101, AN-104, and AN-103*, PNNL-11450, Pacific Northwest National Laboratory, Richland, Washington.

Siciliano, E. R., 1998, *Drill String Gas Data*, HNF-1754, Rev. 0, Fluor Daniel Northwest, Inc., Richland, Washington.

Stewart, C. W., 2000, *Buoyant Response of the Tank 241-SY-101 Crust to Transfer and Back-Dilution*, PNNL-13066, Pacific Northwest National Laboratory, Richland, Washington.

Stewart, C. W., J. D. Hudson, J. R. Friley, F. E. Panisko, Z. I. Antoniak, J. J. Irwin, J. G. Fadeff, L. E. Efferding, T. E. Michener, N. W. Kirch, and D. A. Reynolds, 1994, *Mitigation of Tank 241-SY-101 by Pump Mixing: Results of Full-Scale Testing*, PNL-9959, Pacific Northwest Laboratory, Richland, Washington.

Stewart, C. W., C. L. Shepard, J. M. Alzheimer, T. I. Stokes, and G. Terrones, 1995, *In Situ Determination of Rheological Properties and Void Fraction in Hanford Waste Tank 241-SY-101*, PNL-10682, Pacific Northwest Laboratory, Richland, Washington.

Stewart, C. W., J. M. Alzheimer, M. E. Brewster, G. Chen, R. E. Mendoza, H. C. Reid, C. L. Shepard, and G. Terrones, 1996a, *In Situ Rheology and Gas Volume in Hanford Double-Shell Waste Tanks*, PNNL-11296, Pacific Northwest National Laboratory, Richland, Washington.

Stewart, C. W., M. E. Brewster, P. A. Gauglitz, L. A. Mahoney, P. A. Meyer, K. P. Recknagle, and H. C. Reid, 1996b, *Gas Retention and Release Behavior in Hanford Single-Shell Waste Tanks*, PNNL-11391, Pacific Northwest National Laboratory, Richland, Washington.

Stewart, C. W., J. M. Alzheimer, G. Chen, and P. A. Meyer, 1998, *In Situ Void Fraction and Gas Volume in Hanford Tank 241-SY-101 as Measured with the Void Fraction Instrument*, PNNL-12033, Pacific Northwest National Laboratory, Richland, Washington.

Stewart, C. W., S. D. Rassat, J. H. Sukamto, and J. M. Cuta, 1999, *Buoyancy and Dissolution of the Floating Crust layer in Tank 241-SY-101 During Transfer and Back-Dilution*, PNNL-13040, Pacific Northwest National Laboratory, Richland, Washington.

Stewart, C. W., L. A. Mahoney, and W. B. Barton, 2000, *Analysis of Several Hazardous Conditions for Large Transfer and Back-Dilution Sequences in Tank 241-SY-101*, PNNL-13118, Pacific Northwest National Laboratory, Richland, Washington.

Sullivan, H. L., 1995, *A Safety Assessment for Proposed Pump Mixing Operations to Mitigate Episodic Gas Releases in Tank 241-SY-101: Hanford Site, Richland, Washington*, LA-UR-92-3196, Rev. 14, Los Alamos National Laboratory, Los Alamos, New Mexico.

Van Vleet, R. J., 1996, *Summary of Flammable Gas Hazards and Potential Consequences in Tank Waste Remediation Facilities at the Hanford Site*, WHC-SD-WM-TI-753, Rev. 0, Westinghouse Hanford Company, Richland, Washington.

Webb, B. J., 1994, *Summary Report on the Design of the Retained Gas Sampler System*, WHC-SO-WM-ER-387, Rev. 0, Westinghouse Hanford Company, Richland, Washington.

WHC, 1992, *Test Plan for Tank 101-SY Mitigation by Mixing Test*, WHC-SD-WMTP-140, Rev. 3, Westinghouse Hanford Company, Richland, Washington.

Whitney, P. D., 1995, *Screening the Hanford Tanks for Trapped Gas*, PNL-10281, Pacific Northwest National Laboratory, Richland, Washington.

Whitney, P. D., P. A. Meyer, N. E. Wilkins, F. Gao, and A. G. Wood, 1996, *Flammable Gas Data Evaluation Progress Report*, PNNL-11373, Pacific Northwest National Laboratory, Richland, Washington.

Wilkins, N. E., 1992, *Evaluation of April 1992 Tank 241-SY-101 Gas-Release Event*, WHC-SD-WM-PE-048, Rev. 0, Westinghouse Hanford Company, Richland, Washington.

Wilkins, N. E., 1995, *Tank 241-SY-103 Core Sample: Interpretation of Results*, WHC-SD-WMM-TI-712, Rev. 0, Westinghouse Hanford Company, Richland, Washington.

Wilkins, N. E., 1997, *Tank Characterization Report for Double-Shell Tank 241-AN-103*, HNF-SD-WM-ER-702, Rev. 0, Lockheed Martin Hanford Corp., Richland, Washington.

This page intentionally left blank.

APPENDIX A

A.0 VOID FRACTION DATA REDUCTION MODEL

This page intentionally left blank.

APPENDIX A

VOID FRACTION DATA REDUCTION MODEL

A1.0 GAS VOLUME CALCULATION MODEL

The most general expression for the gas volume contained in a cylindrical waste volume of depth L and radius R is given by the integral

$$V_G = \int_0^L \int_0^{2\pi} \int_0^R \beta(r,\theta,z)\pi r dr d\theta dz \qquad \text{(A-1)}$$

where β is the local instantaneous gas indicator function (Kataoka 1986; Zhang and Prosperetti 1993).

The gas indicator function is the local instantaneous gas fraction which is defined as

$\beta(\mathbf{x}) = 1$: gas is present at point $\mathbf{x}$
$\beta(\mathbf{x}) = 0$: gas is not present.

The area average gas fraction, $\alpha(z)$, which is the fraction of the total cross-sectional area occupied by gas in the plane z, is defined as

$$\alpha(z) = \frac{1}{A} \int_0^{2\pi} \int_0^R \beta(r,\theta,z)\pi r dr d\theta \qquad \text{(A-2)}$$

where $A = \pi R^2$.

The gas fraction is also often termed the void fraction. Substituting Equation A-2 into Equation A-1 gives

$$V_G = A \int_0^L \alpha(z) dz \qquad \text{(A-3)}$$

In evaluating the flammable gas hazard and comparing tanks, we need to adjust the in-situ volume to standard pressure and temperature. Including the pressure and temperature correction in Equation A-1 gives the standard gas volume as

$$\hat{V}_G = \int_0^L \int_0^{2\pi} \int_0^R \frac{p(r,\theta,z)}{\hat{p}} \frac{\hat{T}}{T(r,\theta,z)} \beta(r,\theta,z)\pi r dr d\theta dz \qquad \text{(A-4)}$$

where $p(r,\theta,z)$ and $T(r,\theta,z)$ are the local pressure and temperature, respectively;
$\hat{p}$ is the standard atmospheric pressure of 101,320 Pa; and
$\hat{T}$ is the standard temperature, 298K.

If the area average pressure, $p(z)$, and temperature, $T(z)$, are defined in the same way as the area average gas fraction, and assuming that the pressure, temperature and gas fraction are not correlated in a horizontal plane, the total gas volume at standard temperature and pressure is given by

$$\hat{V}_G = A\int_0^L \frac{p(z)}{\hat{p}}\frac{\hat{T}}{T(z)}\alpha(z)dz \qquad \text{(A-5)}$$

The waste actually comprises several layers: floating crust, convective liquid, and nonconvective solid. Each has markedly different properties and gas content. It is also necessary to further subdivide the major waste layers into sublayers to resolve the gas fraction profile revealed by the local void fraction data and to perform the numerical analog of the integration in Equations A-3 and A-5. Therefore, it is most convenient to consider each layer and sublayer separately. Performing the integration for a layer or sublayer i, of thickness H_i and average void fraction α_i, the in-situ volume, V_i, of the layer is

$$V_i = \alpha_i A H_i \qquad \text{(A-6)}$$

and the standard volume, $\hat{V}_i$, is

$$\hat{V}_i = V_i\frac{p_i}{\hat{p}}\frac{\hat{T}}{T_i} \qquad \text{(A-7)}$$

where H_i is the layer thickness,
p_i is the layer pressure, and
T_i is the layer average temperature.

Because the product of pressure and temperature ratios occurs often, we define the effective pressure ratio, P_i, as

$$P_i = \frac{p_i}{\hat{p}}\frac{\hat{T}}{T_i} \qquad \text{(A-8)}$$

The pressure in layer i is calculated as the hydrostatic pressure exerted by the material above the midpoint of the layer. The nonconvective layer densities obtained from core samples are assumed to represent degassed waste; however, the dimensions of the waste layers include the expansion due to accumulated gas. Therefore, the density used to calculate the local pressure should be reduced to account for the void fraction. The pressure in a nonconvective sublayer, I, is calculated by

$$p_i = \hat{p} + g\rho_L(L_w - H_{NC}) + g\rho_{NC}\left(\sum_{j<i} H_j(1-\alpha_j) + \tfrac{1}{2}H_i(1-\alpha_i)\right) \qquad \text{(A-9)}$$

where ρ_L and ρ_{NC} are the liquid and degassed nonconvective layer densities, respectively;
L_W is the overall waste level;
H_{NC} is the nonconvective layer thickness;
H_i is the nonconvective sublayer thickness; and
α_i is the sublayer void fraction.

Measuring the waste level at the surface of the floating crust layer, which may be a few inches above the free liquid level, introduces a small error into the hydrostatic pressure. But it is much smaller than the effect of variations in the nonconvective layer height and the uncertainty in the density.

The total in-situ gas volume in the nonconvective waste is the sum of the gas volumes in the nonconvective sublayers:

$$V_{NC} = A\sum_{i=1}^{NC}\alpha_i H_i \qquad \text{(A-10)}$$

The total standard volume is similarly computed, making use of the effective pressure ratio definition of Equation A-8, as

$$\hat{V}_{NC} = A\sum_{i=1}^{NC}\alpha_i H_i P_i \qquad \text{(A-11)}$$

The overall average void fraction for the entire nonconvective layer is calculated by

$$\alpha_{NC} = \frac{1}{H_{NC}}\sum_{i=1}^{NC}\alpha_i H_i \qquad \text{(A-12)}$$

The average pressure ratio is back calculated from the gas volumes as

$$P_{NC} = \frac{\hat{V}_{NC}}{V_{NC}} = \frac{1}{H_{NC}\alpha_{NC}}\sum_{i=1}^{NC}\alpha_i H_i P_i \qquad \text{(A-13)}$$

The convective layer extends from the bottom of the floating crust layer to the top of the nonconvective layer. Its thickness is given by

$$H_{CL} = L_W - H_{CR} - H_{NC} \qquad \text{(A-14)}$$

where H_{CR} is the estimated thickness of the floating crust layer.

The convective layer pressure is given by

$$p_{CL} = \hat{p} + g\rho_L(H_{CR} + \frac{1}{2}H_{CL}) \quad \text{(A-15)}$$

The convective layer in-situ gas volume is computed from the average convective layer void fraction as

$$V_{CL} = A\alpha_{CL}H_{CL} \quad \text{(A-16)}$$

The standard volume in the convective layer is the product of the in-situ volume and the pressure ratio from Equations A-8 and A-15:

$$\hat{V}_{CL} = V_{CL}P_{CL} \quad \text{(A-17)}$$

The crust gas volume calculation (except recently in SY-101) is very uncertain as to both the thickness of the crust layer and its gas fraction. The crust thickness is determined at a single location with an uncertainty of 10 to 20 cm (4 to 8 in.). The lateral variability of the crust thickness is unknown but may be significant. The gas fraction is also highly speculative.

Except for SY-101 and one data point in AN-103, the void fraction distribution in the crust layer is unknown. Therefore, a buoyancy model as described in Section 5 of the main report is used to represent crust gas retention behavior. The void fraction necessary to float the crust to a given level of submergence is derived from Archimedes' principle and is given by

$$\alpha_{CR} = 1 - \frac{f_S\rho_L}{\rho_{NC} - (1 - f_S)(1 - \psi)\rho_L\phi} \quad \text{(A-18)}$$

where f_S is the fraction of the total thickness submerged,
ρ_L is the liquid density, ρ_{NC} is the nonconvective layer density,
ϕ is the porosity of the material above the liquid level, and
ψ is its liquid saturation (ψ=1.0 means the porosity is filled with liquid).

Assuming a porosity of 0.4 and an average saturation of 0.5 above the liquid level (see Section 5 for discussion), Equation A-18 becomes

$$\alpha_{CR} = 1 - \frac{f_S\rho_L}{\rho_{NC} - 0.2(1 - f_S)\rho_L} \quad \text{(A-19)}$$

where $\phi(1-\psi)$=0.4*(1-0.5)=0.2.

The effective pressure is the hydrostatic pressure at the midpoint of the submerged portion of the crust:

$$p_{CR} = \hat{p} + \frac{g}{2}\rho_L f_S H_{CR} \tag{A-20}$$

The in-situ crust gas volume is calculated using the void fraction from Equation A-18. The standard crust volume corrects the in-situ volume to standard conditions using Equation A-20 along with Equation A-8. The crust in-situ and standard volumes are given, respectively, by

$$V_{CR} = A\alpha_{CR} f_S H_{CR} \tag{A-21}$$

$$\hat{V}_{CR} = V_{CR} P_{CR} \tag{A-22}$$

The total in-situ and standard gas volumes in the entire tank are the sums of the contributions of individual layers. They are given, respectively, by

$$V_G = V_{NC} + V_{CL} + V_{CR} \tag{A-23}$$

$$\hat{V}_G = \hat{V}_{NC} + \hat{V}_{CL} + \hat{V}_{CR} \tag{A-24}$$

The overall tank effective pressure ratio is computed as the ratio of standard to in-situ volume:

$$P_{EFF} = \frac{\hat{V}_G}{V_G} \tag{A-25}$$

The degassed level represents the waste level after all the in-situ retained gas in the nonconvective layer has been removed. It is computed by

$$L_{NO-GAS} = L_W - V_{NC}/A \tag{A-26}$$

A2.0 STATISTICAL DATA REDUCTION MODEL

As indicated in Equation A-5, the total retained gas volume in a tank at standard temperature and pressure can be calculated by integrating the product of the local void fraction, hydrostatic pressure, and waste temperature, all of which vary with elevation. The spatial variability and measurement error associated with these quantities must be included in the uncertainty of the overall retained gas volume. The multiple sources of variability and the complex chain of calculations make it difficult to calculate the uncertainty analytically. Instead, a Monte Carlo simulation technique is used to propagate the sources of variability through the calculation.

There are two key elements in this statistical simulation model: (1) performing the numerical integration for the overall retained gas volume and (2) combining the various sources of variability to obtain the overall uncertainty using a Monte Carlo simulation technique.

With the measurements of void, density, temperature, and waste configuration (i.e., layer thickness), the numerical integration is performed by dividing the tank waste into many very thin horizontal slices. If the slices are thin enough, the void, hydrostatic pressure, and temperature within a slice can be considered uniform. Values of these quantities in a slice that does not contain a measurement are chosen as those of the nearest measurement. The retained gas volume in each slice can then be calculated as the integrand in Equation A-5. The summation of the gas volumes over a large number of small waste slices is a fair approximation of the integration in Equation A-5 for the total retained gas volume.

The numerical integration step does not assess the uncertainty of the gas volume estimate directly. The sample measurements vary spatially and are subject to measurement error. This implies that the measurements we have are just one set of values from a distribution of all possible values. If we took another set of measurements, we would obtain different values that would give a different total gas volume estimate. If this process were repeated many times, it would produce a distribution of the total gas volume that reflects the combined impact of the uncertainties from the multiple sources.

We can simulate the possible sampling results from estimated or assumed probability distributions of the input parameters and data. These distributions need to be set based on sample data, knowledge of the physical mechanisms of gas retention, and some assumptions. To ensure a reasonable coverage for all possible combinations of void, density, temperature, and waste configuration, 5,000 measurement sets are simulated. The uncertainties of these derived quantities can then be estimated from the outputs of these simulations. The operation of the Monte Carlo model includes the following basic steps:

1. Estimating and assigning the probability distribution for each of the input variables.
2. Simulating a set of measurements of void, temperature, etc., from the assigned distributions.

3. Calculating the mean void fractions, gas volumes (in-situ and standard), and other quantities for the convective, nonconvective, and crust layers and the whole tank from the simulated tank condition through a numerical integration.
4. Repeating steps 2 and 3 many times to create distributions of the output quantities.
5. Calculating the point estimates, standard deviations, and confidence intervals from these output distributions.

This simulation method has several important advantages:

- The major waste layers (e.g., convective, nonconvective) need not be subdivided in a specific way to capture trends of void fraction with elevation. Instead, small subdivisions of uniform thickness can be used to assess the spatial variability of void fraction.
- All important sources of variability can be incorporated directly by assigning probability distributions to input variables without resorting to statistical approximation formulas.
- The model creates probability distributions of average void fraction, total gas volume, and other calculated quantities. Point estimates, standard deviation, and confidence intervals can be easily constructed from these distributions. Confidence intervals can also be determined directly without assuming a specific distribution (e.g., normal).

The measurement methods and estimated measurement error for each of the quantities necessary for calculating the gas volume are discussed in Section 2 (see also Brewster et al. 1995 for a discussion of some of the typical tank instrumentation). The following paragraphs ascribe probability distributions to measurements of temperature, density, layer dimensions, and void fraction. The density and layer thicknesses are necessary to compute the hydrostatic pressure.

A2.1 Temperature

The waste temperature is taken from validation probe measurements in the MITs performed at approximately the same time as the VFI was deployed. The temperature measured at each elevation is assumed to be normally distributed. The measured value is taken as the mean, and the standard deviation is assigned as 2 °C. This distribution, which is applied to all tanks, is assumed to reflect both nominal measurement error and lateral variability of waste temperature.

A2.2 Density

Mean and standard deviations of waste densities in the convective layer are based on density measurements with the ball rheometer. Nonconvective layer densities are determined from laboratory analysis of core samples. The densities are assumed to be normally distributed with the same distribution applied to the entire convective or nonconvective layer. The mean and standard deviations of the normal distribution are estimated by the sample mean and sample standard deviations from all density measurements in each layer assuming that the sample variability includes the effect of measurement error.

A2.3 Waste Configuration

Normal distributions are assumed for waste surface level, nonconvective layer depth, and crust thickness. Means and standard deviations are derived by averaging several kinds of measurements, as discussed in Section 5.1 and listed in Table 5-1. A normal distribution is assumed for the crust submergence fraction, which is used to calculate the void fraction in the crust layer (see Equations A-18 and A-19).

A2.4 Void Fraction

Variability of void fraction, except for the crust layer, is evaluated directly from VFI and/or RGS void fraction measurements. This variability mainly reflects the spatial distribution of gas within a tank. The measurement error associated with individual void measurement is not included in the calculation because it is small compared with spatial variability. The variability of the crust layer void fraction is determined by simulation.

The variability of void fraction is evaluated separately for the convective and nonconvective layers. The data show that convective layer typically contains little gas with an essentially uniform void fraction. Therefore, the void fraction at any location in the convective layer is assumed to follow a common normal distribution. The mean and standard deviations of the normal distribution are estimated by the sample mean and sample standard deviations from all void measurements in the convective layer.

But the void fraction in the nonconvective layer typically shows a relatively large lateral variability and marked trends with elevation. We need to capture the structure of the vertical void profile without attributing it to spatial variability. To do this, the nonconvective layer is divided into sublayers 48-cm (19-in.) thick. This thickness is chosen to match the length of an RGS segment. The RGS measures the average void fraction in a sample of this length, which limits the vertical resolution of RGS measurements to 48 cm. This choice of thickness allows VFI and RGS data to be weighted equally when combined.

For each 48-cm sublayer containing one or more void measurements, a sample mean is calculated as the average of all the measurements in the sublayer. A common lateral variability is assumed for all sublayers in nonconvective layer. This lateral variability is estimated by a pooled sample variance, which is a weighted average of sample variance from all sublayers with more than one void measurement. The pooled sample standard deviation is calculated as

$$\hat{\sigma}_{pooled} = \sqrt{\frac{\sum_i n_i \hat{\sigma}_i^2}{\sum_i n_i}} \qquad \text{(A-27)}$$

where n_i denotes the number of void samples in sublayer i, and
σ_i denotes the sample standard deviation in sublayer i.

The weighting emphasizes the sublayers with the most measurements.

It is assumed that void measurements within a sublayer are from a common normal distribution with the estimated mean void of the sublayer and the pooled sampled standard deviation. The void measurements from the same riser are assumed to be correlated with a covariance equal to the riser-to-riser variability. The VFI data typically show that the void fraction measurements differ between risers, sometimes significantly. The simulated sample measurements should reflect this tendency.

Void fraction measurements with this kind of riser-dependent structure can be simulated by imposing a covariance on a set of completely independent samples. Specifically, a covariance matrix is constructed with a dimension equal to the number of void fraction measurements in the nonconvective layer. The diagonal elements of the matrix are equal to the variance of the distribution from which the measurements are simulated. Because a common variance is assumed for all sublayers, all diagonal elements are the same. The off-diagonal elements in the matrix represent covariance between two void measurements. If two measurements come from the same riser, the covariance is set equal to the riser-to-riser variability; otherwise, the covariance is zero. Based on the properties of normal distributions, this matrix can be used to convert a set of completely independent random samples to a set of samples with the desired riser-to-riser structure.

The riser-to-riser variability was estimated through the following analysis-of-variance (ANOVA) model:

$$\alpha_{ijk} = \overline{\alpha} + R_i + L_j + \varepsilon_{ijk}$$

where

α_{ijk} = local void fraction measurement k in riser i at layer j
$\overline{\alpha}$ = mean void fraction in entire nonconvective layer
R_i = deviation of void fraction at riser i from the mean
L_j = deviation of the void fraction in the jth sublayer
ε_{ijk} = sampling and measurement error.

The riser effect, R_I, is considered a random effect with zero mean and σ_R standard deviation. This standard deviation, which represents the riser-to-riser variability, was estimated by fitting the model to the VFI data for each tank.

A2.5 Calculation Procedure

To numerically integrate the void fraction measurements and to propagate the sources of variability, the waste is divided into many very thin slices. We choose a 4.8-cm (1.9-in.)-thick slice, $1/10^{th}$ of the nominal 48-cm (19-in.) sublayer dimension. The idea is to simulate possible sample measurements (temperature, void, etc.) so the waste condition in each thin slice can be evaluated from a given set of simulated measurements. Then the mean void fraction is estimated as the average void fraction in all the thin slices. The total retained gas volume is estimated as

the sum of the gas volumes in each slice. A set of measurements is simulated from these distributions using the following procedure:

- Simulate a realization of waste level, crust thickness, submergence fraction, nonconvective layer depth, convective layer density, and nonconvective layer density from the pre-defined distributions.
- Divide convective and nonconvective layers into slices 1.9-in. (4.8-cm) thick based on the current realizations of waste layer thickness for numerical integration. The number of slices in each layer may be different for each realization.
- Simulate a realization of temperature at each measuring location. If a waste slice does not contain any measuring location, the temperature of the slice is assigned the value of the realization at nearest elevation containing a temperature measurement.
- Simulate a realization of void fraction at each sampling location. Void fraction realizations at sampling locations within the same 19-in. (48-cm) sublayer are simulated from the same pooled distribution as described in Section A2.4. The void fraction value for each waste slice is calculated using the same procedure as for temperature.

For each simulation, one realization of average void fractions, gas volumes, and dL/dP for convective, nonconvective, and whole tank is calculated. Using i to index a 1.9-inch (4.8-cm) waste slice, the following equations are used for the calculation:

$$\alpha_{mean} = \frac{1}{n_{slice}} \sum_i \alpha_i$$

$$V_G = A \sum_i \alpha_i h_i$$

$$\hat{V} = A \sum_i \alpha_i h_i \frac{p_i}{\hat{p}} \frac{\hat{T}}{T_i}$$

where n_{slice} is the number of slices in a convective or nonconvective layer;
h_i is the height of a slice; and
α_i, p_i, and T_i denote void, pressure, and temperature, respectively, in i^{th} slice.

The total gas volume is the sum of the gas volumes in the three waste layers. A set of 5,000 realizations is obtained for each quantity of interest. A summary of the output distributions, including mean, median, standard deviation, percentiles, etc., is then calculated from these distributions.

A3.0 REFERENCES

Brewster, M. E., N. B. Gallagher, J. D. Hudson, and C. W. Stewart, 1995, *The Behavior, Quantity, and Location of Undissolved Gas in Tank 241-SY-101*, PNL-10681, Pacific Northwest Laboratory, Richland, Washington.

Kataoka, I., 1986, *Local Instant Formulation of Two-Phase Flow*, International Journal of Multiphase Flow, Vol. 12, No. 3, pp. 745-758.

Zhang, D. Z., and A. Prosperetti, 1993, *Ensemble Averaged Euler Equations and Added Mass for Linearized Flows in Gas-Liquid Flows*, ASME Fluids Engineering Division, FED-Vol. 165, pp. 65-70.

This page intentionally left blank.

APPENDIX B

B.0 BAROMETRIC PRESSURE EFFECT MODEL

This page intentionally left blank.

APPENDIX B

BAROMETRIC PRESSURE EFFECT MODEL

The barometric pressure effect (BPE) model for estimating retained gas volume is derived in detail in this appendix, and all the assumptions and requirements are listed. Conditions that may compromise the application of the model are developed based on these assumptions.

B1.1 BPE Model Derivation

The fundamental definition of the gas volume is given by Equation A-3. The barometric pressure response is the derivative of Equation A-3 with respect to ambient atmospheric pressure, p_0:

$$\frac{dV_G}{dp_0} = A\frac{d}{dp_0}\int_{L_0}^{L_1}\alpha(z)dz \tag{B-1}$$

Recognizing that only that volume of the waste that is gas can respond to pressure and applying Leibnitz' rule for differentiation of integrals, we can write Equation B-1 as

$$\frac{dH}{dp_0} = \frac{\alpha(L_1)-\alpha(L_0)}{1-\alpha(L_0)}\frac{dL_1}{dp_0} + \frac{1}{1-\alpha(L_0)}\int_{L_0}^{L_1}\frac{d\alpha(z)}{dp_0}dz \tag{B-2}$$

where $H = L_1 - L_0 = V_G/A$.

If the stored gas is in intimate contact with the waste, the infinitesimal compression and expansion process resulting from barometric pressure fluctuations can be considered isothermal. For an isothermal process in an ideal gas, the product of the pressure and gas volume is constant. This is expressed in differential form as

$$\frac{dV_G}{dp} = -\frac{V_G}{p} \tag{B-3}$$

where p is the pressure of the gas volume, V_G.

Applying the definition of the gas volume fraction yields

$$\frac{d\alpha}{dp} = -\frac{\alpha(1-\alpha)}{p} \tag{B-4}$$

The derivative of local gas pressure in the waste in Equation B-4 is related to external barometric pressure via the chain rule:

$$\frac{d\alpha}{dp_0} = \frac{d\alpha}{dp}\frac{dp}{dp_0} \tag{B-5}$$

Expressions for dp/dp_0 can be derived from models for waste yield stress (Whitney et al. 1996), capillary pressure, time lag between the dome space and atmosphere, changes in the gas elevation due to pressure changes, or any other effects. However, since the waste in the Facility Group 1 DSTs is relatively weak, we assume that the gas in the waste senses the exact, instantaneous effect of a barometric pressure change so that dp/dp_0 is unity.

Substituting Equation B-4 into Equation B-1 gives an expression for the change in waste height in response to barometric pressure change:

$$\frac{dH}{dp_0} = \frac{\alpha(L_1)-\alpha(L_0)}{1-\alpha(L_0)}\frac{dL_1}{dp_0} + \frac{1}{1-\alpha(L_0)}\int_{L_0}^{L_1}\frac{\alpha(z)[1-\alpha(z)]}{p(z)}dz \tag{B-6}$$

The vertical gas distribution, $\alpha(z)$, can be inferred from the waste configuration (determined by temperature profiles or core extrusions, for example) or measured directly (i.e., with the VFI or RGS). In either case, the functional form of $\alpha(z)$ is unknown. Therefore, the average gas fraction in the layer of waste between L_0 and L_1 is applied as a uniform value independent of elevation. However, the pressure is allowed to vary linearly with elevation according to the average density and gas fraction as

$$p(z) = p + (1-\alpha)\rho g(L_1 - z - H/2) \tag{B-7}$$

where p is the pressure at the layer midpoint,
$\alpha = V_W/AH$ is the average gas fraction in the layer,
ρ is the average ungassed density,
L_1 is the elevation of the top of the layer, and
H is the layer thickness, $H = L_1 - L_0$.

Substituting Equation B-7 into Equation B-6, applying the stated assumptions, and performing the integration yields

$$\frac{dH}{dp_0} = -\frac{\alpha}{(1-\alpha)\rho g}\ln\left\{\frac{1+(1-\alpha)\rho gH/2p}{1-(1-\alpha)\rho gH/2p}\right\} \tag{B-8}$$

Equation B-8 can be simplified by expanding the natural log as a Taylor series and retaining the first-order term to give

$$\frac{dH}{dp_0} = -\frac{\alpha H}{p} \tag{B-9}$$

The additional error introduced by this approximation to the natural logarithm can be estimated by $[(1-\alpha)\rho gH/p]^3/12$ (which is the next term in the Taylor series). In the extreme case, where

a single layer is used to represent a deep tank with a small gas fraction and the midpoint pressure is equal to the pressure difference across the layer, this error is less than 10%.

If the entire waste volume is represented by N layers, the overall barometric pressure response of the waste surface, L, is the sum of Equation B-9 over all the layers:

$$\frac{dL}{dp_0} = -\sum_{i=1}^{N} \frac{\alpha_i H_i}{p_i} \tag{B-10}$$

The familiar expression for calculating the total in-situ gas volume in the tank from the barometric pressure response can be derived by rearranging Equation B-10 as

$$V_G = -Ap_{BPE} \frac{dL}{dp_0} \tag{B-11}$$

where the effective pressure for the BPE calculation is defined by

$$\frac{1}{P_{BPE}} = \sum_{i=1}^{N} \left[\frac{f_i}{p_i} \right] \tag{B-12}$$

and f_i is the fraction of the total in-situ gas stored in layer i:

$$f_i = \frac{A\alpha_i H_i}{V_G} \tag{B-13}$$

Equation B-10 provides an estimate of the barometric pressure response when the gas distribution and its pressure are known. If a suitable measurement of the barometric response and an estimate of the gas distribution are available, Equation B-11 gives the in-situ gas volume.

All gas volumes discussed up to now were at their local pressure and temperature. The true measure of the total amount of stored gas is the standard volume, which brings the in-situ volume to standard pressure and temperature as expressed by Equation A-25, which can be written as

$$\hat{V}_G = V_G P_{EFF} \tag{B-14}$$

where the effective pressure ratio, P_{EFF}, is calculated by substituting Equations A-13, A-17, A-22 and A-24 into Equation B-14. The result is:

$$P_{EFF} = \frac{V_{NC}}{V_G} P_{NC} + \frac{V_{CL}}{V_G} P_{CL} + \frac{V_{CR}}{V_G} P_{CR} \tag{B-15}$$

Substituting Equation B-11 for the in-situ volume yields the result for estimating the standard volume from a measured barometric pressure response:

$$\hat{V}_G = -AP_{EFF}\, p_{BPE} \frac{dL}{dP_0} \tag{B-16}$$

B1.2 Assumptions and Requirements of the BPE Model

The assumptions in the above derivations are summarized below. Though not part of the derivation, it is essential to assume the response of the waste surface can be measured frequently and precisely. Assumptions 1 through 5 apply to the in-situ volume determined from Equation B-11. Additional assumption 6 applies to the standard volume computed from Equation B-16:

1. The gas-bearing waste is contained entirely in a cylinder of fixed radius and uniform but temporally variable height (true for a radially stiff tank structure whose waste and gas fraction are relatively uniform radially and azimuthally).
2. The process of expansion and compression due to barometric pressure fluctuation is isothermal (true for expected large gas surface-to-volume ratio and very slow pressure changes).
3. The gas stored in the waste behaves as an ideal gas (true for small pressure changes and relatively low temperatures with the expected gas composition and pressures).
4. The local pressure of all the gas in the waste changes as the barometric pressure (true for relatively weak waste in which the gas elevation does not change significantly with pressure).
5. Vertical waste configuration and in-situ gas volume distribution can be estimated or is known to within an appropriate level of uncertainty (depends on information available).
6. The local pressure is radially and azimuthally uniform or the radial and azimuthal variation of the pressure and gas fraction are not correlated (true if assumption 4 is met).

From these assumptions, it can be inferred that the BPE model should be applied to these tanks only after careful consideration:

- that have been saltwell pumped in which a high lithostatic load results from an interstitial liquid level well below the waste surface where the gas is stored as pore-filling bubbles (potentially violates assumptions 1, 4 and 5)
- with a very low waste level (potentially violates assumptions 1 and 4)
- with a forest of suspended hardware such as airlift circulators, cooling coils, etc. (potentially violates assumptions 1 and 4)
- in which the waste is periodically disturbed by mixing (violates assumption 4)
- in which the gas effective pressure changes during the time of the barometric pressure response measurement (violates assumption 5)

- in which an appropriately precise waste level instrument is not available or readings are not taken with sufficient frequency.

The best prospects for an accurate volume determination with the BPE model are tanks with relatively deep, wet waste in which the vertical gas distribution can be estimated with fair confidence. Currently, this includes the DSTs and few of the SSTs.

Nevertheless, regardless of how well the assumptions of the BPE model are satisfied, it is almost impossible to attribute a correlation of waste level and barometric pressure to anything but the presence of stored gas. Therefore, while a negligible barometric pressure response does not necessarily indicate the absence of gas, a strong measured barometric pressure response should *always* be taken as an indication of stored gas.

B1.3 Uncertainty and Detection Limits

The BPE model has a significant inherent uncertainty in the best of conditions. The smaller the retained gas volume, the less accurately the BPE model can estimate it. We can derive the minimum detectable volume for a given uncertainty threshold and measurement error. The barometric response in Equation B-11 can be rewritten in finite difference form as

$$V_G = -A p_{BPE} \frac{\Delta L}{\Delta p_0} \tag{B-17}$$

where ΔL is the specific level change in response to a corresponding barometric pressure change of Δp_0.[1] Assuming the uncertainties in the barometric pressure change and tank area are small, the relative uncertainty in the volume in Equation B-17 can be estimated by linear error propagation as

$$\left(\frac{\sigma_V}{V_G}\right)^2 = \left(\frac{\sigma_p}{p_{BPE}}\right)^2 + \left(\frac{\Delta L_{min}}{\Delta L}\right)^2 \tag{B-18}$$

Here, the relative uncertainty in level response has been approximated by the instrument precision, L_{min}, divided by the actual level change, ΔL. Solving Equation B-17 for ΔL, substituting the result into Equation B-18, and solving for V_G yields

$$V_{MIN} = A p_{BPE} \frac{\Delta L_{min}}{\Delta p_0 \left[\left(\frac{\sigma_V}{V_G}\right)^2 - \left(\frac{\sigma_p}{p_{BPE}}\right)^2\right]^{1/2}} \tag{B-19}$$

[1] The pressure fluctuation should be only the amount that exceeds twice the yield stress of the material, according to Whitney et al. (1996). However, the yield stress in the DSTs is small, ~150 Pa, compared with barometric pressure changes.

where V_{MIN} is the minimum in-situ gas volume that is measurable with the given uncertainties in volume and pressure and the given instrument precision.

Figure B-1 shows the gas volume and void fraction as a function of barometric pressure change for a typical DST. This tank is assumed to have a 10-m waste level and a 4-m nonconvective layer yielding an effective pressure of 1.8 ± 0.4 atm. An ENRAF™ level gauge with a precision of ± 0.1 cm is used to measure level changes. The effective detection threshold might be defined as 100% error. The nominal barometric pressure change is about 1 kPa, with a maximum of 3 kPa in the late fall and winter and a minimum of 0.3 kPa in the summer (Whitney 1995).

Under these assumptions, it is clear from the figure that the BPE method (assuming all assumptions and conditions prescribed earlier are met) can calculate the in-situ gas volume to within ± 25% only if the gas volume is ~300 m^3 or more and if the pressure change is above about 2 kPa. For nominal conditions, an in-situ volume of volume of 200 m^3 could be measured with an uncertainty under ± 50%. This is consistent with the uncertainties presented in the comparisons of BPE and VFI/RGS volume estimates to follow.

Figure B-2 shows the detection threshold (defined as 100% error) for other measurement instruments as well as the ENRAF™ for the same typical DST. The FIC probe has an assumed precision of 0.2 cm and the manual tape 0.4 cm. The actual uncertainty varies considerably from tank to tank (Whitney 1995). The manual tape requires such a large pressure change and gas volume as to be essentially unusable. The precision afforded by the ENRAF™ gauge is clearly required for reasonably accurate BPE volume calculations.

B1.4 Water Vapor Pressure Effect

The BPE model overpredicts the gas volume when the vapor pressure is high. The partial pressure of water vapor is a function only of the local temperature on the time scale of a barometric pressure swing. Because its partial pressure is constant, the volume fraction of water vapor grows as total pressure decreases and vice versa, which amplifies the effect of expansion and compression of the noncondensable gas. Thus, there is actually less gas present than the measured dL/dP correlation would indicate.

The effect of water vapor can be quantified with the aid of Dalton's and Amagat's laws that relate the mole fractions of the vapor and noncondensable gas to the partial pressure and partial volumes as follows:

$$\frac{n_i}{n_G} = \frac{p_i}{p_G} = \frac{V_i}{V_G} \qquad \text{(B-20)}$$

where n is the number of moles of gas,
p is the average pressure felt by the gas, and
V is the gas volume.

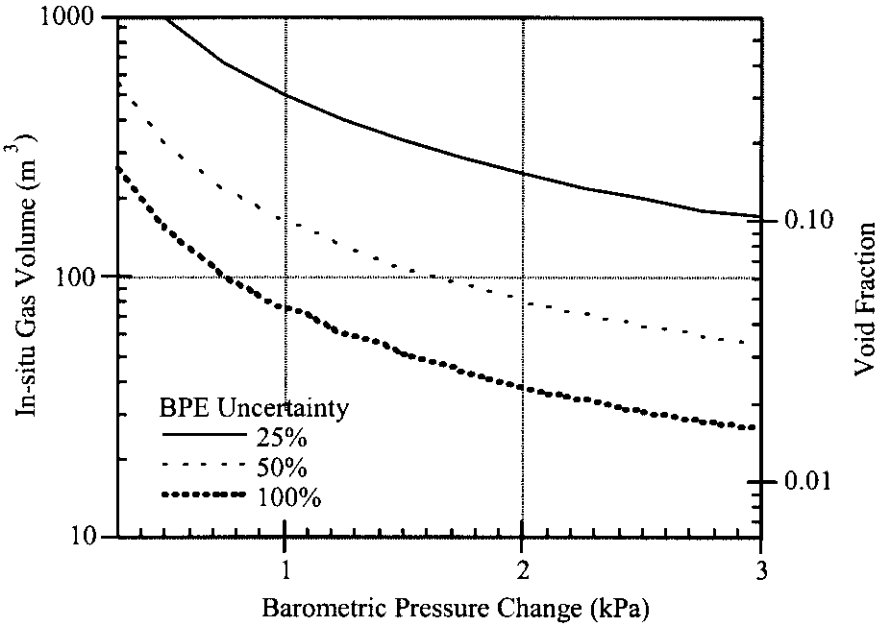

Figure B-1. Barometric Pressure Effect Uncertainty for a Typical Double-Shell Tank

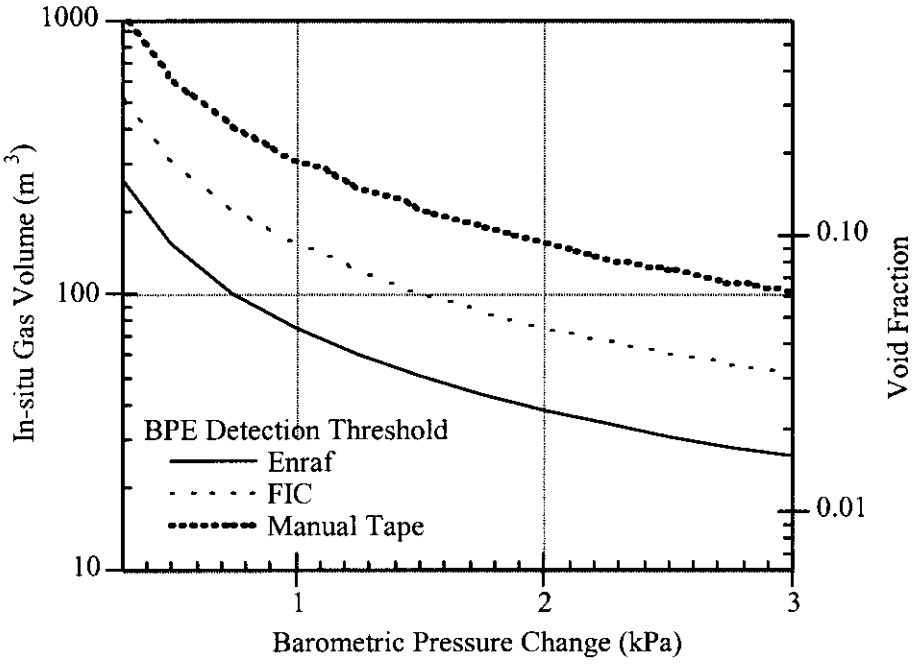

Figure B-2. Threshold Barometric Pressure Effect Gas Volume for Several Level Instruments

The subscript i refers to either the vapor or noncondensable component, and the subscript G refers to the gas mixture. The partial pressure, p_i, is the pressure that would be exerted by n_i moles of gas i contained in the total volume, V_G. The partial volume, V_i, is the volume that n_i moles of gas i would occupy under the total pressure, p_G.

Considering only the vapor (subscript V) and noncondensable (subscript N) components in Equation B-20 the total gas volume can be related to the noncondensable gas partial volume by

$$V_G = \left(1 + \frac{p_V}{p_N}\right) V_N \tag{B-21}$$

The change in waste level with barometric pressure is assumed due solely to compression and expansion of the gas (both vapor and noncondensable). This can be expressed with the aid of Equation B-21 by

$$A\frac{dL_w}{dp_0} = \frac{dV_G}{dp_0} = \frac{d}{dp_N}\left[\left(1 + \frac{p_V}{p_N}\right) V_N\right]\frac{dp_N}{dp_0} \tag{B-22}$$

Taking the derivative, recognizing that $dp_N = dp_0$ since p_V is a function only of temperature, and assuming isothermal pressure changes such that $pV_N = n_N RT$ = constant, Equation B-22 becomes

$$A\frac{dL_w}{dp_0} = -\left(1 + \frac{p_V}{p_N}\right)\frac{V_N}{p_G} - \frac{p_V}{p_N^2} V_N \tag{B-23}$$

Converting V_N to V_G via Equation B-21, using $p_G = p_N + p_V$, and rearranging Equation B-23 yields

$$V_G = -Ap_G\left(1 - \frac{p_V}{p_G}\right)\frac{dL_w}{dp_0} \tag{B-24}$$

Thus, if the water vapor pressure in the bubbles is 10% of the total pressure, the total gas volume is 90% of the value indicated by the unmodified BPE model, Equation B-11. The void fraction including the vapor is computed with the analog to Equation B-24 as

$$\alpha = -\frac{p_G}{L_G}\left(1 - \frac{p_V}{p_G}\right)\frac{dL_w}{dp_0} \tag{B-25}$$

The noncondensable portion of the total gas volume can be found by substituting Equation B-21 for V_G in Equation B-24 as follows:

$$V_N = -Ap_G\left(1-\frac{p_V}{p_G}\right)^2 \frac{dL_w}{dp_0} \qquad \text{(B-26)}$$

The volume fraction of water vapor in the retained gas is plotted versus temperature in Figure B-3 at a total pressure of 2 atm. The water vapor volume fraction in the bubbles is less than 6% for waste temperatures less than about 120 °F, which includes the tanks of interest to this study. This means that the actual void fraction is 94% of the value that would be computed if water vapor is ignored. We conclude that water vapor is not an important contributor to waste buoyancy and barometric pressure response under typical DST conditions and need not be accounted for, except possibly as a diluent in flammability calculations. However, its effect could be important in tanks with elevated temperatures.

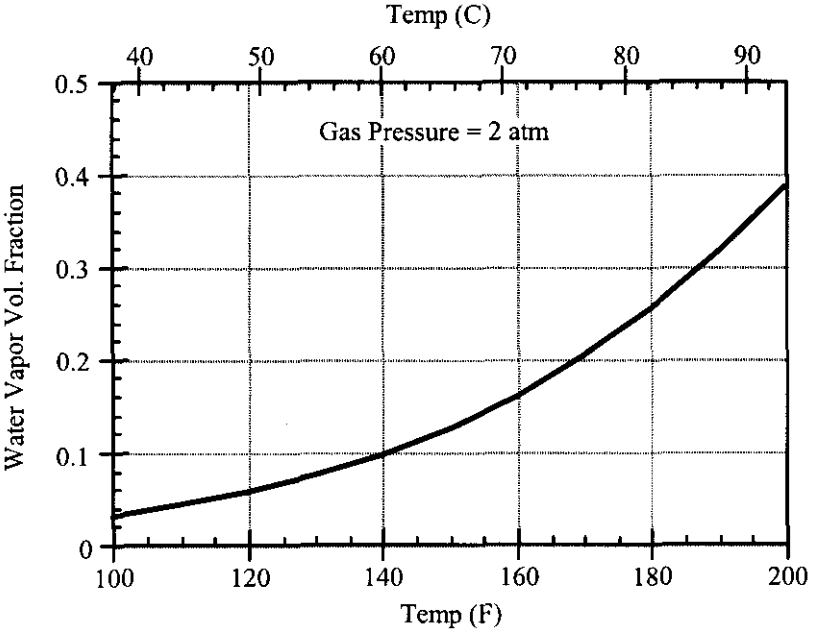

Figure B-3. Bubble Water Vapor Fraction Versus Waste Temperature

B2.0 REFERENCES

Whitney, P. D., 1995, *Screening the Hanford Tanks for Trapped Gas*, PNL-10281, Pacific Northwest National Laboratory, Richland, Washington.

Whitney, P. D., P. A. Meyer, N. E. Wilkins, F. Gao, and A. G. Wood, 1996, *Flammable Gas Data Evaluation Progress Report*, PNNL-11373, Pacific Northwest National Laboratory, Richland, Washington.

APPENDIX C

C.0 STATISTICAL ANALYSIS OF CORRELATION OF GAS RELEASES WITH BAROMETRIC PRESSURE FLUCTUATIONS

This page intentionally left blank.

APPENDIX C

STATISTICAL ANALYSIS OF CORRELATION OF GAS RELEASES WITH BAROMETRIC PRESSURE FLUCTUATIONS

The number of GREs in each month in Tanks AN-103, AN-104, AN-105, AW-101 and SY-103 as indicated by sudden elevations of the headspace hydrogen concentration for January 1995 through December1999 are listed in Table C-1. The average barometric pressure drop and pressure rise during each month for the same period is also included. The number of GREs per month for the entire 60-month period is plotted in Figure C-1. The magnitudes of barometric pressure rises and drops for 1994-98 is plotted in Figure C-2.

To examine the potential periodic behavior of the 12 month summed GRE count of Table C-1, a chi-squared test for goodness-of-fit in a multinomial setting was used to test the null hypothesis that GREs occur at the same proportions for all 12 months. The alternative hypothesis is that the proportion of GREs is different for some months than it is for others. One would expect to see evidence in favor of the alternative hypothesis if GREs actually do exhibit periodic behavior as would be dictated by an association to the barometric pressure fluctuations. The test statistic for this chi-squared test was 12.973, which yields a p-value of 0.2951, so the null hypothesis is not rejected. Admittedly, this is a very crude test to use to test for periodic behavior.

Table C-1. Average Pressure Fluctuations and Gas Release Events Count per Month for 1995-1999

Month	Average Pressure Drop (atm)	Average Pressure Rise (atm)	GRE Count
January	-0.010	0.009	4
February	-0.011	0.010	5
March	-0.010	0.009	3
April	-0.008	0.010	4
May	-0.009	0.007	9
June	-0.008	0.005	4
July	-0.008	0.006	5
August	-0.008	0.005	9
September	-0.008	0.007	8
October	-0.008	0.010	7
November	-0.008	0.009	3
December	-0.011	0.013	11

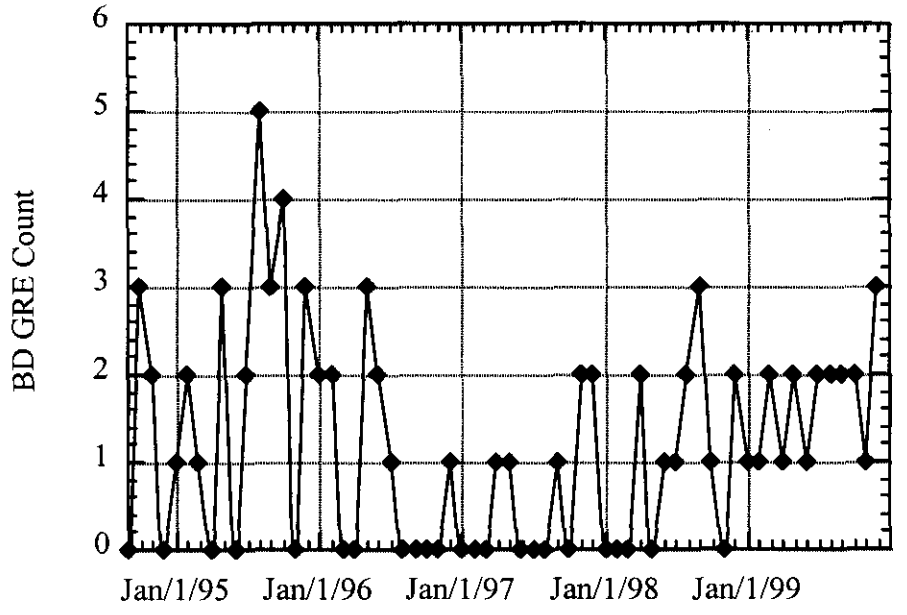

Figure C-1. Monthly Count of Gas Release Events

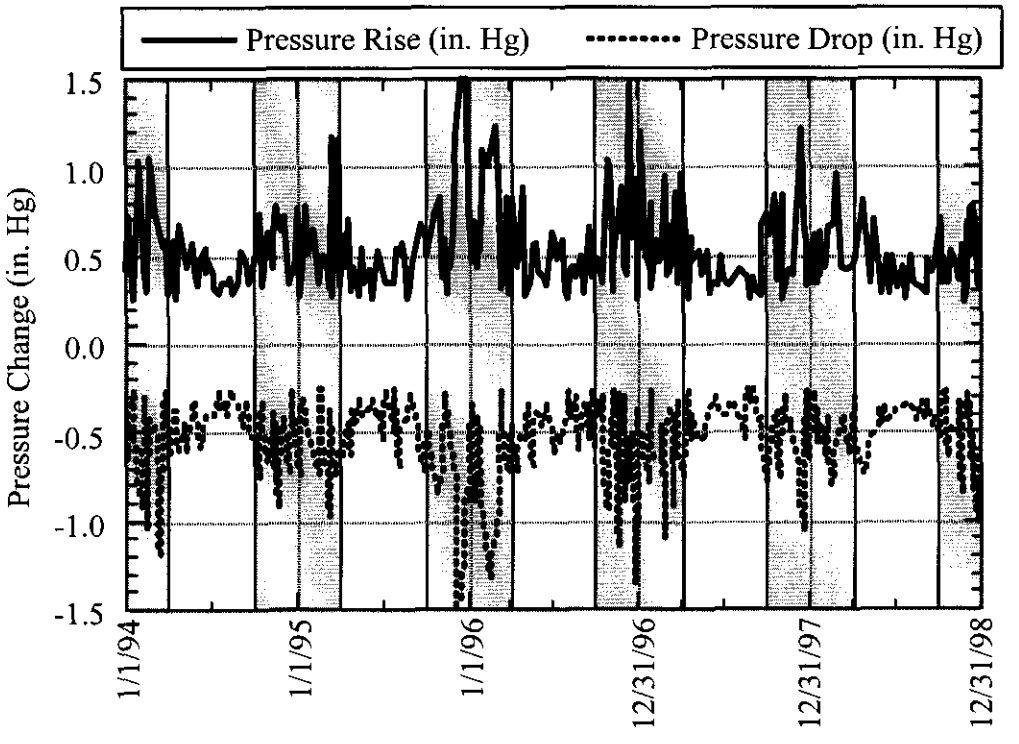

Figure C-2. Barometric Pressure Fluctuations as a Function of Time

A more suitable test would be the runs up and down test, as it should be much more sensitive to periodic behavior than the chi-squared test. The null hypothesis for the test is that the sequence of GREs by month is random, the alternative hypothesis is that the runs tend to cluster. The test statistic is the total number of runs in the data, either up or down. If the combined data over the 12 months is used, the test statistic is V=7 which yields a p-value of 0.4453. So again, the null hypothesis is not rejected.

Additionally, it was determined that there is no significant linear correlation between the 12-month summed number of GREs and the 12-month summed average monthly pressure fluctuations. The p-value is 0.977, and Pearson's correlation coefficient is 0.009. These values indicate that based on this data set there is no statistical basis to suppose that GREs are linearly correlated with pressure fluctuations.

If the runs up and down test is conducted using the data over the 60 months (Figure C-1), the null hypothesis is that the sequence is random and the alternative hypothesis is that the runs tend to cluster. In this case, there are 35 runs total, so the z-score (based on the asymptotic distribution for the test statistic) is -1.8697 which yields a p-value of 0.0308. This indicates that the null hypothesis should be rejected and thus that the runs tend to cluster. Therefore, there are noticeable up-and-down patterns in the data. If the GREs are actually periodic, up-and-down patterns should be seen in the data. Note, however, the presence of these patterns does not necessarily imply that the data is periodic.

The 60-month GRE totals per month (Figure C-1), as well as that of the barometric pressure changes (Figure C-2), were investigated for periodic behavior using the fast Fourier transform (FFT) data analysis tool in Excel®.

The lack of discernable peaks in the power spectrum resulting from the application of a FFT to the monthly GRE count provides no indication of periodic behavior, Figure C-3. Even by applying various windowing schemes to examine the data, no distinct peaks were identifiable. The power spectrum of the barometric pressure fluctuations does contain distinct peaks, so period behavior, as expected, is indicated, Figure C-4.

The 60-month histories were analyzed for correlation between them. The p-value is determined to be 0.491, and the correlation coefficient is 0.088. Again, there is no statistical basis to suppose that GREs are linearly correlated with pressure fluctuations, Figure C-5.

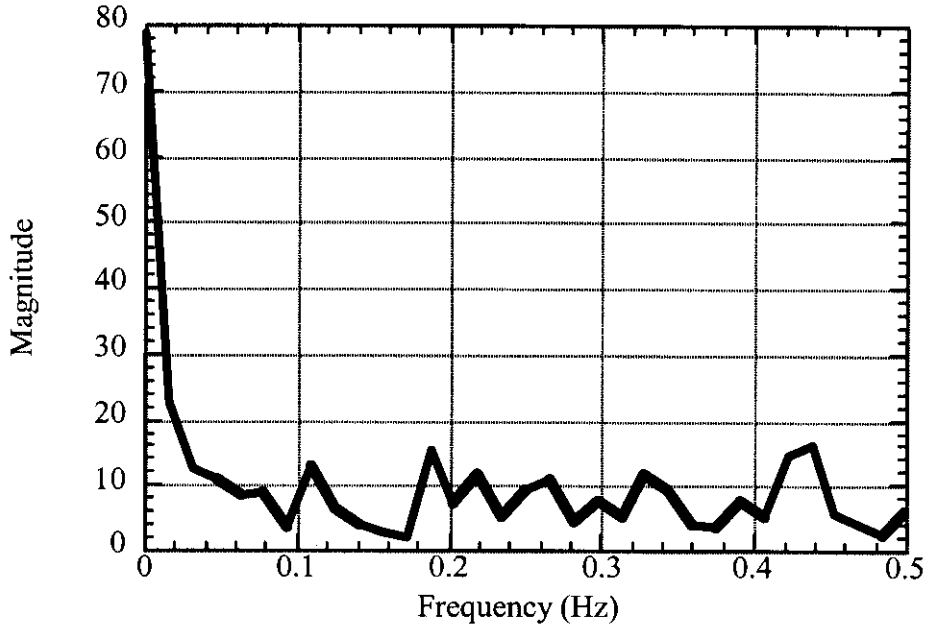

Figure C-3. Power Spectrum of Gas Release Event Count

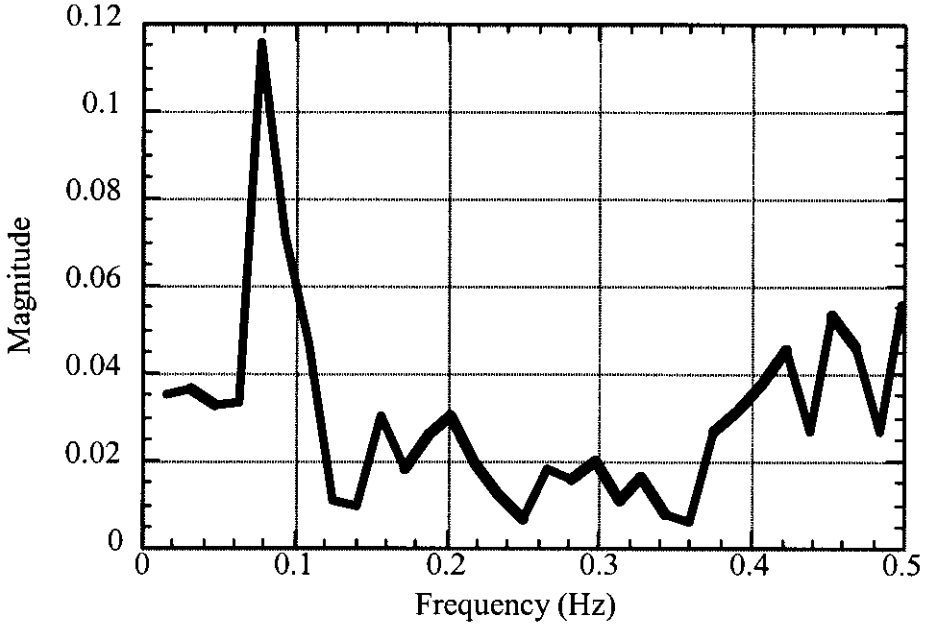

Figure C-4. Power Spectrum of Barometric Pressure Fluctuations

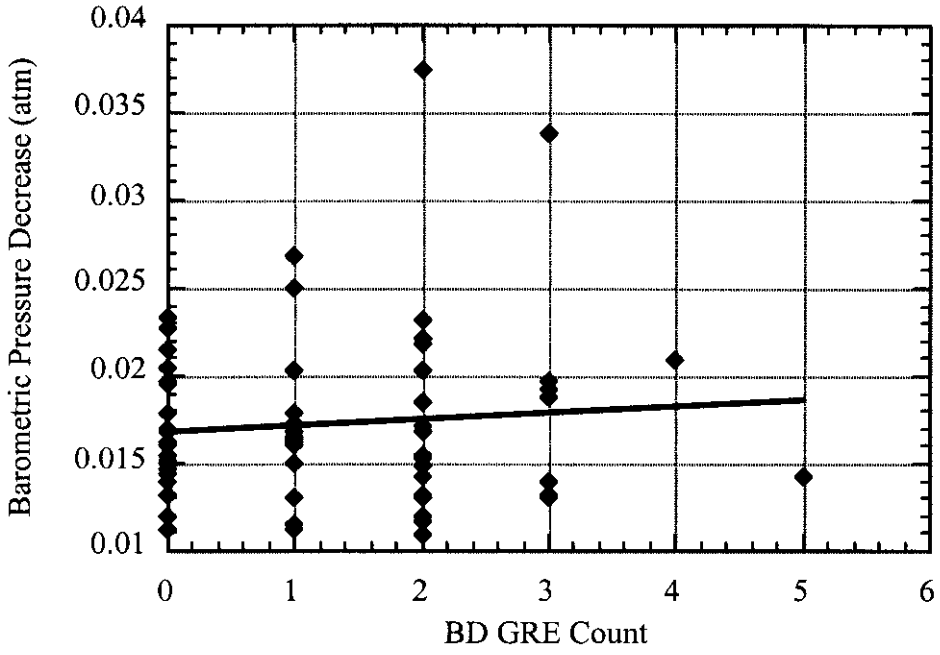

Figure C-5. Correlation Between Gas Release Event Count and Barometric Pressure Decrease

This page intentionally left blank.